NON-EQUILIBRIUM AND QUANTAL ASPECTS

OF

RELATIVISTIC HEAVY ION COLLISIONS

By

Joseph J. Molitoris

A DISSERTATION

Submitted to

Michigan State University

in partial fulfillment of the requirements

for the degree of

DOCTOR OF PHILOSOPHY

Department of Physics and Astronomy

1985

ABSTRACT

NONEQUILIBRIUM AND QUANTAL ASPECTS

OF

RELATIVISTIC HEAVY ION COLLISIONS

By

Joseph J. Molitoris

The approach to local kinetic equilibrium in relativistic heavy ion collisions is studied by following the time evolution of the Wigner function in configuration and momentum space using the Vlasov-Uehling-Uhlenbeck theory. This theoretical approach includes the nuclear mean field, two body collisions, particle production, relativistic kinematics, and the Pauli principle in a microscopic model. A Newtonian Force Model, Time Dependent Hartree Fock, the Vlasov equation, intranuclear cascade, and macroscopic nuclear fluid dynamics are studied as reference cases. In the VUU theory, for central nucleus-nucleus interactions, rapid equilibration of the participants is observed within time spans of the order of 10 fm/c. Total stopping of the projectile occurs at small impact parameters for heavy systems: a sidesplash of nuclear matter is seen due to the interplay of the nuclear compressional potential energy and the collision term. The intranuclear cascade model lacks this essential compressional energy and Pauli blocking and so does not give a realistic representation of medium and high energy heavy ion collisions. Density, temperature, and entropy of the interacting nuclei are extracted. The formation of complex nuclear fragments is studied by applying a six dimensional coalescence model to the final state. The

conjectured nuclear liquid-vapour phase transition is examined. The theory is compared to recent data mainly from the GSI/LBL Plastic Ball collaboration. The pion yields, transverse momentum transfer, and kinetic energy flow effects are found to be sensitive to the nuclear compressibility and the Pauli principle: thus there is the possibility of extracting the nuclear equation of state from the data. Preliminary evidence for a surprisingly stiff nuclear equation of state is presented.

Dedication

To my parents: John and Irene

All the aim of learning is to achieve consciously what to youth is given freely.

...Turgenev in Rudin

Acknowledgements

I have enjoyed writing this doctoral dissertation. Also, I would like to express my gratitude to Horst Stöcker, my thesis adviser, without whom this thesis would never have been written. I am also grateful to Gary Westfall, Konrad Gelbke, S. Mahanti, and Wayne Repko for a careful reading of the manuscript. I want to thank my collaborators Hans Kruse, Detlev Hahn, Barbara Jacak, Jim Hoffer, and Brian Winer for physics and programming contributions and fruitful discussions. In particular, I am indebted to Jim Hoffer and Hans Kruse for code development. Also, during the last few months of my dissertation research, Brian Winer's help was invaluable. I have also appreciated Shari Conroy's help throughout my PhD work.

TABLE OF CONTENTS

List of Tables

List of Figures

III.12 Entropy for Au + Au at b = 3 fm versus energy extracted by the non-interacting fermion formula in the VUU model.

III.13 The evolution in momentum space in the VUU theory of Ar (137 MeV/nucleon) + Ca at b = 0 fm. The collision term (bottom) results in substantial equilibration.

III.14 Initial and final states in configuration and momentum space in the VUU theory for C (85 MeV/nucleon) + C at b = 1 fm. The nucleons which equilibrate are those that collide.

III.15 The number of uncollided projectile nucleons in the VUU model emitted for C (85 MeV/nucleon) induced reactions is used to extract a mean free path.

III.16 In the VUU theory, the evolution of Ar (770 MeV/nucleon) + Pb in configuration space at b = 1, 3, and 5 fm.

III.17 The time development of Ar (770 MeV/nucleon) + Pb in momentum space in the VUU approach at various impact parameters.

III.18 Nb (1050 MeV/nucleon) + Nb at b = 1, 3, and 5 fm in configuration space as a function of time (VUU).

III.19 Nb (1050 MeV/nucleon) + Nb in momentum space in the VUU approach.

III.20 Single particle inclusive proton spectra experimentally and theoretically (histograms) in the VUU theory for the Ar + Ca system.

III.21 The VUU approach explains well recent data which show the lack of a knockout component in a C (40 MeV/nucleon) + C in-plane/out-of-plane pp coincidence experiment.

III.22 The liquid-gas phase transition in nuclear matter in the pressure density plane.

III.23 Density around the origin for an expanding compressed (ρ/ρ_0 = 1.50) system at 5, 10, 15, and 20 MeV initial temperatures in the VUU and NFM models.

III.24 Central density versus time for Au + Au at b = 3 fm and E = 50 MeV/nucleon versus 250 MeV/nucleon in the VUU model shows the same transition behaviour as in the previous figure.

III.25 Pion multiplicities per nucleon versus bombarding energy calculated in a simple shock model with the linear EOS and K_1= 1200, 1600, and 2000 MeV for the solid, dashed, and dotted lines, respectively.

III.26 Number of π^- versus energy for Ar + KCl in the cascade, VUU, and for the experimental data.

I. Nuclear Matter

1. Prospectus

For decades, nuclear physicists have occupied themselves with essentially one point on the phase diagram of nuclear matter, the ground state at $\rho_o = 0.15\ fm^{-3}$ and T = 0 MeV. Studies of low energy nuclear physics (E_{lab} < 10 MeV/nucleon) only probe moderate degrees of excitation. Certainly, there are still many unsolved problems relating to the ground state of nuclei and what happens in such low energy nucleus-nucleus collisions.

However, we have just begun to realize the wide vista open to our study on the phase diagram of nuclear matter. We are just beginning to study the properties of hadronic matter at finite temperatures and densities other than the ground state. There are conjectures about a nuclear liquid-vapor phase transition at temperatures T < 20 MeV and $\rho < \rho_0$, abnormal nuclear matter (density isomers and pion condensates) at high densities $\rho \approx 3 - 5\ \rho_0$, pionization of nuclear matter for high temperatures T > 50 MeV, and the possibility of the deconfinement phase transition from hadronic matter into the quark-gluon plasma at high densities $\rho \approx 5 - 10\ \rho_0$ and/or high temperatures T ≈ 150 - 250 MeV (see Figure I.1). Even more exotic objects such as nuclearites of quark matter are possible [Wit 85].

These different regions of the phase diagram can be probed briefly by nucleus-nucleus collisions at different beam energies. Nuclear physics has continually been driven to higher energies by the need to probe and understand the complicated short range nuclear force which may result in such phases. Consider the present capabilities of our

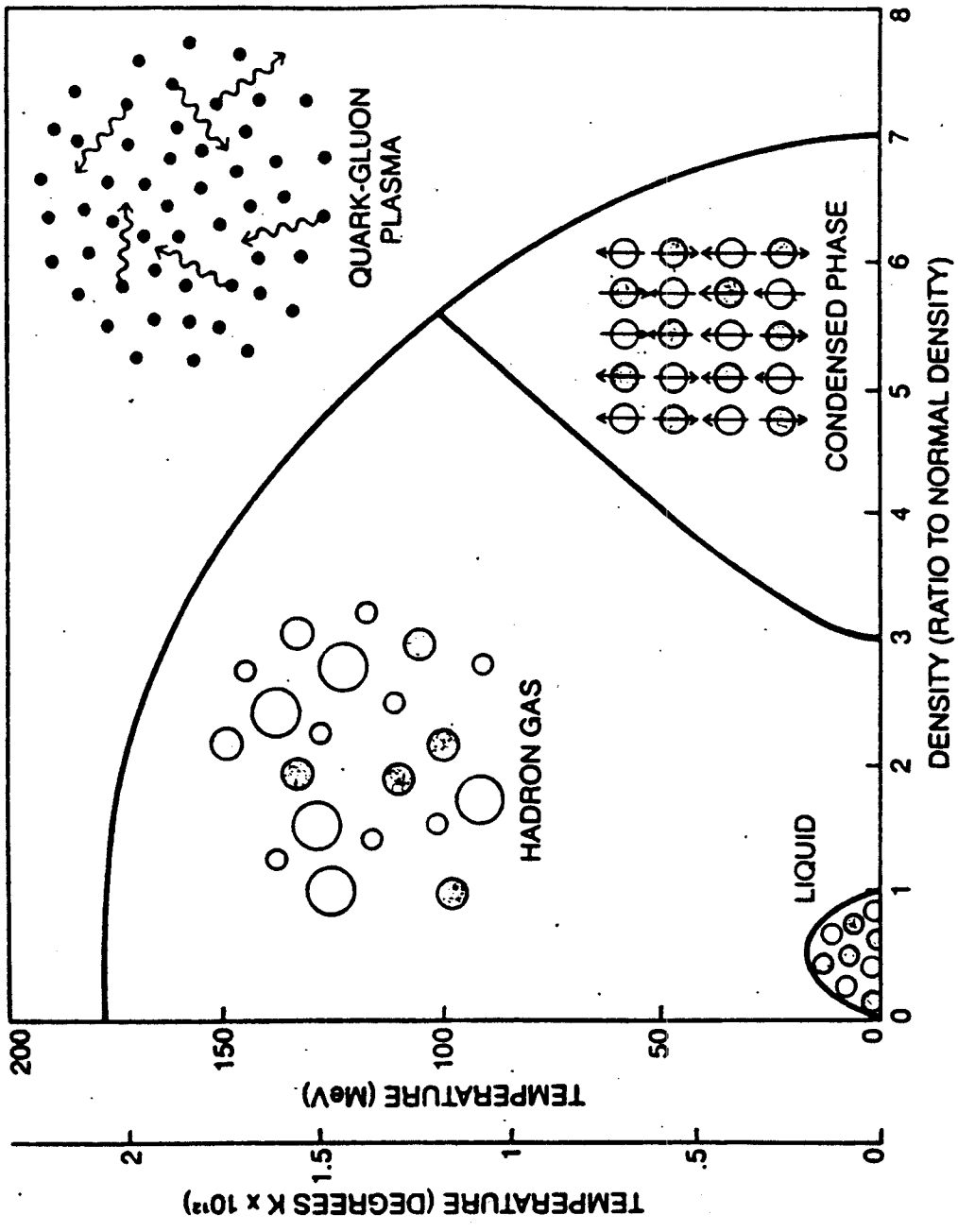

Figure I.1 Possible phase diagram of nuclear matter shows the various transformations that have been conjectured. Experimentally, we still know very little about any of these.

accelerators for a heavy projectile. The present (or soon to be operating) facilities range in energy from 20 MeV/nucleon with the Unilac at GSI to 100 MeV/nucleon at Ganil or the MSU Phase II through the Bevalac at 1000 MeV/nucleon. Only recently have ions with A > 40 been accelerated at this highest energy.

At the greatest available beam energies, densities > $3\rho_o$ and temperatures > 90 MeV are probed. Such extreme densities (10^{15} g/cm^3) and temperatures (10^{12} Kelvin) have prevailed before only in the first fractions of a second during the birth of the universe (in the big bang) and during the death of stars (in supernova explosions and neutron star or black hole formation) [Bow 82, Bet 83, Wil 85]. Thus, in the laboratory we seek to create a little bang, to probe even the parton degrees of freedom. Nuclear physics and high energy physics come to overlap and share theoretical ideas, experimental facilities, and vast manpower.

Clearly today the field of relativistic and ultra-relativistic nucleus-nucleus collisions is exciting and where much of the future of nuclear physics lies. The goal experimentally is to reproduce in the lab these conditions of high density and temperature. Currently, experiments are being done at the Bevalac in Berkeley and the Synchrophasotron at Dubna. Experiments have been approved for the Alternating Gradient Synchrotron at Brookhaven (S + Pb at 16 GeV/nucleon) and for the PS at CERN beginning in 1986. By 1988, there should be HI collisions in the SPS at CERN. Finally, the aborted Isabelle/CBA at BNL may be a HI collider by 1992 (Au + Au at 100 GeV/nucleon).

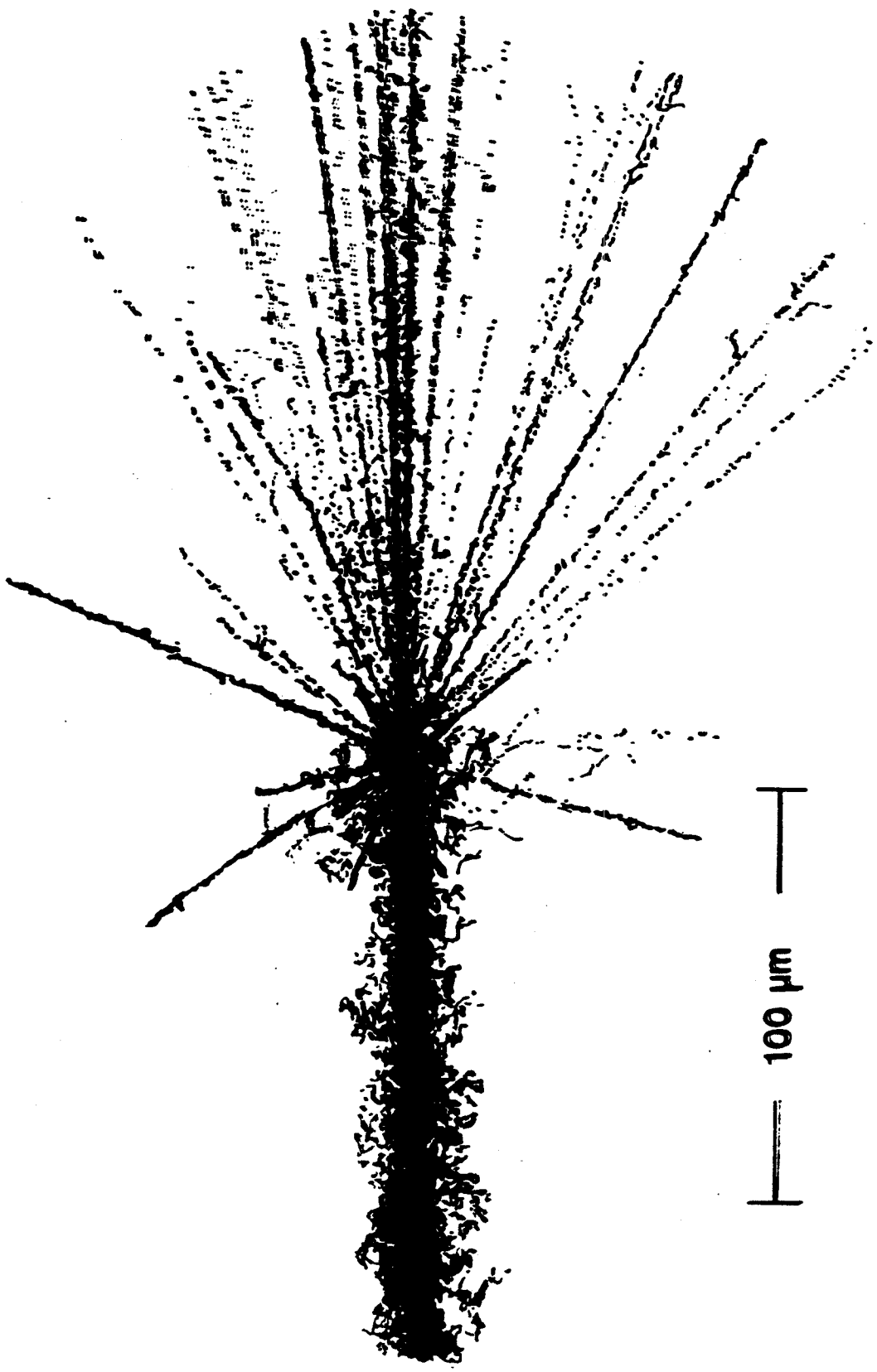

Figure I.2 U (960 MeV/nucleon) + Ag collision in emulsion: we see only the remnants of this central collision. What happened in the 10 fm/c that we do not see?

Experimental information on this unexplored domain is thus now being sought by analyzing high energy collisions of heavy nuclei (see Figure I.2). If the nuclei can stop each other (if the longitudinal momentum can be sufficiently degraded), high energy densities can be obtained for $t \approx 10^{-22}$ seconds. All that is accessible experimentally are the final state fragments. From these and theoretical models, we must try to understand what happens in this very short time. The fact that the duration of a relativistic nuclear collision is so short makes the physics problems even more challenging.

In this thesis a recent theoretical approach is presented and a survey is given of recent experimental and theoretical developments in the field of high energy heavy ion reactions. First the statistical concepts necessary to study the properties of infinite hadronic systems at high density and temperatures are discussed. Then an overview is given of various theoretical approaches developed to describe the finite time and size effects in the dynamical evolution of the highly excited strongly interacting system in an ephemeral heavy ion collision. Finally, the recent 4π experiments on fragment formation, pion production and collective flow are discussed. The implications of these experiments for the nuclear equation of state are pointed out.

2. Statistical and Thermodynamical Concepts

High density matter is formed in nuclear collisions only for brief moments, and global equilibrium can not be reached. However, statistical concepts have been successfully applied to nuclear collisions, e.g. in the Nuclear Fluid Dynamical model, which assumes that local (rather than global) equilibrium is closely approached even

on these short time scales. But the assumption of statistical equilibrium in nuclear collisions must be checked via microscopic theories, which are able to describe the evolution of the system from the non-equilibrium situation to the locally equilibrated state. These theories and the questions related to the equilibration are discussed in detail in the second and third chapters of this thesis.

What are the general statistical concepts appropriate to describe the near equilibrium situation? The nuclear matter properties can be characterized by two canonical variables: for example the density ρ and the temperature T. The discussion of the properties of a piece of hadronic matter at rest usually starts with the definition of the energy per baryon, $E(\rho,T)$, as a function of these two variables. It is convenient to divide the total energy per baryon into a thermal and a compression part:

$$E(\rho,T) = E_T(\rho,T) + E_C(\rho) + E_o \qquad (1)$$

where

$$E_C(\rho) = E(\rho,T=0) - E(\rho_o,T=0) = E(\rho,T=0) - E_o \qquad (2)$$

is defined to be the compressional energy and E_T is the thermal excitation energy per baryon. Note that E_T is zero if the temperature vanishes and $E_C(\rho_o) = 0$. $E_o \approx 939\text{-}16 = 923$ MeV is the rest energy of a nucleon at equilibrium density and zero temperature.

In order to understand the physical significance of $E(\rho,T)$ consider a piece of nuclear matter of volume V. It's energy content is given by $E_V = \int_V \rho\, E(\rho,T)\, dV$, where $e = \rho\, E$ is the energy density of the matter. In evaluating this quantity the Coulomb energy and the long range part

of the Yukawa energy are excluded since these lead to divergence for infinite systems. Hence only the short range part of the nuclear interaction has been considered. This is the origin of the binding energy of 16 (rather than 8) MeV/nucleon: it comes from the volume term of the Bethe-Weizäcker formula (surface and Coulomb terms are neglected).

Once the functional form of E is given, standard thermodynamic relations can be used to calculate the pressure p, entropy S, and enthalpy H of the system at a given density and temperature. For example, the pressure is calculated from the internal energy as

$$p = - \left.\frac{\partial E}{\partial V}\right|_S = \rho^2 \left.\frac{\partial E}{\partial \rho}\right|_S \qquad (3)$$

and can also be separated into two parts p_C and p_T. Similarly one obtains the entropy of the system from the thermal energy alone: because of Nernst's theorem (1906), the T = 0 part of the equation of state does not contribute to the entropy. The entropy of a body vanishes at the absolute zero of temperature.

3. Relativistic Field Theory

The total energy per baryon can also be expressed in kinetic and potential terms. This becomes particularly useful in the field theoretical approach. A relativistic description of the nucleus using the Dirac equation may give a more coherent view of nuclear phenomena than the Schrödinger equation. The relativistic field theory or Quantum Hadro-Dynamics developed by Walecka [Wal 74, Ser 85], Boguta [Bog 77, Bog 83], and others is of special interest. This relativistic field model consists of nucleons obeying the time-dependent Dirac equation, a

classical spin zero attractive meson field (sigma) obeying the Klein Gordon equation, a spin one repulsive meson field (omega) obeying the Proca equation and a meson-baryon interaction between them. This approach starts directly from a Lagrangian involving the exchange of bosons. The resulting coupled field equations are solved simultaneously in a mean field approximation.

QHD is a relativistic field theory of nuclear systems which is based on baryons and mesons and so at the hadron level offers a complete, consistent, and unified treatment of nuclei. The most successful results of QHD are based on the relativistic Hartree approximation. By fitting a minimal number of coupling constants and masses to bulk nuclear properties [Wal 74, Ana 81], the relativistic Hartree solutions predict charge densities, matter densities, and rms radii of the ground state of closed shell nuclei [Due 56 and 58, Mil 72, Jam 81]. An RPA like treatment of excited states is also possible, but the effective interaction involves strong and often sensitive cancellations of large potentials, unlike the usual nonrelativistic approach. QHD can be based on baryons and neutral vector and scalar mesons σ and ω or include in addition charged vector ρ and pseudoscalar π fields in a renormalizable field theory. Feynman rules for the meson-nucleon vertices and meson propagators have been developed [Ser 85].

The Hartree approximation yields an effective Lagrangian where masses and coupling constants for the mesons are phenomenological and are adjusted to fit static nuclear matter properties. The model Lagrangian density is

$$\mathcal{L} = -\hbar c\, \bar{\psi}\left(\gamma_\mu \partial/\partial x_\mu + \frac{m_B c}{\hbar}\right)\psi - \frac{1}{2}(\hbar c)^2(\partial\sigma/\partial x_\mu)^2 - U(\sigma)$$

$$- \frac{1}{4} (\hbar c)^2 F_{\mu\nu} F_{\mu\nu} - \frac{1}{2} (m_v c^2)^2 \omega_\mu \omega_\mu + i g_v \hbar c \bar{\psi} \gamma_\mu \psi \omega_\mu - g_s \hbar c \bar{\psi} \psi \sigma, \qquad (4)$$

where

$$F_{\mu\nu} = (\partial / \partial x_\mu) \omega_\nu - (\partial / \partial x_\nu) \omega_\mu \ . \qquad (5)$$

ψ is the baryon field, σ is the sigma field, and ω is the omega field. Some typical [Cus 85] model parameters are $m_B c^2 = 938$ MeV, $m_S c^2 = 500$ MeV, $m_V c^2 = 780$ MeV, the scalar coupling constant $g_S = 18.030$ MeV-fm, and the vector coupling constant $g_V = 33.141$ MeV-fm.

The potential function is taken to be a quartic polynomial in the field σ [Bog 77, Bog 83]:

$$U(\sigma) = \frac{1}{2} (m_s c^2)^2 \sigma^2 + \frac{1}{3} b \sigma^3 + \frac{1}{4} c \sigma^4 \ . \qquad (6)$$

The addition of nonlinear terms to the Lagrangian allows for a more realistic fit to other nuclear properties, such as the compressibility and effective nucleon mass [Sar 85].

This model has been applied to dynamical calculations [Cus 85]. But let us here discuss the equation of state resulting from these relativistic mean field theories for infinite nuclear matter, neglecting the space and time derivatives in the equations of motion and assuming thermal equilibrium. The compression energy $E_C(\rho)$ of nuclear matter has been calculated in this relativistic field theory with additional nonlinear terms in the Lagrangian and in non-relativistic many-body calculations using the variational method [Bog 83]. The results of both approaches agree for $\rho < 1.2\ \rho_0$ for any reasonable set of parameters for the compressibility K and effective nucleon mass m^* at saturation density ρ_0. However, at higher densities $\rho > 1.2\ \rho_0$ the nuclear

equation of state is so sensitive to K and m^* at ρ_o that differences of several hundred percent arise even if K and m^* are only varied within their present experimental 10-20% uncertainties. These results demonstrate the obvious fact that even a precise determination of the nuclear properties at ground state densities does not enable us to predict the high density behavior of nuclear matter. A theoretical determination of these properties is also very difficult in view of the fact that many body forces may play an essential role.

It is a shortcoming of this relativistic field model that the nucleons and mesons are point particles. Another problem is the explicit lack of the delta. Furthermore, a field theoretical treatment beyond the mean field approximation is not yet developed. To describe the collision dynamics in a time dependent theory, semi-classical approaches must be used which include the nuclear potential, but also the effects of two body collisions (see Chapter II). For such approaches, phenomenological equations of state are used. The compression energy $E_C(\rho)$ then incorporates phenomenologically the nuclear binding energy, the Fermi energy of the nucleons, hard core effects and the exchange part of the nuclear forces. It is often loosely referred to as the "nuclear equation of state (EOS)." Two commonly used functional forms for $E_C(\rho)$, the linear and the quadratic, originate from the extended liquid drop model of Scheid and Greiner [Sch 68]:

$$E_C(\rho) = K_1(\rho-\rho_o)^2/(18\rho\rho_o) \qquad (7a)$$

$$E_C(\rho) = K_q(\rho-\rho_o)^2/(18\rho_o^2) \; . \qquad (7b)$$

4. Finite temperatures

The temperature of the system is the second thermodynamic variable of importance. The total energy of the system at finite temperature is described by the interaction energy plus the kinetic energy of the particles in the system. The latter is given by interacting relativistic Fermi-Dirac and Bose-Einstein distributions, hence the total energy per baryon is [Hei 79, Hah 85a]

$$E = U + \sum_{i=1}^{\sigma_b} \left\{ \frac{\rho_i^{\circ} m_i c^2}{\rho} + \frac{4\pi g_i}{\rho(2\pi\hbar c)^3} \int_{m_i c^2}^{\infty} \frac{\varepsilon^2\sqrt{(\varepsilon^2 - m_i^2 c^4)}}{\exp[\varepsilon/T]-1}\, d\varepsilon \right\}$$

$$+ \sum_{i=\sigma_b+1}^{\sigma} \frac{4\pi g_i}{\rho(2\pi\hbar c)^3} \int_{m_i c^2}^{\infty} \frac{\varepsilon^2\sqrt{(\varepsilon^2 - m_i^2 c^4)}}{\exp[(\varepsilon+U-\mu))/T]+1}\, d\varepsilon \qquad (8)$$

where the first sum runs over the Bose-degrees of freedom (the pion, heavier mesons, and the photon) while the second sum is over all the excited states of the nucleon (the $\Delta(1232)$ resonance being the most important resonance in the GeV/nucleon energy region).

Here it is assumed that all nucleonic resonances feel the same interaction energy per particle U, which depends only on the total baryon density ρ [Hei 79, Hah 85a]. This potential energy must be included into the Fermi-Dirac distribution function in a self-consistent way. It is also assumed that all the particles are in chemical and thermal equilibrium and that the chemical potential μ is the same for all baryons. Both the chemical potential and the interaction potential for the bosons are taken to be equal to zero.

Since at least the baryons feel a potential, this approach is thus more physical than Hagedorn's approach where the dynamics is shifted to the density of states. In Hagedorn's thermodynamics, if a system of

particles interacts through the formation of a new resonance or bound state R, then for all thermodynamic purposes, this interaction may be ignored and in its place a new non-interacting species may be added to the system with the quantum numbers of R [Hag 68].

In (8), ρ_i^o is the contribution of the Bose ground-state to the density of the boson-phases. The photon naturally has no Bose condensate. The connection between the baryon density and the chemical potential reads [Hah 85a]

$$\rho = \sum_{i=\sigma_b+1}^{\sigma} \frac{4\pi g_i}{(2\pi\hbar c)^3} \int_{m_i c^2}^{\infty} \frac{\varepsilon \sqrt{(\varepsilon^2 - m_i^2 c^4)}}{\exp[(\varepsilon+U-\mu)/T]+1} \, d\varepsilon \, . \qquad (9)$$

The number of mesons can be calculated via [Hah 85a]

$$N_i = \frac{g_i}{\exp(m_i c^2/T)-1} + \frac{4\pi g_i V}{(2\pi\hbar c)^3} \int_{m_i c^2}^{\infty} \frac{\varepsilon \sqrt{(\varepsilon^2 - m_i^2 c^4)}}{\exp[\varepsilon/T]-1} \, d\varepsilon \qquad (10)$$

The connection between U and the compression energy E_C is also needed. This is found by letting $T \to 0$ in eq. (8) and (9) to get [Hah 85a]:

$$E(T=0) = 0.75X + U + \frac{m^2c^4}{8} \left\{ \frac{3X}{X1^2} - \frac{3m^2c^4}{X1^3} \ln[(X+X1)/mc^2] \right\} \qquad (11)$$

with $g = 4$, $mc^2 = 939$ MeV, $C = 6\pi^2(\hbar c)^3$, $X1 = (\rho C/g)^{1/3}$, and $X = \sqrt{(m^2c^4 + X1^2)}$ assuming that for T=0 only the nucleonic ground state is populated (which should be true for small densities unless the nucleon-Δ interaction is much stronger than the nucleon-nucleon interaction [Bog 82]). Expanding (11) for small densities, the well known $\rho^{2/3}$ dependence for the energy is obtained [Hah 85a]

$$E \approx U + mc^2 + 0.3 \, (\rho/\rho_o)^{2/3} \hbar^2/m \, (6\pi^2\rho_o/g)^{2/3} + \ldots \qquad (12)$$

The relation between U and E_C is then [Hah 85a]:

$$U(\rho) = E_C + E_o - 0.75\ X - \frac{m^2c^4}{8}\left\{\frac{3X}{X1^2} - \frac{3m^2c^4}{X1^3}\ln[(X+X1)/mc^2]\right\} \qquad (13)$$

Finally, the pressure is [Hah 85a]

$$p = -T \sum_{i=1}^{\sigma_b} \frac{4\pi g_i}{(2\pi\hbar c)^3} \int_{m_i c^2}^{\infty} \varepsilon\sqrt{(\varepsilon^2 - m_i^2c^4)}\ \ln(1-\exp[-\varepsilon/T])d\varepsilon$$

$$+ T \sum_{i=\sigma_b+1}^{\sigma} \frac{4\pi g_i}{(2\pi\hbar c)^3} \int_{m_i c^2}^{\infty} \varepsilon\sqrt{(\varepsilon^2 - m_i^2c^4)}\ \ln(1+\exp[(\mu-U-\varepsilon)/T])d\varepsilon$$

$$+ \rho^2 \frac{\partial U}{\partial \rho} \qquad (14)$$

and the entropy per baryon is

$$S/N_B = P/(\rho T) - \frac{\rho}{T}\frac{\partial U}{\partial \rho} - 1/N_B \sum_{i=1}^{\sigma_b} g_i \ln(1-\exp[-m_i c^2/T])$$

$$+ (E-\mu)/T\ . \qquad (15)$$

5. Pionization in Hot Systems

These equations have been used in simplified models of heavy ion reactions [Hah 85a] to extract the temperature in the reaction from pion multiplicities. The dependence of the number of pions per nucleon on the temperature as calculated with the above approach, which includes all firmly established resonances, the pion, the η meson, and the photon is shown in Figure I.3. Observe that the pion yield increases rapidly with temperature from zero to about one per nucleon at $T \approx 100$ MeV, and then flattens out - nuclear matter is gradually transformed into a hadron plasma. This becomes obvious in Figure I.4, which shows the

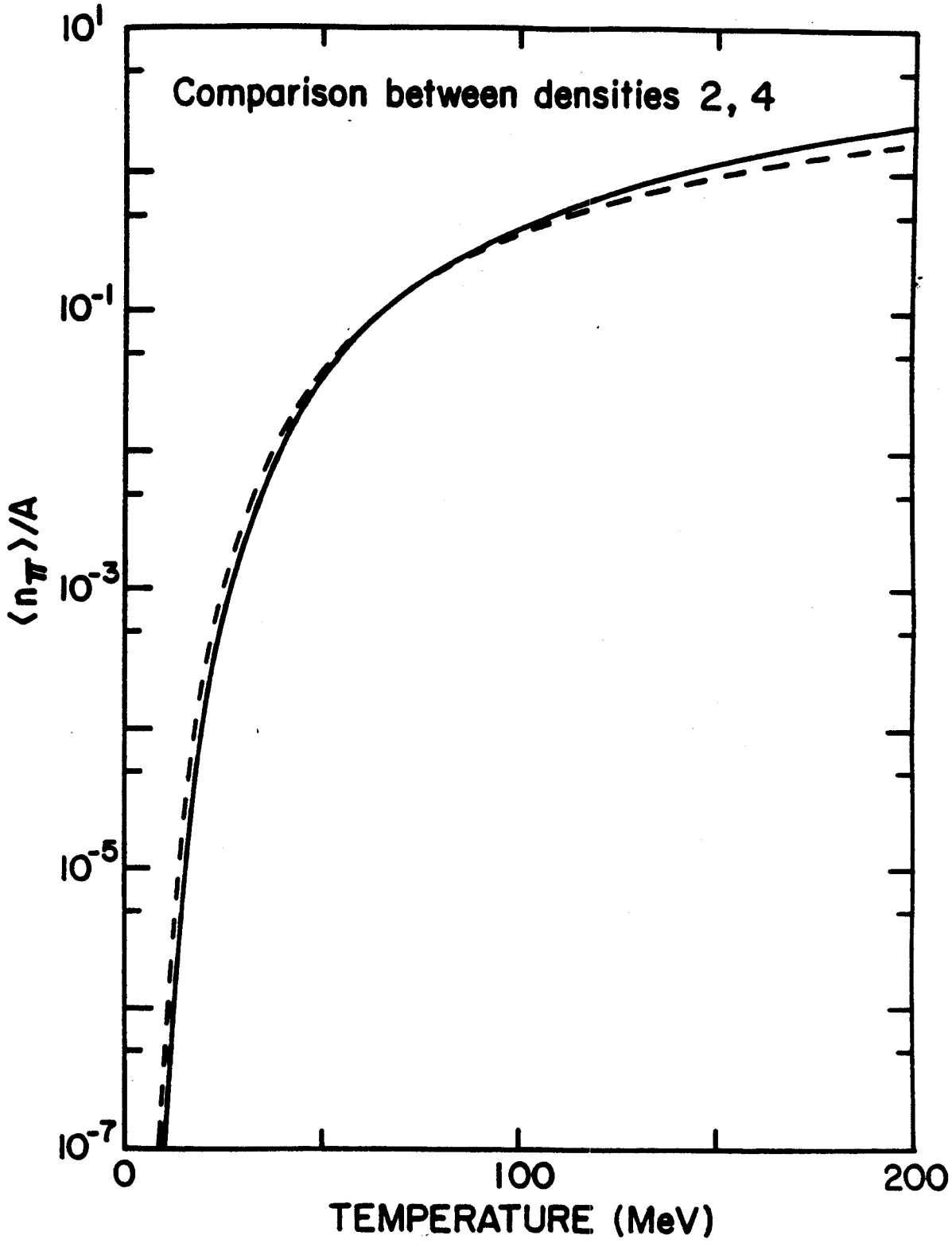

Figure I.3 Pion multiplicities versus the temperature for baryon densities two times (solid line) and four times (dashed line) normal nuclear matter density.

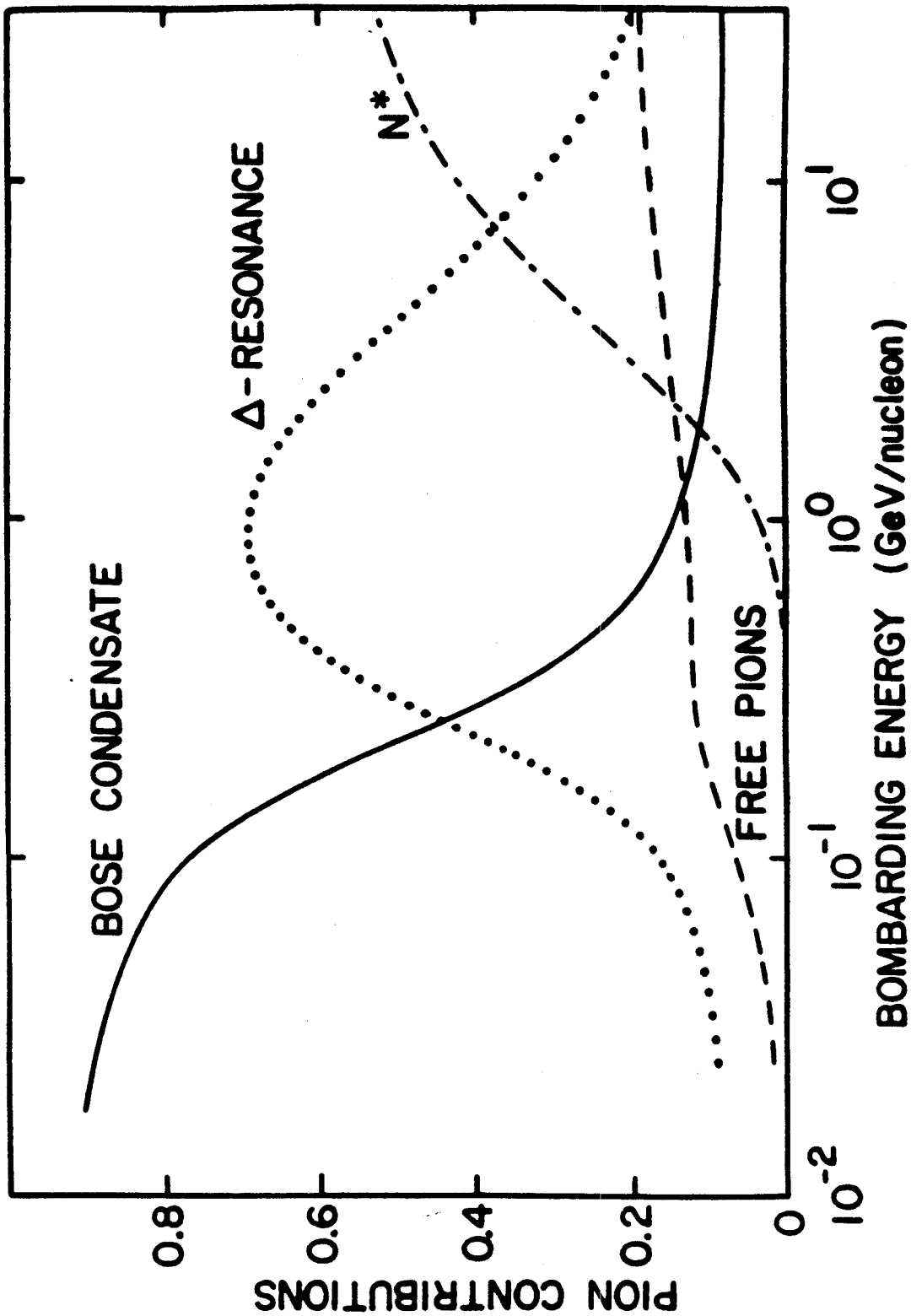

Figure I.4 Contributions to the pion yields per baryon for a C + C reaction with the quadratic equation of state in the shock model.

distribution of pions over the various pion producing channels [Hah 85a]. At low energy, temperatures of the order of 50 MeV or less, most of the pions reside in the Bose condensed zero momentum state. At higher temperatures, the pion yield is due to nuclear resonances. The $\Delta(1232)$ resonance is of particular importance in the Bevalac energy regime, $E_{lab} \approx 1$ GeV/nucleon, while the more massive resonances become important at temperatures above 100 MeV. In the evaluation of the relativistic integrals, it is seen that most of the pions stem from the decay of the Δ resonance. The direct production of pions due to equilibrium evaporation [Gal 84, Aic 84a], equilibrium hot spot emission [Aic 84b] and nuclear pion bremsstrahlung [Vas 80ab,84] has been studied by others.

Figure I.3 can be used to extract the temperatures in the moment of pion emission from the observed pion yields [Hah 85a] - see Figure I.5. One finds that the temperature rises smoothly with the bombarding energy, reaches $T \approx 100$ MeV at the top Bevalac energies and can be extrapolated to temperatures exceeding the critical temperature for deconfinement, $T \approx 200$ MeV, at energies in the range of relativistic heavy ion facilities presently under construction at CERN and Brookhaven, $E_{lab} > 10$ GeV/nucleon. This equation of state (14) is too complicated to be of practical importance for many three dimensional model calculations. Therefore simpler approximations are widely used to determine the energy and density dependence of the thermal energy.

The simplest ansatz for the thermal energy is the classical ideal gas relation $E_T = 3/2\ T$. This is actually the asymptotic value for the full non-interacting non-relativistic Fermi gas: it neglects the

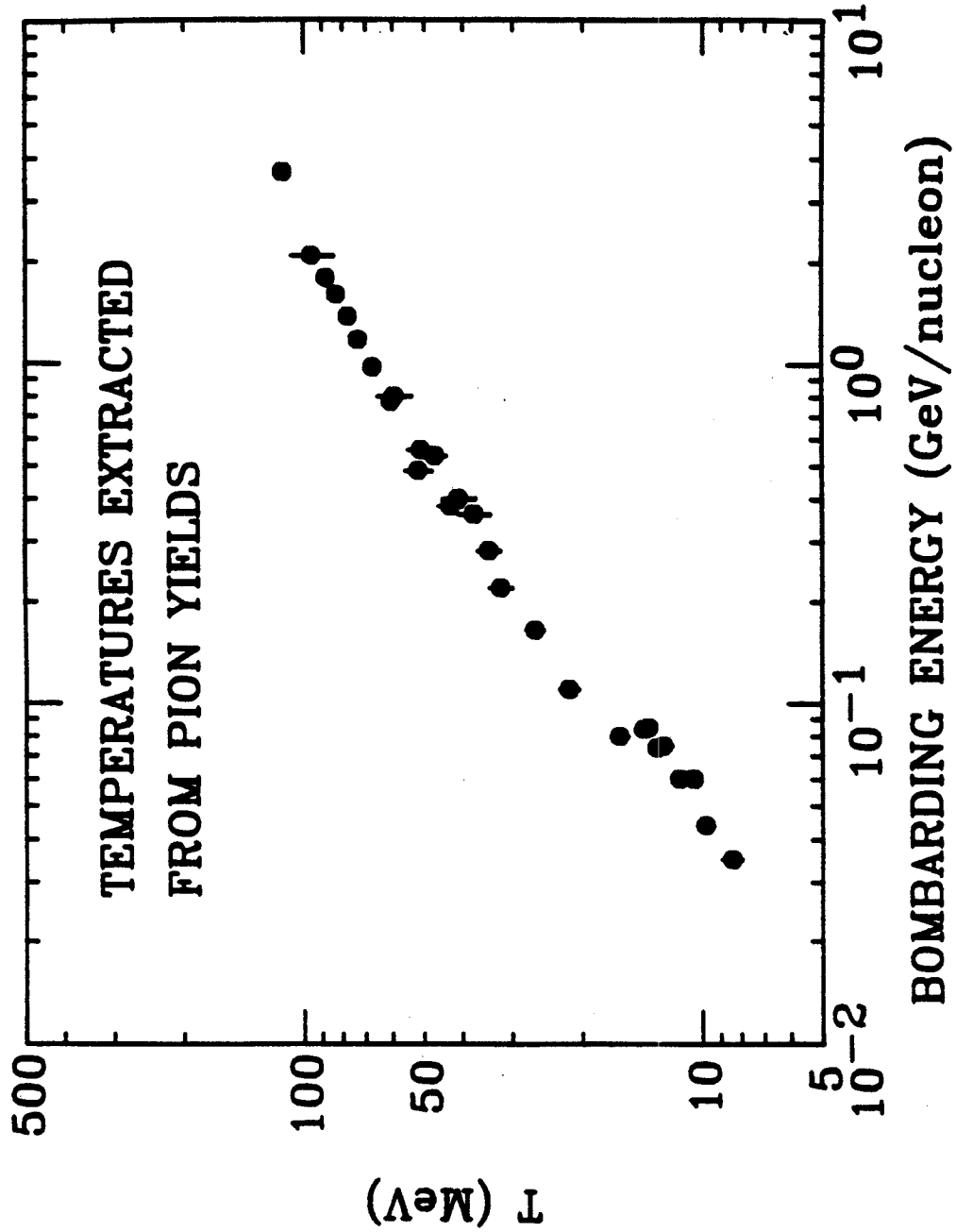

Figure I.5 The freeze out temperature of the pions calculated from the pion multiplicity data per nucleon.

influence of the interactions on the thermal energy, but it contains the Fermi degeneracy energy. However, the classical approximation is only reasonable if the temperatures are considerably larger than the chemical potential or the Fermi energy at a given density.

6. Exotic Matter

The possible existence of density isomers in nuclear matter has been suggested repeatedly by many authors [Fee 46, Bod 71, Mig 72, Lee 74]. Lee and Wick observed that the nonlinear scalar meson self-interaction model - the chiral sigma model - can lead to an abnormal state at high density, $\rho/\rho_0 \approx 3\text{-}5$. They found that chiral symmetry is restored in this state - the nucleons become massless. The binding energy can be enormous, leading to secondary minima in the compressional energy which are several hundred of MeV/nucleon deep. Another mechanism proposed to create secondary minima in $E_c(\rho)$ is the collective excitation of zero frequency spin-isospin modes in nuclear matter called pion condensation (since these modes carry the quantum number of the pion [Mig 72]).

However many of these proposals did not attempt to describe the nuclear EOS at other densities or (as in the case of the linear sigma model) the description of the known properties of nuclear matter was incorrect. Since the existence of isomeric superdense matter is speculative, it is desirable to study this question in models which describe normal nuclear matter in a self consistent way. A recent calculation [Bog 82] fulfills this requirement and still predicts abnormal superdense states.

The model used is the relativistic mean field theory discussed above, which is well able to describe normal nuclear matter. The abnormal state comes in by introducing the Δ resonance into the theory. The abnormal state occurence depends now on the strength of the scalar interactions of the Δ. If the coupling constant for this interaction is only one third larger than the corresponding coupling of the nucleon, secondary minima occur in E_C and the abnormal state is predominantly populated by the resonance rather than the nucleon. A similar mechanism has been discussed at high temperatures, leading to abundant resonance formation above a critical temperature [Hei 79, Gar 79]. Since the scalar coupling of the Δ is unknown, the possible existence of these baryonic resonance isomers can not be ruled out.

More exotic possibilities include that of nuclearites or balls of u,d,s quarks in possible islands of nuclear stability [Wit 85] beyond the A values of the nuclear table. Only by doing a careful analysis of high energy experiments can the existence or non-existence of such objects be ascertained.

II. Many Body Theory of Nuclear Collisions

1. Hierarchy of Theories

A comprehensive theory of nuclear collisions at high energies should describe relativistic quantum mechanical wave packets interacting via an apropo many body interaction. Such a relativistic quantum mechanical treatment has not yet been attempted: even the formulation of the interaction itself poses formidable problems. A natural suggestion for a simpler treatment - and one that has been very successfully employed in the cascade calculations [Yar 79,81; Cug 80,81,82] - is to use measured free N-N cross sections as the primary physical input for a model. This is legitimate if only binary N-N interactions occur and the scattered nucleons always reach their asymptotic states before encountering another nucleon - in other words, if the system is dilute. Thus, the cascade models and all other models that assume point N-N scattering, require diluteness.

If one does not want to assume this diluteness, then the simultaneous interaction of many nucleons has to be allowed. In this case, scattering can no longer be described in terms of asymptotic states and cross sections, but an explicit interaction potential is required. The models that use this approach generally describe the nucleon motion in terms of classical trajectories and forces and are therefore called Classical Equations of Motion or Newtonian Force Models [Bod 77,80,81; Wil 77,78; Cal 79; Mol 84a]. A classical description might be considered a reasonable approach for intermediate energies 100-800 MeV/nucleon because of the high degree of thermal excitation that

tends to smear out nuclear structure and the quantum mechanical features of the system.

In the relativistic realm there are problems even with the formulation of the theory - the meson fields, which have to be included in a relativistic theory, do not obey classical equations even approximately, although it is possible to replace the Dirac equations by relativistic Newton equations. The only possibility to obtain a solvable model seems to be to ignore second quantization and treat the meson fields classically. The closest tractable treatment of the many-body aspect thus occurs in a model which solves the non-relativistic equations of motion.

2. Newtonian Force Model - the Classical Limit

Consider the classical Γ space description of an A body system with fixed degrees of freedom: I have in mind the colliding system of $A = A_P + A_T$ nucleons. Recall that the Γ space is a 6A dimensional phase space and the state of the system is represented by one point in this space. Let $\rho(\vec{r}_1,\ldots,\vec{r}_A,\vec{p}_1,\ldots,\vec{p}_A,t)d\Gamma$ be the probability to find the system at the point $(\vec{r}_1,\ldots,\vec{r}_A,\vec{p}_1,\ldots,\vec{p}_A)$ in Γ space at time t: ρ is the A-body distribution function. The classical Liouville equation then follows from considering ρ as an incompressible probability fluid:

$$\frac{\partial\rho}{\partial t} + \sum_{i=1}^{A} \left(\frac{\partial}{\partial \vec{r}_i} \cdot (\rho\, \dot{\vec{r}}_i) + \frac{\partial}{\partial \vec{p}_i} \cdot (\rho\, \dot{\vec{p}}_i) \right) = 0 \qquad (1)$$

$$= \frac{\partial\rho}{\partial t} + \sum_{i=1}^{A} \left(\dot{\vec{r}}_i \cdot \frac{\partial\rho}{\partial \vec{r}_i} + \dot{\vec{p}}_i \cdot \frac{\partial\rho}{\partial \vec{p}_i} \right) .$$

Hamilton's equations imply that:

$$\frac{\partial \rho}{\partial t} = \{H, \rho\} \qquad (2)$$

This is the classical Liouville equation which describes a microcanonical ensemble. For equilibrium, one has the condition $\{H, \rho\} = 0$ and hence $\rho = C\delta(E - H(\vec{r}_1, \ldots, \vec{r}_A, \vec{p}_1, \ldots, \vec{p}_A))$.

The Newtonian Force Model of heavy ion physics solves Newton's or Hamilton's equations of motion for the A interacting nucleons. This is thus a theory for the full non-equilibrium classical situation. Hence the NFM is more fundamental than a kinetic equation (see below): it solves the A-body Liouville equation. In the NFM model there are all classical degrees of freedom so that non-equilibrium as well as equilibrium events can be described. This classical description is the only method which can account for the dual role of forces in determining the nuclear equation of state and the collisional relaxation effects. The main objective in considering a classical approach here is as a model which can roughly describe the N-N interaction (both in terms of cross sections and binding energies) and to use it to study the approach to equilibrium and the influence of the short range repulsion in nucleus-nucleus collisions.

Historically, NFM has some similarities with the molecular dynamics approach to the theory of liquids [Ald 57]. There the Newtonian equations of motion for spherical molecules or the coupled Newton-Euler equations of motion for translations and rotations (in the case of rigid non-spherical molecules) are solved. The first molecular dynamics calculations used hard sphere and square well potentials [Ald 57, 59, 72]. The first NFM calculations used Yukawa potentials in three

dimensions [Bod 77, Wil 77] and Lennard-Jones potentials in two dimensions [Nun 77] introducing this type of approach into nuclear physics. The former two groups applied the NFM approach for the energy range 100-300 MeV/nucleon whereas the latter were interested in few MeV/nucleon reactions.

Of course, there are no quantum effects in this model. However, one does have information about the A-body classical distribution function once one has chosen some classical potential. The choice of this potential is subtle since over the years nuclear physicists have been driven to more and more complicated nucleon-nucleon interactions culminating e.g. in the Paris potential [Cot 73] in order to accommodate the spin, isospin, etc. degrees of freedom.

The standard problem of scattering theory is to determine the scattering amplitude $f(\theta)$ from the interaction potential between projectile and target. Generally the potential may be non-local

$$V\psi(r) = \int V(r,r')\psi(r')d^3r' \quad . \tag{3}$$

The inverse problem is to gain information on the potential from the observed differential scattering cross section

$$\frac{d\sigma}{d\Omega} = |f(\theta)|^2. \tag{4}$$

One can get information on the amplitude from polarization experiments. If the interaction is local, $V = V(r)$, then the potential is unique. However, the N-N interaction is known to be non-local - there is an $\vec{l}\cdot\vec{s}$ term and a complicated momentum dependence. Then the scattering amplitude does not determine the potential uniquely - there exist many phase equivalent potentials which give the same phase shifts and hence the same amplitude. The problem is that one doesn't have information on

off-shell ($E \neq p^2/2m$) scattering: the wave function at finite distance is not fixed by the asymptotic behaviour [Pei 79].

The N-N interaction has been studied by np and pp scattering for many years. Cross sections, analyzing powers, polarizations, spin-transfer, and spin correlation parameters have been measured to try to more completely describe the process in terms of the scattering matrix. The isospin T=1 phase shifts are fairly well-known from pp data, but T=0 ones less so (because of the imprecision of np data). With a classical potential, one can only hope to fit some part or moment of the differential cross section.

Yet it is through the potential that the NFM attempts to give some explanation of ground state properties, at the very least in terms of nuclear size and binding, and also via the same forces to explain the interaction of nuclei. One must of course note that the NFM can't hope to do more than produce roughly stable nuclei to be used in studying the short range repulsion in nucleus-nucleus collisions: nuclei are fundamentally quantum mechanical in the ground state. Thus the defining characteristic of NFM is the use of some potential V(r) acting between each nucleon and all the others. This is both the key ingredient of the approach and also a major problem because the potential demanded by the model may be different from these standard quantum mechanical potentials for the NN interaction: the potential must be deduced in a classical way from the available experimental data (binding energies, cross sections, nuclear size).

A simple ansatz for a classical central potential that acts between each nucleon and all other A-1 nucleons consists of repulsive and attractive Yukawa terms [Bod 77, Wil 77]:

$$V_Y = (V_R\, e^{-k_R \cdot r} - V_A\, e^{-k_A \cdot r})/r. \qquad (5)$$

The attractive part serves to bind the nucleons and the repulsive core prevents nucleons from approaching each other closely (which amounts to a strong correlation).

The parameters in the phenomenological potential have been chosen in a compromise between reproducing the np differential scattering cross section at $\theta_{CM} \approx 90^{\circ}$ (which has the largest influence on the transverse momentum transfer) and giving reasonable binding energies and stable nuclei in a completely classical calculation. For Nb nuclei, typical parameters are $K_A = 1.75\ fm^{-1}$, $K_R = 2.66\ fm^{-1}$, $V_A = 765.$ MeV-fm, and $V_R = 2970$ MeV-fm [Mol 84a]. Recall that the cross section classically is calculated from:

$$\frac{d\sigma}{d\Omega} = \frac{b}{\sin(\theta)} \left|\frac{db}{d\theta}\right| . \qquad (6)$$

It is not adequate to compare this quantity directly with the experimental differential cross section, because of the purely quantum mechanical diffraction and exchange effects, which can't be reproduced in this classical theory. A meaningful quantity to fit is the viscosity moment of the scattering cross section:

$$\sigma_v = 2\pi \int \sigma(\theta)\sin^2(\theta) d(\cos(\theta)) \qquad (7)$$

which is related to the viscosity and thermal conductivity in a Boltzmann equation approach [Bod 77].

In a two dimensional model [Nun 77] made an even simpler ansatz for the potential. Each nucleus was taken to consist of seven equally charged nucleons confined to two dimensions and interacting via a Coulomb and a Lennard Jones 6-12 potential. One may write their potential in the general form:

$$V_{LJ}(r) = D[(\frac{a}{r})^m - 2(\frac{a}{r})^n] \qquad (8)$$

where [Nun 77] took m = 12, n = 6, a = 2 fm and D = 10 MeV. Fermi energy is completely neglected but Coulomb effects are included and simulations were done with initial energies up to twice the Coulomb barrier. Some features of Heavy Ion reactions at few MeV/nucleon energies are reproduced such as fully and partially damped scattering and orbiting (a deflection to negative angles) [Nun 77]. Low energy studies with a classical model have not been pursued further since the quantum mechanical aspects of the interaction are then very important.

In the NFM approach in three dimensions [Bod 77, Wil 77, Mol 84a], nuclei are described as an ensemble of protons and neutrons initially distributed at random throughout a sphere with the nuclear radius

$$R = R_0 A^{1/3} \qquad (9)$$

where R_0 = 1.2 fm. Some cutoff on the interparticle positions, say 1.2 fm, must be imposed so that nucleons do not evaporate with large amounts of energy due to the repulsive potential. There is, of course, always some evaporation since it is a difficult problem to put the particles into stable orbits. The nucleons may be subjected to a minimization procedure to find more stable positions in phase space: the use of such

a procedure is discussed below. The nucleons are also given random Fermi momenta.

For a numerical simulation of a collision process, the nuclei are Galilei boosted with the respective center of mass momenta at given impact parameter. The Newtonian equations of motion are then integrated using a fourth order Adams-Moulton predictor-corrector method [Hof 83]. This routine requires three previous positions and momenta so that a fourth order Runge-Kutta routine is also used. The use of a predictor-corrector routine makes available an estimate of the error by comparing the predicted with the corrected values. If this error becomes too large (small), then the time step is reduced (increased). Energy conservation to better than 1% has always been demanded. Of course, both momentum and angular momentum are conserved. All calculations are done using the double precision available on a VAX 11/780 or FPS 164.

A slightly modified version of this integration routine is used to effect the minimization [Bod 77, Wil 77]. The only modification is to cause each nucleons momentum to be cut by a factor of one half in each integration step, thus effectively damping the motion of the particles. This is equivalent to introducing an artificial viscosity term [Wil 77]. The configuration of minimum energy is then a crystalline structure. Thus one finds (for $p_F = 0$) a linear structure for the deuteron, a triangle for three nucleons, a tetrahedron for four, etc. The characteristic interparticle distance corresponds to that of the potential minimum.

Newton's equations of motion are solved for the $A = A_P + A_T$ interacting nucleons:

$$\vec{F}_i = \frac{d\vec{p}_i}{dt} = -\frac{\partial U}{\partial \vec{r}_i} \tag{10}$$

where

$$U(r_i) = \sum_{\substack{j=1 \\ j\neq i}}^{A} V(r_{ij}) \, . \tag{11}$$

Shown in Figure II.1 is how a Nb + Nb collision at 400 MeV/nucleon evolves in this approach. Note the strong bounce-off or side-splash of nuclear matter [Mol 84a].

Bodmer and Panos [Bod 77] initially chose the four Yukawa parameters based on the potentials of Bethe and Johnson [Bet 74] but adjusted to give reasonable values of the viscous cross section. Their calculations for A=50 on A=50 at 117 and 300 MeV/nucleon were done to look for shock-like phenomena. Some transverse peaking for small impact parameter b and even large fused residues with A~60 for the 117 MeV/nucleon case were found. Results for Ne on Ne at 117, 400, and 800 MeV/nucleon and for Ca on Ca at 400 MeV/nucleon [Bod 80] compare a static two body potential and a scattering equivalent momentum dependent potential to test for finite range effects. For Ca on Ca a transverse peaking in the momentum distribution is found.

A classical two body potential with a momentum dependent two body core which roughly satisfies $p_{ij}r_{ij} \geq \hbar$ has also been used [Wil 77]. The Pauli core is

$$V_p(r,p)=(\xi^2\hbar^2/5mr^2)\exp(-2.5[(pr/\xi\hbar)^4-1]) \tag{12}$$

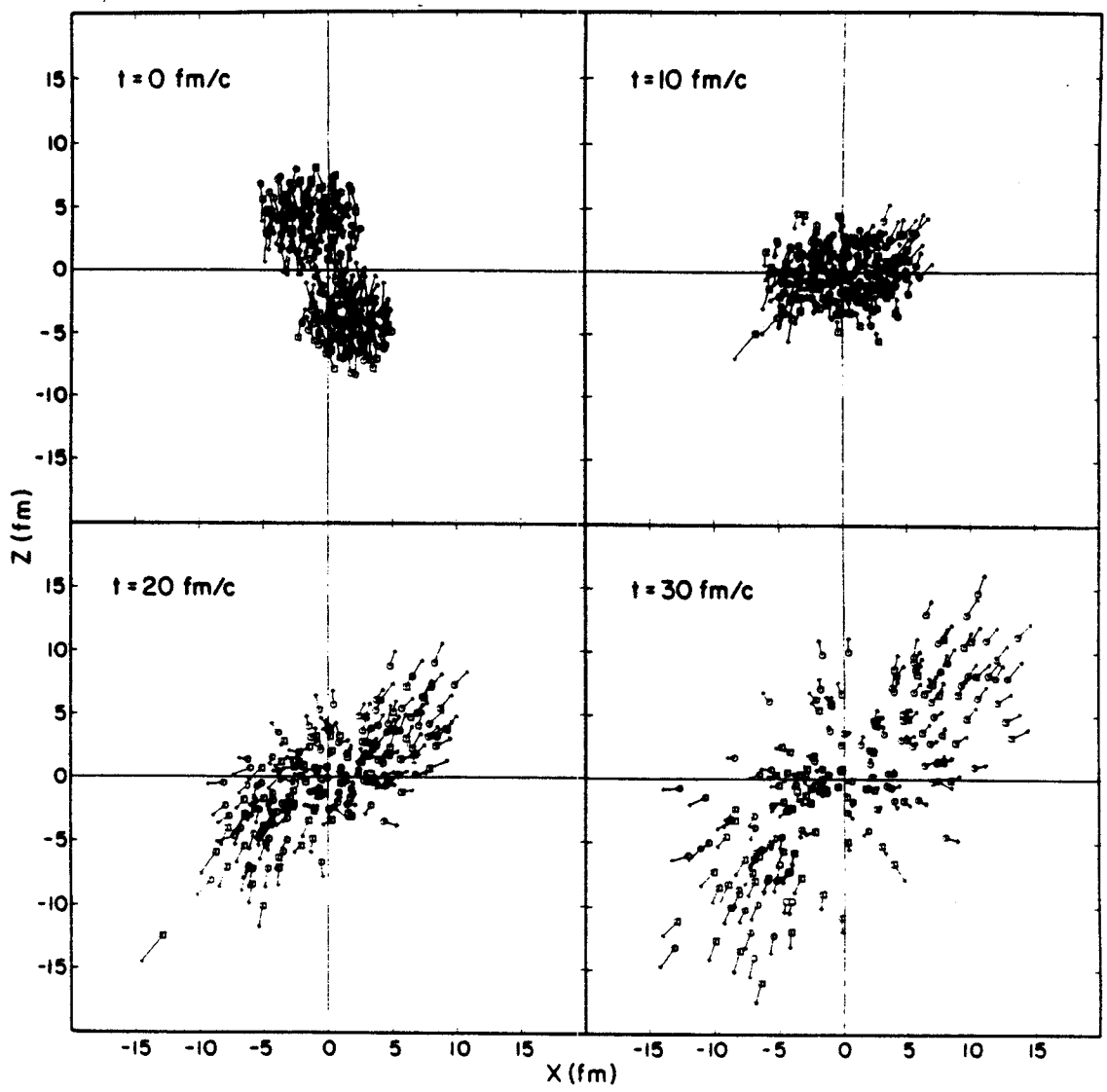

Figure II.1 Nb (400 MeV/nucleon) + Nb as a function of time in the Newtonian Force Model: strong collective flow is sensitive to the short range repulsive nuclear force.

where ξ is a number of order one. At minimum, the nucleonic velocities will all be zero but the momenta will not. The Pauli core may include spin-isospin by

$$V_P(r,p) \rightarrow V_P(r,p)\delta_{s_i s_j} \tag{13}$$

where s_i and s_j are a spin isospin index. In 20 on 20 and 40 on 40 collisions at 800 MeV/nucleon [Cal 79] there is only qualitative agreement with the fireball/firestreak model: the NFM is found to exhibit shear viscosity and incomplete thermalization.

A relativistic approach to $O(v^2/c^2)$ may be obtained by including a retarded momentum dependent correction to the nonrelativistic static potential $V = V_{sta} + V_{ret}$ [Bod 77]. An alternate approach [Wil 76] included retardation effects but ignored the acceleration of the source particle to obtain a relativistic momentum dependent potential. One may try [Kun 81] to extend this model to include the meson field. Nucleons are then treated as relativistic Dirac particles coupled to the isovector pion field through pseudoscalar γ_5 coupling. The problem of one nucleon interacting with a pion field is solved and the Δ_{33} resonance is qualitatively reproduced. A many body extension is not tractable.

Other forms for the potential are possible. The attractive Yukawa potential may be replaced with a Woods-Saxon potential [Kit 81]:

$$V_{WS}(r) = V_R\, e^{-K_R \cdot r}/r - V_A/(1+e^{K_A \cdot (r-r_{WS})}). \tag{14}$$

With the potential parameters given by these authors, the greatest possible potential energy that one can obtain for Ar is -17 MeV/nucleon

(neglecting Coulomb energy); adding 20 MeV of Fermi energy would then produce an unbound state.

Kiselev [Kis 84] has used a double parabolic form for the N-N potential and have also included spin and isospin projections. Calculations for Ne + U and Nb + Nb at 400 MeV/nucleon and for Ca + Ca at 800 MeV/nucleon yield the same collective flow phenomena (see below) that has been observed experimentally and attributed to the short range component of the nuclear force [Mol 84a]. The NFM approach can't hope to be realistic since it is classical; however, one can see qualitatively the effect of the short range repulsion.

Furthermore, a simple mechanism whereby the formation of fragments in the final state may be accounted for has been utilized: whenever the total energy of a fragment becomes about -8 MeV/nucleon its internal motion is frozen. The problem with this approach to fragmentation is that the NFM cannot be expected to apply to light systems where the binding energy is not roughly 8 MeV/nucleon (see below); such systems correspond to the majority of fragments which will be formed (d,t,Li,Be, etc.)!

It is also possible to introduce [Kis 84] a Woods Saxon density function for the nucleus:

$$\rho(r)=\rho_0/(1+\exp((r-R)/a)) \qquad (15)$$

where R is as above in (9) and a = .53 fm is the skin thickness. In particular, adding the surface improves the stability of the nuclei since the Fermi momentum will then be lower near the surface. This refinement has been neglected here.

Bodmer and Panos [Bod 77, 80, 81] discovered that for the potentials they used with r_o = 1.23-1.37 fm, the ground state nuclei are too small. This may be understood as follows. The NFM considers the nucleus as a classical system governed by classical forces. The volume available per nucleon is $4/3\pi R_o^3$. With R_o = 1.2 fm and equating this volume to that of a cube one finds l = 1.9 fm for the cube edge length. This cube edge corresponds to the smallest interparticle distance in a simple lattice with nucleons at the center of each cubic cell. Thus this distance should roughly correspond to the location of the classical two body potential minimum. In the configuration of minimum energy, the ground state, all the particles will lie on such a lattice in the $p_F = 0$ limit: thus the NFM allows a solid phase of nuclear matter. The ground state with $p_F \neq 0$ has interparticle distances smeared about l.

A convenient potential form for study is the Morse potential, which is parametrized as follows:

$$V_M(r) = V_R\, e^{-K_R \cdot r} - V_A\, e^{-K_A \cdot r} \qquad (16)$$

The more usual form for the Morse potential is

$$V_M(r) = V_o\,(e^{-2(r-r_o)/a} - 2e^{-(r-r_o)/a}) \qquad (17)$$

where there are only three parameters: r_o, V_o, and r(0). The first two specify the minimum and the last is the zero crossing where $a = (r_o - r(0))/\ln 2$. One advantage of using the Morse potential is that these may be varied independently to fit the viscous cross section: this is a much simpler parameter space than that of Yukawa potentials. In particular

the constraint r_0 = 2.25 fm and σ_v(E = 400 MeV/nucleon) = 25 mb implies the following V_0 and a values:

Table II.1

V_0	2.23	4.00	4.67	6.30	8.76	12.
a	.65	.74	.76	.84	.91	1.01

Furthermore the finite V(0) value does not present a problem so long as it is sufficiently large; indeed this is why Morse introduced the potential [Mor 29].

To substantiate this idea about $r_0 \approx 2$ fm, consider Morse potentials of constant depth V_0 = -4.67 MeV and vary r_0 subject to the constraint that σ_v = 25 mb at E_{lab} = 400 MeV. We use an ensemble of Ar nuclei minimized for t = 200 fm/c so that the nucleons have drifted to more stable positions. The desired average radius is 2.82 fm (R_0 = 1.1 fm) or 3.08 fm (R_0 = 1.2 fm), assuming a uniform distribution for the density. The results are:

Table II.2

r_0	1.85	2.05	2.25	2.45	2.65
<r>	2.38	2.54	2.71	2.82	2.98

It is clear that a potential with $r \geq 2.25$ fm is necessary to ensure the correct value for <r>. Note that these potentials do not all give the same average potential energy after minimization. Using a Morse potential such as the last is clearly not desirable because r(V = 400 MeV) is too small (.26 fm) and also the range of the potential becomes too long r(V = -.1 MeV) = 7.29 fm.

Note that there is an easy way to get a Yukawa type potential from a Morse potential. Multiply the Morse potential by r_o/r. Then by the use of the more usual form for the Morse potential and a Taylor expansion about r_o to first order one can obtain a quadratic equation for the new minimum. It may also be necessary to rescale V_A and V_R to get the same value for the depth at this new minimum.

The Morse, Yukawa, Yukawa-Woods Saxon, and Lennard Jones type potentials have been studied for their stability (Ar nuclei) with parameters given by:

Table II.3

Potential	K_A	K_R	V_A	V_R	r_{WS}	<r>	ρ(100)	ρ(200)
Morse	1.308	2.616	177.1	1680.	-	2.71	.69	.68
Yukawa	.9763	1.953	207.0	1088.	-	2.66	.72	.66
Yuk/WS	5.0	4.0	4.7	4700.	3.2	2.39	.78	.67
	a	n	D	m				
LJ	2.25	2.3	2.9	4.6	-	2.65	.60	.56

Note that all of these potentials have $r_o \approx 2.25$ fm, a sufficient depth to give a binding energy of -9 MeV/nucleon with an average of 20 MeV of Fermi energy, and give $\sigma_v = 25$ mb at $E_{lab} = 400$ MeV. Shown after the potential parameters is the average radius after 200 fm/c of minimization.

The last two columns give the density within an $r = 4.1$ fm sphere after the specified time of integration. Note that there is clearly not an order of magnitude stability improvement for any of these potentials when compared with the other [Kit 81]. Neither a shorter range

potential (Yuk/WS has r(V = -.1 MeV) = 3.97 fm) nor an extremely longer range potential (LJ has r(V = -.1 MeV) = 13 fm) improves the stability of the nuclei to the evaporation of particles. The instability must thus be due to something else, e.g., from both the fact that the nucleons at the surface with high Fermi momenta tend to escape, and also that correlations between $\vec{r}$ and $\vec{p}$ are not taken into account in the initialization. Furthermore, the initial Fermi distribution of the nucleons is not the equilibrium distribution for a finite collection of particles interacting via classical forces: hence the Fermi gas distribution must be driven to a Maxwell-Boltzmann distribution.

One might expect that there is some effect of the degree of minimization on the stability. Consider a collection of Ar nuclei minimized for various times and then allowed to evolve for 100 fm/c:

Table II.4

t_{min}	0	50	100	200
<r>	3.07	2.81	2.72	2.71
ρ(100)	.62	.71	.70	.69

For t_{min} = 0 a Morse potential is used with V_o = 6.6 MeV, whereas for the later times the Morse potential of Table II.3 is used. For unminimized nuclei, one must use a deeper potential to get the same binding. Thus one satisfies <K> = 20 MeV and BE = -9 MeV in all cases. Note that once the minimum energy has been obtained, further minimization only decreases the average radius but does not increase the stability. Furthermore, the momentum distribution is degraded much quicker for the minimized nuclei: <K> goes from 20 to 11 during the first 10 fm/c of integration for a minimized collection whereas this

same degradation takes 200 fm/c for an unminimized collection. Thus a deeper potential and unminimized nuclei are called for.

To fit a fair range of nuclei (Ca to U), both in terms of binding energy and average radii, a repulsive tail can be added in the form of a third Morse or Yukawa potential [Wil 78]; this increases the number of parameters from three to four. Let us choose two potentials for further study. The first is a Morse (but with a small long range repulsion to simulate nuclear saturation effects) soft potential,

$$V(r) = V_M(r) + V_W \cdot e^{-K_W \cdot r}, \tag{18}$$

and a hard potential that is identical to the first for distances probed by the ground state nucleons

$$V(r) = \begin{cases} V_Y(r) + V_M(1.2) - V_Y(1.1) + 0.1b + 0.115m, & r < 1.1 \text{ fm} \\ -br - 0.5mr^2 + V_M(1.2) + 1.2b + 0.72m, & 1.1 < r < 1.2 \text{ fm} \\ V_M(r), & r > 1.2 \text{ fm}. \end{cases} \tag{19}$$

Thus the two forces only differ in the repulsive cores and effects due to the core can be investigated.

The average potential energy per nucleon of the nuclei is

$$U = 0.5 \sum_{i=1}^{A} (U_N(r_i) + \sum_{\substack{j=1 \\ j \neq i}}^{A} V_C(r_{ij}))/A \tag{20}$$

where the first term is the nuclear potential energy (11) and the second is the Coulomb potential energy where $V_C(r) = 1.44/r$. For the nuclear potential energy, one sums over all pairs of nucleons whereas the Coulomb sum is only over all proton pairs. Note that the Coulomb energy reproduces well the standard liquid drop result $U_C/A = 0.705\ Z^2/A^{4/3}$

[Nix 69], as it shoud. A theoretical binding energy is then BE = U + <K> where <K> is the average Fermi kinetic energy. Note that experimentally the average Fermi kinetic energy varies with atomic number [Mon 71]: for ^{6}Li, <K> = 9 MeV whereas for elements from Ni to Pb, <K> = 22 MeV. Let us compare the theoretical binding energies with the experimental ones [Mat 65] for A = 1-300 for the two potentials

Table II.5

A	BE	BE_{exp}
Ne	-2	-8.03
Ca	-5	-8.55
Nb	-9	-8.66
Ba	-8	-8.40
Pb	-6	-7.87
U	-8	-7.57

Note that the lower elements are underbound and the higher ones (Ca to U) are approximately bound correctly.

A second constraint is how well these potentials can fit the N-N scattering cross section. Experimental viscous cross sections have been calculated from tabulated np and pp data [Sig 85]. The Coulomb peak is removed from the pp data using the formula of Rutherford. Then:

$$\sigma_v=(\sigma_v(np) + \sigma_v(pp))/2 \ . \qquad (21)$$

One then uses the integration routine described above without Coulomb forces. From an initial state of fixed impact parameter b one can then produce a final state. With respect to the viscous and 90 degree scattering cross sections, these potentials compare as follows to the experimental data:

Table II.6

energy	soft potential		hard potential		experimental	
E	σ_v	$\frac{d\sigma}{d\Omega}(90)$	σ_v	$\frac{d\sigma}{d\Omega}(90)$	σ_v	$\frac{d\sigma}{d\Omega}(90)$
20	328	9.05	328	9.05	263	30.2
100	64.2	4.30	64.0	4.30	42.5	4.30
200	40.7	2.68	40.2	2.80	27.6	2.75
300	31.0	1.80	31.9	2.34	26.5	2.65
400	25.1	1.33	27.4	2.03	25.0	2.62
770	13.6	0.42	19.5	1.42	11.7	0.54

Note that these potentials give identical values for E < 100 MeV/nucleon as they should. Both the hard and the soft potentials compare moderately well with the experimental values. The hard potential tends to give higher cross sections than the soft one. The experimental values compare well with those previously compiled by Bodmer and Panos, even though they use a parameterization of N-N data [Bod 76]. Note that the experimental values of σ_v are overestimated. One can't expect more than 10-20% agreement over the whole energy range since the full differential cross section calculated classically is a monotonically decreasing function of the angle and hence can't reproduce the charge exchange peak.

The for our purposes reasonable stability of the ground state in configuration and momentum space is illustrated in Figure II.2 for Ca and Figure II.3 for Nb nuclei. Figures II.4 and II.5 show the fraction of particles within the Fermi sphere defined by (9) versus time. All of the particles are not within the sphere initially because of the necessary shifting of the center of mass. Note that the Ca nuclei are

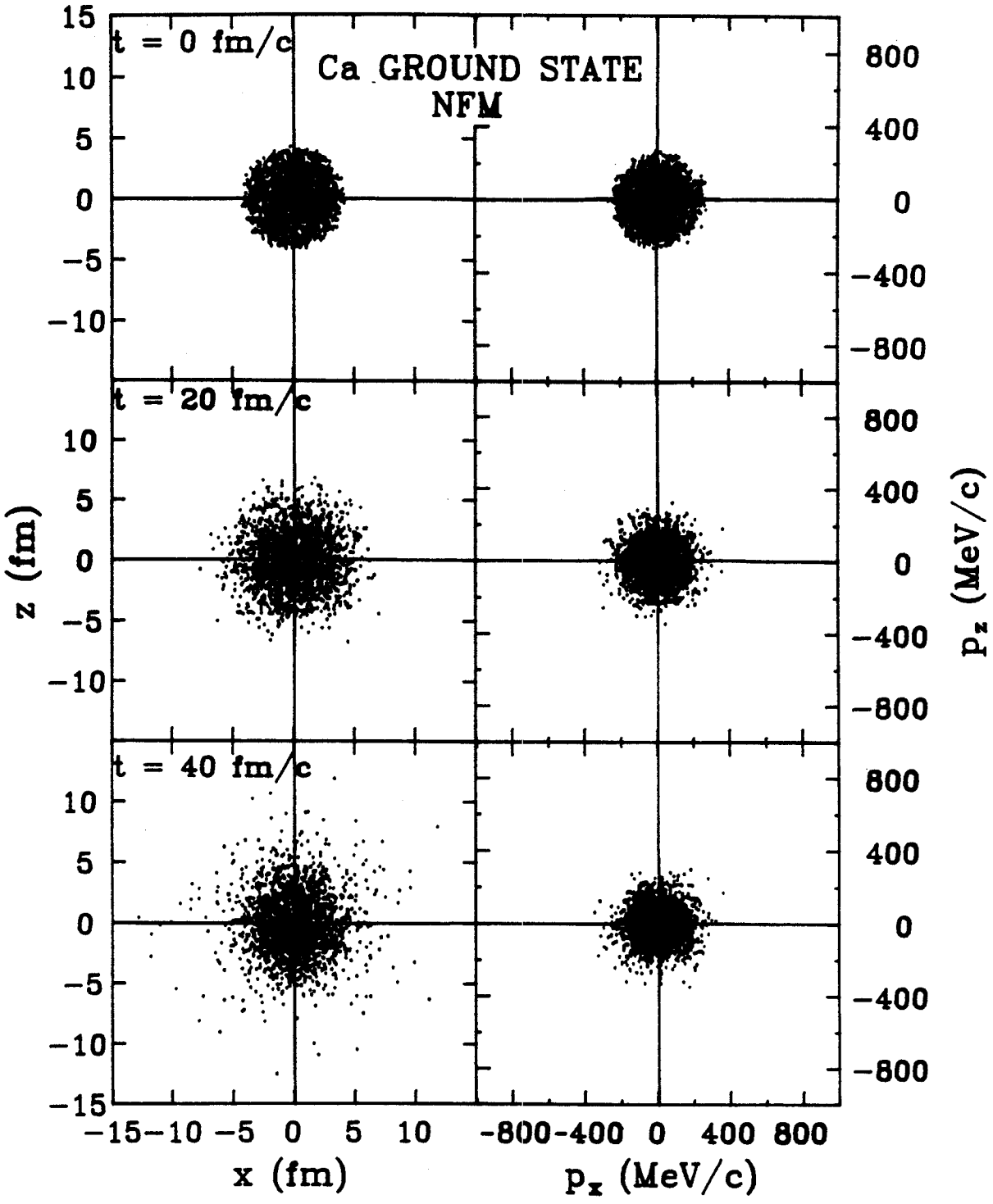

Figure II.2 Ca nuclei evolve in configuration and momentum space in the NFM. Forty-five nuclei are superposed to represent the distribution function.

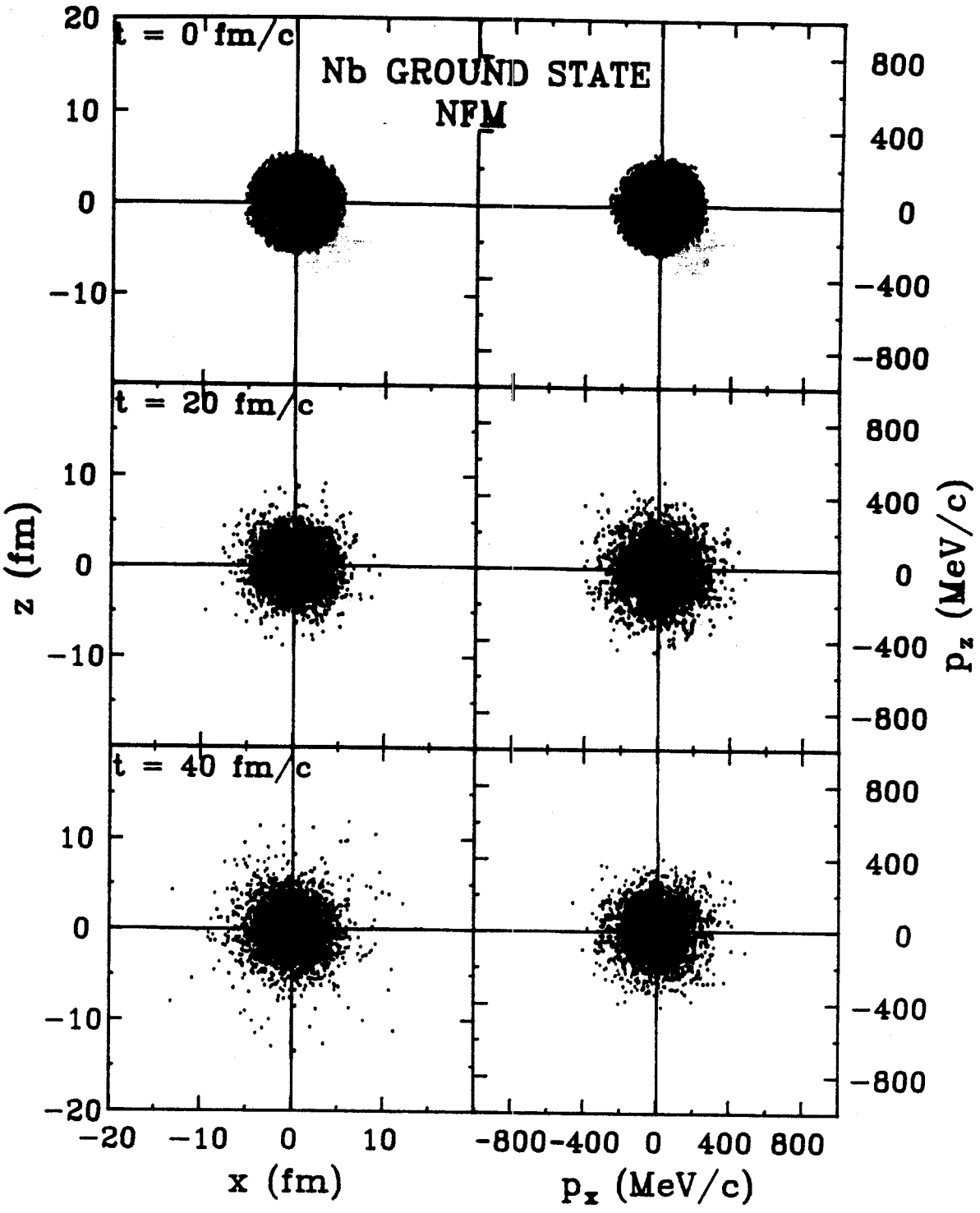

Figure II.3 Nb nuclei evolve in configuration and momentum space in the NFM model. Thirty nuclei are superposed.

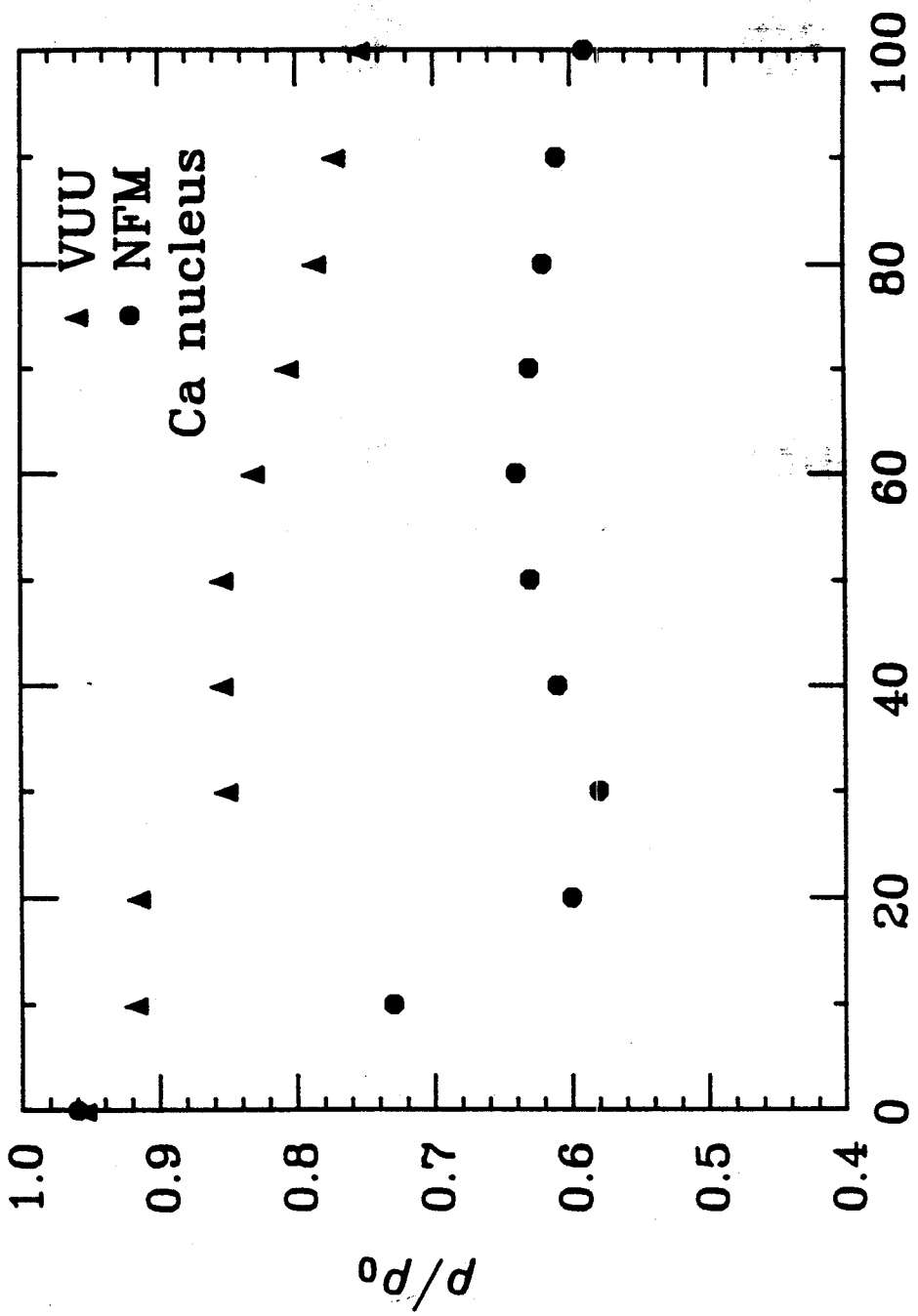

Figure II.4 Fraction of particles within a Ca nucleus versus time for the NFM and Vlasov-Uehling-Uhlenbeck models.

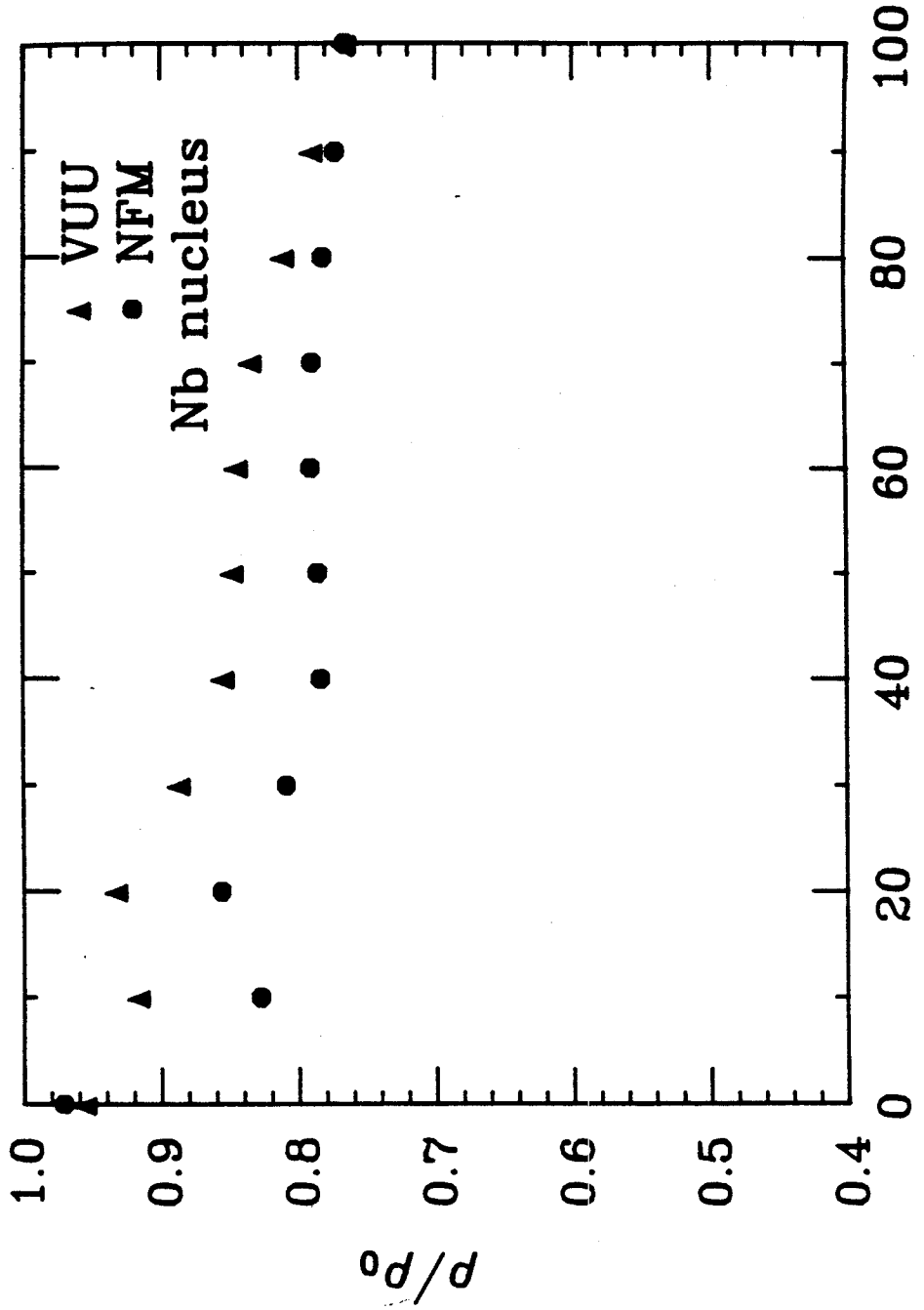

Figure II.5 Fraction of particles within a Nb nucleus versus time for the NFM and VUU models.

less stable than the Nb nuclei. This is probably due to surface effects, which are not taken into account by using a uniform density distribution - these are more important for the smaller nucleus since it has less interior. In both type of nuclei, note how the momentum distributions degrade and note also the generation of some high energy evaporated particles. The degradation is due to the lack of a Pauli principle: particles fall into regions of phase space that are already fully occupied (in the quantum mechanical sense). The evaporated particles come from both the surface and the adjusting of the particles to a more stable distribution in phase space. Classically, it is not so easy to hold together a cloud of nucleons. However, they are held together well enough, especially for the heavier atomic numbers, to simulate a collision.

One may also give justification to this classical potential in terms of its compressional potential energy. In fact, this interpretation is an explanation of why the NFM method may provide similar observable results as a kinetic or fluid dynamic approach with a nuclear EOS. Using a collection of 150 Nb nuclei and the soft and hard potentials, the particle positions are scaled and a classical analog to the Skyrme potential (neglecting the Fermi contribution) is calculated. Compare this to the values obtained from using a medium and a stiff Skyrme potential [Kru 85a]:

Table II.7

ρ/ρ_0	.5	1.	1.5	2.0	2.5	3.0
E_{sof}	-22	-33	-36	-34	-29	-21
E_{har}	-22	-33	-35	-31	-20	-5

E_{med}	-27	-38	-43	-42	-38	-30
E_{sti}	-25	-39	-40	30	-8	25

Note that the potential energy per nucleon from the NFM agrees qualitatively with the Skyrme potential energy. However the EOS and the compressibility K are underestimated. A minimization of the nuclei would increase K by as much as a factor of five; this is another reason why the minimization process is undesirable.

Once one has a potential with reasonable binding and scattering properties, one can then study many physical collision observables in this model. In Chapter III, the NFM will be confronted with these experimental observables.

Before leaving the theoretical discussion of the NFM approach, consider some possible future improvements. In particular, how can the effects of the Pauli principle be incorporated into a classical model? It is not possible to directly incorporate the Pauli principle since every movement of particles in phase space is given deterministically by Newton's laws. In a Hamiltonian formulation, one can introduce momentum dependent potentials; however, these should be related to free N-N potentials in some way, which has not been done. One easy way to include the Pauli principle in a hybrid model is the following. From a classical viewpoint in pp scattering:

$$d\sigma/d\Omega = |f(\theta)|^2 + |f(\pi-\theta)|^2 \text{ for } s=0 \qquad (22)$$

and

$$d\sigma/d\Omega = |f(\theta)-f(\pi-\theta)|^2 \text{ for } s=1 \qquad (23)$$

Thus if only s-waves are important, one may alter the above classical cross section:

$$d\sigma/d\Omega = d\sigma/d\Omega_{cl}(\theta) + d\sigma/d\Omega_{cl}(\pi-\theta) \text{ for } s=0 \qquad (24)$$

Of course this approach can only be used if one does a 2π impact scattering for $r < r_{cor}$ where r_{cor} is some core radius and one selects the cross section from cross section tables. The Pauli blocking may perhaps be included in such a hybrid NFM model by looking at the occupation of phase space.

What about relativistic effects? An approach valid to $O(v^2/c^2)$ is not a significant improvement. There is a fundamental problem which must be solved before there can be any relativistic NFM model. This is the Coulomb scattering problem for relativistic particles of equal mass. The only relativistic treatment that exists is that of Mott scattering in the Born approximation where the one particle is infinitely massive [Dar 13].

The main problem with the NFM approach is that classical potentials can provide only a poor approximation to N-N scattering and nuclear binding properties. Additional complications occur in the relativistic generalization [Kun 81] due to difficulties with second quantization and considerations of covariance [Eks 65, Cur 65, Lus 81]. However, the NFM is the model which comes closest to the solution of the many-body aspect and enables a study of finite range effects of the repulsive core [Mol 84a]. Certainly for the non-ultra-relativistic domain, NFM is a valuable tool to gain insight into the short range nature of the nuclear force. It would be most important to study also retardation effects in an appropriate generalization, which for $v \ll c$ reduces to the NFM.

3. Time Dependent Hartree Fock and Beyond

To solve the quantum non-relativistic A body nuclear physics problem, one has to solve the time dependent Schrödinger equation:

$$i\hbar \frac{\partial \Psi}{\partial t} = H\Psi \tag{25}$$

where

$$\Psi = \Psi(1,2,\ldots,A,t) \tag{26}$$

is the time dependent many-body wave function, A is the total number of nucleons, and H is the many body Hamiltonian. This is in general an impossible task just as the complete relativistic problem is.

The finite many body problem is of course less tractable than the few body one. Recall that an approach to the static many body problem for atomic electrons is Hartree's theory of the self-consistent field. There one starts with a set of single particle wave functions, generates with this set a single particle potential by averaging the many body interaction, solves the single particle problem and gets a new set of single particle wave functions. These steps are iterated until consistency between the wave functions and the potential is achieved.

Static Hartree-Fock theory includes an additional exchange term. The many body wave function is approximated as a Slater determinant of single particle wave functions, the Hamiltonian containing the Hartree field and a non-local single particle potential. Again one proceeds iteratively to achieve consistency between the averaged interaction and the wave functions. The HF method constructs a Fermi sea of particles with a sharp Fermi surface, since in calculating the HF determinant one selects the A lowest single particle wave functions in energy. In the HF method, the use of a Slater determinant neglects all correlations

between the nucleons except those required by the Pauli principle. The fact that two identical nucleons with parallel spin must not be very close to each other is represented by the antisymmetrization.

Euler [Eul 37] first used the HF method with a Gaussian force to calculate the energy of infinite nuclear matter, neglecting the divergent Coulomb repulsion. Nucleons are bound together solely by their mutual interaction: there is no external central field as in the case of atomic electrons. The HF method is an approximation for reducing the problem of these interacting particles to one of non-interacting particles in a potential and neglects residual interactions.

Static Hartree Fock theory has had much success in the shell models for electrons and later nucleons. In heavy ion nuclear physics, however, one has a time dependent problem of A colliding scattering nucleons. The complete nuclear wave function Ψ contains lots of information - perhaps more than we will ever need or be able to use. Therefore, some approximations to get a tractable Time Dependent Hartree Fock theory are justified. TDHF is used to describe excited states and to take into account the long range or field part of the residual interaction.

Recall that TDHF can be derived in the formalism of second quantization [Koo 75]. Let

$$|abc\ldots\rangle = 1/\sqrt{A!}\sum_{(ab\ldots)}\psi_a\psi_b\ldots \mathrm{sgn}(abc\ldots) \qquad (27)$$

be the Slater determinant, where the subscripts label space, spin, and isospin. Define the particle creation and destruction operators $a_i^\dagger$ and a_i, respectively. Antisymmetry and the Pauli principle yield the anti-commutation relations [Row 70]:

$$\{a_i^\dagger, a_j^\dagger\} = 0 \text{ and } \{a_i^\dagger, a_j\} = \delta_{ij}. \tag{28}$$

The state Ψ of the nucleus is a linear combination of such Slater determinants.

The many body Hamiltonian is

$$H = K + V$$

$$= \sum_{ij} K_{ij} a_i^\dagger a_j + \frac{1}{2} \sum_{ijkl} U_{ijkl}\, a_i^\dagger a_j^\dagger a_l a_k \tag{29}$$

where the kinetic energy is a single particle operator and U is the two body interaction. The one body density matrix is

$$\rho_{ji} = \langle \Psi | a_i^\dagger a_j | \Psi \rangle \ . \tag{30}$$

The von Neumann equation

$$i\hbar\, d\rho/dt = \langle \Psi | [a_i^\dagger a_j, H] | \Psi \rangle \tag{31}$$

follows from the Schrödinger equation and the assumption that H is hermitian. After inserting the many body Hamiltonian and some algebra, this time dependent density equation will <u>not</u> reduce to a purely one body equation. The two body force couples ρ to the two body density matrix $\rho^{(2)}$, leading to the so called BBGKY hierarchy [Koo 75]. The TDHF approximation is based on the assumption that the matrix elements of $\rho^{(2)}$ factor:

$$\rho^{(2)}_{ijkl} = \rho_{jk}\rho_{il} - \rho_{jl}\rho_{ik} \ . \tag{32}$$

This terminates the BBGKY hierarchy and yields the TDHF equation

$$i\hbar\, d\rho/dt = [h, \rho] \tag{33}$$

where h is the HF hamiltonian:

$$h = \sum_{ij} (K_{ij} + \sum_{kl} (V_{ikjl} - V_{iklj})\rho_{lk}) \ . \tag{34}$$

It is not difficult to show that particle number and the energy are conserved in TDHF [Koo 75]. Furthermore, each of the single particle orbitals satisfies the time-dependent Schrodinger equation with the HF hamiltonian h.

TDHF has been applied with some success at energies up to 10 MeV/nucleon. Fusion, compound nucleus formation, dissipation, strongly damped collisions, shock wave propagation, and fragmentation are all reportedly found in TDHF [Bon 76, Stö 82a, Cus 82]. Beyond this range, TDHF and mean field theory in general are not sufficient because of the lack of two body collisions and the assumption of a long mean free path for the nucleons. The mainly potential scattering of TDHF implies only a single particle viscosity so that the nuclei are rather transparent for $E_{CM} > E_F = 38$ MeV. Furthermore, the solution of the TDHF equations becomes difficult for higher energies. This transparency is illustrated in Figure II.6 for C (85 MeV/nucleon) + C [Stö 80a,81b].

However, in TDHF, the sensitivity of the observables, e.g. dynamic fusion thresholds, to the particular effective two body interaction may be large [Mar 85]. Nevertheless, what is important for us is that TDHF is approximately equivalent to a classical pseudo-particle simulation [Won 82]; the dynamics is then determined by following the pseudo-particle trajectories, which are identical to the trajectories of real particles moving in the self-consistent field.

To go beyond TDHF, consider that some perturbing two body interaction causes particles to scatter from their unperturbed orbitals. In first order perturbation theory, the perturbed wave function is [Ber 84a]:

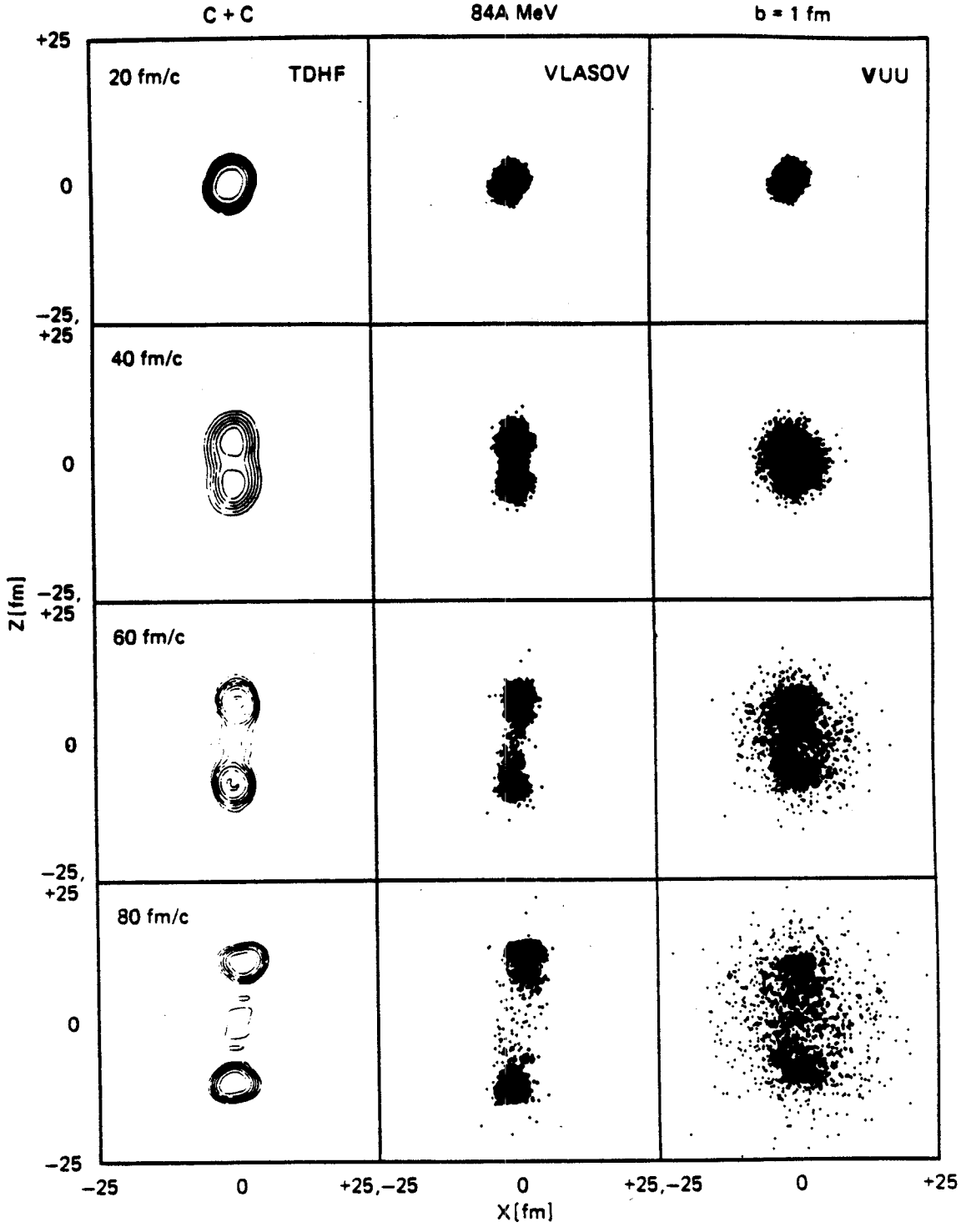

Figure II.6 Time evolution in configuration and momentum space for C (85 MeV/nucleon) + C at b = 1 fm for Time Dependent Hartree Fock (left), the Vlasov equation (middle), and the VUU theory (right). Transparency occurs in both cases with a mean field only.

$$|\Psi> = |\Psi_o> + 1/i\hbar \sum_{klk'l'} \int dt\ e^{i\omega t} V_{k'l'kl} a^\dagger_{k'} a^\dagger_{l'} a_l a_k |\Psi_o>$$

$$= |\Psi_o> - \sum_{klk'l'} \frac{e^{i\omega t}-1}{\hbar\omega} V_{k'l'kl} a^\dagger_{k'} a^\dagger_{l'} a_l a_k |\Psi> . \qquad (35)$$

The density matrix then evolves according to the von Neumann equation:

$$d\rho_{ii}/dt = \frac{1}{i\hbar} <\Psi| a^\dagger_i [a_i, V] + [a^\dagger_i, V] a_i |\Psi>. \qquad (36)$$

Proceeding is now complicated by the fact that one has to evaluate octupole Fock space operators. Let us therefore consider a one body perturbing interaction as an illustrative example [Ber 84a]. Then the first order perturbed wave function is:

$$|\Psi> = |\Psi_o> - \sum_{kk'} \frac{e^{i\omega t}-1}{\hbar\omega} V_{k'k}\ a^\dagger_{k'} a_k |\Psi_o> . \qquad (37)$$

In the one body case, it is easily shown using the anti-commutation rules that

$$[a_i, V] = \sum_j V_{ji} a_j \quad \text{and} \quad [a^\dagger_i, V] = -\sum_j V_{ij} a^\dagger_j . \qquad (38)$$

With the additional assumption that the one body density matrix is diagonal

$$\rho_{ji} = n_i\ \delta_{ij} \qquad (39)$$

the occupation number n_i obeys the equation

$$dn_i/dt = 1/i\hbar \sum_j V_{ij} <\Psi| a^\dagger_i a_j - a^\dagger_j a_i |\Psi>. \qquad (40)$$

Substituting the bra and the ket first order perturbed wave functions, one gets terms of first, second, and third order in V. The first order terms are already in the mean field and the third order

terms may be neglected with respect to the second order ones. A typical second order term is

$$\langle\Psi_o|a_i^\dagger a_j a_{l'}^\dagger a_l|\Psi_o\rangle = \langle\Psi_o|a_i^\dagger(\delta_{jl'}-a_{l'}^\dagger a_j)a_l|\Psi_o\rangle$$

$$= \rho_{li}\delta_{jl'} - \rho_{ljl'i}$$

$$= \rho_{li}\delta_{jl'} - \rho_{jl'}\rho_{li} + \rho_{ji}\rho_{ll'}$$

$$= n_i(1-n_j)\delta_{li}\delta_{jl'} + n_i n_l \delta_{ij}\delta_{ll'} . \qquad (41)$$

Combining the above equations, one finds

$$dn_i/dt = 1/\hbar^2 \sum_j [2V_{ij}^2 \sin(\omega_{ji}t)/\omega_{ji}][n_j(1-n_i)-n_i(1-n_j)]$$

$$= 2\pi/\hbar \sum_j V_{ij}^2 \delta(E_j - E_i)[n_j(1-n_i)-n_i(1-n_j)]. \qquad (42)$$

where the time limit has been extended to infinity and one definition of the delta function made use of. This is a standard Boltzmann equation with the golden rule applied for the interactions.

Consider the physical import of letting $t \to \infty$. Qualitatively, there are three important times for the interacting nucleons: t_{int} the duration of an interaction between nucleons O(1-5 fm/c), t_{col} the mean time between collisions O(5-10 fm/c), and t_{cro} the time to cross the nucleus at high speed O(10-20 fm/c). In the initial stage of the collision, where $0 < t < t_{int}$ the full quantum Liouville equation is necessary to describe the interaction. For $t_{int} < t < t_{col}$ one may have a kinetic stage where approximately the A-body distribution function is an antisymmetric product of one body ones. Finally, $t_{col} < t < t_{cro}$ is

the hydrodynamic stage where Local Thermodynamic Equilibrium may be a useful approximation.

The extension to the δ-function (42) requires that the time t_{int} of the transition be sufficiently large but also less than t_{col}, so that double and higher order collisions (formally higher order in V) can't take place. It is part of the famous stosszahl-ansatz of Boltzmann that the one particle has no correlation with the other with which it is going to collide. The particle can't be rescattered by the first scatterer unless it is in the meantime collided with another. The delta function or sinusoid has height $t/\hbar\pi$ and width $\pi\hbar/t$ so that the area is one. For large times, the width is negligible and one get a delta function. However one needs $t < t_{col}$ so that double and higher order collisions don't occur - this implies width $> \hbar/t_{col}$. One still neglects this width provided that other factors in the equation vary little with energy over it. Thus the question of the appropriateness of the δ function is subtle [Pei 79].

In the two body case, one expects by analogy the corresponding equation [Ber 84a]:

$$dn_i/dt = 2\pi/\hbar \sum_{ji'j'} V^2_{ijj'i'} \delta(E_{i'} + E_{j'} - E_i - E_j)$$

$$[n_{i'} n_{j'} (1-n_i)(1-n_j) - n_i n_j (1-n_{i'})(1-n_{j'})]. \qquad (43)$$

This provides some plausible justification for Uehling and Uhlenbeck's original ansatz for a collision term [Ueh 33].

4. The Vlasov-Uehling-Uhlenbeck Kinetic Equation

One way to include two body collisions is thus to couple to the TDHF equation a master equation involving the occupation probabilities of the single particle states n_i [Rem 84]. Now replace the summation over the discrete single particle levels by continuous integrals over momenta:

$$\sum_{ji'j'} \rightarrow \int d^3p_2 d^3p_1' d^3p_2'/(2\pi\hbar)^9 \tag{44}$$

Furthermore, the continuous analog of the occupation probability is the Wigner function [Wig 32]

$$f(\vec{p},\vec{r}) = \int d^3s\ e^{i\vec{p}\cdot\vec{s}/\hbar} \rho_{\vec{r}+\vec{s}/2,\vec{r}-\vec{s}/2}$$

$$= \int d^3q\ e^{-i\vec{q}\cdot\vec{r}/\hbar} \rho_{\vec{p}+\vec{q}/2,\vec{p}-\vec{q}/2} \tag{45}$$

which has the properties that

$$\rho(\vec{r}) = \int d^3p\ f(\vec{p},\vec{r})/(2\pi\hbar)^3 \text{ and } \rho(\vec{p}) = \int d^3r\ f(\vec{p},\vec{r})/(2\pi\hbar)^3 \tag{46}$$

One can also eliminate the matrix element $\langle \vec{p}_1\vec{p}_2|V|\vec{p}_1'\vec{p}_2'\rangle$ with the Born approximation [Ber 84a]. Then one obtains from eq. (43) the Uehling-Uhlenbeck collision term

$$\left(\frac{df}{dt}\right)_{coll} = \int d^3p_2 d^3p_2'\ d\sigma v_{12} \times$$

$$[f_1'f_2'(1-f)(1-f_2) - ff_2(1-f_1')(1-f_2')]\delta^3(\vec{p}+\vec{p}_2-\vec{p}_1'-\vec{p}_2') \tag{47}$$

where f_1 has been replaced by f and where the f's represent the phase space distribution, except in the Pauli blocking terms where it represents the dimensionless occupation numbers. Also $v_{12} = v_{1'2'}$ is

the relative speed of the two colliding nucleons and $\frac{d\sigma}{d\Omega}$ is the differential cross section in the two particle center of mass system.

The imaginary part of the mean field relates to the Uehling-Uhlenbeck collision term and gives a relaxation time [Köh 80]. However the transport equation collision term is more complete since it not only describes how a state decays, but also what final states will be populated.

Finally, one may also write the total derivative as:

$$\frac{df}{dt} = \frac{\partial f}{\partial t} + \vec{v}\cdot\frac{\partial f}{\partial \vec{r}} + \frac{d\vec{p}}{dt}\cdot\frac{\partial f}{\partial \vec{p}} \quad . \tag{48}$$

This last equation set equal to zero is the Vlasov equation. Combining these, one gets the Vlasov-Uehling-Uhlenbeck equation [Ueh 33]:

$$\frac{\partial}{\partial t} f + \vec{v}\cdot\frac{\partial}{\partial \vec{r}} f - \nabla U \cdot \frac{\partial}{\partial \vec{p}} f = \int d^3p_2 d^3p_2' \; d\sigma v_{12} \times$$

$$\left[f_1' f_2' (1-f)(1-f_2) - f f_2 (1-f_1')(1-f_2')\right] \delta^3(\vec{p}+\vec{p}_2-\vec{p}_1'-\vec{p}_2') \tag{49}$$

The main input is now a potential and the free nucleon-nucleon differential cross section. The Fermi-Dirac distribution, which is a solution of the Vlasov equation, is also the equilibrium solution of the collision term. The VUU collision term is in fact only valid for a dilute quantum gas. However, the strongly interacting system of a nucleus-nucleus collision can be considered to be such if the Pauli principle is respected. The Pauli principle prevents phase space from becoming over-occupied.

The Vlasov part of the VUU equation can alternatively be derived. The single particle density operator is an inverse Laplace transform of

the single particle propagator [Rem 84]. The Wigner transform of the propagator can be expanded in powers of $\hbar$ [Rem 84]. From truncating the Wigner transform of the Liouville-von Neumann equation [Neg 82]

$$i\hbar \frac{\partial \rho}{\partial t} = [H, \rho] \tag{50}$$

one then obtains the Vlasov equation.

What is the relativistically correct form of this VUU transport equation? Let $\underline{r} = r^i = (ct, \vec{r})$ and $\underline{p} = p^i = (E/c, \vec{p})$ be contravariant four vectors. and g_{ij} be the standard metric tensor $g_{00} = 1$, $g_{\alpha\alpha} = -1$, and $g_{ij} = 0$ for $i \neq j$. Recall that $\vec{r}$ and $\vec{p}$ define six dimensional μ space and $\vec{r}, \vec{p}, t$ seven dimensional Π space. Then $f(\vec{r}, \vec{p}, t) d^3r d^3p$ is a number of particles such that $f(\vec{r}, \vec{p}, t) = f'(\vec{r}', \vec{p}', t')$ [Kam 69]. The relativistic VUU equation without interaction is then

$$p^i \partial_i f = m^2 c^2 \int d^3p_2 \, d\sigma v_{12} \gamma_{12} / E_2 \times$$
$$[f_1' f_2' (1-f)(1-f_2) - f f_2 (1-f_1')(1-f_2')] \tag{51}$$

where

$$p^i \partial_i = \frac{E}{c^2} \frac{\partial f}{\partial t} + \vec{p} \cdot \frac{\partial f}{\partial \vec{r}} \, . \tag{52}$$

The above is form invariant under a Lorentz transformation since $\gamma \frac{d}{dt} = \frac{d}{d\tau}$ where τ is the time measured in the inertial frame where $\vec{p}$ vanishes [Ran 79]. All the well known properties of the non-relativistic Boltzmann equation - conservation laws, H- theorems, equilibrium, heat flow, and viscosity can be obtained from this covariant equation [Mal 81].

One should describe particle propagation in a quasi-classical model of relativistic nucleus-nucleus collisions. Then one needs a reformulation of field theory in terms of functions defined on a classical phase space using the four dimensional Wigner transform to obtain Covariant Distribution Functions. Such a CDF expresses part of the solution to a field-theory problem. Classical particle trajectories are used and one can interpret the results as meaning the stochastic scattering of particles. However, in a succession of scatterings, there are negative as well as positive contributions to probabilities with only the net probability being positive. In such a field theory model, a real scalar field Ψ describes any hadron with rest mass m [Rem 85a]. A one particle CDF is a real function of the position and momentum four-vectors. Results of such a formal approach show how, classically, particles can propagate off-shell and yet be found on-shell asymptotically [Rem 85a].

What shall actually be solved in the VUU model - see below - will incorporate as much of the essential physics as is possible with an interaction U. For the interaction U, a local Skyrme interaction is used. Let us briefly review the Skyrme model [Sky 58, 59]. Skyrme's interaction can be written as a potential:

$$V = \sum_{ij} V^{(2)}_{ij} + \sum_{ijk} V^{(3)}_{ijk} \qquad (53)$$

with two and three body parts. In configuration space, the two body part is [Vau 72, Bei 75]:

$$V^{(2)}(\vec{r}-\vec{r}') = t_0(1 + x_0P_\sigma)\delta(\vec{r}-\vec{r}') + 1/2\ t_1(\vec{k}'^2\delta(\vec{r}-\vec{r}') + \delta(\vec{r}-\vec{r}')\vec{k}^2) +$$

$$t_2\vec{k}'\cdot\delta(\vec{r}-\vec{r}')\vec{k} + iW_0\vec{k}'\cdot\delta(\vec{r}-\vec{r}')\vec{\sigma}\hat{}\vec{k} \qquad (54)$$

where

$$\vec{k} = (\partial/\partial\vec{r} - \partial/\partial\vec{r}')/2i \quad \text{and} \quad \vec{k}' = \vec{k}^{\dagger} \tag{55}$$

are the relative momentum operators and

$$P_{\sigma} = 1/2\ (1 + \vec{\sigma}_1 \cdot \vec{\sigma}_2) \tag{56}$$

is the spin exchange operator.

The three body part is

$$V^{(3)}(\vec{r}_1, \vec{r}_2, \vec{r}_3) = t_3\delta(\vec{r}_1 - \vec{r}_2)\delta(\vec{r}_2 - \vec{r}_3). \tag{57}$$

Hartree-Fock calculations are usually done with this Skyrme interaction. The expectation value of the total energy is:

$$E = \langle\Psi|T + V|\Psi\rangle$$

$$= \int H(\vec{r})\, d^3r \tag{58}$$

where H is the Hartree-Fock functional energy density. For the Skyrme interaction, this energy density is an algebraic function of only three quantities: the nucleon density $\rho(\vec{r})$, kinetic energy density $\tau(\vec{r})$, and spin density $\vec{J}(\vec{r})$. For the case of a symmetric nucleus, N = Z, and neglecting the Coulomb field, the densities for neutrons and protons are equal:

$$\rho_n = \rho_p = 1/2\ \rho\ ,\ \tau_n = \tau_p = 1/2\ \tau\ ,\ \vec{J}_n = \vec{J}_p = 1/2\ \vec{J}. \tag{59}$$

In nuclear matter $\vec{\nabla}\rho = 0 = \vec{\nabla}\cdot\vec{J}$, $\rho = \frac{2}{3} k_F^3/\pi^2$, and $\tau = 3/5\ k_F^2\rho$. Then the binding energy per particle reads

$$E/A = H/\rho = \frac{3}{5} E_F + \frac{3}{8} t_o\rho + \frac{1}{16} t_3\rho^2 + \frac{3}{80}(3t_1+5t_2)\rho k_F^2 \tag{60}$$

and the potential is

$$U(\vec{r}) = \frac{3}{4} t_o\rho + \frac{3}{16} t_3\rho^2 + \frac{3}{40}(3t_1 + 5\ t_2)\rho k_F^2. \tag{61}$$

Note that the potential and the energy density are related by

$$U = \left(\frac{\partial H}{\partial \rho}\right)_{\tau,\vec{J}} . \tag{62}$$

For colliding relativistic nuclei in the non-ultra-relativistic case, one can to first order neglect the problems of the relativistic field and calculate the potential locally. In the spirit of the Skyrme interaction in nuclear matter, the potential is taken in a density expansion

$$U = a\rho + b\rho^2 \tag{63}$$

so that the binding energy is

$$E/A = \frac{3}{5} E_F + \frac{1}{2} a\rho + \frac{1}{3} b \rho^2 \tag{64}$$

[Ber 84ab, Kru 85ab]. The long range Coulomb and Yukawa interaction are neglected here as well as the nuclear surface. Now measure ρ in units of $\rho_0 = 0.17/fm^3$. Then impose the three conditions $E/A = -16$ MeV, $\frac{3}{5} E_F = 23$ MeV, and $K = 380$ MeV to get a stiff potential. The saturation condition $\frac{\partial(E/A)}{\partial k_F} = 0$ is equivalent to the zero pressure condition

$$p = \rho^2 \frac{\partial(E/A)}{\partial \rho} = 0 \tag{65}$$

and the compressibility $K = k_F^2 \frac{\partial^2(E/A)}{\partial k_F^2}$ may also be written as

$$K = 9 \rho \frac{\partial p}{\partial \rho} . \tag{66}$$

These three conditions fix the parameters $a = -124$ and $b = 70.5$ [Ber 84ab, Kru 85ab]. Similarly, for a medium potential, take the expansion

$$U = a\rho + b\rho^{7/6} \tag{67}$$

and impose K = 200 MeV to find a = -356. and b = 303 [Ber 84ab, Kru 85ab].

The incompressibility of nuclei is directly related to the energy of the giant monopole resonance [Lui 85]. K is extrapolated from K_A for finite nuclei. Recall the empirical relation

$$K_A = K_{vol} + K_{sur}A^{-1/3} + K_{sym}(\frac{N-Z}{A})^2 + K_{cou} \qquad (68)$$

K_{vol} is to be identified with K for infinite nuclear matter [Pan 70, Bla 76]. Recently, it is found that K_{vol}= 270 MeV is the best average value [Lui 85]. The values for the two chosen Skyrme EOS thus span the experimental value for K. However, one must remember that that these potentials are stiff and medium is more a reflection of their difference at high densities than their ground state compressibilities.

In Figure II.7, these two local Skyrme interactions are plotted and compared to the equation of state extracted recently from pion multiplicity data [Sto 82]. Note that the cascade and chemical model analysis, which derive a nuclear EOS from the differences of the calculated pion multiplicities and the observed pion yields, tend to agree with the stiff EOS.

5. Application of the VUU theory -

The VUU equation (49) is difficult to solve since it is a highly non-linear differentio-integral equation in six dimensional phase space. Since this equation comes close to the classical limit, one may solve it in terms of quasi-particles, whose mean positions are solutions of Newton's equations [Won 82, Ber 84ab, Kru 85ab, Mol 84b,85a]:

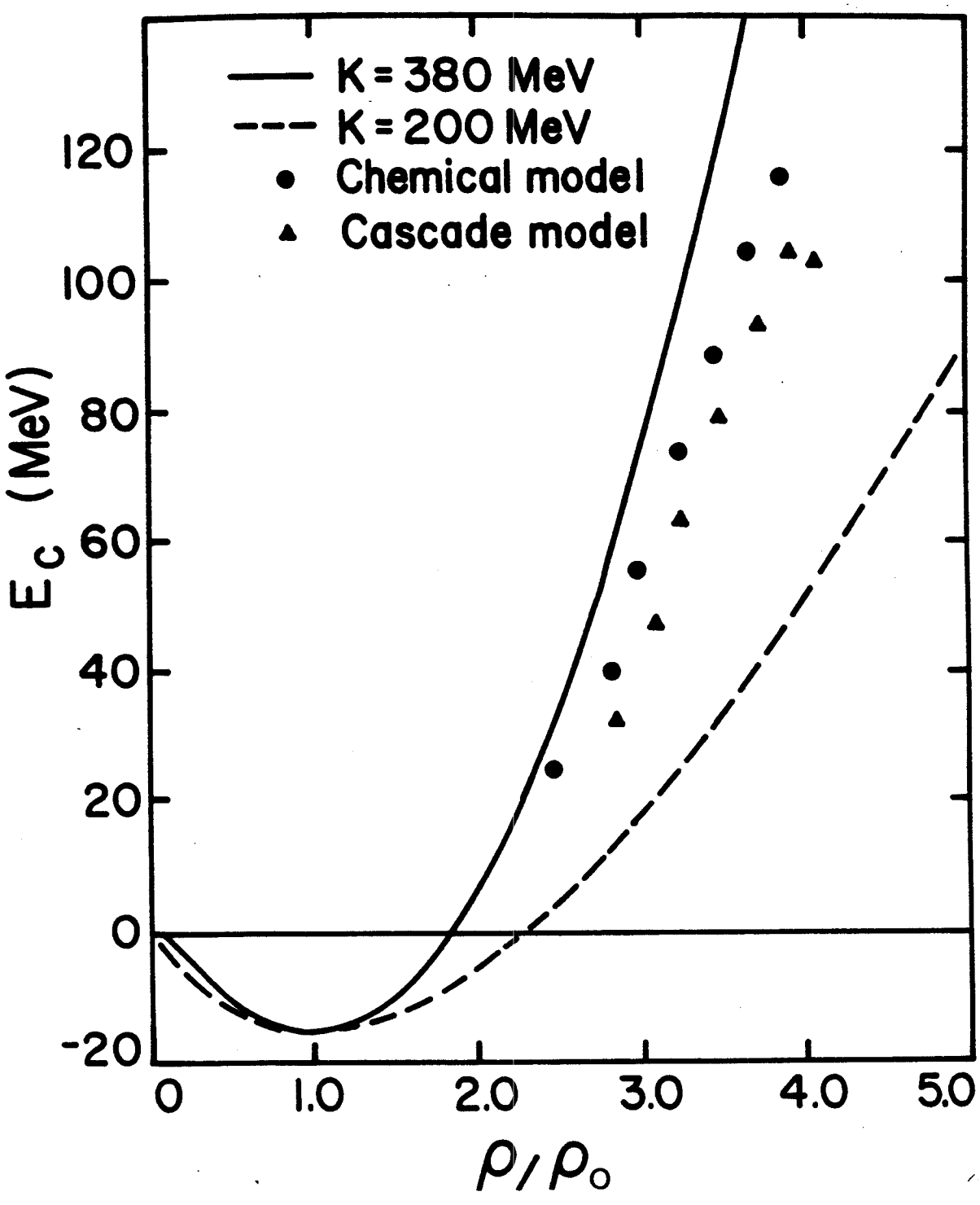

Figure II.7 The Skyrme equation of state with K = 200 MeV and K = 380 MeV as used in the VUU theory compared with values extracted from pion yields.

$$\vec{p}/m = d\vec{r}/dt \quad \text{and} \quad d\vec{p}/dt = -\partial U/\partial \vec{r} \ . \tag{69}$$

One actually goes beyond the VUU equation by including not only a mean field and Pauli Blocking of the final state, but also relativistic kinematics and particle production. This can be loosely termed the VUU theory.

Recall the simple gas model where the number space is related to the momentum space by

$$dn = g \frac{d^3r}{(2\pi)^3} d^3k \, F \tag{70}$$

where $F = \dfrac{1}{e^{(E-\mu)/T} + \lambda}$ and $\lambda = \begin{cases} -1 & \text{Bose-Einstein} \\ 0 & \text{Maxwell-Boltzmann.} \\ 1 & \text{Fermi-Dirac} \end{cases}$ For a zero temperature Fermi gas of nucleons, this yields a density in configuration space

$$\frac{dN}{d^3r} = \frac{4}{(2\pi\hbar)^3} \cdot \frac{4}{3} \pi p_F^3 \tag{71}$$

and a density in momentum space

$$\frac{dN}{d^3p} = \frac{4}{(2\pi\hbar)^3} \cdot \frac{4}{3} \pi R^3. \tag{72}$$

Thus in both configuration and momentum space, the nucleons are initialized within their respective Fermi spheres just as in the NFM approach. For finite nuclei, a Woods Saxon density distribution would be more appropriate in configuration space; however this would be a future refinement.

The stability of the ground state nuclei in this VUU theory is an important issue to address in testing the method [Mol 85b]. Figure II.8 shows the effect of the time step on the stability of Ca nuclei.

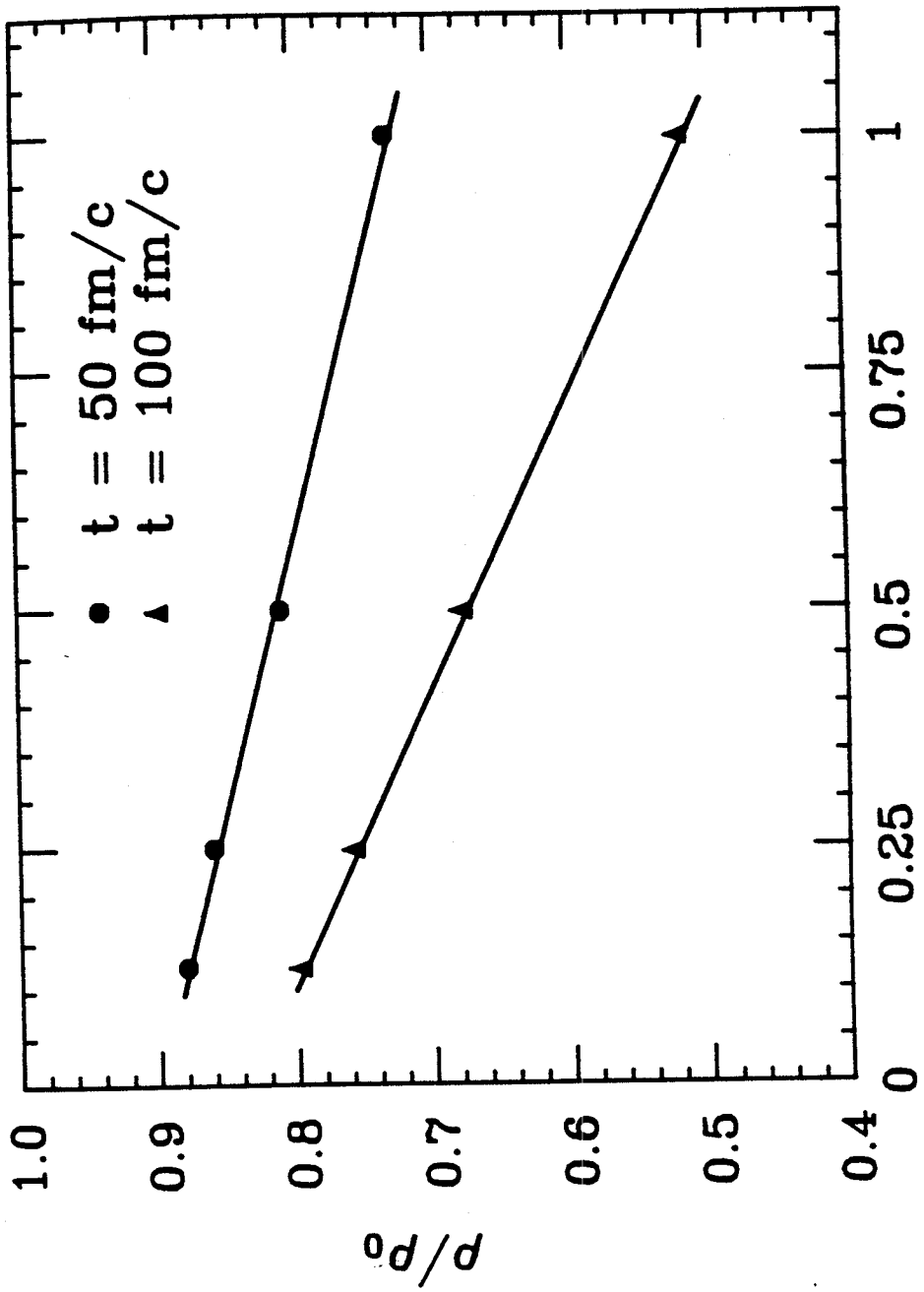

Figure II.8 The effect of the time step on the stability of the ground state nuclei in the VUU model for Ca nuclei.

Clearly, one must be careful and use a small time step to do calculations for light nuclei. Figures II.9 and II.10 show that the ground state nuclei (Ca and Nb, respectively) are quite stable up to times of the order of 40 fm/c in both position and momentum space. See also figures II.4 and II.5, which illustrate how well the nucleons remain confined within their respective Fermi spheres in position space. Also note how in Figures I.9 and I.10 the Pauli blocking prevents nucleons from falling down in momentum space as is the case in a classical model (Figures II.2 and II.3).

To solve the VUU equation, fifteen collision simulations are followed in parallel and the ensemble averaged phase space density in a sphere of radius r_t = 2 fm around each particle is computed [Kru 85a]. The ensemble averaging results in statistical fluctuations at the 10% level and thus reasonably smooth single particle distribution functions, which are used to determine the mean field and the Pauli blocking probability. About a hundred such parallel ensembles are followed to simulate an actual reaction.

The gradient of the potential at the position of each test particle is calculated from the difference between the particle densities in two hemispheres centered around the test particle, e.g.

$$\frac{\partial \rho}{\partial x} = \frac{\rho_+ - \rho_-}{3r_t/4} \qquad (73)$$

where for delta x, the centroid location has been used. The force is then $F_x = - \frac{\partial U}{\partial \rho} \frac{\partial \rho}{\partial x}$ by the chain rule. This force changes the momentum of the particle according to the relativistic Newton equation.

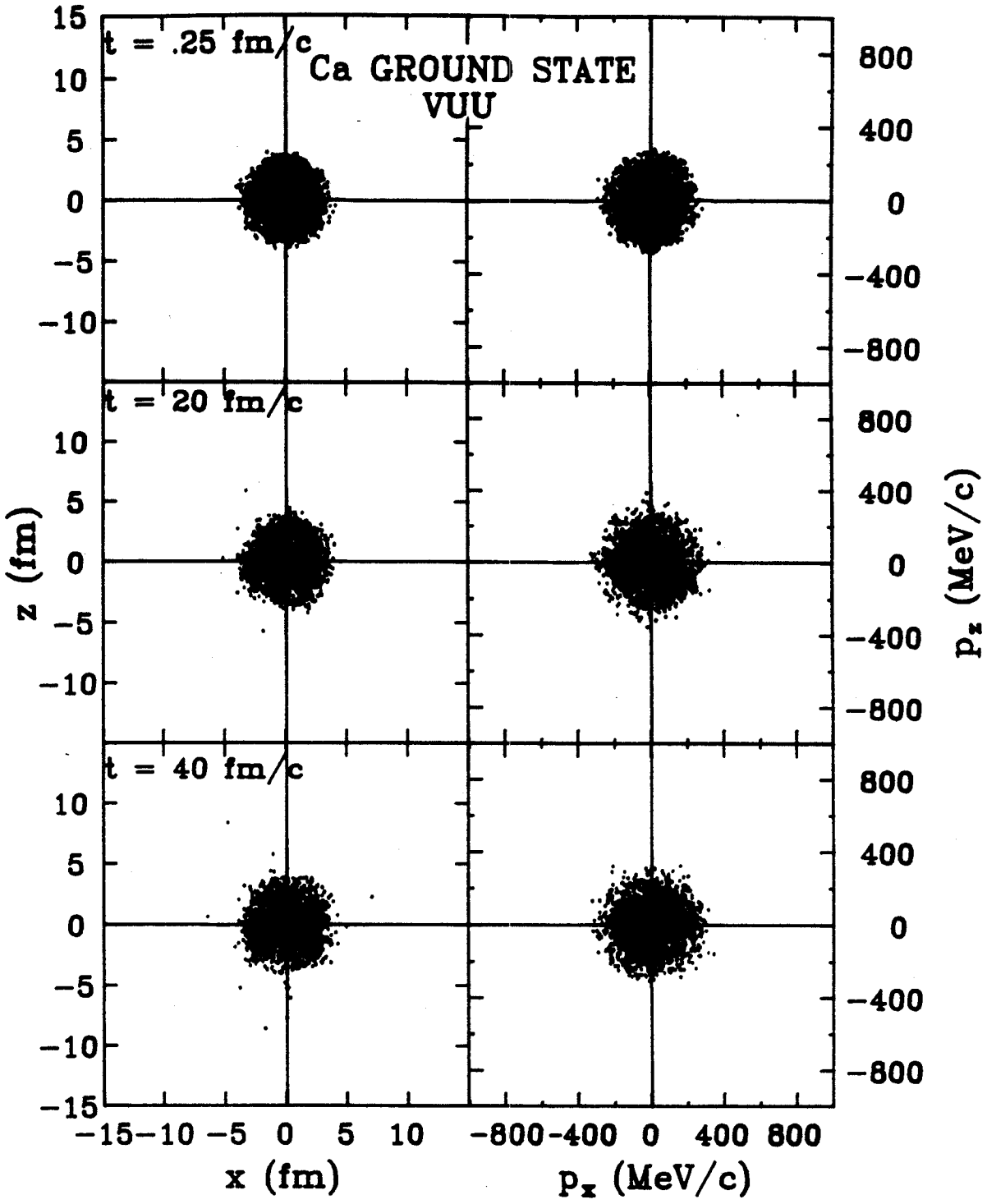

Figure II.9 Ca nuclei evolve in configuration and momentum space in the VUU approach with a time step of 0.25 fm/c.

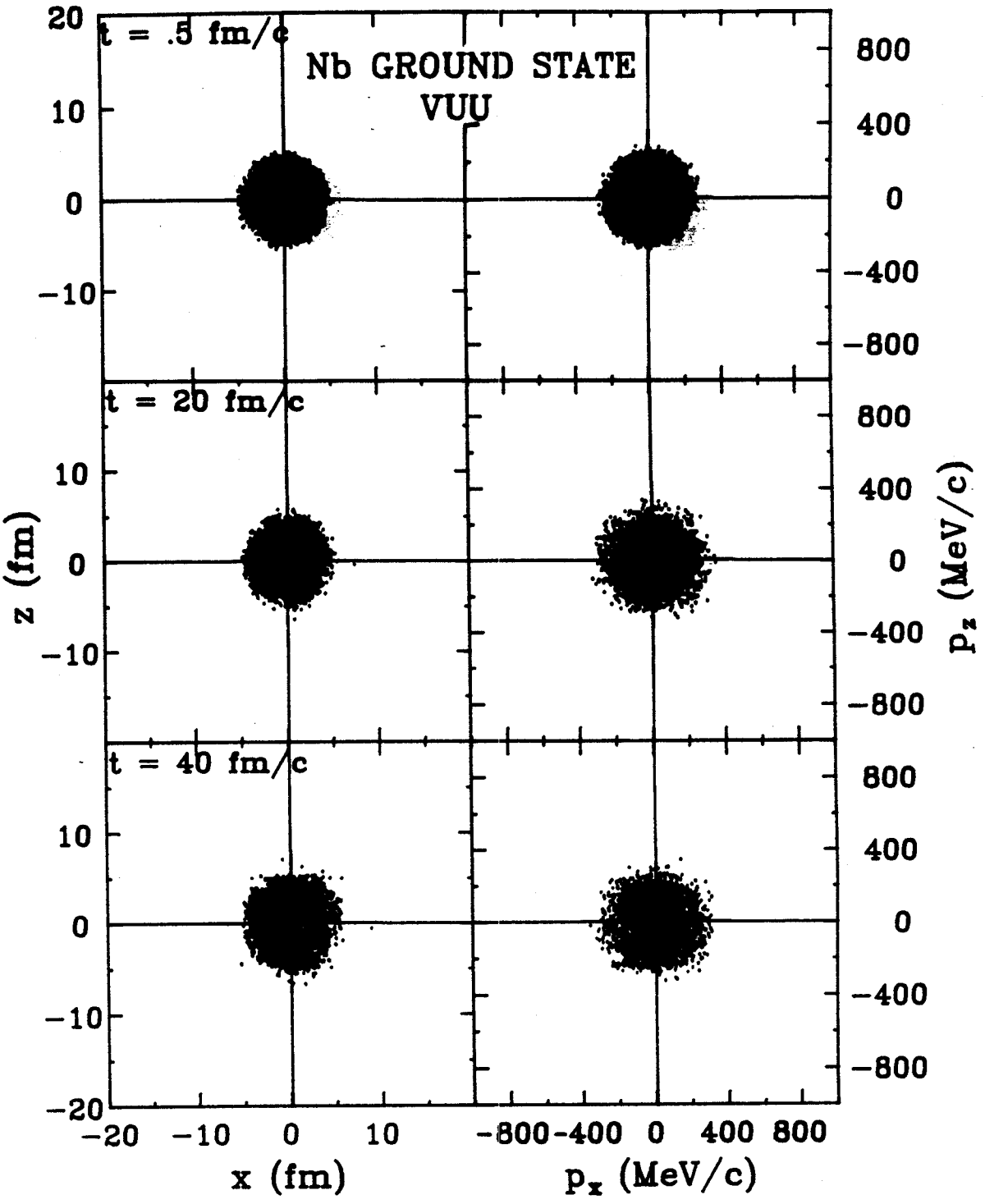

Figure II.10 The stability of Nb nuclei in the VUU approach is illustrated by their evolution in configuration and momentum space.

A constant time-step integration routine is used to insure synchronization of the ensembles. The acceleration of the test particles due to the field gradient is calculated prior to each transport step from the force components and is assumed to be constant within a synchronization time step. The local gradient of the field is computed via a finite difference method (73) between two hemispheres centered around the test particle. This method is analogous to Lagrange's method in fluid dynamics, in contrast to the space-fixed Eulerian mesh.

Protons, neutrons, deltas and pions of different isospin are included separately with their experimental scattering cross sections. The $p + n \rightarrow d + \pi^0$ channel is neglected. The following processes occur

$$N + N \rightarrow N + N,\ N + \Delta \rightarrow N + \Delta,\ \Delta + \Delta \rightarrow \Delta + \Delta$$
$$N + N \rightarrow N + \Delta,\ N + \Delta \rightarrow N + N \qquad (74)$$

where N = n or p and $\Delta = \Delta^-, \Delta^0, \Delta^+$, or Δ^{++}.

For N-N elastic scattering, $\sigma^{el}_{exp}(\sqrt{s})$ is used [Kru 85ab] with an angular distribution given by

$$\frac{d\sigma}{d\Omega} \sim e^{A(s)t} \text{ where } A(s) = 6\,\frac{3.65^6(\sqrt{s}-1.876)^6}{1 + 3.65^5(\sqrt{s}-1.876)^6} \qquad (75)$$

and $t = -(\text{momentum transfer})^2$ [Cug 81]. This form provides a good fit from low energies where the cross section is fairly isotropic to higher energies where it is forward peaked.

The process $N + N \rightarrow N + \Delta$ is given a cross section $\sigma^{ine}(\sqrt{s}) = \sigma^{tot}_{exp} - \sigma^{el}_{exp}$ with isotropic angular distribution. $N + \Delta \rightarrow N + N$ is obtained

by detailed balance and $N + \Delta \rightarrow \Delta + \Delta$ is neglected. The mass of the Δ is chosen randomly according to a Lorentzian with $E_0 = 1232$ MeV, width $\Gamma_0 = 120$ MeV, and finite lifetime τ chosen with exponential weight [Cug 82]. The Δ decay width is mass dependent; it is a function of the pion momentum in the Δ rest frame [Ran 79, Rit 71]:

$$\Gamma = \Gamma_0 \frac{p_\pi^3 \left(1 + \left(\frac{227}{238}\right)^2 + \left(\frac{227}{318}\right)^4\right)}{227^3 \left(1 + \left(\frac{p_\pi}{238}\right)^2 + \left(\frac{p_\pi}{318}\right)^4\right)} \qquad (76)$$

When an inelastic collision occurs, m_Δ is chosen randomly with a cut on the low energy side at the pion threshold [Cug 82, Ran 79]. An isotropic angular distribution is used for delta production - it has been shown [Cug 81] that an acceptable anisotropic distribution does not significantly change the results. Pauli blocking of the delta decay is not taken into account: this would perhaps reduce the final pion yields by 5% or so.

Pion production thus occurs via the delta resonance and in the s-wave channel below the delta resonance energy. The formation probabilities are given by the squares of the appropriate Clebsch-Gordon coefficients. The Δ (T=3/2) has isospin states $T_z = -3/2, -1/2, 1/2,$ and $3/2$; the proton $T = 1/2$ has $T_z = 1/2$ and the neutron $T_z = -1/2$; and the pion $T = 1$ has $T_z = -1, 0,$ and 1. Then the various probabilities are for formation

$$\begin{aligned} &n + n \rightarrow n + \Delta^0 \ (1/4), \ p + \Delta^- \ (3/4) \\ &n + p \rightarrow n + \Delta^+ \ (1/2), \ p + \Delta^0 \ (1/2) \\ &p + p \rightarrow p + \Delta^+ \ (1/4), \ n + \Delta^{++} (3/4); \end{aligned} \qquad (77)$$

decay

$$\Delta^0 \rightarrow n + \pi^0 \ (2/3),\ p + \pi^- \ (1/3)$$

$$\Delta^- \rightarrow n + \pi^-$$

$$\Delta^+ \rightarrow n + \pi^+ \ (1/3),\ p + \pi^0 \ (2/3) \qquad (78)$$

$$\Delta^{++} \rightarrow p + \pi^+;$$

and absorption

$$\pi^0 + n \rightarrow \Delta^0,\ \pi^0 + p \rightarrow \Delta^+$$

$$\pi^- + n \rightarrow \Delta^-,\ \pi^- + p \rightarrow \Delta^0 \qquad (79)$$

$$\pi^+ + n \rightarrow \Delta^+,\ \pi^+ + p \rightarrow \Delta^{++}.$$

Clearly the end result of such a process is not easy to predict. After one formation and decay step, the proportion of $\pi^-:\pi^0:\pi^+$ is 7:10:7 with equal numbers of protons and neutrons. A neutron abundance tends to enhance the proportion of π^-, whereas a proton abundance that of π^+.

Relativistic kinematics is used, but the one time nature of the model results in a lack of Lorentz invariance. However, as in the relativistic cascade model, this should give rise to an uncertainty of a few % in the observables [Cug 81] for the non-ultra-relativistic realm.

The question of double counting of the mean field and the collision term is a basic restriction for the VUU approach [Kru 85b]. The following operational point of view is taken here: the phenomenological Skyrme potential incorporates the real part of the potential, i.e. the attractive one meson exchange (the linear term in U) and repulsive mean field interactions, while the two body scattering accounts for the residual interactions. It should be pointed out that energy and

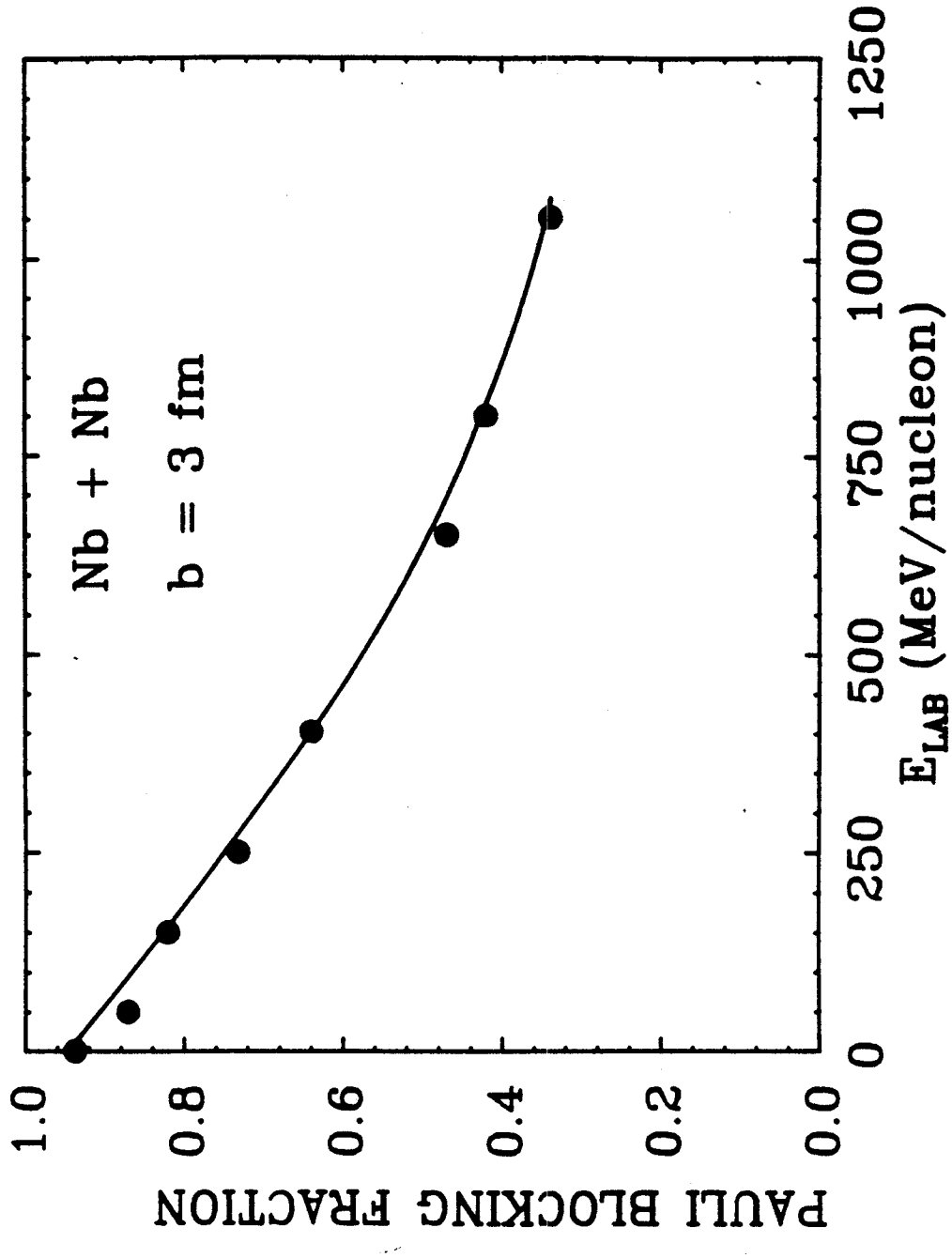

Figure II.11 Fraction of Pauli blocked collisions in the VUU theory versus energy for the Nb + Nb system at b = 3 fm.

momentum conservation is fulfilled in the present approach for individual two body scatterings and for the ensemble average on the mean but not within each separate ensemble, because of the coupling between different ensembles (energy conservation problems have been studied for a similar approach [Köh 80] using the relaxation time ansatz).

The free particle cross sections have to be corrected for "in medium" effects, the most important one being the Pauli blocking of collisions [Kru 85ab]. Two particles may undergo s-wave scattering if they approach each other with a minimum distance of less than $\sqrt{(\sigma(\sqrt{s})/\pi)}$ and if the final states are not Pauli blocked. The Pauli blocking factor for each nucleon is given by $(1-f)$, and the scattering probability is then reduced by the Uehling-Uhlenbeck factor $(1-f_1)(1-f_2)$. The Pauli blocker has been tested on ground states of nuclei and forbids there about 97% of all collisions. It is very important at intermediate bombarding energies, too: even at 137 MeV/nucleon, 80% of the attempted collisions are blocked due to lack of available final state configurations (Figure II.11) [Kru 85b]. Many of these attempted collisions are between nucleons of the same nucleus.

As we shall discuss in detail below, the effect of the collision term is to cause equilibration. The repulsive part of the field results in bounce-off or collective flow effects. We will return to these collective effects in more detail in Chapter III.

6. Intranuclear Cascade Models

The intranuclear cascade model represents the limit of the VUU theory where there is no mean field and no sophisticated Pauli blocking. Historically, the intranuclear cascade idea is due to Serber [Ser 47].

His idea was that nuclear reactions at high energies might be understood in terms of a quite simple picture different from the description needed at low energies. Because the collision time between an incident high energy nucleon and one in the nucleus is short compared to the time between collisions of the nucleons in the nucleus itself, he suggested that the high energy reaction could be regarded as a cascade process. Collisions occur between the incident particles and those particles which are directly struck in the nucleus. This model was first investigated in two dimensions by Goldberger [Gol 48], who performed his calculations by hand for the case of high energy neutrons interacting with heavy nuclei. The first three dimensional calculations were done [Met 58] for incident protons and neutrons using the MANIAC computer; also a second stage was added to the cascade calculation during which the excited residual nucleus evaporates particles, as had also been suggested by Serber.

Many others have contributed to the development of the intranuclear cascade model. The two most commonly used versions of the cascade code in the theory of high energy heavy ion reactions are due to Yariv and Fraenkel [Yar 79,81] and Cugnon et. al. [Cug 80,81,82]. These codes simulate a heavy ion reaction at high bombarding energies on a microscopic level by treating nuclear collisions as a superposition of independent two-body nucleon-nucleon collisions. Nucleons move on straight line trajectories (since there is no field) until they collide, with a probability given by the free nucleon-nucleon scattering cross section. The creation of deltas, pions, and other particles and the interaction of all these particles occur according to experimental cross sections. Relativistic kinematics is included.

Target and projectile nucleons are initialized in configuration and momentum space with random Fermi momenta and then Lorentz boosted to an appropriate frame, where the collision simulation proceeds. Momentum and energy are conserved in the particle-particle interactions and the evolution of the system is computed up to a time where the majority of interactions has ceased. Collisions are Pauli blocked according to the simple criterion that the collisions are forbidden if the total center of mass energy is less than the Fermi energy in ground state nuclear matter [Cug 80,81,82] or if the outgoing particle would scatter into momentum space regions originally occupied by projectile or target [Yar 79,81].

Both the Yariv-Fraenkel and the Cugnon cascade satisfy the above criteria. They differ in two respects: (1) the particles in the Yariv-Fraenkel simulation sit in a potential well of constant depth V_0; (2) in the original Yariv-Fraenkel approach the incoming particles (projectile nucleons) are cascading independently through a medium (the target) - in the updated version, this scheme has been improved by including the so-called cascade-cascade interactions.

In the Cugnon cascade, one has the problem that the nucleons are not bound; hence one may get spurious effects [Cug 84a] due to nuclear instability, see Figure II.12 [Mol 85b]. It is possible to bind the nucleons by letting each nucleon move only with the beam velocity until it interacts with another nucleon, at which point it 'remembers' it's Fermi momentum [Gyu 82]. However, this bound Cugnon cascade is not very satisfying either, since in real nuclei, nucleons can travel in all directions.

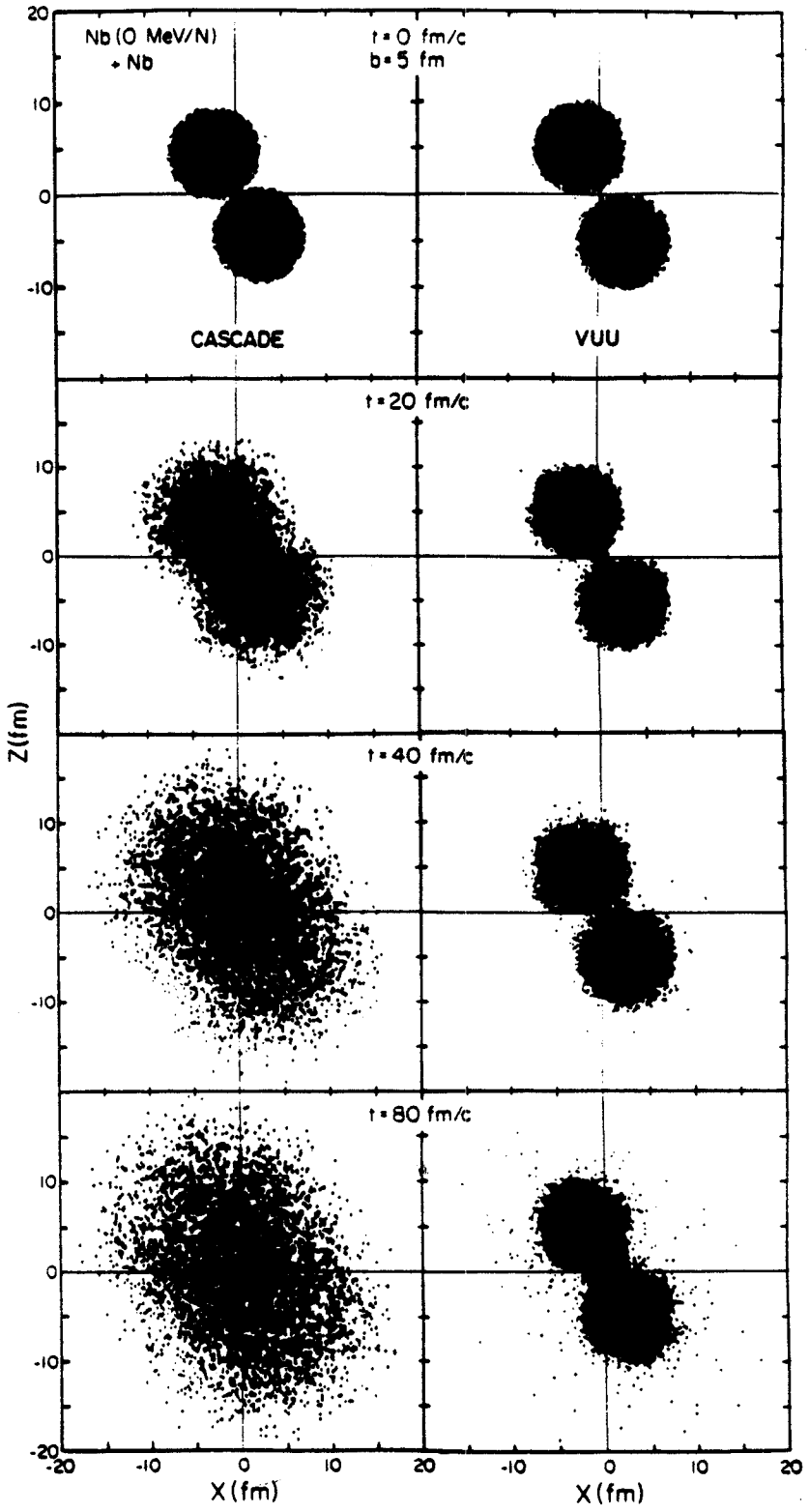

Figure II.12 The stability of Nb nuclei in the VUU approach versus a corresponding instability in the Cugnon cascade for Nb (0 MeV/nucleon) + Nb.

7. Nuclear Fluid Dynamics

Just as in the classical case, one can derive from the VUU equation general transport equations. Let us re-write the VUU equation in the simple form:

$$\left(\frac{df}{dt}\right)_{coll} = \frac{\partial f}{\partial t} + \vec{v}\cdot\frac{\partial f}{\partial \vec{r}} + \vec{F}\cdot\frac{\partial f}{\partial \vec{p}} \quad . \tag{80}$$

Assume for simplicity that the force $\vec{F} = d\vec{p}/dt$ is momentum independent. Then an integration of this equation over p produces:

$$\frac{\partial \rho}{\partial t} + \vec{\nabla}\cdot(\rho\vec{u}) = \int d^3p \left(\frac{df}{dt}\right)_{coll} \tag{81}$$

The term containing the force vanishes by partial integration. The collision term on the right hand side of eq. (81) describes the net gain rate of particles at position $\vec{r}$ and with momentum $\vec{p}$. Since the collisions take place at one point and only redistribute particles in momentum space while conserving their number, the integral over all momenta must vanish. Thus the first equation of nuclear fluid dynamics, the continuity equation, is obtained:

$$\frac{\partial \rho}{\partial t} + \vec{\nabla}\cdot(\rho\vec{u}) = 0 \quad . \tag{82}$$

This equation of continuity is valid for any fluid, viscous or not. To get an equation for the momentum density, integrate the VUU equation with a weight of $\vec{v}$:

$$\frac{\partial}{\partial t}(\rho\vec{u}) + \vec{\nabla}\cdot\int d^3p \vec{v}\vec{v}f + \sum_j F_j \int \vec{v}\frac{\partial f}{\partial p_j} d^3p = 0 \quad . \tag{83}$$

Again the collision term yields a vanishing contribution, because momentum is conserved in the collisions locally. In the second term on the left, one may separate an average and a fluctuating part:

$$\int d^3p \vec{v}\vec{v}f = \int d^3p \vec{u}\vec{u}f + \int d^3p (\vec{v}-\vec{u})(\vec{v}-\vec{u})f + \int d^3p \vec{u}(\vec{v}-\vec{u})f + \int d^3p (\vec{v}-\vec{u})\vec{u}f \quad (84)$$

The last two terms vanish because the average of $\vec{v} - \vec{u}$ is zero. The fluctuating part defines the kinetic stress tensor:

$$\underline{P}(\vec{r},t) = \int d^3p (\vec{v}-\vec{u})(\vec{v}-\vec{u}) f(\vec{r},\vec{p},t) \ . \quad (85)$$

Note that the stress tensor is identically zero only if all the particles have exactly the mean velocity $\vec{u}$. The external force contribution can be rewritten using

$$p_i \frac{\partial f}{\partial p_j} = \frac{\partial}{\partial p_j}(p_i f) - \delta_{ij} f \quad (86)$$

and then the first term on the right hand side vanishes in partial integration. The momentum conservation equation is then:

$$\frac{\partial}{\partial t}(\rho \vec{u}) + \vec{\nabla} \cdot (\rho \vec{u}\vec{u}) = - \vec{\nabla} \cdot \underline{P} + \frac{\rho}{m} \vec{F} \ . \quad (87)$$

Define the energy density as:

$$\rho E = \frac{m}{2} \int d^3p \ v^2 f(\vec{r},\vec{p},t) \ . \quad (88)$$

Then, through the introduction of the average velocity, ρE may be split up into a flow kinetic energy and a thermal contribution:

$$\rho E = \frac{m}{2} \rho u^2 + \frac{m}{2} \int (\vec{v}-\vec{u})^2 f(\vec{r},\vec{p},t) d^3p \ . \quad (89)$$

Integrating the VUU equation with a weight of $mv^2/2$ gives

$$\frac{\partial}{\partial t}(\rho E) + \nabla \cdot \int d^3p \frac{m}{2} v^2 \vec{v} f + \vec{F} \cdot \int d^3p \frac{m}{2} v^2 \frac{\partial f}{\partial \vec{p}} = 0 \quad (90)$$

where again the collision term gives no contribution because it conserves the kinetic energy of the particles. The second term is split up into a number of parts:

$$\int d^3p \frac{m}{2} \vec{v} v^2 f = \int d^3p \frac{m}{2} (\vec{v}-\vec{u})^2 (\vec{v}-\vec{u}) f + \int d^3p \ f \frac{m}{2} u^2 \vec{u} +$$

$$m \int d^3p \vec{u}\cdot(\vec{v}-\vec{u})(\vec{v}-\vec{u})f + \int d^3p \frac{m}{2} (\vec{v}-\vec{u})^2 \vec{u} f$$

$$= \vec{q} + \rho E\vec{u} + \vec{u}\cdot \underline{P} \qquad (91)$$

wherein the first term $\vec{q}$ describes the transport of thermal energy by thermal motion (thermoconductivity). The second and third term are combined to give the transport of total energy by collective flow and the last term describes the work done against the stresses. Finally the external force contribution can be re-written by partial integration:

$$\vec{F}\cdot\int d^3p \frac{1}{2} v^2 \frac{\partial f}{\partial \vec{p}} = - \vec{F}\cdot\int d^3p \vec{v} f = -\rho \vec{u}\cdot\vec{F} \qquad (92)$$

and the equation for energy conservation reads:

$$\frac{\partial}{\partial t}(\rho E) + \vec{\nabla}\cdot(\rho E\vec{u}) = -\vec{\nabla}\cdot(\vec{u}\cdot\underline{P} + \vec{q}) + \rho\vec{u}\cdot\vec{F} \; . \qquad (93)$$

These then are the general fluid dynamics equations (82, 87, and 93). One obtains the usual Nuclear Fluid Dynamical equations by using $P_{ij} = p\delta_{ij}$ and $q_i = 0$. Also, a potential $\vec{F} = -\nabla U$ is introduced. These Euler equations are for local equilibrium and the Navier-Stokes equations (see below) are for near local equilibrium.

For the applicability of the fluid dynamical concepts it has to be ensured that fast equilibration and thermalization of the incident momentum and energy occurs in high energy heavy ion collisions. Some support for this conjecture is seen for the most central collisions and heavy projectile and target combination in the results of the VUU theory (see Chapter III). A simple argument is that this is the case if the mean free path λ is small compared to the typical dimension, $L = 2R$, of the system

$$\lambda/L << 1. \qquad (94)$$

The mean free path λ is given by

$$\lambda = \frac{1}{\sigma \cdot \rho} \qquad (95)$$

where σ is the total nucleon-nucleon scattering cross section and ρ is the actual nuclear density. For normal nuclear matter density ρ_0 and a free N-N scattering cross section $\sigma_{NN} \sim 40$ mb at high energies ($E_{Lab} >$ 200 MeV/nucleon), the mean free path is $\lambda \approx 1.5$ fm, which is not too small against the nuclear dimensions $L \approx 10$ fm for heavy nuclei [Sch 68, Sch 74].

The large longitudinal momentum decay length calculated from the free N-N scattering cross section was interpreted as a complete transparency for the two nuclei at high energies and as the death for compression (shock) waves at energies above 1 GeV/nucleon [Sob 75]. However, in the early interaction time of ensembles of nucleons, collective scattering phenomena cannot be neglected, namely compression effects and the enlargement of the cross section due to precritical scattering [Gyu 77, Ruc 76], so that the scattering cross section and the density can be modified drastically leading to a decrease of the mean free path:

$$\lambda \approx 1.4 \frac{\sigma_{NN}}{\sigma_{coll}} \cdot \frac{\rho_0}{\rho} \text{ fm} \quad . \qquad (96)$$

This would mean that even at bombarding energies above one GeV/nucleon, nuclei do not become transparent to each other: on the contrary, very violent collisions can be expected. One should keep in mind, however, that nucleus-nucleus collisions are a quantum mechanical process. Hence--in the sense of quantum mechanical fluctuations--under the same initial conditions processes with violent randomization (e.g.

the occurrence of pronounced shock waves) may occur as well as processes with less pronounced interaction. It is a formidable experimental task to separate the former from the latter. Recent experiments show that up to lab-energies of 4 GeV/nucleon a considerable part (~30%) of the total cross section is due to violent events with very high multiplicities and large momentum transfer.

There is a formal relationship between quantum mechanics and fluid dynamics which was noticed immediately after the discovery of quantum mechanics [Mad 26]. One uses the Schrödinger equation

$$-\frac{\hbar^2}{2m}\nabla^2\psi + V(r)\psi = i\hbar\frac{\partial\psi}{\partial t} \tag{97}$$

and the separation of a phase S in the wave function

$$\psi(r,t) = \phi(r,t)\cdot e^{imS(r,t)/\hbar} \tag{98}$$

to get

$$\frac{\partial}{\partial t}\phi^2 + \vec{\nabla}\cdot(\phi^2\vec{\nabla}S) = 0\ . \tag{99}$$

This is the well known continuity equation describing the conservation of probability density in quantum mechanics. The probability density and average velocity are

$$\rho(r,t) = \phi^2(r,t) \text{ and } \vec{u} = \nabla S \tag{100}$$

from which it can be shown that

$$\frac{\partial}{\partial t}(m\rho\vec{u}) + \vec{\nabla}\cdot(m\rho\vec{u}\vec{u}) = -\rho\vec{\nabla}U - \rho\vec{\nabla}\left(-\frac{\hbar^2}{2m}\frac{\sqrt{\rho}\nabla^2\sqrt{\rho}}{\rho}\right). \tag{101}$$

This is identical with the conservation equation of the momentum with an external force due to a potential U as in equation (87). Only the last term on the right-hand side is different. It depends solely on the

density and may be interpreted as an inner pressure caused by quantum mechanical effects. It disappears in the classical limit $\hbar \to 0$.

Equations (99) and (101) have been obtained for the probability density of one single particle. The analogy to a quantum mechanical many body system, behaving like interpenetrating fluids with interaction, is obvious. It is important to note that (in contrast to kinetic theory) each single quantum mechanical particle is a continuum itself. Therefore the problem of granulation of the microscopic density does not occur. However, the main problem is a reasonable definition for the many particle densities and velocities. An important question is whether all quantities entering the equations of motion may be described as functions of these macroscopic variables (and a temperature) or not.

It is also possible to derive continuity equations for many particle systems. In particular, linearization of the Hartree equations yields formulae similar to the equations of motion of an ideal compressible fluid [Zyr 56]. A derivation of the hydrodynamic equations by analogy to the TDHF equations is also possible [Stö 85]; this is less general, but the principal argument [Won 77, Mar 77] is the same as the one used above.

After this brief analogy with quantum mechanics, let us collect the general equations of dissipative fluid dynamics. These are continuity equations for the baryon density ρ, momentum density $\vec{M} = \rho\vec{u}$, and energy density $e = \rho E$ with the gradients of the pressure p and the potential U [Stö 85]:

$$\partial_t \rho + \partial_i (\rho u_i) = 0, \tag{102}$$

$$\partial_t(\rho u_i)+\partial_j(\rho u_j u_i)=-\frac{1}{m}\partial_i p+\frac{1}{m}\partial_j[\eta(\partial_i u_j+\partial_j u_i-\frac{2}{3}\delta_{ij}\partial_k u_k)+$$

$$\xi\delta_{ij}\partial_k u_k]-\frac{\rho}{m}\partial_i U,$$

$$\partial_t(\rho E_T)+\partial_j(\rho E_T u_j)=\kappa\partial_j^2 T+\partial_i u_j[-p_T\delta_{ij}+\eta(\partial_i u_j+\partial_j u_i-\frac{2}{3}\delta_{ij}\partial_k u_k)+\xi\delta_{ij}\partial_k u_k].$$

If the viscosity coefficients may be regarded as constant and if the fluid is incompressible ($\nabla\cdot\vec{u}=0$), then the momentum equation is called the Navier-Stokes equation [Lan 59]. The indices i, j and k are running over the space coordinates and the Einstein summation convention is used. κ is the heat conductivity, η is the shear viscosity, and ξ is the bulk viscosity. The coupled nonlinear equations for the density fields $\rho(\vec{r},t)$, momentum density fields $\rho(\vec{r},t)\vec{u}(\vec{r},t)$, and energy density fields $\rho(\vec{r},t)E(\vec{r},t)$ must be solved simultaneously. A three dimensional solution of these equations for nuclear physics has only recently been attempted. Deviations from local equilibrium have been treated before by phenomenologically incorporating viscosity [Stö 78,79].

How do these equations change if relativistic effects become important? The range of validity of the non-relativistic formalism is not sharply defined, but at bombarding energies $E_{lab} > 500$ MeV/nucleon, the classical relative velocity of projectile and target exceeds the speed of light and at best qualitative results may be obtained.

There are two ways in which a system may become relativistic: (a) macroscopically relativistic when the flow velocity becomes large or (b) microscopically relativistic when the excitation energy is non-negligible in comparison to the rest energy (the fluid particles have a large velocity). Case (a) is reflected by the equations of motion and

case (b) by the equation of state. As in the nonrelativistic case, the fluid dynamic equations reflect the conservation of baryon number, momentum and energy, and may be brought into the continuity equation form [Stö 85]:

$$\partial_t \rho_L + \partial_k(\rho_L u_k) = 0$$

$$\partial_t M_i + \partial_k(M_i u_k) = -\partial_i p$$

$$\partial_t e_L + \partial_k(e_L u_k) = -\partial_k(p u_k) \ , \qquad (103)$$

where long range potentials and dissipative terms have been dropped.

The quantities ρ_L, M and e_L are the densities for baryon number, momentum and energy as specified in a fixed ("lab") reference frame. These are related to the "proper" or "co-moving" densities in the local rest frame by

$$\rho_L = \gamma\rho$$

$$M_i = \gamma^2(e + p)u_i$$

$$e_L = \gamma^2(e + p) - p \qquad (104)$$

where $\gamma = 1/\sqrt{(1-\beta^2)}$ is the usual Lorentz factor, ρ = the proper baryon number density, p the pressure, and $e = \rho(E_o + E_C(\rho) + E_T(\rho,T))$ the proper internal energy density including the rest energy. The proper densities ρ, e and the velocity $\vec{u}$, which are the physically interesting quantities, must be obtained from the lab densities ρ_L, M, e_L by inverting the nonlinear equations with $p=p(\rho,e)$ from the equation of state. This nontrivial technical problem is a complication over the

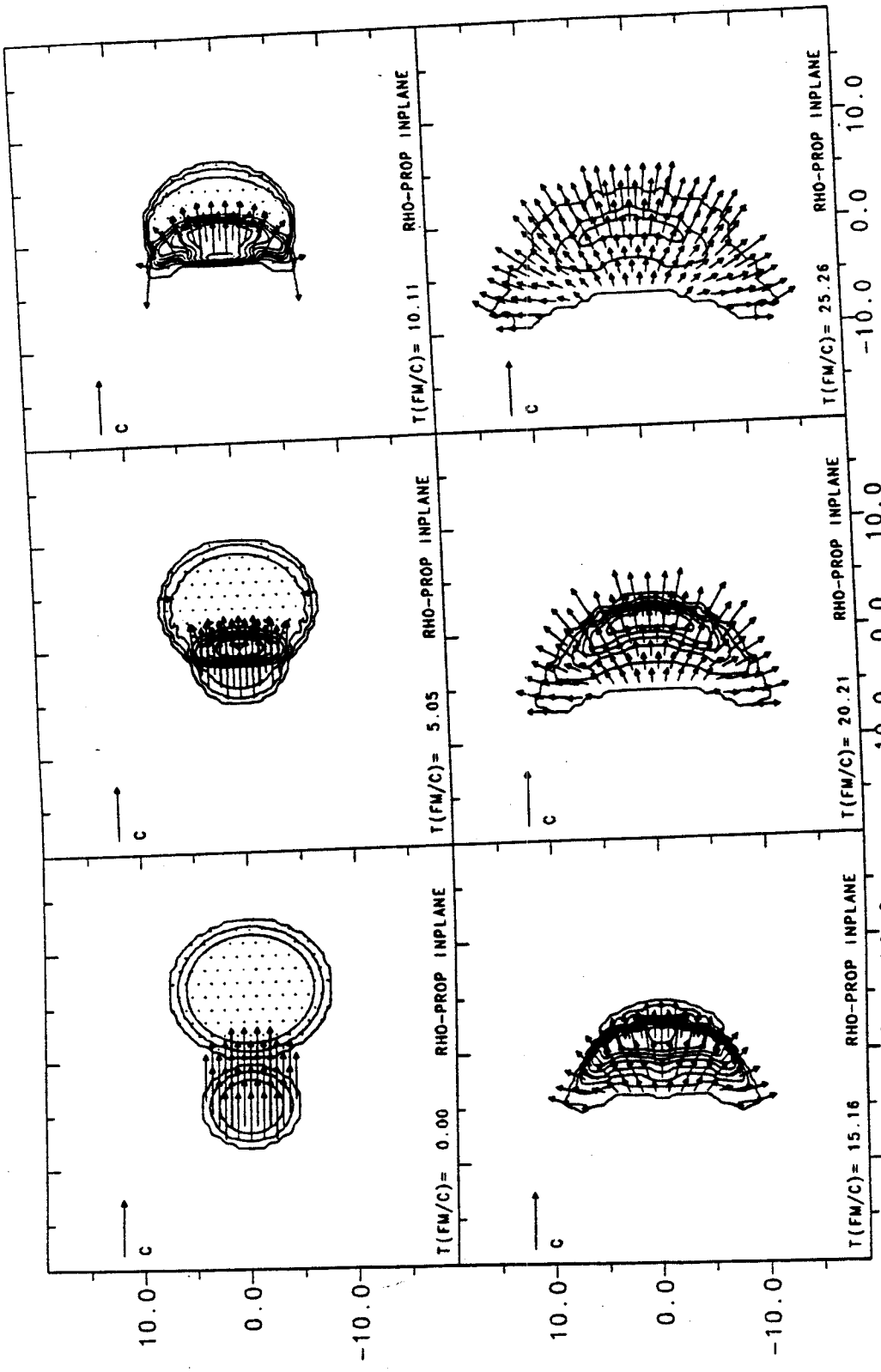

Figure II.13 Collision of Ar (770 MeV/nucleon) + Pb at b = 0 fm in the Nuclear Fluid Dynamic model.

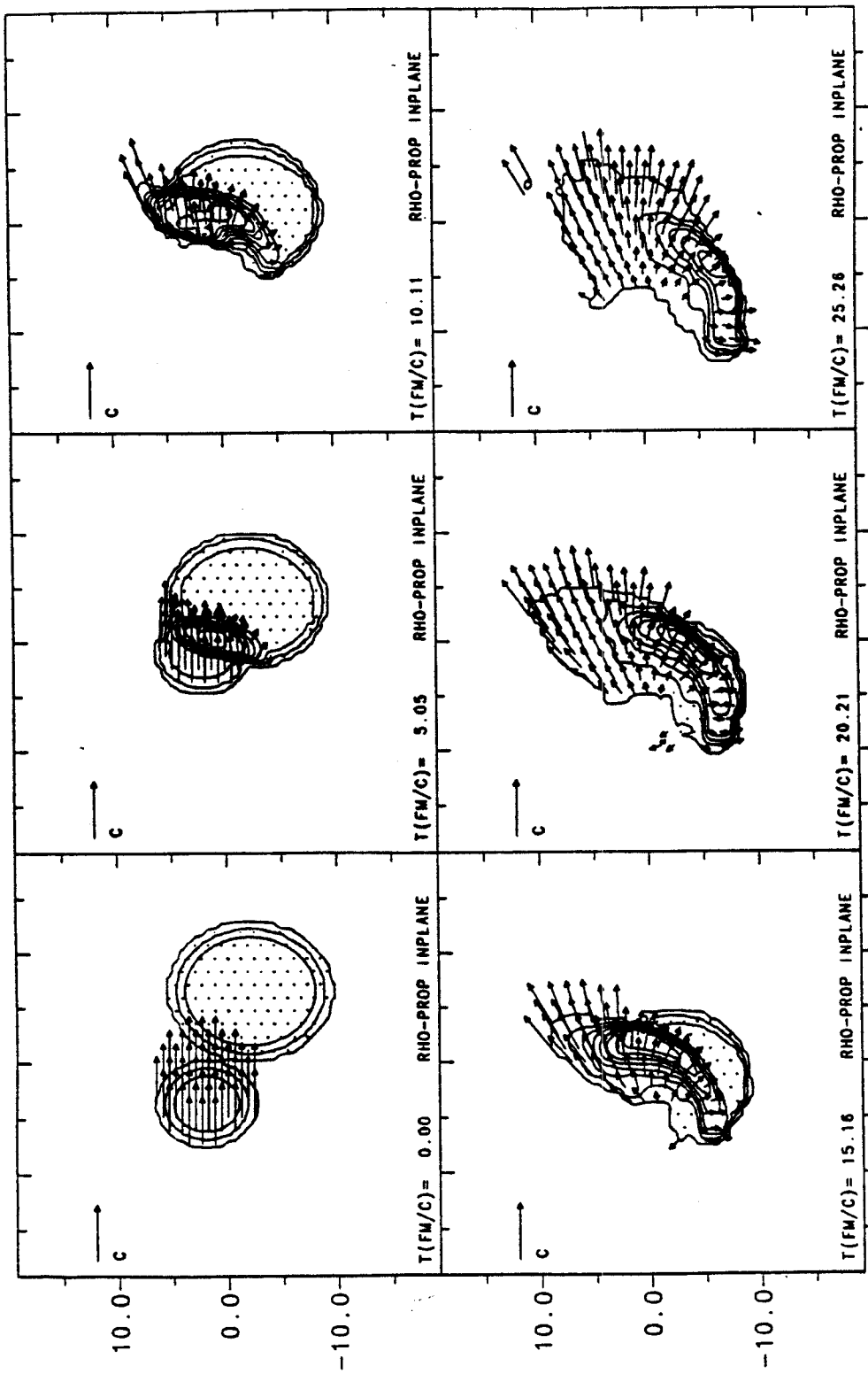

Figure II.14 Collision of Ar (770 MeV/nucleon) + Pb at b = 4 fm in the Nuclear Fluid Dynamic model.

nonrelativistic case, where the velocity can be calculated directly from ρ and $\rho\vec{u}$.

Both the potentials and the dissipative terms become harder to handle in relativistic fluid dynamics where the covariant formulation adds time derivatives and implies retardation for the potential.

Shown in Figures II.13 and 14 is the relativistic nuclear fluid dynamical model calculations [Gra 84] for the reaction Ar (770 MeV/nucleon) + Pb at b = 0 and 4 fm, studied below in the VUU nonequilibrium theory. Note the superposition of the head and sidewards Mach shock waves which results in collective flow. Similar results between VUU and NFD (see below) are however only expected when heavy projectile and targets are studied, because only in this case the VUU approach does predict local thermal equilibrium for the most central impact parameters. For light systems like C + C the fluid dynamical model does not apply - there is simply not enough target material in the way of the projectile to result in nuclear stopping.

8. One Dimensional Shocks

It is often advantageous to gain more insight into the physical processes by solving more simplified, schematic models, which can be solved (at least to some extent) analytically. In this case another set of equations is applied in the more schematic treatment of the fluid-dynamical description of high energy heavy ion collisions, namely the shock equations. In contrast to sound waves, shock waves are connected with a strong, density dependent mass flow velocity v_f. The shock front itself propagates with the shock velocity $v_s > v_f$ and also depends

strongly on the compression amplitude [Bau 75]. Shock waves are non-linear phenomena--for large amplitudes ($\rho >> \rho_0$) both v_s and v_f tend to the velocity of light, while for small perturbations $\rho \approx \rho_0$ they approach the linear limit of sound waves. Shock waves imply a large entropy production: the matter flow through the shock front is highly irreversible, it is not only connected with strong compression, but also with large thermal excitation [Hof 76, Stö 77 ,78].

The shock calculations have to be viewed as an idealization, assuming a zero width of the shock front together with a discontinuous jump of the state variables (e.g. ρ, T, e, p). However, comparison of the one dimensional nuclear shock wave calculations with the result of the two dimensional Navier Stokes calculations [Stö 79] shows that the resulting compression rates and temperatures are very similar, although in the Navier Stokes calculations the compression front is smeared out over 1-2 fm due to the viscosity. Such a width seems to be realistic, as the width of a shock front is approximately given by 2-3 times the mean free path, which can be less than half a fermi in high energy nuclear collisions [Stö 79]. For a large nuclear transparency, the shock front width may be of the order of the nuclear radius. However, no indication for transparency has been found in the high energy experiments up to now.

Let T_{ij} be the energy-momentum 4-tensor for a fluid in motion [Lan 59]:

$$T_{ij} = hu_iu_j + pg_{ij} \qquad (105)$$

where g_{ij} is the metric tensor. Also, $\underline{u} = u_i = \gamma(1,-u/c)$ is the covariant 4-velocity. The relativistic Rankine-Hugoniot equations can

be derived from the continuity of particle flux density, energy flux density, and momentum flux density [Lan 59]. Eliminating the velocities u_x from the continuity equations yields the relativistic Rankine-Hugoniot equation

$$\frac{h_0^2}{\rho_0^2} - \frac{h^2}{\rho^2} + (p-p_0)\left(\frac{h_0}{\rho_0^2} - \frac{h}{\rho^2}\right) = 0 \qquad (106)$$

which gives a unique connection between the free enthalpy $h = e + p$, pressure p, and density ρ within the respective rest frame of the matter (nought stands for the undisturbed matter in front of the shock wave, quantities without subscript refer to matter in the compressed state). When we insert $h=\rho E+p$, $h_0=\rho_0 E_0$, and $p_0=0$ the equation

$$E^2 - E_0^2 + p\left(\frac{E}{\rho} - \frac{E_0}{\rho_0}\right) = 0 \qquad (107)$$

is obtained. This is the relativistic generalization of the Rankine-Hugoniot equation, which determines the temperature T as a function of ρ, i.e. $T(\rho)$. If $E = E_C + E_T + E_0$ is equated with the center of mass energy one can solve eq. (107) for the density $\rho(E_{lab})$ and therefore for the bombarding energy dependence of any other thermodynamic quantity.

The shock velocities v_s and v_f are given by the continuity of the energy and momentum flux density. From the relative velocities of the matter with respect to the shock front

$$\frac{v_s}{c} = \sqrt{\left\{ \frac{pE\rho}{(E\rho-E_0\rho_0)(E_0\rho_0+p)} \right\}} \text{ and } \frac{v_{s'}}{c} = \sqrt{\left\{ \frac{p(\rho_0E_0+p)}{(E\rho-E_0\rho_0)\rho E} \right\}} \qquad (108)$$

the relative matter flow velocity v_f is found by the relativistic law of addition of velocities:

$$\frac{v_f}{c} = \sqrt{\left\{ \frac{p(\rho E-\rho_0E_0)}{\rho E(p+\rho_0E_0)} \right\}} . \qquad (109)$$

A simple model can be constructed to calculate the shock compression and temperature in the central collision of two heavy nuclei as a function of the bombarding energy [Bau 75, Stö 78, Hah 85a]. This model assumes the compressed fluid to be at rest in the center-of-momentum system. Three-dimensional fluid dynamical calculations show that this requirement is fulfilled fairly well for central collisions of heavy nuclei near the collision axis: a sort of stationary compression stage develops. Practically all of the incident kinetic energy is transformed into internal energy (compression and excitation).

Calculations have been done with this model for Nb + Nb [Hah 85a] in the 50 to 1000 MeV/nucleon range. The compresssional and thermal energies versus K_{lab} or K_{CM} for the stiff equation of state (Figure II.7) are:

Table II.8

K_{lab}	K_{CM}	E_C	E_T
50	13.5	8.0	5.5
150	37.5	18.0	19.5
250	61.2	26.4	34.8
400	94.2	37.4	56.8
650	151.4	56.4	95.0
800	184.5	67.0	117.5
1050	233.9	83.0	150.9

For the medium EOS, the compressional energy will be smaller and the thermal energy larger.

Though this model will, due to its lack of kinetic energy of the compressed matter and its neglection of the outflow of matter

perpendicular to the collision axis, give large values for compression and temperatures as function of the bombarding energy (as compared to three dimensional NFD [Gra 84]), it is sufficient to give a rather qualitative overview about the expected compression and the thermal excitation. The influence of the beam energy and the nuclear equation of state and the importance of resonance and pion production in the collision dynamics can be studied almost analytically.

III. Confrontation of the Theory with Experimental Data

1. Compression and Expansion

In the preceding chapter, both microscopic and macroscopic theoretical approaches to nucleus-nucleus collisions have been discussed. Fluid dynamics was historically the first approach to be applied to high energy nuclear collisions; it refers directly to thermodynamical concepts and therefore the underlying physics of high compression and excitation can be discussed in a macroscopic language. However, local thermodynamic equilibrium is probably a poor assumption except for the heaviest systems and the most central collisions. Therefore, microscopic approaches such as the Newtonian Force Model, The Vlasov-Uehling-Uhlenbeck approach, and the Intranuclear Cascade model are essential. For these models, the dependence of the observables and thermodynamic variables (to the extent that these latter can be inferred from the non-equilibrium situation) on the impact parameter, bombarding energy, and projectile-target combination can be studied. The VUU, NFM, and NFD models include the compression energy and so effects of the nuclear EOS can be probed.

Consider first the fluid dynamic model that has just been discussed, the simple shock model [Hah 85a]. The laboratory bombarding energy dependence of the thermodynamic variables density, temperature, and entropy of the shocked matter for the two different EOS (Figure II.7) are:

Table III.1

	medium EOS			stiff EOS		
K_{lab}	ρ/ρ_o	T	S	ρ/ρ_o	T	S
50	1.84	12	1.03	1.60	11	1.03

150	2.28	27	1.80	1.90	24	1.78
250	2.56	39	2.27	2.09	35	2.25
400	2.89	52	2.76	2.30	47	2.73
650	3.32	67	3.36	2.60	62	3.35
800	3.56	75	3.70	2.74	69	3.65
1050	3.88	85	4.13	2.93	78	4.06

The softer EOS allows 15-30% higher densities, 10% higher temperatures, and only a few % higher entropies to be probed. That the temperatures are higher with a soft EOS is however not a necessary prediction; it has been shown that two different EOS can predict the same temperatures [Hah 85a]. In general, shear viscous effects will increase S. Even a one dimensional model thus predicts effects due to the nuclear equation of state; collective effects that are dependent on impact parameter or event multiplicity are, of course, beyond the capabilities of such a simple model. These simple shock model values will serve as references for the three dimensional models.

Now consider that the full three dimensional evolution of a heavy ion collision typically proceeds in the following way (Figures III.1 and 2): when the two nuclei collide at high energy the overlap zones are stopped and a hot dense interaction zone (Figures III.1,2) or a strong nonlinear shock wave (Figures II.13,14) is formed. The nuclear matter in the interaction zone is compressed and heated: high density, pressure and temperature are created in this region. At E_{lab} = 400 MeV/nucleon, for example, a maximum compression of two to three times equilibrium density (Figure III.3,4) and a temperature of about 40 to 50 MeV can be reached. During the compression stage the entropy of the system rises to a certain final value which depends on the nuclear EOS, the

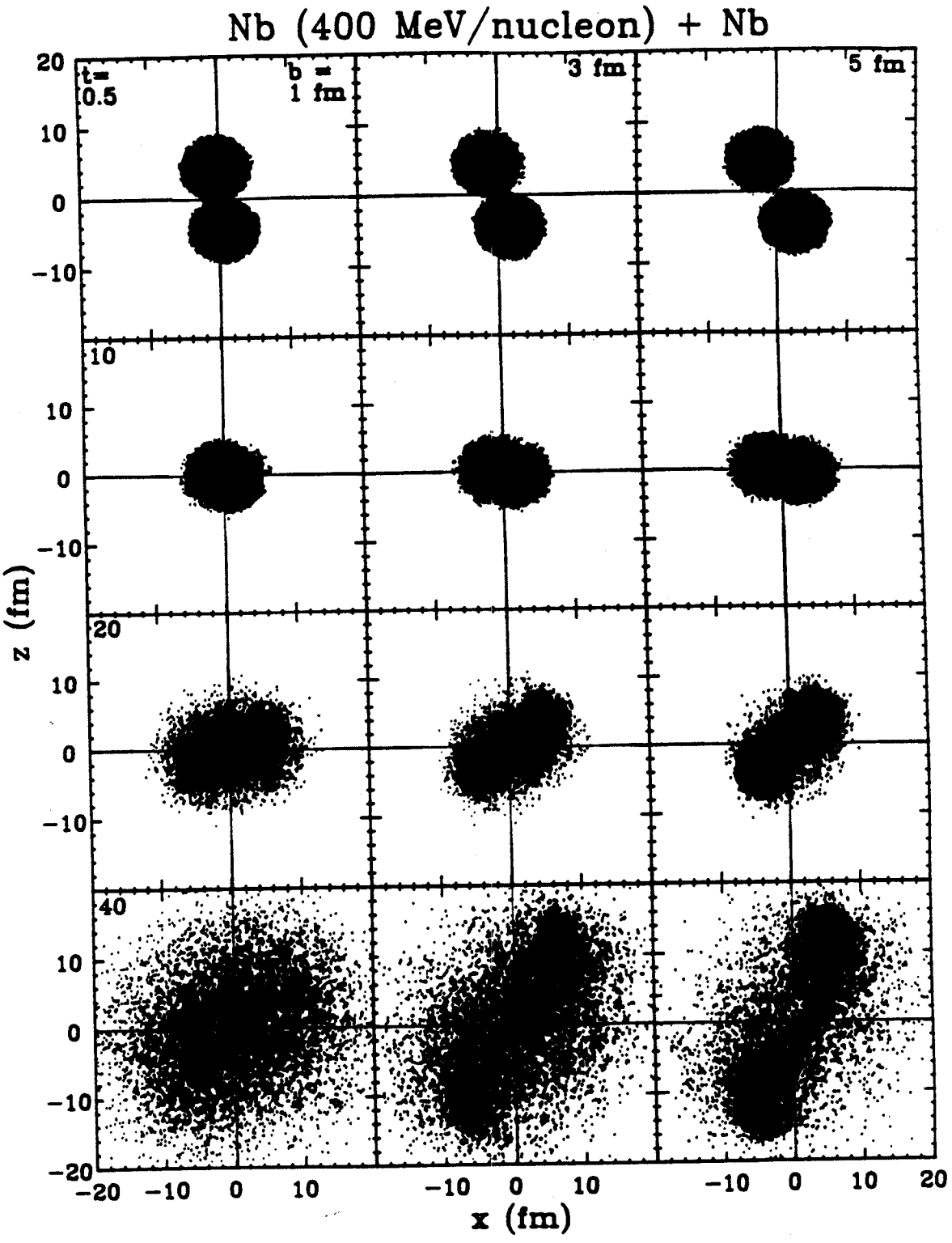

Figure III.1 Nb (400 MeV/nucleon) + Nb at b = 1, 3, and 5 fm in configuration space as a function of time (VUU).

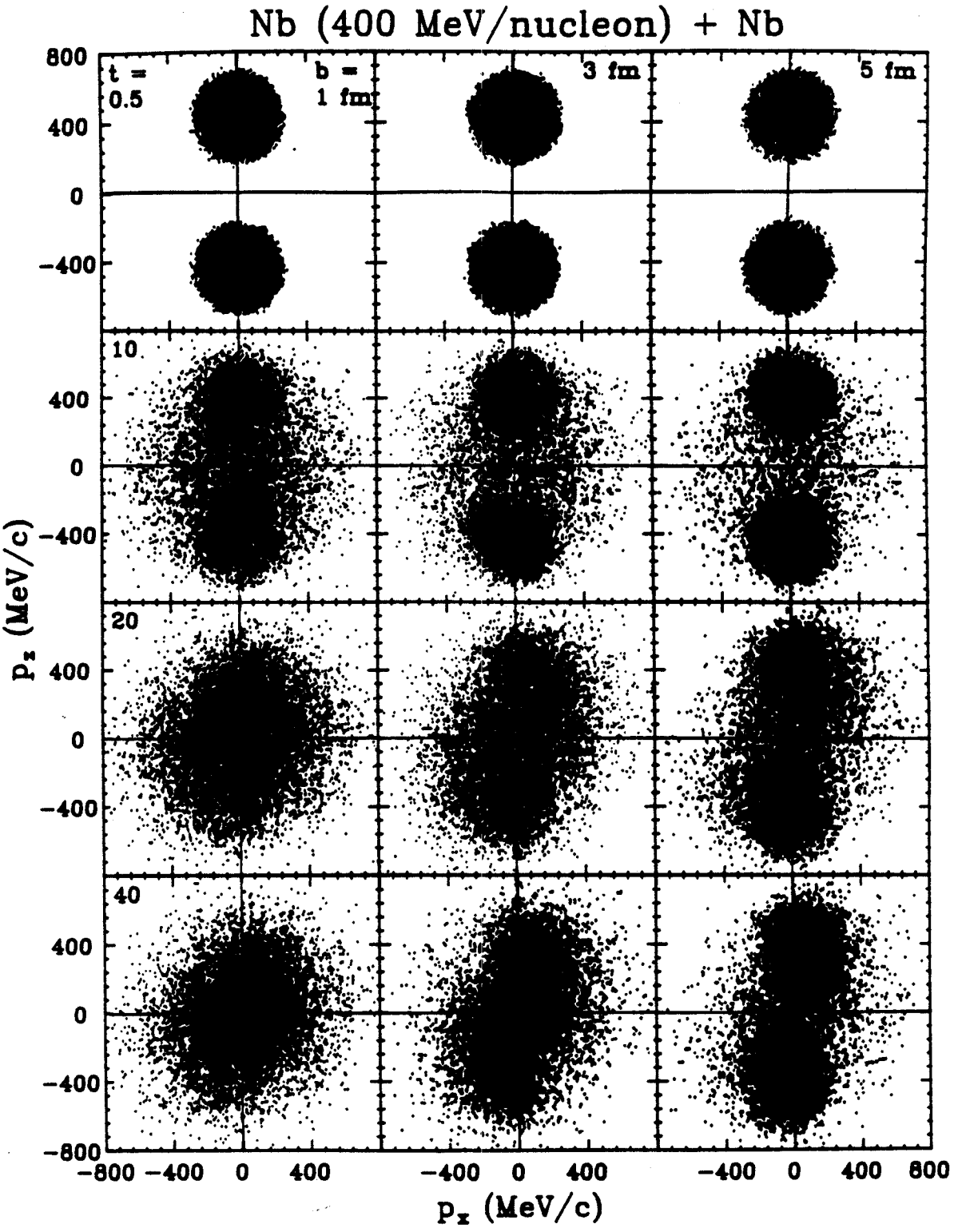

Figure III.2 Nb (400 MeV/nucleon) + Nb in momentum space in the VUU approach.

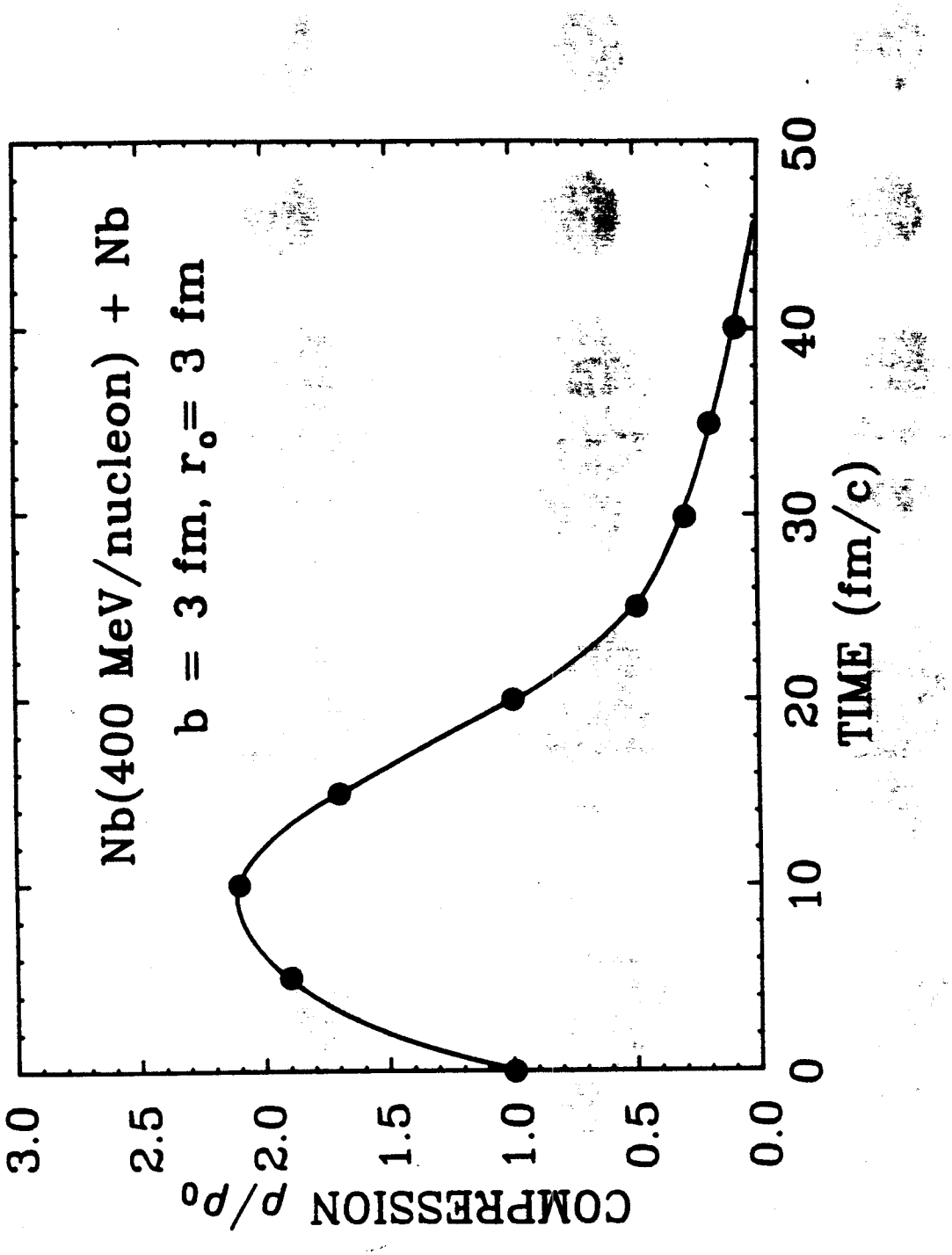

Figure III.3 The compression for Nb (400 MeV/nucleon) + Nb at b = 3 fm in a central region of radius 2 fm versus time (VUU).

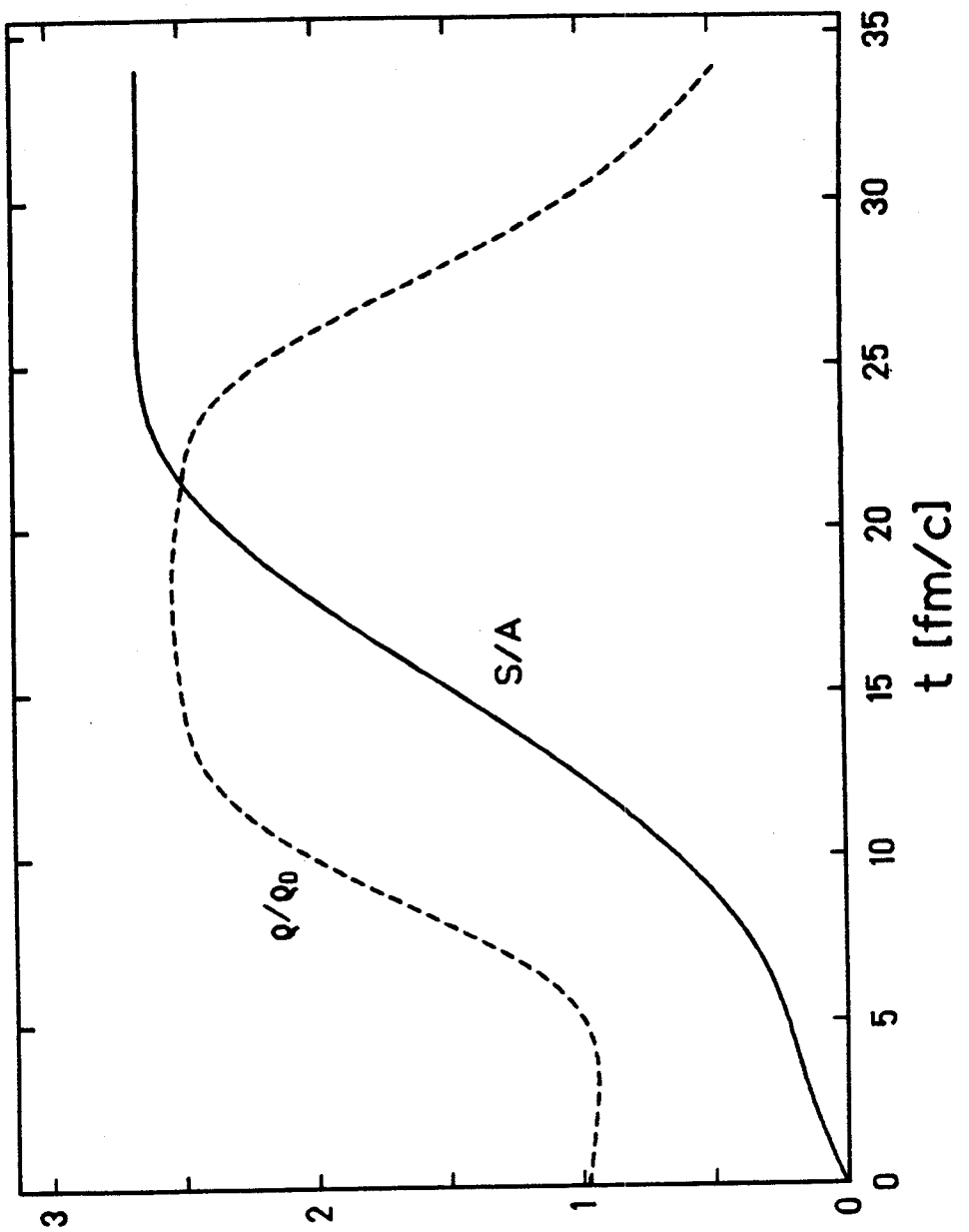

Figure III.4 The compression for Nb (400 MeV/nucleon) + Nb at b = 3 fm in a central region in the NFD approach.

bombarding energy, the viscosity in the system, and the degree of fragmentation.

In particular, the density rises to a maximum of 2.2 at t = 9 fm/c (Figure III.3) for Nb (400 MeV/nucleon) + Nb at b = 3 fm in the VUU approach. The density drops to 0.5 of the ground state density by t = 25 fm/c. The simple one dimensional shock model with the same stiff EOS predicts a density for the shocked matter of 2.3, very similar to that achieved in a central region. In the NFD model, the density in one cell of size 0.5 fm reaches the slightly larger value of 2.5 (with a softer EOS) (Figure III.4). At a higher energy, for Nb (1050 MeV/nucleon) + Nb in the VUU approach, the density rises to a maximum of 2.7 at t = 5 fm/c (compare the shock model value of 2.9) and then falls to 0.5 by 18 fm/c (Figure III.5). There is thus a somewhat less interaction time at the higher energy.

As a function of energy, the density reached in heavy ion collisions is very similar in Au + Au (see Figure III.6), Nb + Nb, or Ar + KCl collisions for the VUU model. What is important for the maximum density is not the atomic number, but the EOS: higher densities are achieved with softer equation of states just as the simple shock model predicts (Table III.1). Let us compare the central density achieved for the NFM, VUU, and INC models for the reaction Nb (1050 MeV/nucleon) + Nb at b = 2 fm:

Table III.2

	NFM		VUU		INC
	hard	soft	stiff	medium	
K_{lab}	$(\frac{\rho}{\rho_o})_{max}$	$(\frac{\rho}{\rho_o})_{max}$	$(\frac{\rho}{\rho_o})_{max}$	$(\frac{\rho}{\rho_o})_{max}$	$(\frac{\rho}{\rho_o})_{max}$

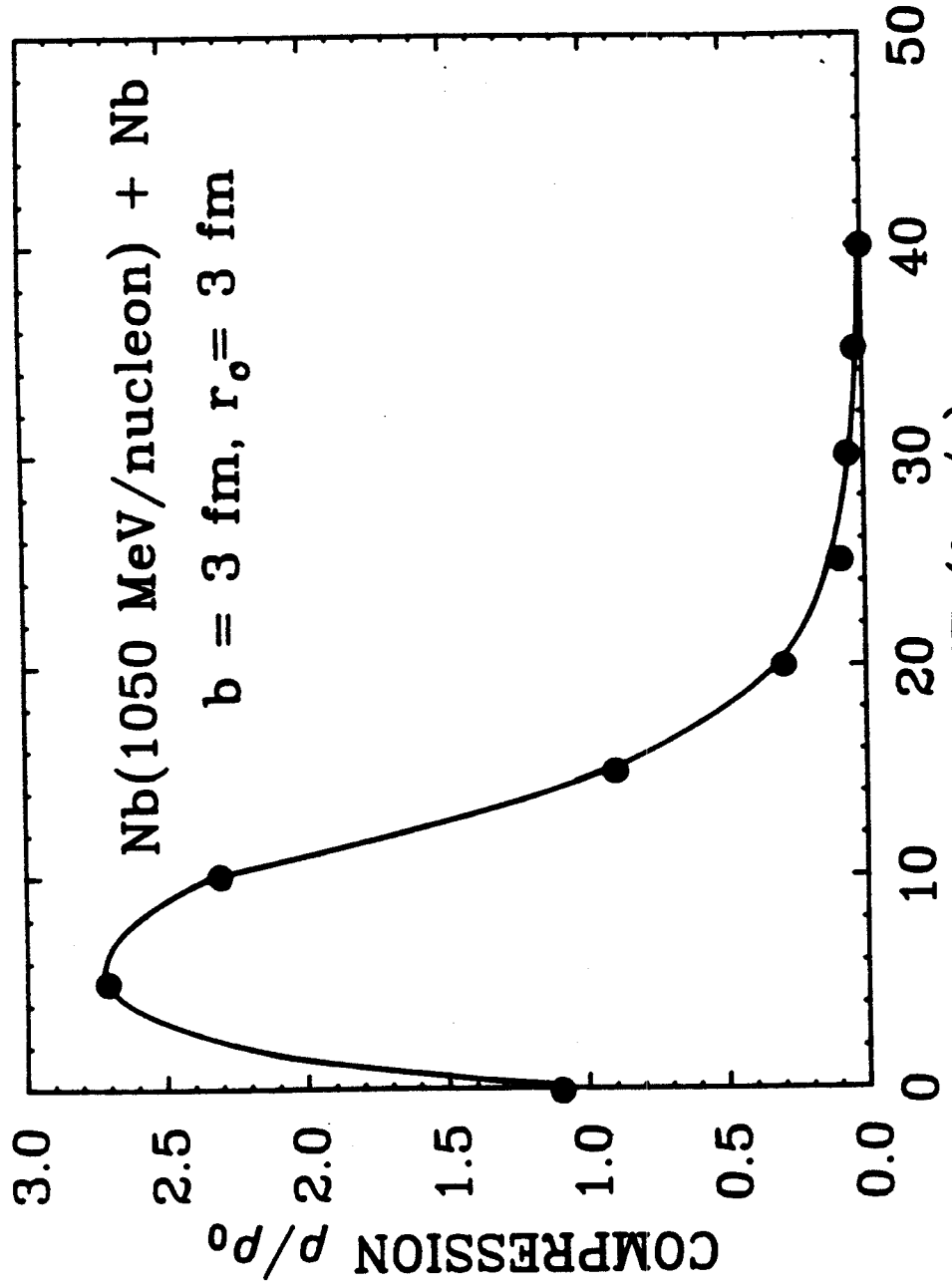

Figure III.5 The compression for Nb (1050 MeV/nucleon) + Nb at b = 3 fm in a central region of radius 2 fm versus time (VUU).

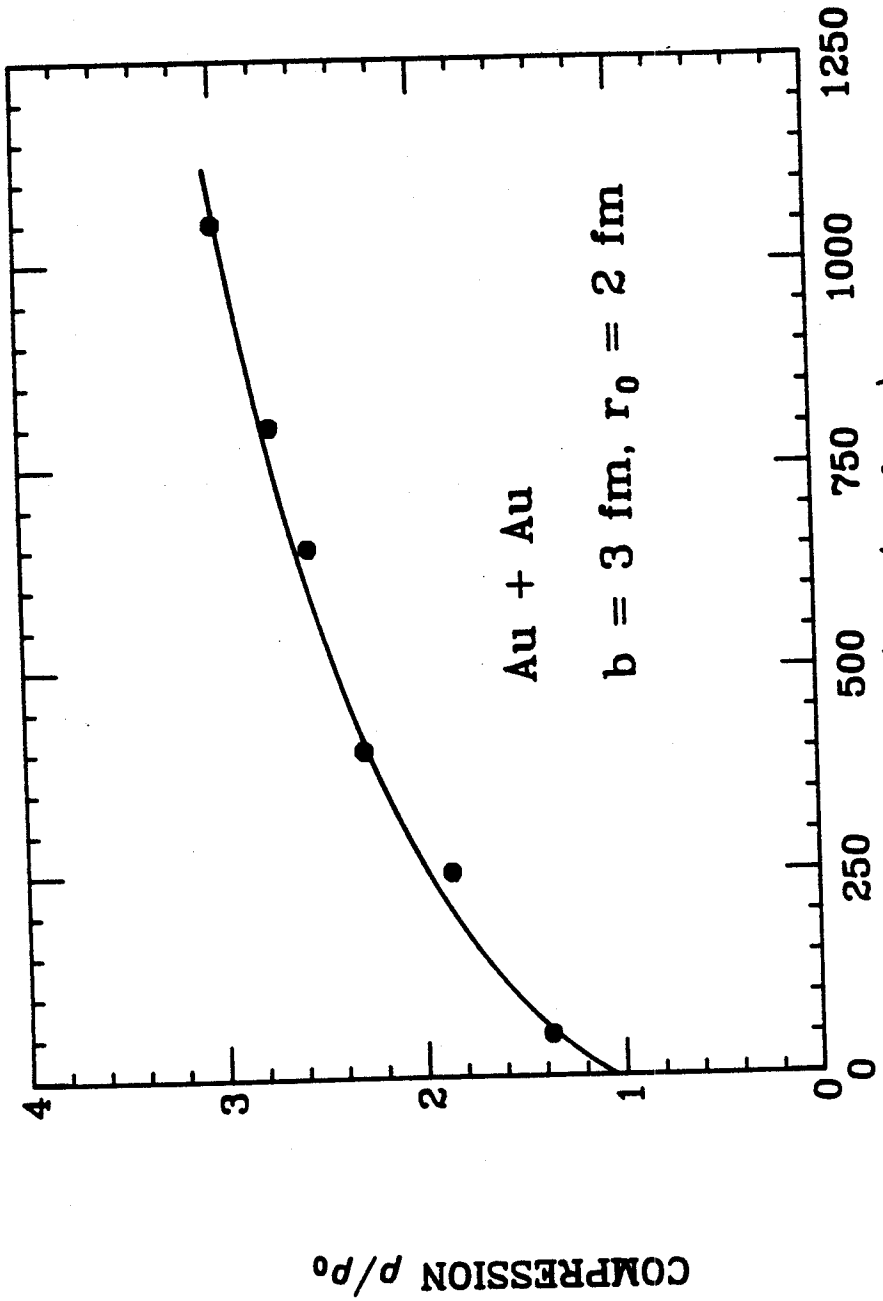

Figure III.6 Maximum density in the center of mass frame for Au + Au collisions at b = 3 fm (VUU).

150	2.65	3.18	1.61	1.90	3.25
400	3.05	3.63	2.29	2.50	3.60
650	3.28	3.62	2.55	2.95	3.75
1050	3.34	3.91	3.00	3.60	4.00

Notice that the soft potential in NFM or the medium EOS in VUU allows greater densities to be probed. Also notice that the densities calculated with the VUU theory are much lower than those reached with the less realistic intranuclear cascade model [Cug 81]; this is due to the compressional energy which the cascade model lacks.

One would also expect that the temperature increases in this interaction region. For this strongly interacting system, it is not at all a trivial matter to define the temperature. One can however gain some insight from Hagedorn's thermodynamics [Hag 71] where in the large mass limit

$$\langle p_\perp \rangle^2 = \pi m T/2 \ . \qquad (1)$$

This corresponds to the non-relativistic case where the two transverse degrees of freedom obtain the classical equipartition of kinetic energy. The $\pi/4$ instead of one comes out from calculating $\langle p_\perp \rangle^2$ instead of $\langle p_\perp^2 \rangle$. The y-direction alone may be further used to avoid some of the possible contribution from collective effects in the x-z reaction plane; the use of a small sphere centered around the origin also helps. This temperature is then a classical one simply calculated as twice the kinetic energy out of the reaction plane (the y - direction).

For Nb (1050 MeV/nucleon) + Nb in the VUU approach, the temperature rises to 80 MeV by t = 9 fm/c (Figure III.7) and then falls away as the the density does (Figure III.5). This temperature compares quite well with the temperature of 78 MeV extracted from the simple shock model

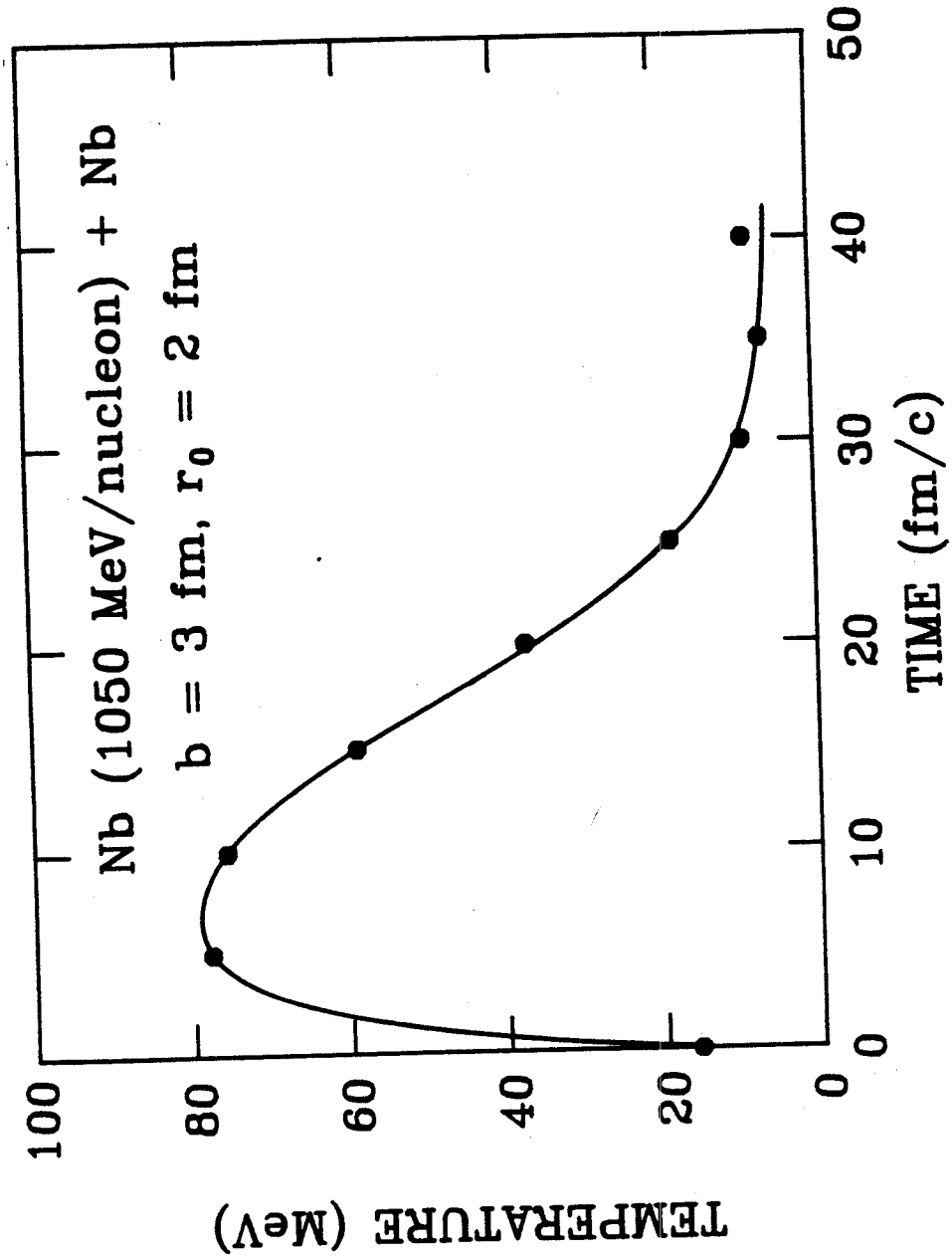

Figure III.7 Classical temperature versus time for Nb (1050 MeV/nucleon) + Nb at b = 3 fm in a central region of radius 2 fm in the VUU model.

with the same stiff EOS. Thus after the compression phase the temperature drops during the expansion; the system expands due to it's large internal pressure and at densities $\rho \approx 0.5\text{-}0.7\ \rho_0$ most of the collisions between the particles cease: the single nucleon or fluid dynamic description then loses its validity.

Temperature or slope parameter values may also be extracted from the invariant cross section at 90 degrees in the center of mass assuming a Maxwell-Boltzmann form. In fact the invariant cross sections for the NFM approach are completely Maxwell-Boltzmann. A shoulder appears in the VUU model; nevertheless, one can use the tails of the invariant cross section spectra to extract T_0 (Figure III.8). The slope parameters overestimate the maximum temperature achieved by large amounts at the highest energies (Figure III.8). Experimentally, one finds that T_0 varies with increasing multiplicity from 42 to 65 MeV for Nb (400 MeV/nucleon) + Nb collisions [Gut 85]; these values compare well with the NFM (T_0 = 57) or VUU (T_0 = 73 MeV) results. A more detailed comparison would require a connection of multiplicity with impact parameter. For Ca (400 MeV/nucleon) + Ca, one finds similar experimental values for the same multiplicity bins [Gut 85].

The temperatures T as calculated in the microscopic theories and fluid dynamics [Stö 81b] may be compared to the experimentally determined slope factors T_0 [Nag 81] of protons and pions emitted from violent nuclear collisions at various bombarding energies (Figure III.9). The data seem to rule out a pure nucleon Fermi gas at energies $E_{LAB} > 800$ MeV/nucleon. A mixture of noninteracting gases of the different hadrons with an exponentially increasing hadronic mass spectrum is in much better agreement with the data. However, one must

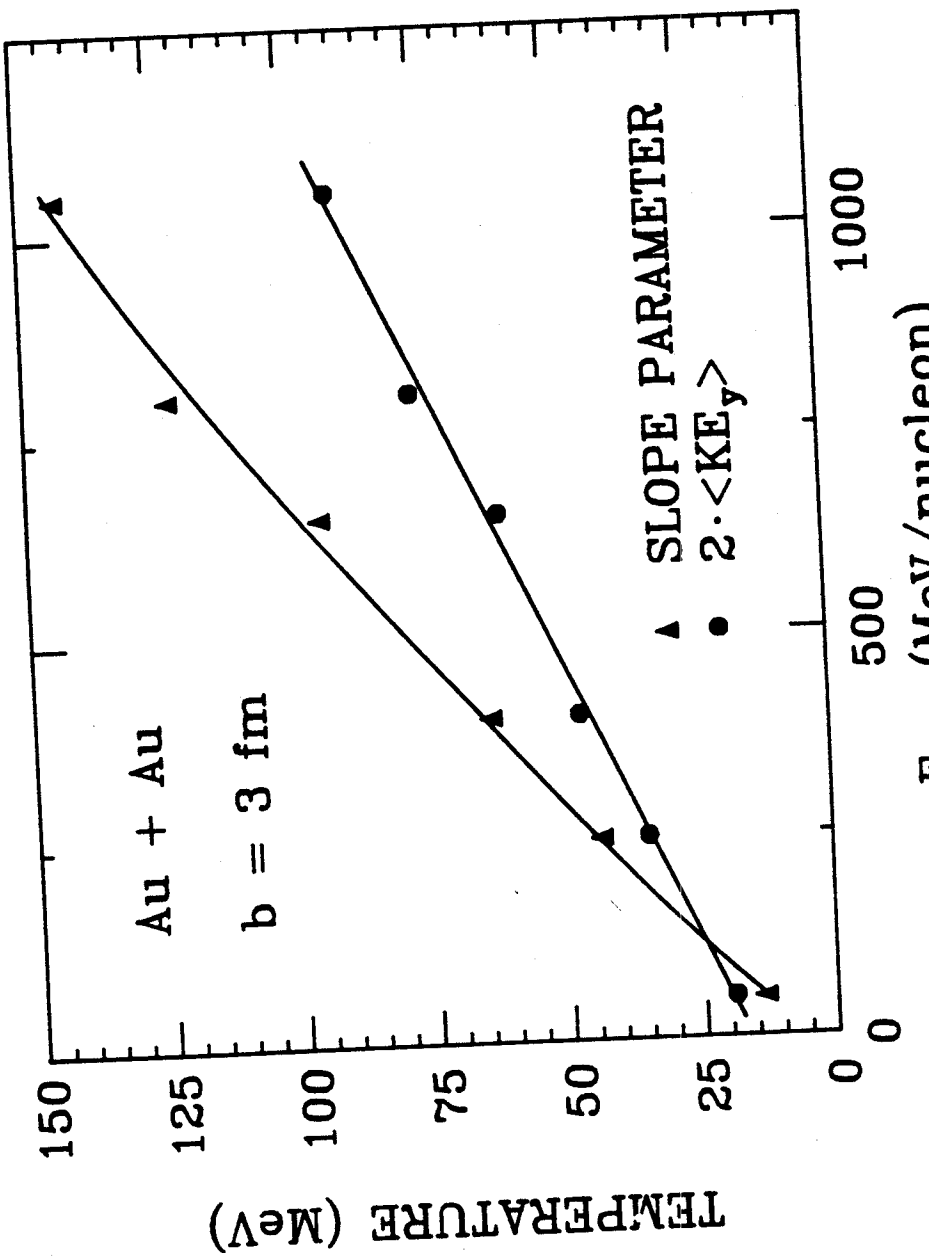

Figure III.8 Slope parameter T_o and maximum central classical temperature versus energy for Au + Au at b = 3 fm (VUU).

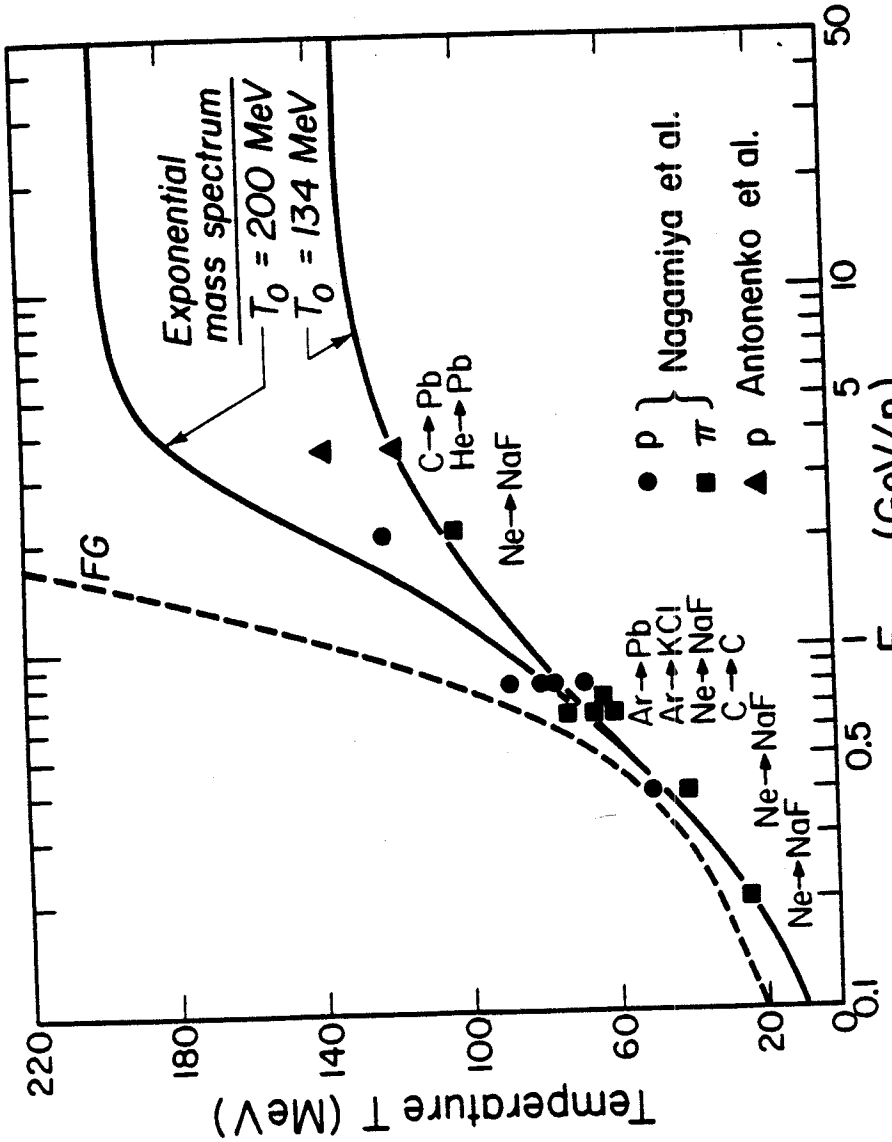

Figure III.9 Experimental slope factors compared to fluid dynamic calculations for a pure Fermi gas and for a classical ideal hadron gas.

keep in mind that the finally observed slope factors do not give a direct measure of the temperature [Sie 79, Stö 81b]. The actual temperature in a central region at the moment of maximum compression is lower than that extracted from assuming a Maxwell Boltzmann form for the invariant cross sections (Figure III.8).

2. Entropy

One may also try to calculate the entropy production in the VUU model, although this is more difficult. Consider the simple case of a system of non-interacting fermions. Then the entropy is

$$S = - \int d\Gamma (f \ln(f) + (1-f)\ln(1-f)] \qquad (2)$$

where $d\Gamma = \frac{4}{(2\pi\hbar)^3} d^3r d^3p$ is the phase space element and $f = \frac{n}{n_{ens} d\Gamma}$ is the average occupation number. What is to be expected for the behaviour of S in an expanding system?

One must remember that in a reversible adiabatic expansion the entropy does not change (2nd law of thermodynamics). In an irreversible, adiabatic expansion between two equilibrium states, the entropy generally increases. Adiabatic only means that there is no transfer of heat with the environment. Even if the finite system could be restored to its initial state, the increases in S can't be eradicated - at most it can be passed from one system to another. In a non-equilibrium closed system, the processes occur in such a way that the system continually passes to states of higher entropy until a complete statistical equilibrium ($S = S_{max}$) is achieved. However, interacting nuclei are not a closed system: the nucleons and fragments expand into the vacuum.

Suppose we have an expansion of non-interacting fermions and the momentum distribution is fixed in time. Then it seems that since f is proportional to ρ that as $t \rightarrow$ infinity, one might expect from (2) that S increases without bound. However, locally the momentum distribution shrinks with time since $\vec{r}$ and $\vec{p}$ become strongly correlated at late times: a particular distance from the origin of the expansion implies specific values of the momentum [Sie 79]. The mean field in the nucleus may produce an additional viscosity; thus it is not clear that one should expect isentropic expansion after a certain time in a heavy ion collision, as is assumed by non-viscous NFD.

Consider first equation (2) which will strictly be valid only for late times if one can neglect the fragmentation phenomenon. Really there should be a sum over the distribution function of different fragment types [Rem 85b] in (2): fragments continually form as the nuclear reaction proceeds. Note further that once the fragment's momentum distribution is fixed, then the entropy is fixed. Thus a calculated S value for times after fragmentation may also not be meaningful. Furthermore, for $t = 0$, S must be equal to 0 since the nuclei start in the ground state.

To evaluate (2) for the primordial baryon distribution, one must calculate a six-dimensional integral. The volume element is $(4\pi)^2 r^2 dr p^2 dp$, $8\pi^2 r^2 dr d(\cos\theta_r) p^2 dp$, or $8\pi^2 r^2 dr p^2 dp d(\cos\theta_p)$ depending on whether none of the angles is important, $\cos\theta_r$ is, or $\cos\theta_p$ is. The integral must then be converted to a sum to investigate the sensitivity to these variables. For Nb (1050 MeV/nucleon) at b = 3 fm in the VUU model, one finds

Table III.3

t	none	$\cos\theta_r$	$\cos\theta_p$	full 6D
10	5.04	5.02	4.82	4.21
20	6.82	6.79	6.66	5.35
30	8.20	7.98	7.88	5.85
40	8.69	8.55	8.55	6.38

For intermediate and later times, where the computation may be meaningful, there is thus very little sensitivity to the variable θ_r and θ_p. However, the full 6D Cartesian coodinate calculation shows that there is sensitivity to some other variable: in fact this is $\cos\theta_{pr}$ [Ber 81]. Furthermore, the full 6D calculation agrees well with the results of doing the integration with this new variable (Figure III.10). There is little sensitivity to the binning in r and p since the entropy is such a smooth function, but one must be careful with the $\cos\theta_{pr}$ binning.

At first sight, it is surprising that S does not approach a constant in this computation. (The cascade does however saturate - see below.) However, in the NFD model, S will approach a constant for the Euler equations and even when there is shear viscosity present but not when there is a bulk viscosity (Figure III.11). Thus, the VUU model mean field produces a similar effect. This does not imply that S increases without bound, since it will in fact be fixed at the time of nucleation when the fragmentation distribution becomes fixed or, more correctly, when the wavefunctions approach asymptotia.

Equation (2) has been used in a cascade model to calculate S [Ber 81]. For Ca (800 MeV/nucleon) + Ca at b = 0 fm, it is found that S = 4.5 for $10 < t < 20$ fm/c; as has been seen above for Nb, the $\cos\theta_{pr}$ correlation is important. Without incorporating the $\cos\theta_{pr}$ correlation, S = 5.5 is found. One may redo these calculations with the Cugnon INC

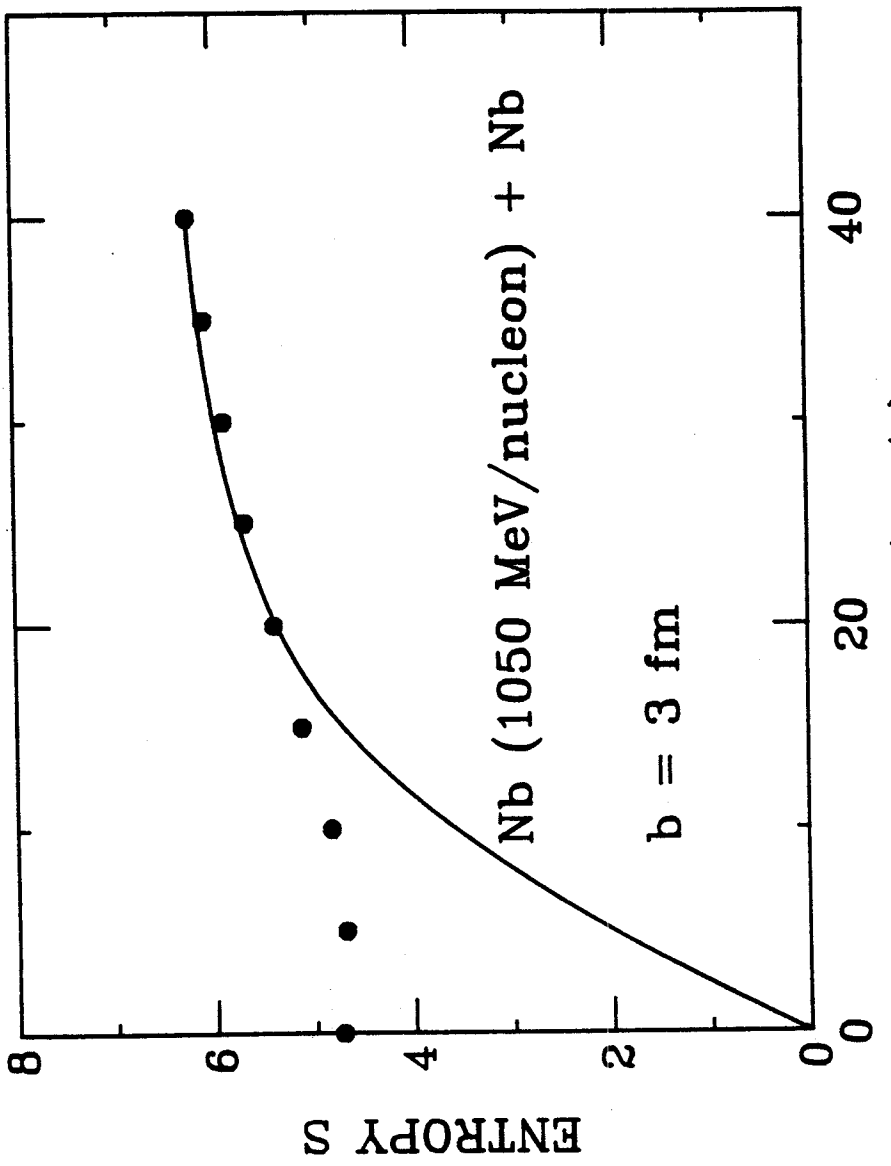

Figure III.10 Entropy calculated from the non-interacting fermion formula versus time for Nb (1050 MeV/nucleon) + Nb at b = 3 fm (VUU).

(frozen) both as a check on the method and to compare with the VUU approach:

Table III.4

t	S_{INC}	S_{VUU}
10	3.91	4.09
20	4.43	4.50
30	4.81	4.80
40	4.92	4.99

One thus finds the same value as [Ber 81] for t = 20 fm/c. However, the entropy goes beyond this value at later times and does not approach a constant saturation value so quickly. Theoretically, since the cascade model solves the Boltzmann equation, S must become constant after the collisions cease. The VUU approach shows a slightly faster increase of S. This is due to the mean field, which reduces the compression achievable, thus increasing the available volume and keeps the system from a rapid freeze-out. Collisions still occur at late times in bound clusters not present in the cascade. Note further that there is a strong impact parameter dependence of S: in the INC model the final entropy rises from 4.5 to 7.5 as the impact parameter is increased from 0 to 6.5 fm [Cug 84b].

The entropy production in the NFD model is shown in Figures III.4 and III.11 for a Nb + Nb collision at 400 MeV/nucleon and an impact parameter of 3 fm. Entropy is created during the first 20 fm/c of the collision. During that time the colliding participant zones of the two nuclei are stopped and compressed. When the maximum density of the system starts to drop (after 20 fm/c) the entropy has reached its saturation value of about 2.7 per nucleon (identical to the shock model

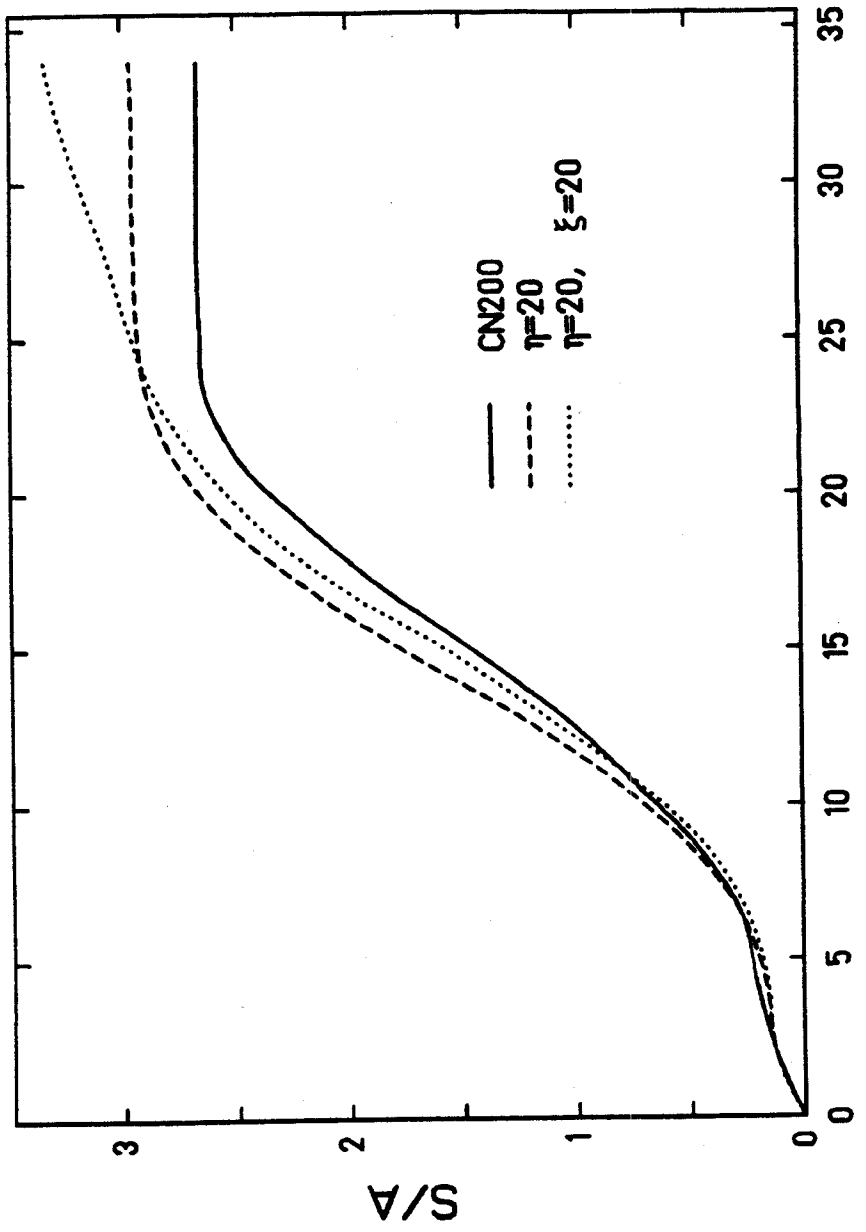

Figure III.11 Entropy versus time for Nb (400 MeV/nucleon) + Nb at b = 3 fm in the NFD approach.

value - but not with the same EOS). The entropy even saturates when a large shear viscosity η is present in the Navier-Stokes equations. Then, the absolute value of the entropy rises from 2.66 (nonviscous) to 2.96 (η=20 MeV/fm^{2}c - see Figure III.11) to 3.17 (η=60 MeV/fm^{2}c), but still remains constant after 20 fm/c [Cse 80ab, Stö 84, Buc 84a]. However, note that when the bulk viscosity is included (η = 20 and ξ = 20), then the entropy does not saturate; the bulk viscosity causes a non-isentropic expansion because of the divergence in the volume.

A method that would allow the determination of the entropy from experiment could yield important insight into the state of the matter in the moment of highest compression and excitation during the collision. Unfortunately, such an experimental determination is model dependent. Note that there are other approaches to calculating the entropy if one does have fragments. In particular, the formula [Sie 79, Ber 81]

$$S = 3.95 - \ln \frac{d_{like}}{p_{like}} \qquad (3)$$

has been used. This follows from the Sackur-Tetrode relation in a kinetic model for ideal gases where

$$d_{like} = d + 1.5\ (t + {}^3He) + 3\ \alpha \qquad (4)$$

and

$$p_{like} = p + d + t + 2({}^3He + \alpha) \qquad (5)$$

This formula (3) has been used to extract entropy values from the inclusive fragment data [Nag 81] and in cascade models [Ton 83]. The experimental values of S vary from 5 - 5.5 for C + C, Ne + NaF, and Ar + KCl and are thus larger than the shock model or fluid dynamic values. A more sophisticated calculation using an approximation of (2) [Rem 85b] on the experimental Ne (400 and 2100 MeV/nucleon) + NaF central

collision data [Nag 81] gives entropy values of 3.69 and 5.40 respectively; the nucleons only contribute 2.54 and 3.83 units respectively. By summing over the different fragments in (2), contributions from pions and light fragments are incorporated.

For Ar (42-137 MeV/nucleon) + Au, one finds S = 2 - 2.4 using a quantum statistical model and S = 4 - 6 using the d/p formula [Jac 83]. The QSM gives S = 4.0 for mid-rapidity fragments (participants) and S = 1.8 for heavy fragments (spectators) [Jac 84] from 30 MeV/nucleon to 350 GeV/nucleon. The d/p ratios tend to give higher S than the thermodynamic formula I.19. In fact, the d/p formula is only valid for high T [Hah 85b]. Recently extracted values from Nb + Nb high multiplicity data are 3.4 and 3.7 for 400 and 650 MeV/nucleon and for Ca + Ca 3.9 and 4.3 at 400 and 1050 MeV/nucleon. These values are from a full quantum statistical calculation from fitting the observed asymptotic d/p, t/p, He/p, and α/p values [Hah 85b]; they also agree with values extracted using an approximation to (2) [Rem 85b] and summing over the different fragment types [Hah 85b]. This quantum statistical model includes the decay of the particle unstable excited nuclei [Stö 84],

$$A^{*} \rightarrow (A-1) + p, \qquad (6)$$

which are important especially at intermediate and low energies [Stö 84].

Recent data from the GSI/LBL Plastic Ball collaboration have made clear that experimentally the d to p ratio depends strongly on the multiplicity of the event in which the particles are emitted: in peripheral collisions, which dominate the inclusive particle spectra,

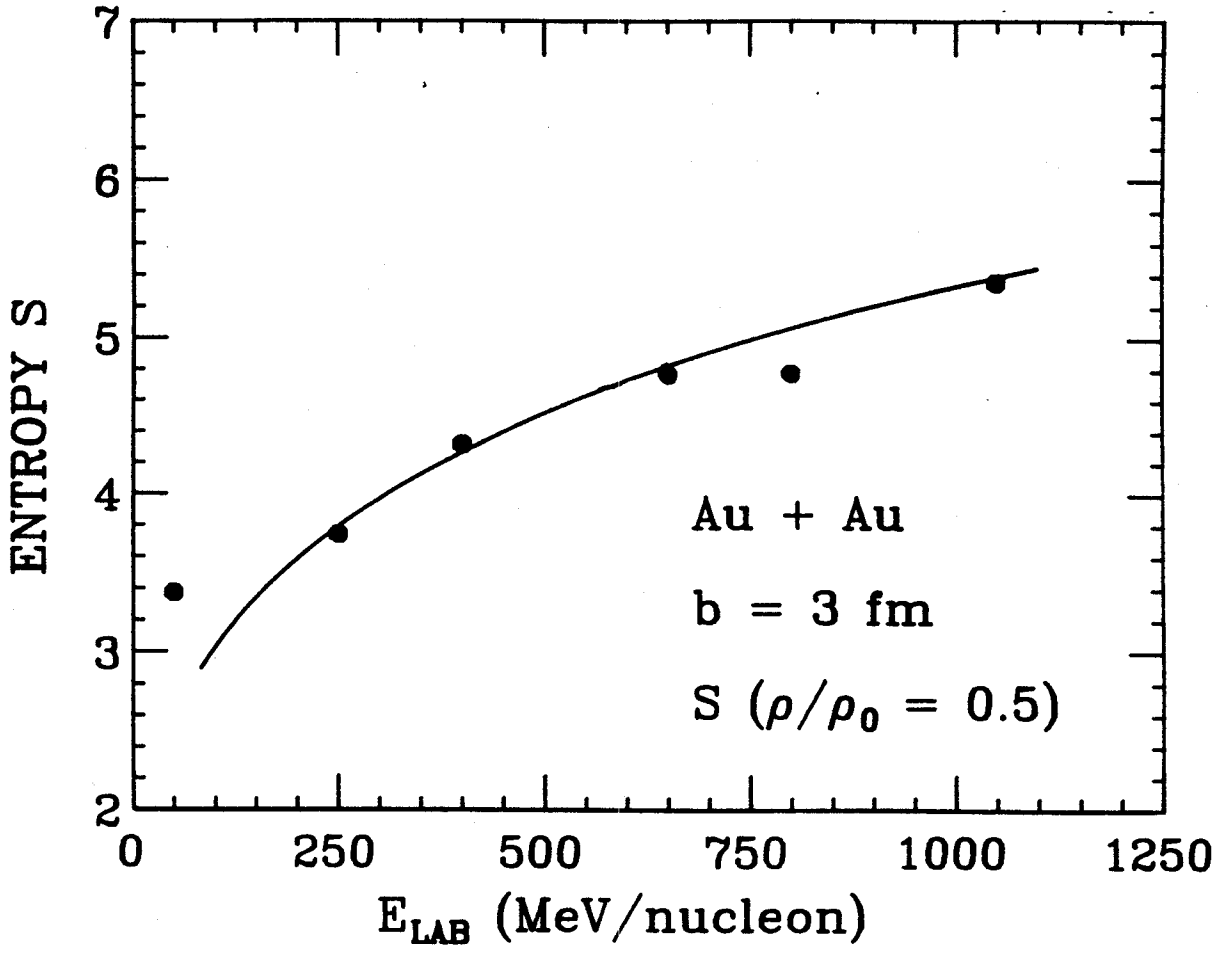

Figure III.12 Entropy for Au + Au at b = 3 fm versus energy extracted by the non-interacting fermion formula in the VUU model.

the ratio is much smaller than in central collisions with high multiplicity [Dos 85].

One may also try in the VUU model to extract the energy dependence of the entropy values from (2) at the time when the density in a central region is 0.5 ρ_0 or from (3) by clustering the nucleons into fragments (see below) (Figure III.12). The shock model values are somewhat less than the values extracted from (2) for Au + Au; this may be due to the finite impact parameter b = 3 fm [Cug 84b] and the fact that fragments have not been incorporated into the calculation. The values extracted from the d/p formula after a six dimensional coalescence are S ≈ 5, although the constancy with energy may be an artifact of the chosen half density time. These VUU results are meant to be only qualitative.

3. Equilibration

What is the effect of collisions in a heavy ion reaction? For p + A reactions, the mean time between collisions is relatively long and there is little multiple scattering of other than the projectile; so it is questionable whether thermal or chemical equilibrium can be established [Boa 85a]. The VUU model has been used to study this question for nucleus-nucleus collisions. In particular, the system Ar + Ca has been studied in the mean field approximation without two body collisions [Kru 85b], thus mimicking TDHF by solving the Vlasov equation.

The lack of two body collisions results in strongly forward peaked angular distributions, in qualitative agreement with 3D TDHF calculations [Stö 80a, 81a] in this energy regime. The top of Figure III.13 shows the initial state in momentum space for Ar (137 MeV/N) +

Ca; note that at this energy the Fermi spheres of target and projectile nuclei are well separated. The Ar projectile moves in the positive z-direction, while the Ca target moves in the negative z-direction in this center of mass frame. The middle and bottom of Figure III.13 show the final state of this reaction as obtained in this approach without and with the Uehling-Uhlenbeck collision term. Note that the momentum space distribution is practically unchanged in the mean field calculation--equilibration of the momenta is not observed--while the inclusion of the Uehling-Uhlenbeck collision term results in strong equilibration: the isotropy in the bottom of Figure III.13 is indicative of substantial thermalization.

A convenient way to compare momentum distributions is to use the ratio of transverse to longitudinal momenta

$$R = 2/\pi \; \Sigma \; p_{\perp} / \Sigma \; p_{||} \; , \qquad (7)$$

where $p_{\perp}$ and $p_{||}$ are the momenta perpendicular to and parallel to the beam. For an isotropically expanding system, one finds R = 1 in the center of mass frame [Str 83]. Comparing the ratio of final to initial R values, one finds 1.08 for the mean field only case and 2.05 for the mean field + collisions approach. At lower energies, the difference is not as dramatic; the initial R values are already high (but less than one) since the nuclei overlap more in momentum space--furthermore, most of the collisions are Pauli blocked. But the collision term always leads to increased isotropy. In configuration space, one finds transparency when the Vlasov equation is solved and a substantial degrading of the initial momentum occurs once the collision term is included [Kru 85b, Aic 85a].

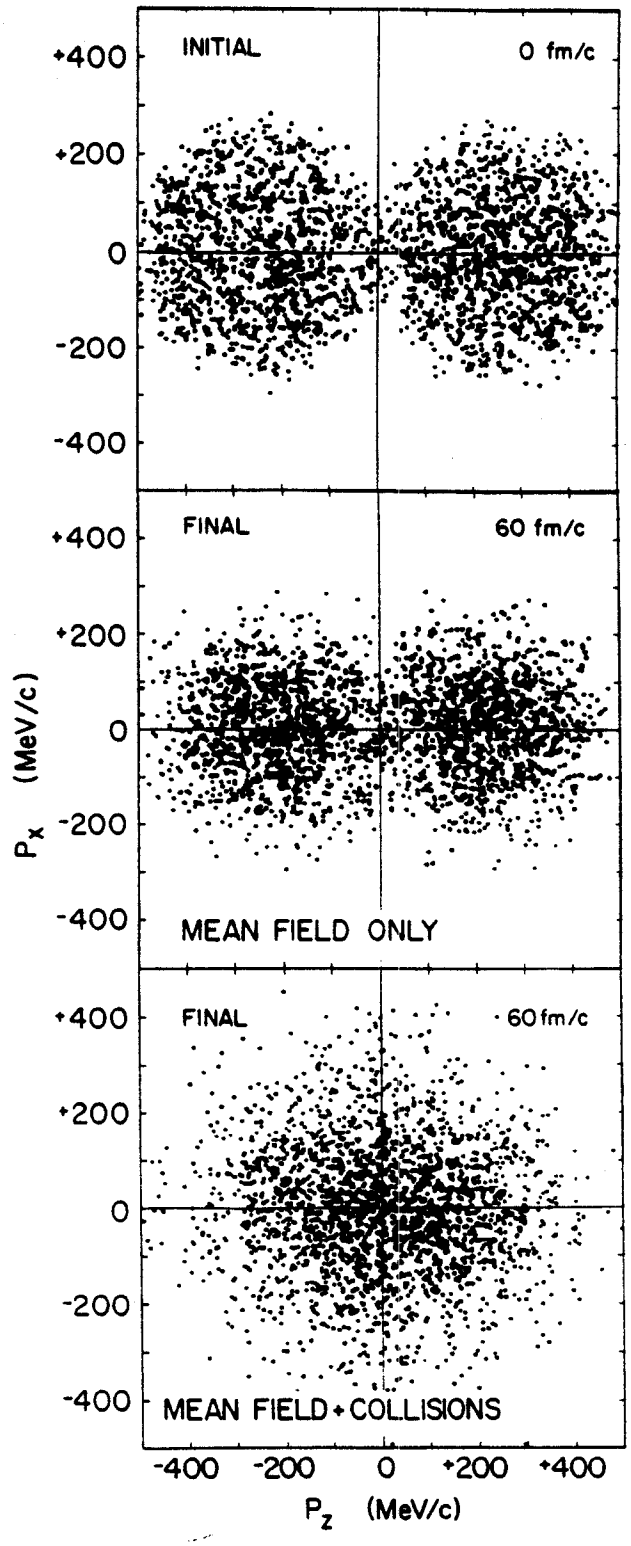

Figure III.13 The evolution in momentum space in the VUU theory of Ar (137 MeV/nucleon) + Ca at b = 0 fm. The collision term (bottom) results in substantial equilibration.

The time evolution in configuration space in the three dimensional TDHF [Stö 80a,81a] and Vlasov equation calculations [Aic 85a] is shown in Figure II.6 in the left and middle for the lighter system C (85 MeV/nucleon) + C at b = 1 fm . There is a very similar behavior in both the quantum mechanical and classical mean field theories: both calculations exhibit transparency and nearly identical small longitudinal and transverse momentum transfers. The lack of two body collisions results in strongly forward peaked angular distributions, in sharp contrast to the data in this energy regime [Kru 85b, Aic 85a]. Both theories predict that for central collisions of C + C the nuclei slip through each other and survive the reaction rather intact.

Just like for the Ar + Ca system [Kru 85b], the inclusion of the Uehling-Uhlenbeck collision integral changes this drastically (right of Figure II.6): each individual reaction can now be separated into two clearly distinct components. First, observe the slipped-through projectile- and target-like fragments, which now retain about 40% of the nucleons and less than 20% of the initial longitudinal c.m. momentum. As one sees in Figure III.14, these slipped-through residues contain mostly particles which have not scattered at all [Aic 85a].

The second component consists of the 60% of the nucleons which have undergone at least one nucleon-nucleon scattering and form a non-equilibrated mid-rapidity system with an almost isotropic emission pattern. At even higher energies, Ar (800 MeV/N) + Pb (see below), complete stopping of the projectile in the target is predicted [Mol 84b]. What then is the reason for the incomplete deceleration for the C + C system? At these low energies a rather large fraction of the attempted nucleon-nucleon collisions are forbidden by the Pauli blocking

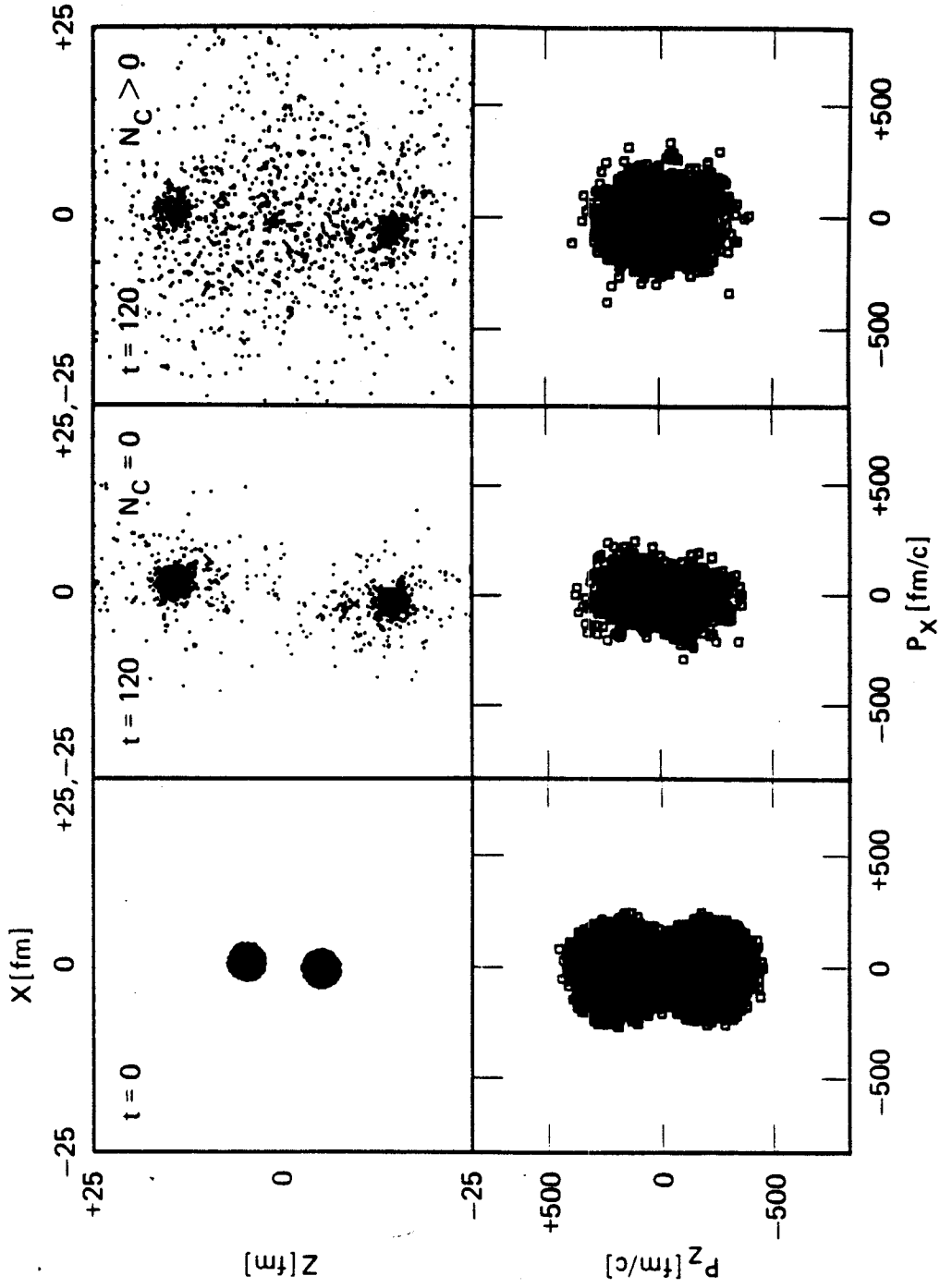

Figure III.14 Initial and final states in configuration and momentum space in the VUU theory for C (85 MeV/nucleon) + C at b = 1 fm. The nucleons which equilibrate are those that collide.

of the exit channels and the nucleon's mean free path is effectively longer as a result of the Pauli principle [Aic 85a]. Furthermore, the C + C system is rather small, hence the chances for a nucleon-nucleon collision to occur is smaller than in a bigger system.

At intermediate impact parameters, negative angle scattering is observed in both pure mean field approaches, and again the classical and the quantum approach agree remarkably well [Aic 85a]. Inclusion of the collision term results in less inward scattering. The midrapidity source is much less apparent; two slightly decelerated and excited residues survive the collision. The effect of the collision term is less dramatic at these larger impact parameters due to the smaller geometrical overlap of the nuclei, which reduces the number of nucleon-nucleon collisions.

Figure III.14 shows the reaction C (85 MeV/N) + C at b = 1 fm in more detail [Aic 85a]. The initial and the final distributions in configuration and momentum space are displayed. Particles which did not undergo any collision ($N_c = 0$) and scattered particles ($N_c > 0$) are distinguished between. The mid-rapidity region consists almost exclusively of scattered particles. The high momentum components of the initial momentum space distribution get most effectively depleted by collisions because for them the Pauli blocking is least effective. A collective deceleration of the projectile-like fragments is caused by the mean field. Those particles which have undergone collisions exhibit a nearly isotropic distribution in momentum space.

The dependence of the nuclear stopping power on the target mass has also been studied [Aic 85a] in the VUU approach. Central collisions of C (85 MeV/nucleon) projectiles with 6 different targets from C to Au have

been analyzed. The number of projectile nucleons undergoing at least one collision increases from about 60% for the C target to about 97% for the Au target. An almost complete stopping of the projectile in the target occurs for the heavier targets.

The number of projectile nucleons being emitted without having undergone a collision up to a time t = 160 fm/c is shown in Figure III.15 as a function of the target diameter D_t for 100 parallel ensembles [Aic 85a]. Observe the exponential fall-off with D_t of the number of un-collided nucleons. This can be reproduced by assuming that the mean free path of the nucleons in heavy ion collisions in this energy region is $\lambda \approx 2.6$ fm, which is larger than the mean free path estimated from classical kinetic theory, $\lambda_c = 1/\sigma = 1.5$ fm. This difference is mainly due to the effects of the Pauli-principle. Other counter-acting effects are the density increase in the collision (which decreases λ) and the finite deceleration due to the mean field (which also decreases λ). The extraction of the mean free path is important since at low energy it is related to the question of one body versus two body dissipation and at medium to high energy to the question of the validity of the NFD approximation; clearly, with such mean free paths, it can only be coincidental if nuclear fluid dynamics describes the correct physical observables especially for light systems where $\lambda \approx D_t$. Fluid dynamics may well be a reasonable approximation for the heaviest systems like Au + Au. This is another reason why one needs a tractable approach like VUU or NFM.

The momentum degradation for C + C at these low energies and central impact parameters is a good introduction to results obtained with the VUU method for Ar + Pb at 92, 400 and 800 MeV/nucleon

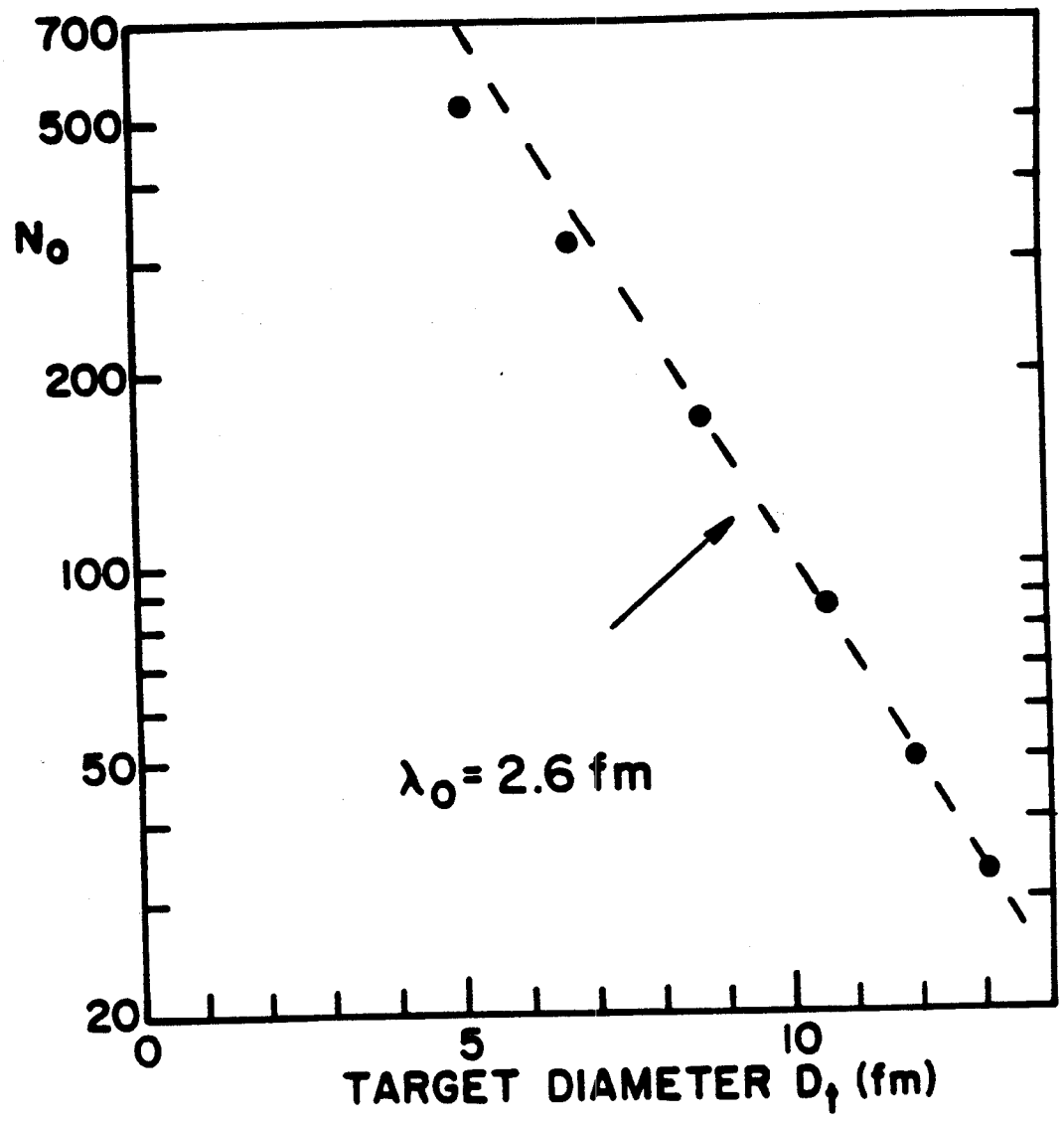

Figure III.15 The number of uncollided projectile nucleons in the VUU model emitted for C (85 MeV/nucleon) induced reactions is used to extract a mean free path.

bombarding energy [Mol 84b]. Let us examine the evolution of the single particle distribution function as calculated from the VUU approach for Ar (770 MeV/nucleon) + Pb collisions. In Figure III.16 and 17 one displays projections of the distribution function into configuration and momentum space for this system. It is remarkable how closely these figures resemble Figure II.13 and 14, calculated with the Nuclear Fluid Dynamic model [Gra 84]. In the VUU approach, the collision term is essential at both intermediate and high energies, as one expects intuitively; in NFD, the fluid assumption mocks up a collision term.

At low impact parameter the Ar projectile is completely consumed by the Pb target as well in configuration as in momentum space (see Figure III.16 and 17). The t=0 configuration space plots show the correct nucleon-nucleon center of momentum frame Lorentz length contraction by a factor $1/\gamma = .85$. In configuration space, for t = 10 fm/c, the squashed elliptical to octupole shape is an indication of the high density formed in these collisions. For example, at 1 fm impact parameter, the density within a sphere of radius 2 fm centered at the origin reaches 2.7 ρ_o at 5 fm/c; then, the density falls very rapidly - by 17 fm/c it is below the ground state value.

The directed sidewards flow of nucleons is easily seen in configuration space (Figure III.16) at b = 3 and 5 fm by the excess of nucleons in the quadrant with $x < 0$ and $z < 0$ with non-zero p_x as early as t = 20 fm/c. Spectator fragments are also observed, namely at b = 5 fm. The projectile is seen to not just shear off the target; it rather experiences a substantial transverse momentum transfer away from the region of high density - the bounce-off effect predicted earlier on the basis of nuclear fluid dynamics [Stö 80b, Buc 83a,84a]. Thus, simple

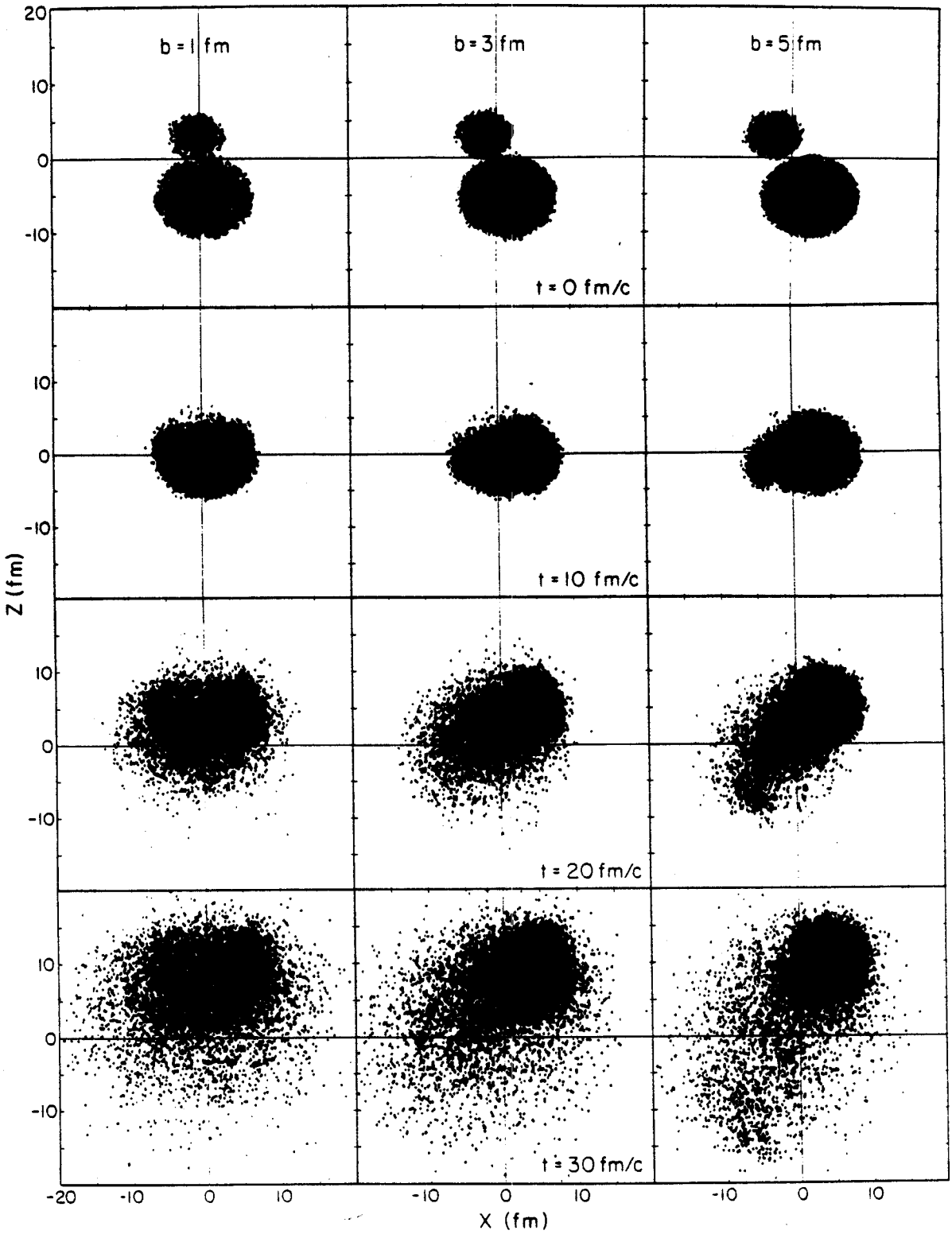

Figure III.16 In the VUU theory, the evolution of Ar (770 MeV/nucleon) + Pb in configuration space at b = 1, 3, and 5 fm.

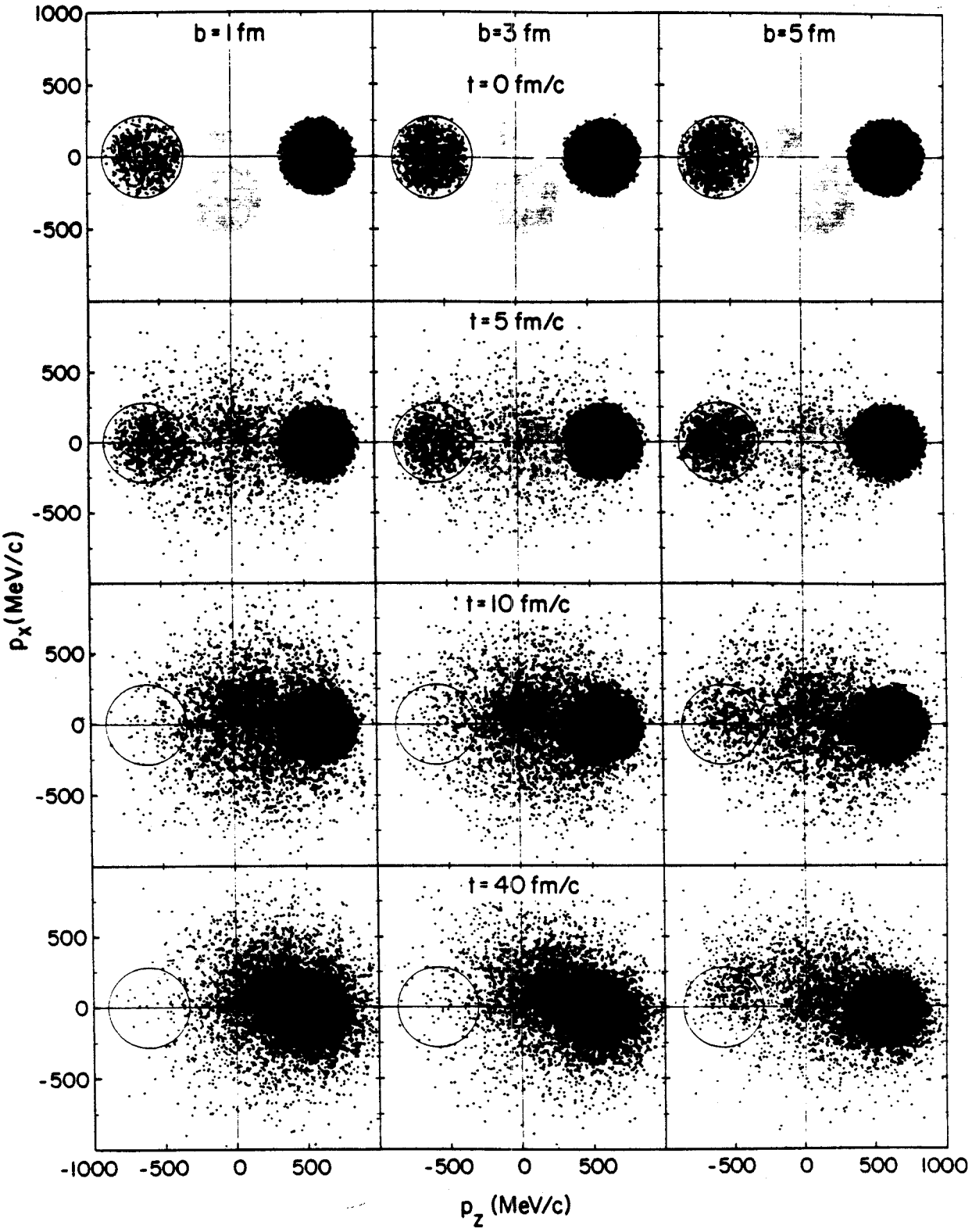

Figure III.17 The time development of Ar (770 MeV/nucleon) + Pb in momentum space in the VUU approach at various impact parameters.

geometric models [Wes 76, Gos 78] are only a very poor approximation to the rather complicated reaction dynamics illustrated here.

The momentum space evolution of the single particle distribution function displayed in Figure III.17 shows rapid equilibration at low impact parameters: the projectile sphere in momentum space is rapidly depopulated by two body collisions at b = 1 and 3 fm. At t = 5 fm/c substantial filling of the nucleon-nucleon center of momentum region is seen, indicating the formation of a participant zone. At t = 10 fm/c, there are practically no nucleons left in the originally densely populated projectile momentum sphere; almost all of the projectile nucleons have been scattered out of their initial momentum states. At b = 1 fm, this scattering has been with about equal probability into the positive and negative p_x direction. At b = 3 fm, a preference for the positive p_x direction can clearly be observed - this is due to the expansion of the compressed participant matter away from the high density repulsive interaction into the vacuum. At t = 40 fm/c the number of hard nucleon - nucleon collisions has become negligible, the final state in momentum space is closely approached. Secondary, tertiary, and higher order collisions of the participants have resulted in a further decrease of the number of fast particles and in a more diffuse momentum distribution in the projectile hemisphere, with a very pronounced visible sidewards flow at b = 3 fm.

At the intermediate impact parameter, b = 5 fm, the situation is even more complicated: since projectile and target exhibit only about half overlap, there are a substantial number of projectile nucleons or spectators which do not collide at all with the target nucleons. Hence there is only a partial depopulation of the projectile momentum sphere:

part of the projectile is stopped and forms the participant zone together with the struck nucleons from the target, while the projectile spectators move ahead with nearly their initial longitudinal momentum. The behavior of the participant nucleons is almost the same as at the lower impact parameters - equilibration is achieved rapidly ($t \approx 10$ fm/c) and sidewards flow is observed.

The projectile nucleons which have not undergone collisions, and thus the projectile-like fragments formed from them, exhibit a finite transverse momentum transfer into the same direction as the directed participant side splash. This bounce-off of the participants is a result of the repulsive interactions felt by the spectators in the vicinity of the compression zone. The simultaneous occurrence of this bounce off and the sidesplash has recently been observed experimentally in symmetric [Gus 84] and asymmetric [Ren 84] systems with high statistical confidence.

The equilibration at low impact parameter goes hand in hand with nuclear stopping; without the collision term, the nuclei are transparent. As a reference case, one may also solve the Vlasov equation by turning off the collision term; then the final momentum distribution looks very much like the initial one, as was seen above at lower energies (Figure III.13). The filling of the intermediate rapidity region is thus a consequence of the collision term.

An accessible experimental quantity is the longitudinal momentum (p_z) distribution in the laboratory frame. The multiplicity dependence of this quantity should give information on the nuclear stopping. Initially the Ar nuclei form a bump at beam momentum $p_z = 1430$ MeV/c, whereas the Pb nuclei are at rest. In the final state at the lower

impact parameter one sees evidence of nuclear stopping: there is no projectile remnant and the Pb target is accelerated. At the higher impact parameter, there is less stopping: one sees some projectile remnants and the target-like fragments are less accelerated [Mol 84b].

An analysis of these processes for symmetric systems has also been done. Figures III.1 and 2 show the evolution in momentum and configuration space of Nb (400 MeV/nucleon) + Nb collisions and Figures III.18 and 19 at 1050 MeV/nucleon in the VUU transport equation approach. The above discussion for Ar + Pb holds almost verbatim for the symmetric case. In particular, note how the depopulation of the projectile and target Fermi spheres depend on impact parameter. Of course, the reaction proceeds faster at the higher energy: the interaction time is smaller since the time for which a hot compressed interacting zone exists is shorter (see Figures III.3 and 5).

Note in the configuration plots that the collision term is not much less effective at the higher energy. Consider however that the final degree of isotropy is less at the higher energies:

Table III.5

	VUU				NFM	
	stiff			medm	hard	soft
	R					
E_{lab}	b= 1	b= 2	b= 3	b= 2	b= 2	
50	-	-	0.90	-	-	0.98
150	0.90	0.80	0.70	0.75	0.93	0.90
250	0.92	0.79	0.65	-	-	-
400	0.94	0.78	0.64	0.73	0.86	0.76
650	0.92	0.77	0.61	0.71	0.82	0.67

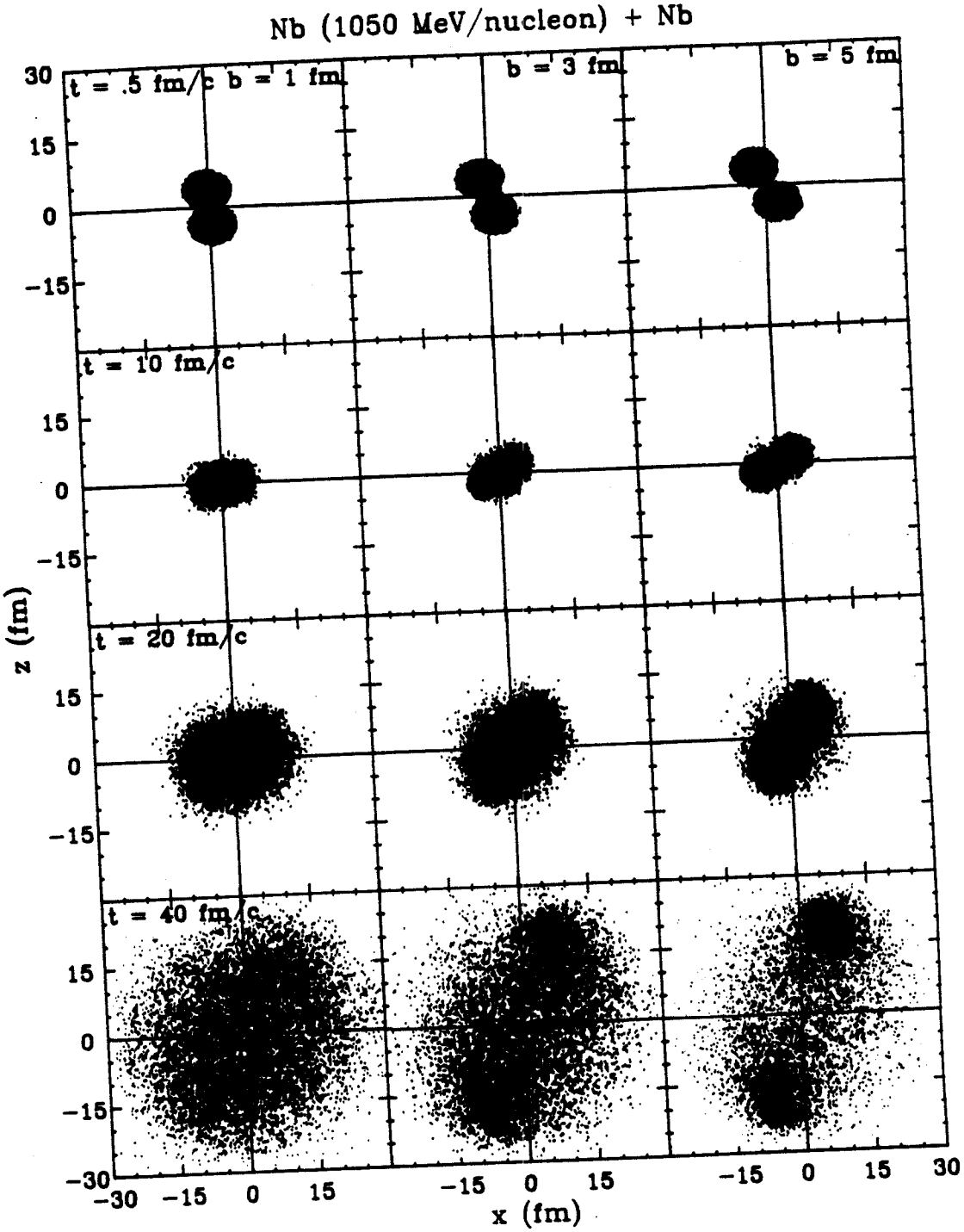

Figure III.18 Nb (1050 MeV/nucleon) + Nb at b = 1, 3, and 5 fm in configuration space as a function of time (VUU).

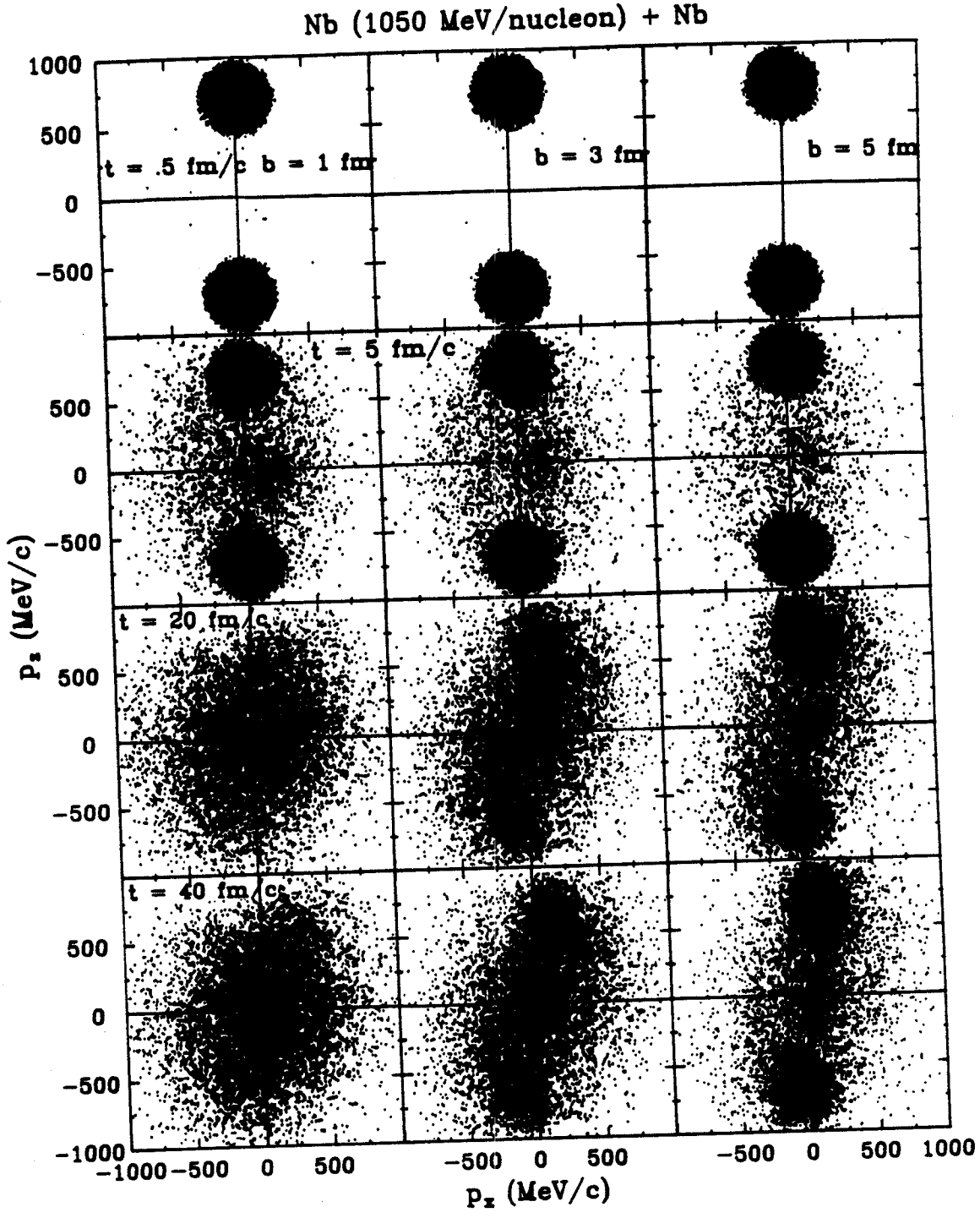

Figure III.19 Nb (1050 MeV/nucleon) + Nb in momentum space in the VUU approach.

800	0.91	0.75	0.61	-	-	-
1050	0.87	0.73	0.58	0.68	0.74	0.48

One thus sees how sensitive the degree of isotropy is to the stiffness of the EOS or the short range part of the nuclear force. The larger repulsion has the effect of causing greater isotropy. However, the decrease of R for the participants with energy in both VUU and NFM may be less because the spectators tend to have higher $p_{||}$ at the higher energies. This R calculated for all the protons is thus not a sensible measure of the degree of local equilibration of the participants.

However note that at a given energy, the degree of equilibration is, of course, the greatest for the most central impact parameters and this is reflected in the above R values. The collision term fills the mid-rapidity region in momentum space more strongly at the lower impact parameters. The softer equation of state results in less equilibration, as one would expect. Furthermore, turning off the Pauli blocking increases the R values by about 10%. The classical NFM generally results in a greater degree of isotropy.

4. Fragmentation and the Liquid-Gas Phase Transition

Clearly the questions of equilibration and entropy production are related to the fragmentation problem. The fragments and the pions are the only messengers from the reaction which are observed experimentally. They carry all the available information about the initial dense state of the system, modified by the ensuing expansion and any freeze-out. The physics of their formation is a topic of great current interest because of their possible relation to the entropy and the nuclear liquid gas phase transition [Stö 83, Cse 85]. Experimentally, it is found that a

great number of composites are produced in nucleus-nucleus collisions in the same range of energy and angles as the detected nucleons [San 80a, Lem 79]. Mainly peripheral collisions produce composites through evaporation since they result in excited projectile and target fragments [Gol 78]. The possibility of direct knock-out of pre-formed composite clusters would require the existence of very strong correlations and a low average momentum transfer [Aic 84c].

How does one handle fragments in a single nucleon model or in fluid dynamics? In practice, the hydrodynamic calculation is stopped when the average density is $\approx 0.5\rho_0$. Then the light fragment composition may be determined from a statistical model by assuming that the baryon number and energy per particle of the interacting nucleon fluid is conserved. The quantum statistical model [Gos 78, Sub 81, Stö 83, Hah 85b] used to calculate the fragment yields assumes that chemical equilibrium between the different fragments (p, n, d, t, ^{3}He and α's ...) is established at this late stage of the reaction. This assumption is supported by rate calculations for the appropriate densities and temperatures [Mek 78ab]; however, it is probably only marginally true at best.

The idea of final state interactions [But 63] between participants fits naturally into the VUU approach since these have to do with the rescattering contribution (participant-participant interaction). Physically, nucleons collide with each other to form composites. In this spirit, a generalized 6-dimensional coalescence model has been used to find the nucleons bound in clusters and prevent them from contributing to the proton cross sections [Kru 85b]. This coalescence

is especially important at medium energies, where a large fraction of the emitted protons are found to be bound in fragments.

In this coalescence scheme, a nucleon is part of a cluster, if it is within a configuration space distance r_0 from some other member of the cluster and within a momentum space distance p_0 from the center-of-momentum of the cluster. The sequential evaporation of protons from residual fragments is neglected: one would improve the calculation by including these. The generalized coalescence prescription has been used to calculate inclusive proton spectra from the primordial nucleon distribution with r_0 = 2-3 fm and p_0 = 200-300 MeV/c [Jac 85]. This approach gets further support from the agreement of the predicted fragment yields as a function of fragment mass to the experimental data for masses 1 - 14 [Jac 85].

Figure III.20 shows the comparison between calculated and measured proton spectra for 42 and 92 MeV/nucleon Ar + Ca. The calculated absolute cross sections and the slopes of the spectra agree reasonably well with the data. In contrast, a simple cascade simulation cannot reproduce the medium energy data [Kru 85b]. [Aic 85c] has shown that un-coalesced proton spectra from the VUU approach compare very well with experimental data if they are simply scaled.

The VUU approach may shed some light on the relative importance of direct N-N reactions versus phenomena involving many nucleons simultaneously by considering coincidence cross sections. Experimentally, the relative contributions of direct versus multiparticle interactions has been studied for C + C, Ar + KCl, and C + Pb at 800 MeV/nucleon [Tan 80], for C + C at 85 MeV/nucleon [Car 85], and recently for C + C at 40 MeV/nucleon [Fox 85]. When the ratio of in

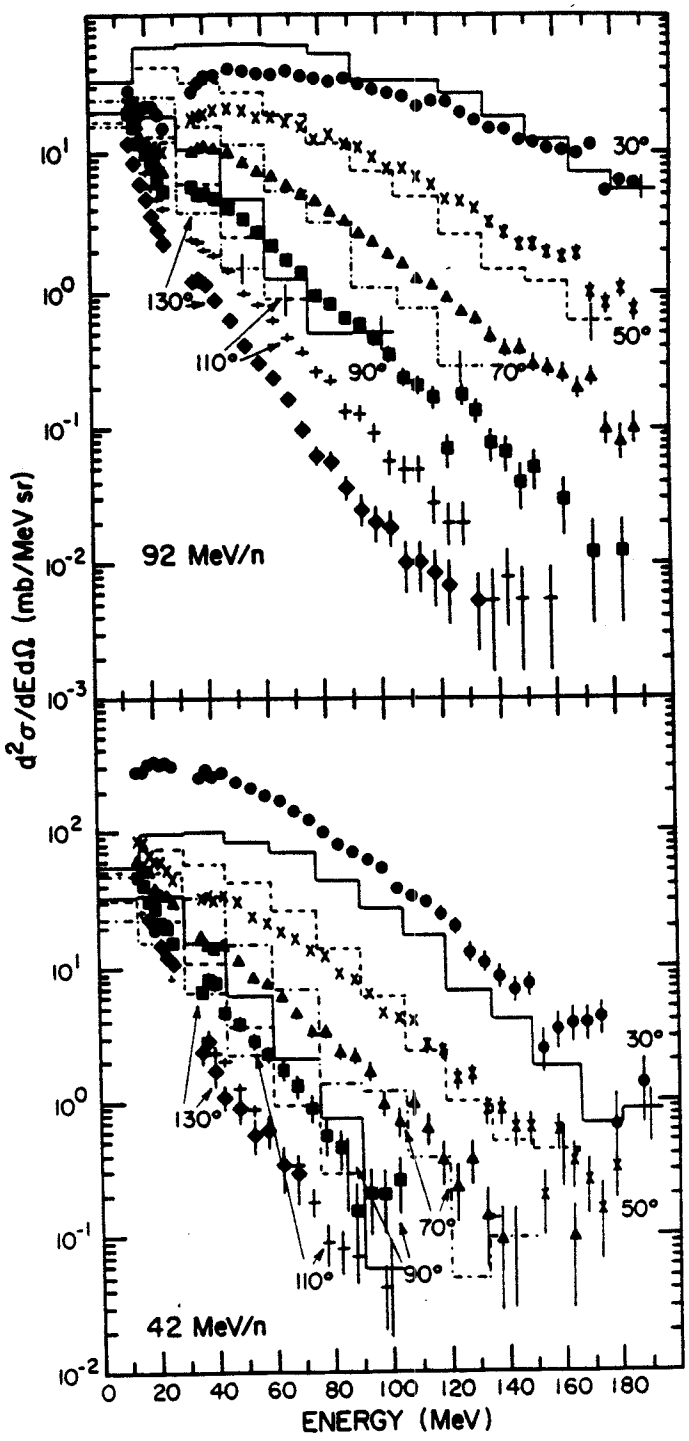

Figure III.20 Single particle inclusive proton spectra experimentally and theoretically (histograms) in the VUU theory for the Ar + Ca system.

to out-of-plane correlations was measured for the higher energy C + C cases, a significant enhancement was observed at energies and angles corresponding to quasi-elastic N-N scattering. For the heavier system Ar + KCl, similar measurements showed less enhancement. Using the reaction C + Pb the ratio was nearly constant as a function of the observed proton energy. At 40 MeV/nucleon, one might expect that the low multiplicity of protons might lead to a strong apparent direct component. On the other hand, the Fermi spheres of the projectile and target do overlap somewhat in momentum space possibly masking any quasi-elastic component. The experimental results and the VUU calculation support the latter conclusion (Figure III.21).

At these intermediate bombarding energies, $E_{lab} < 100$ MeV/nucleon, the temperatures are not high enough ($T < 20$ MeV) to cause substantial hadronization. However, another interesting phenomenon, a liquid-gas phase transition, has been predicted to occur in the late stages of the collisions when the density has dropped below normal nuclear matter density [Dan 79]. This is one of three different scenarios possible for the fragmentation of large nuclei by medium energy projectiles: statistical emission from a hot system (governed mainly by the available phase space) [Fai 82, 83, Fri 83ab], the passage of energetic nucleons from a hot spot (random shattering of the cold spectator matter) [Aic 84cd], expansion of the hot nucleus leading to lower densities and a liquid-vapor phase transition [Hir 84, Ber 83, Pan 84, Lop 84]. In this third scenario, which is considered here, the study of fragment yields offers a possibility to study the nuclear EOS at higher temperatures and lower densities than the ground state.

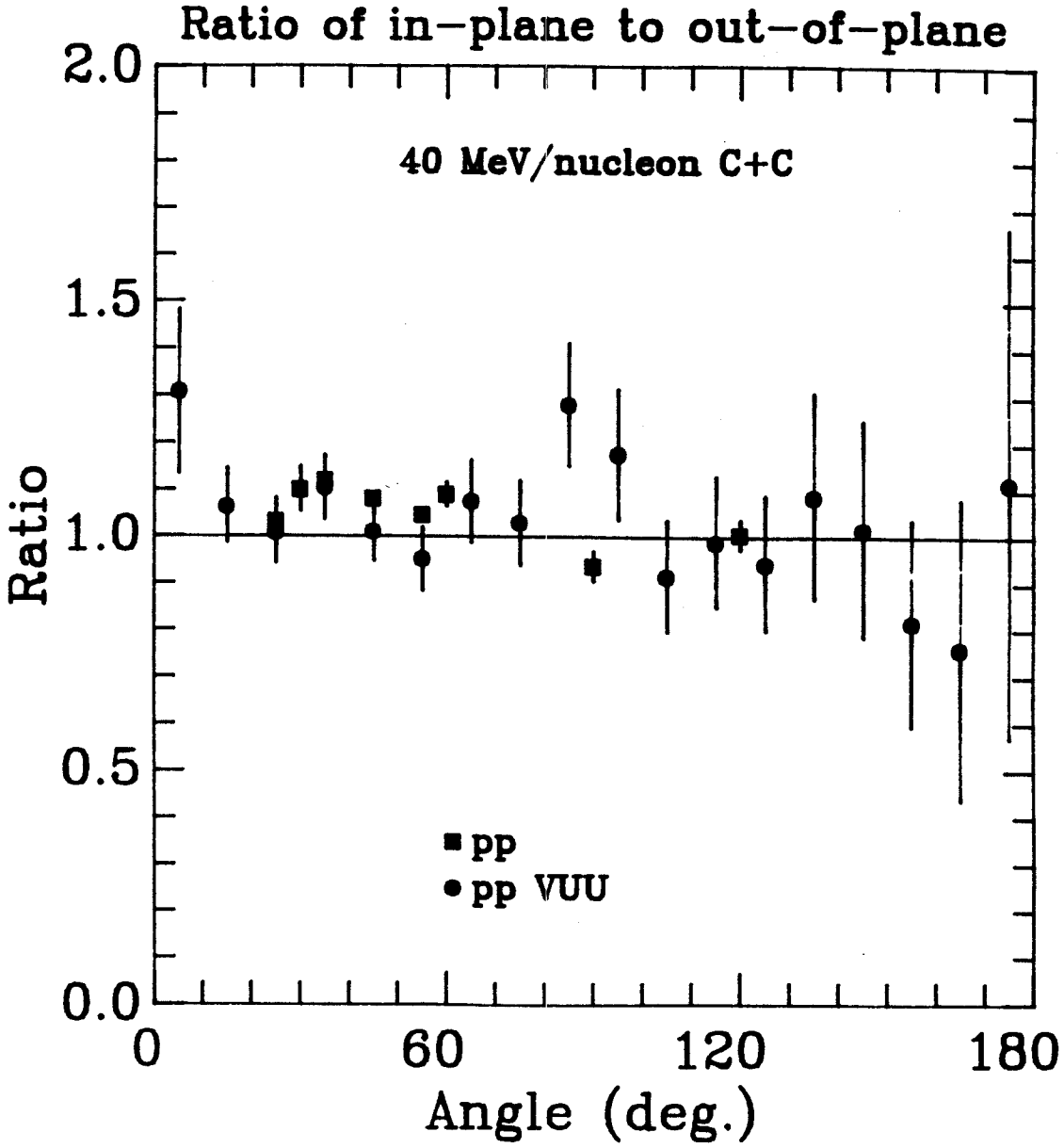

Figure III.21 The VUU approach explains well recent data which show the lack of a knockout component in a C (40 MeV/nucleon) + C in-plane/out-of-plane pp coincidence experiment.

The pressure diagram $P(\rho, T=\text{const})$ of infinite nuclear matter shown in Figure III.22 [Stö 83] exhibits the maximum-minimum structure typical for matter with long range attraction and short range repulsions (e.g. a van der Waals gas). This can be interpreted as a liquid-vapour phase transition in low density nuclear matter. The nuclear EOS exhibits a critical point at $\rho_c \approx 0.4\rho_0$, $T_c \approx 18$ MeV, and $S_c = 3$ [Stö 83]. It turns out that these values are not too sensitive to the details of the assumed interaction [Kap 84, Cse 85]. Experimental estimates for T_c for finite nuclei currently vary around 10 MeV [Pan 84]; from Ne (20 MeV/nucleon) + Au data, it has been estimated that T_c is as low as 5.0 MeV [Mac 85].

The liquid and the vapour phase can coexist in a well determined density regime once the temperature is less than the critical T_c (the shaded area in Figure II.22). Moderate T values may also be achieved in the late expansion stage at higher energies due to the cooling that is associated with expansion. The condition for thermodynamic stability of the two phase system is:

$$T_{liquid} = T_{gas}, \quad P_{liquid} = P_{gas}, \quad \mu_{liquid} = \mu_{gas}. \tag{8}$$

At the critical point, $P_c(\rho_c, T_c)$, the isothermal has a saddle point .

One can make a first step towards a realistic microscopic nuclear EOS by solving for thermal properties of finite nuclei within a mean field approximation using a realistic Hamiltonian in finite temperature Hartree Fock [Boz 85, Blo 58]. By studying the dynamics of the nuclear disassembly, one sees how the mass spectra and multiplicities vary with temperature to indicate a phase transition [Kno 84].

Unfortunately, the question of entropy is important also for this hypothetical phase transition. From rough calculations of the entropy

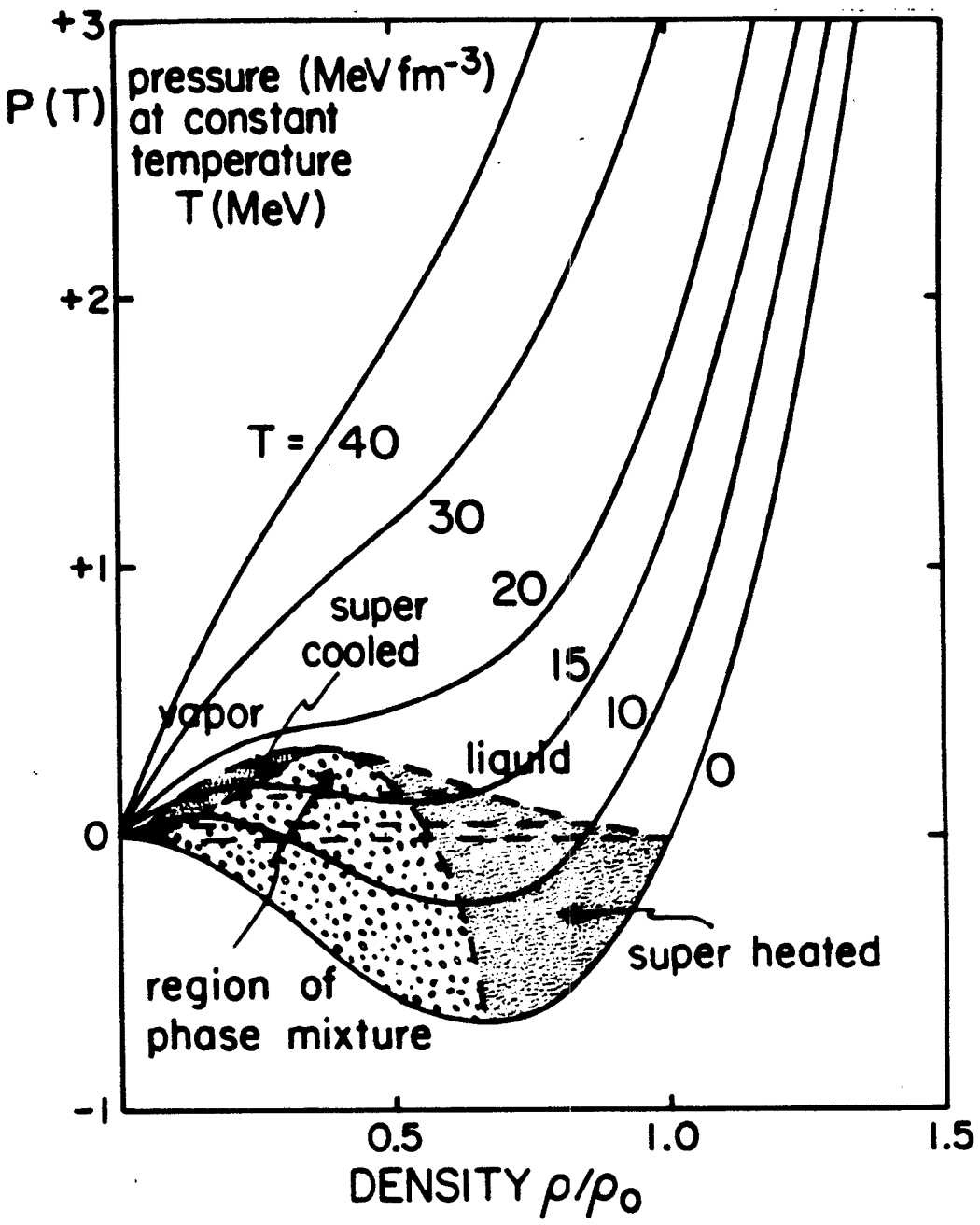

Figure III.22 The liquid-gas phase transition in nuclear matter in the pressure density plane.

from (2) in a cascade approach to p + A reactions, it is found that for the reaction path near the liquid gas phase transition, fragmentation more resembles bubble growth than droplet formation [Boa 85a]. Experimental p (500 MeV/nucleon) + A reactions give S ≈ 1.6 - 2.0 [Jac 84]. Using the cascade model, one finds S ≈ 0.15 - 0.5 in the 100-500 MeV/nucleon region [Boa 85a]. One can estimate a 0.3 increase in S due to the EOS and that the fragment surface and droplet kinetic motion also contribute 0.3 units [Boa 85a]. As has been seen above, the calculation or extraction of the entropy is non-trivial - thus such results are only preliminary.

The language of percolation theory is appropriate to discuss phase transitions [Sta 79]. Suppose one has an infinite lattice of sites which can be occupied or not. Physically, we have in mind a rough analogy to a lattice in phase space. Let p be the probability that a lattice site is occupied. Then there is a critical probability p_c analogous to a critical temperature T_c. For $p > p_c$, there is one infinite cluster; for $p < p_c$, no percolating network exists. Thus percolation is a phase transition since the system or lattice exhibits a qualitative change at a sharply defined parameter value. For physical phase transitions, $p-p_c$ is analogous to T_c-T. To describe the condensation process (nucleation) in a gas, one may group the gas molecules in a cluster or droplet [Fis 67, Vic 85]. The coalescence model which is applied to the final state is essentially percolation in phase space [Bau 85, Cam 85, Vic 85]; however, connections between a critical probability and any nuclear dynamics still need to be made.

One may thus look for qualitative changes of e.g. the central density time evolution in a dynamic model of the nuclear disassembly

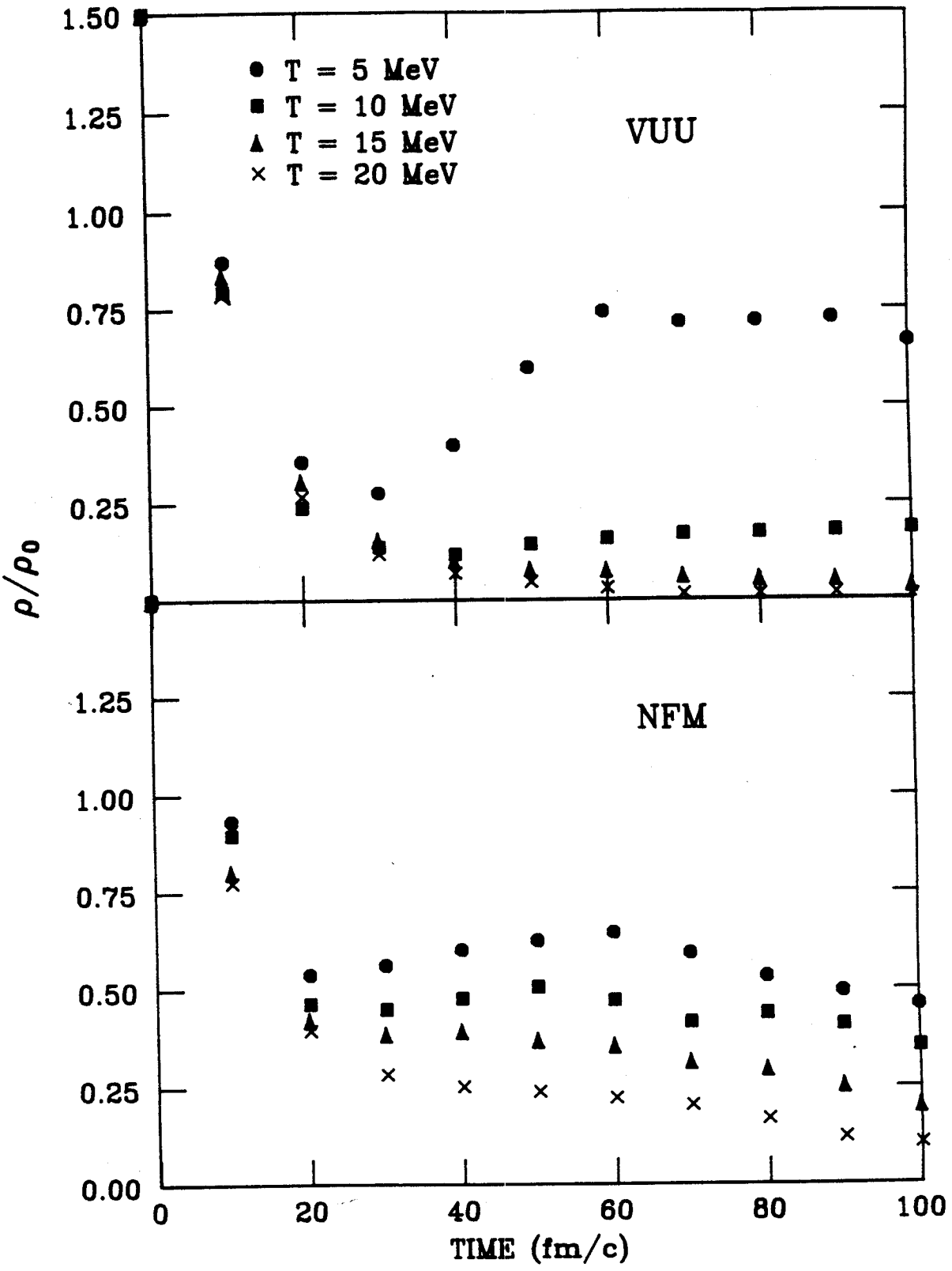

Figure III.23 Density around the origin for an expanding compressed (ρ/ρ_0 = 1.50) system at 5, 10, 15, and 20 MeV initial temperatures in the VUU and NFM models.

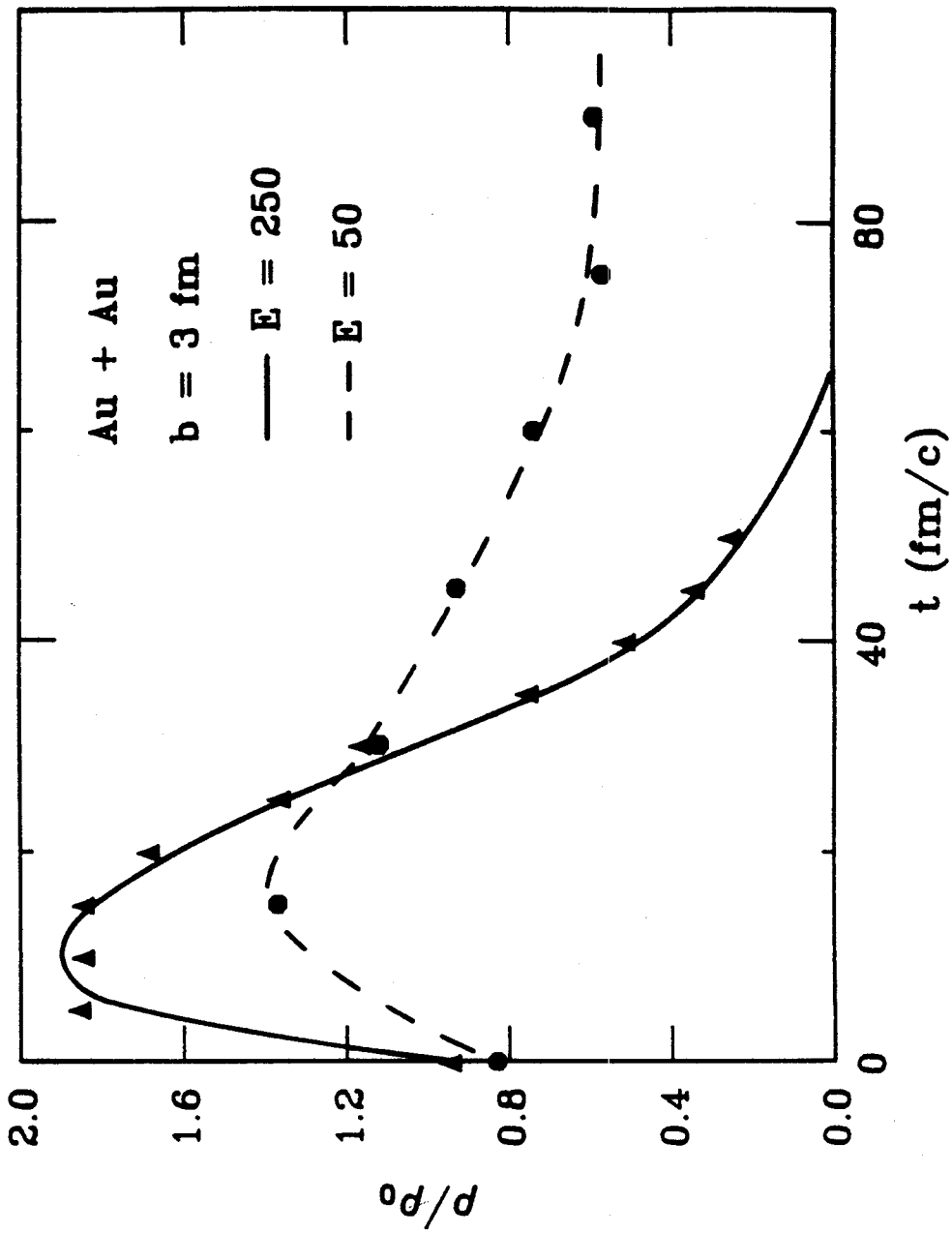

Figure III.24 Central density versus time for Au + Au at b = 3 fm and E = 50 MeV/nucleon versus 250 MeV/nucleon in the VUU model shows the same transition behaviour as in the previous figure.

[Vic 85]. Let us use the VUU and NFM models and initialize a hot (T = 5,10,15, and 20 MeV) compressed ($\rho/\rho_0 = 1.5$) system of 20 protons and 20 neutrons using a finite temperature Fermi gas distribution. Then allow the system to expand.

In Figure III.23, the central density for this hot expanding system at the different initial temperatures is shown. Note the sharp critical behaviour for $5 < T < 10$ MeV, especially for the VUU case (top). For the NFM model, the Coulomb force tends to reduce the change somewhat; the density at t = 60 fm/c increases by 7% when the Coulomb force is turned off. However, the NFM many nucleon force never allows the density to dip as low as quickly as it does in the VUU approach.

One may also look at nucleus-nucleus collisions for the same qualitative change. For Au + Au at 50 MeV/nucleon and 250 MeV/nucleon, the evolution of the central density in the VUU approach is shown in Figure III.24. Note again the sharp difference between the two temperatures. The inferred maximum temperatures are T = 19 and 35 MeV; these values are in fact overestimates since classically the T = 0 Fermi gas has an apparent temperature since there is non-zero kinetic energy. One must also realize that for E < 100 MeV/nucleon, one should more realistically base T on the relative population of states (which are not included in the VUU model); experimentally, one then finds temperatures of about 5 MeV at the lower energy [Poc 85].

5. Pion Production and the Equation of State

Let us now return to the high temperature and density domain and consider how pion yields can be used to study the nuclear equation of state [Stö 78, Dan 79, Hah 85a]. Stöcker, Scheid and Greiner first

proposed to measure the stiffness of the nuclear EOS via the pion multiplicities. The first exclusive measurements of the pion multiplicities as a function of the participant multiplicity [San 80b] have been used recently to extract the compressional energy via the proposed method [Hah 85a, Har 85] and via a substraction procedure, which used the cascade model (which does not employ any compressional energy) as input [Sto 82]. The data can only be reproduced if a very stiff compression potential is assumed (see Figure II.7). The assumption of immediate freeze-out in the high density stage in this procedure could overestimate the pion multiplicities [Stö 81c, 84]. However, cascade calculations indicate that the pion degree of freedom decouples from the baryonic 'heat bath' very early in the collision (see Figure III.27 for the VUU time dependence), namely in the high density stage [Cug 80, Sto 82].

Shown in Figure III.25 is the pion multiplicities calculated with the simple shock model [Hah 85a]. The linear equation of state with K_l = 1400 MeV and the quadratic one with K_q = 800 MeV give the best fit to the observed pion yields over the whole BEVALAC bombarding energy range. With respect to the large values of K, one must keep in mind that they are fitted for densities far away from normal nuclear matter density [Hah 85a].

To study thermodynamic variables and pion production on the microscopic level the VUU theory has been employed [Kru 85a]. Pions of different isospin are produced in this model via the production of Δ-resonances in elementary nucleon-nucleon collisions: thus both production and absorption mechanisms are treated microscopically. The VUU approach has been tested by turning off the Pauli blocking and mean

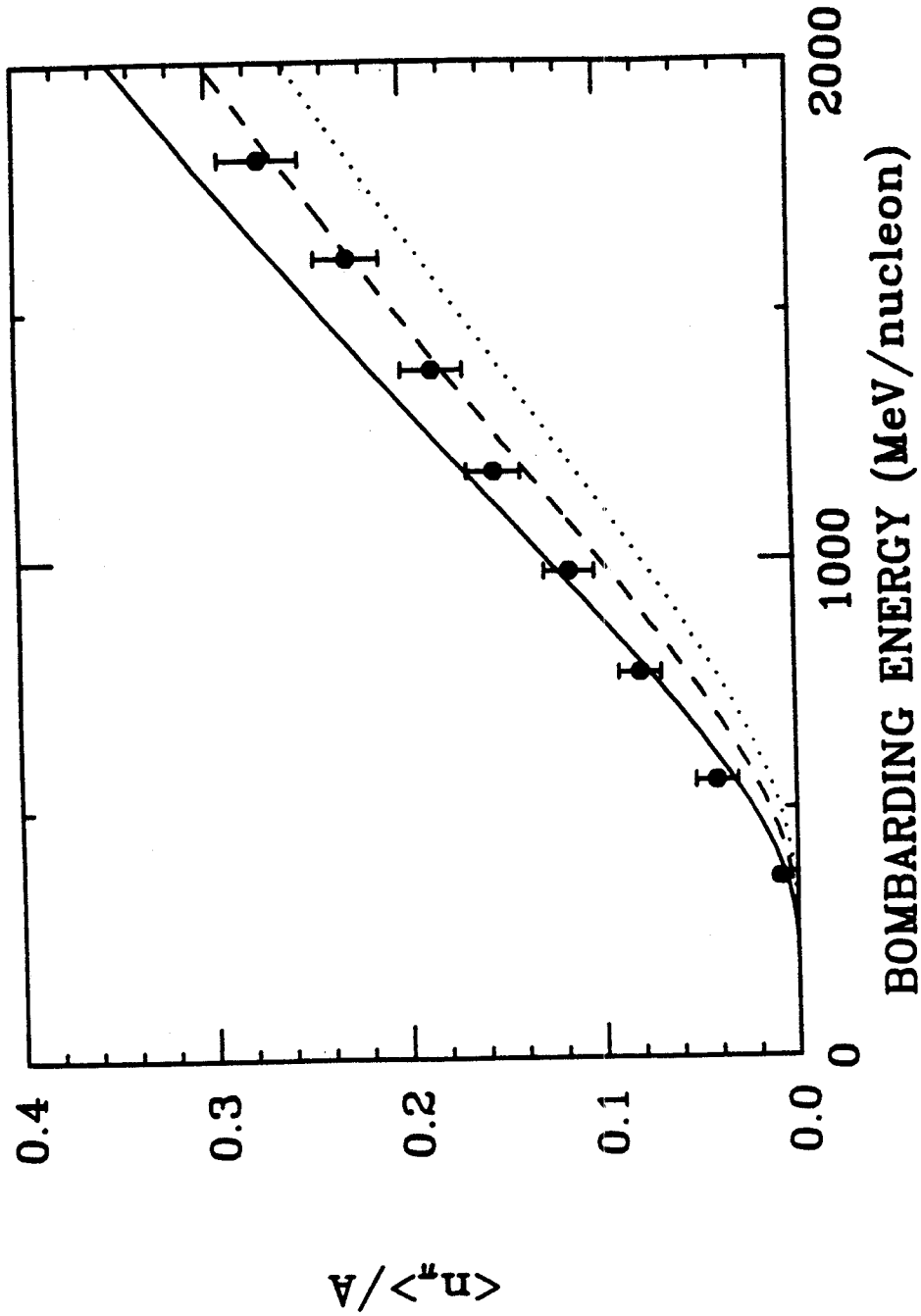

Figure III.25 Pion multiplicities per nucleon versus bombarding energy calculated in a simple shock model with the linear EOS and K_1= 1200, 1600, and 2000 MeV for the solid, dashed, and dotted lines, respectively.

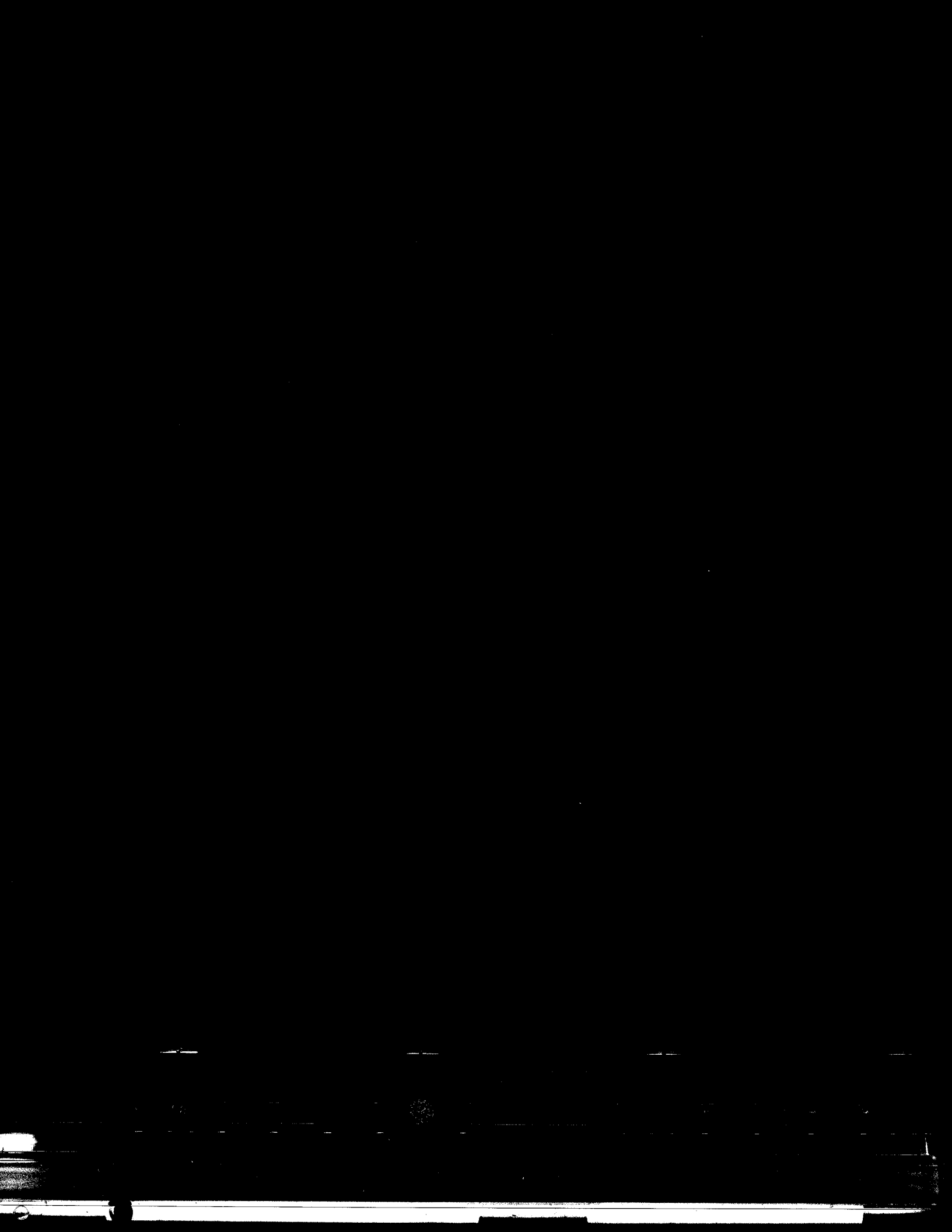

potential field. Then the parallel ensembles decouple and the test particles move on straight line trajectories until they scatter: the intranuclear cascade model is recovered. The pion yields calculated with the VUU method in this cascade mode agree quantitatively with results obtained with the conventional cascade [Cug 80, Yar 81]. Both results differ substantially from the data (Figure III.26).

If the nuclear compression energy and the Pauli blocking are introduced in the VUU method, the pion multiplicities change dramatically, as shown in Figure III.26 [Kru 85a]. Take the 360 MeV/nucleon case, for instance. The π^- yield is 1.05 in the cascade mode, but drops to 0.56 if the compression energy (stiff EOS) is included; the suggested large difference due to the nuclear matter EOS is observed. The pion yield drops further to 0.46 when the VUU Pauli blocking is applied. These results have been confirmed by an alternative VUU program [Aic 85c].

The pion multiplicities as calculated with the full VUU theory are also shown in Figure III.26 as a function of the bombarding energy. The VUU theory with stiff EOS plus phase space Pauli blocker compares well with the data whereas the cascade mode overestimates the data by factors > 2 at energies up to 1 GeV/nucleon. The required drop in the predicted pion yield is due to the transformation of kinetic energy into potential energy during the high density phase of the reaction as well as due to Pauli blocking. To check the sensitivity of the pion yields to the EOS the calculations have been repeated with the medium EOS. At 772 MeV/nucleon one finds $n_{\pi^-} = 2.45$ and 2.13 with the medium and the stiff EOS, respectively. At lower energies, statistical errors of 10% prevent an accurate assessment of the effect of the potential. At other

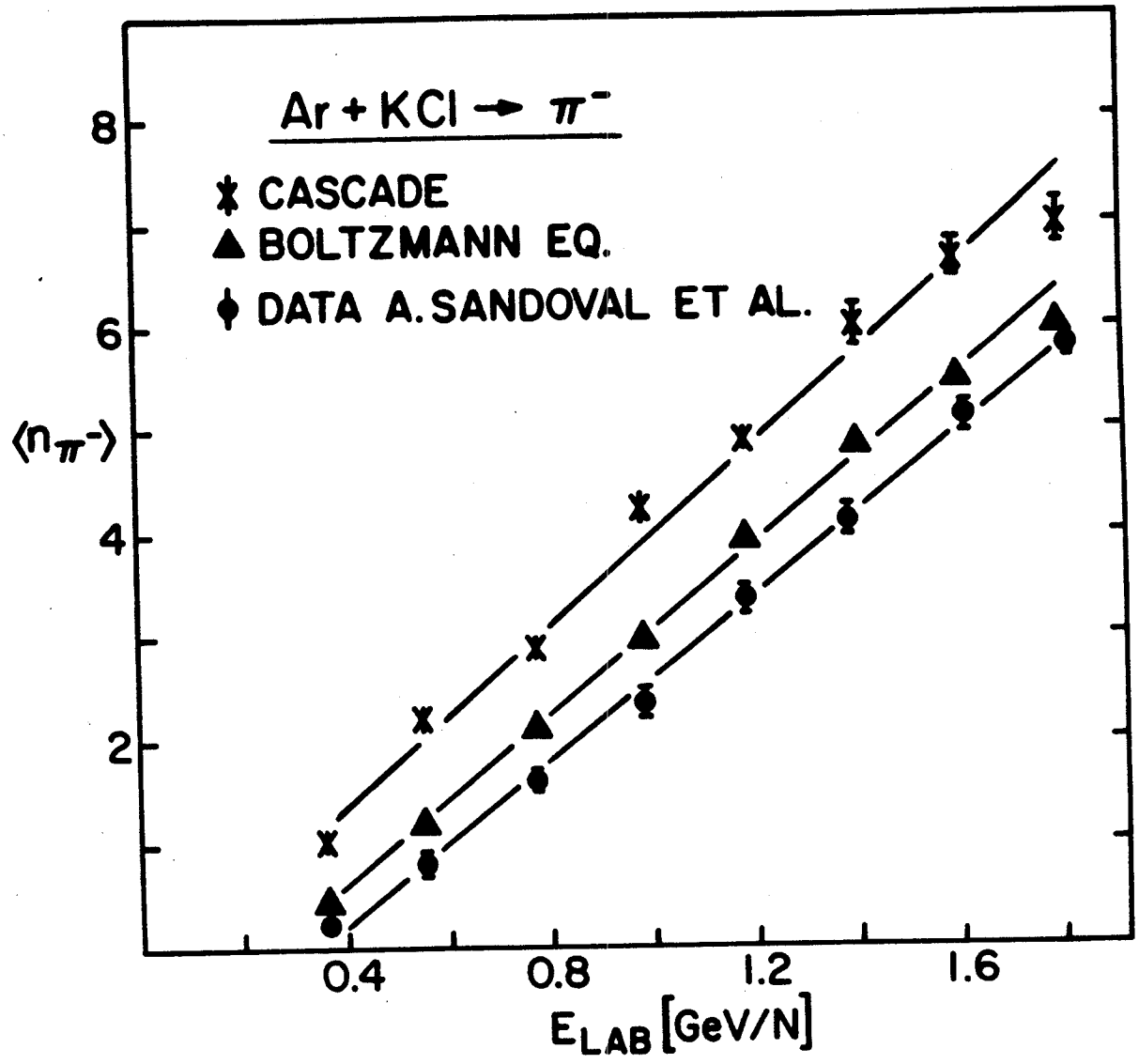

Figure III.26 Number of π^- versus energy for Ar + KCl in the cascade, VUU, and for the experimental data.

energies, where the errors are < 3%, the calculation with the medium EOS overestimates the yields systematically by about 10%.

The time dependence of the total pion multiplicity as calculated from the VUU approach for Nb (1050 MeV/nucleon) + Nb collisions at b = 3 fm is shown in Figure III.27. The pion number rises rapidly to a maximum value at t = 10 fm/c and drops then to a stable final value at 20 fm/c. There is a small but significant effect due to re-absorption until the pions escape the hot interaction zone. It should be emphasized that in this theory - as in the previously discussed cascade calculations - the pion yield approaches it's asymptotic value at a time, which nearly coincides with the moment of highest compression (Figure III.5) and temperature (Figure III.7), thus demonstrating that information on the high density stage can be obtained [Sto 82, Cug 82].

The bombarding energy dependence of the total pion multiplicity at b = 3 fm for Nb + Nb collisions is shown in Figure III.28. The agreement with the shock model values with the same stiff EOS

Table III.5

K_{lab}	n_{pi}^{med}	n_{pi}^{sti}
50	0.0	0.0
150	0.2	0.07
250	1.9	1.0
400	7.7	4.7
650	20.7	15.3
800	30.1	22.5
1050	43.7	33.9

is remarkable. In the VUU approach, there is a strong energy dependence (Figure III.28) as there was for Ar + KCl (Figure III.26). The decrease

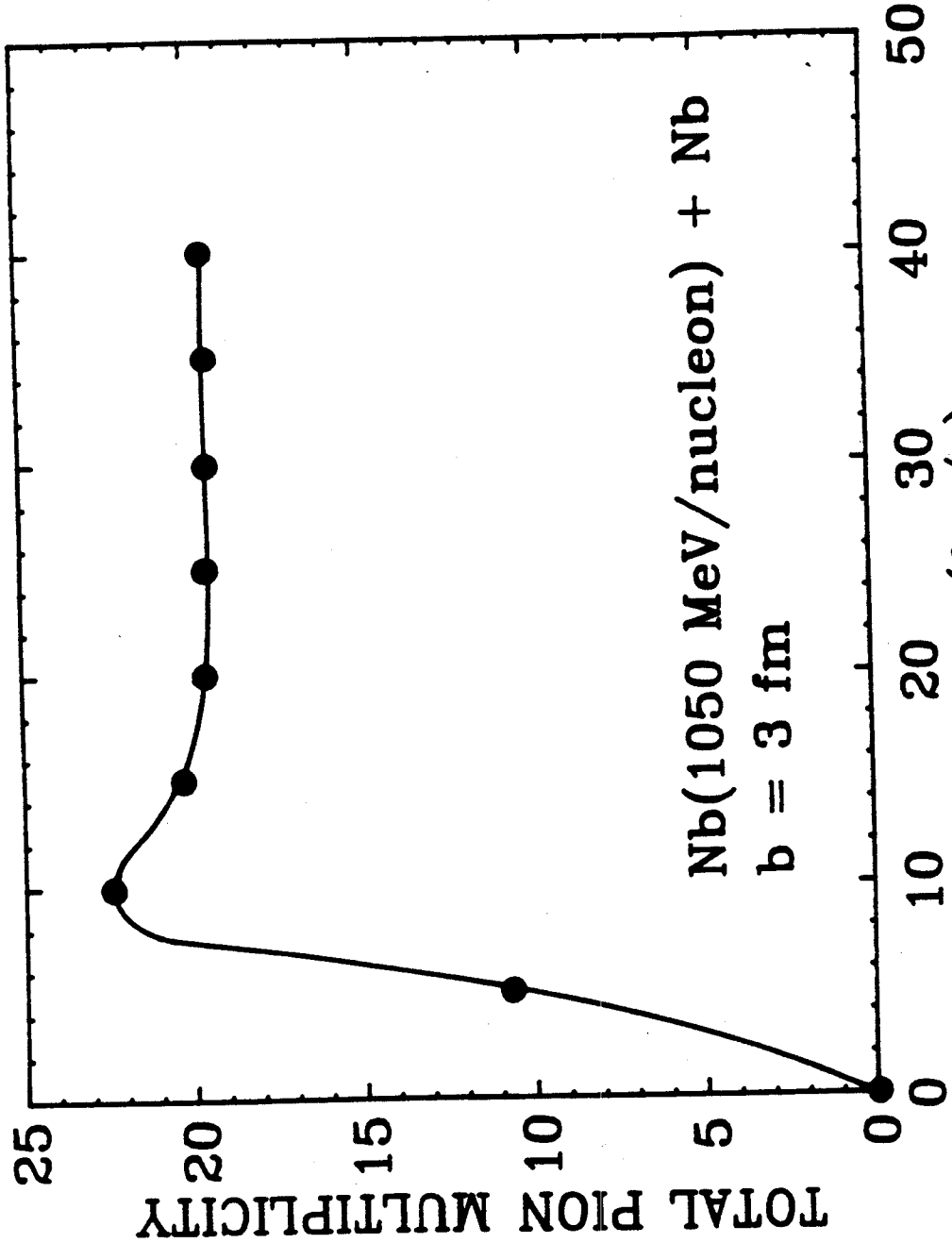

Figure III.27 The total pion multiplicity versus time in the VUU approach for Nb (1050 MeV/nucleon) + Nb at b = 3 fm; note the small but significant effect of re-absorption.

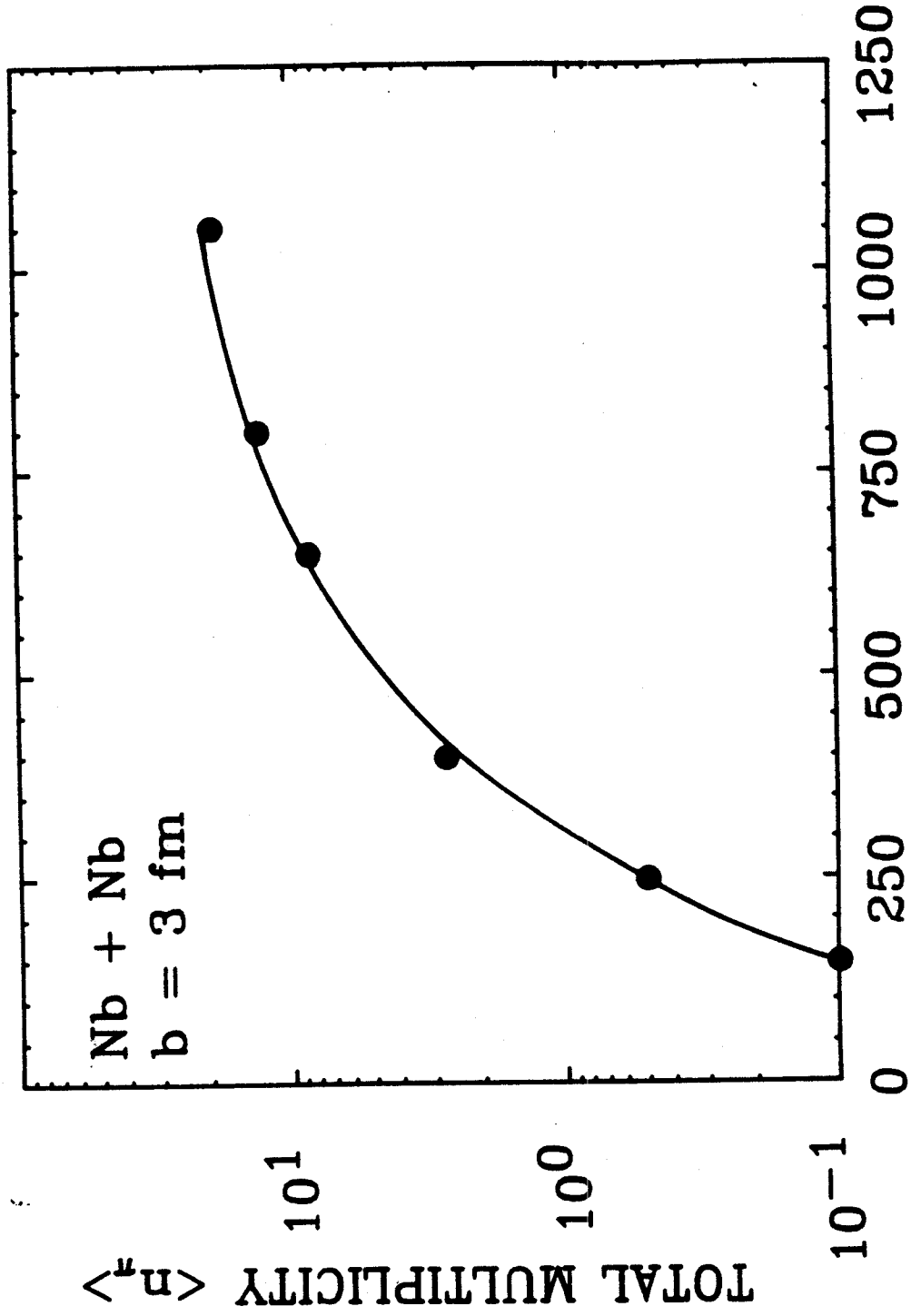

Figure III.28 Total pion multiplicity versus energy for Nb + Nb at b = 3 fm in the VUU theory.

of the total pion yield with impact parameter is almost linear (the decrease is faster when the impact parameters are nearly peripheral). This provides some justification for the usual extrapolation of multiplicity selected pion data to zero impact parameter. There is also a large effect due to atomic number: for Nb + Nb at 400 MeV/nucleon and b = 3 fm, we have n_π = 2.9, wheras for Au + Au n_π = 5.7. For the system Au + Au, the pion multiplicity for b = 3 fm collisions is shown in Figure III.29 for the different isospin channels in the final state. Note that the VUU theory predicts a distinct difference of the pion multiplicity with a charged pion ratio π^- / π^+ = 2 (Figure III.29) for the neutron rich Au + Au system.

The VUU approach has also been used to study pion production in asymmetric nucleus-nucleus collisions [Mol 84b]. How do asymmetric collisions compare with symmetric ones of the same atomic mass, when the same number of nucleons is involved? For the Ar (770 MeV/nucleon) + Pb case at b = 3 fm we obtain n_π = 9.9, which is less than the pion multiplicity for Nb + Nb at the same energy (n_π = 12.0) even though the united mass is greater for the asymmetric system. Thus asymmetric systems appear to be more efficient in absorbing pions; this is due to the large amount of cold spectator matter. For the Ar + Pb system, the total pion multiplicities vary from 10.6 at b = 1 fm to 3.7 at b = 7 fm; again, an almost linear relation with b is found. About 25-30% more pions are created when the Pauli blocking is turned off; equivalently, with the Pauli principle turned on, many collisions that would otherwise produce pions are forbidden by Pauli blocking.

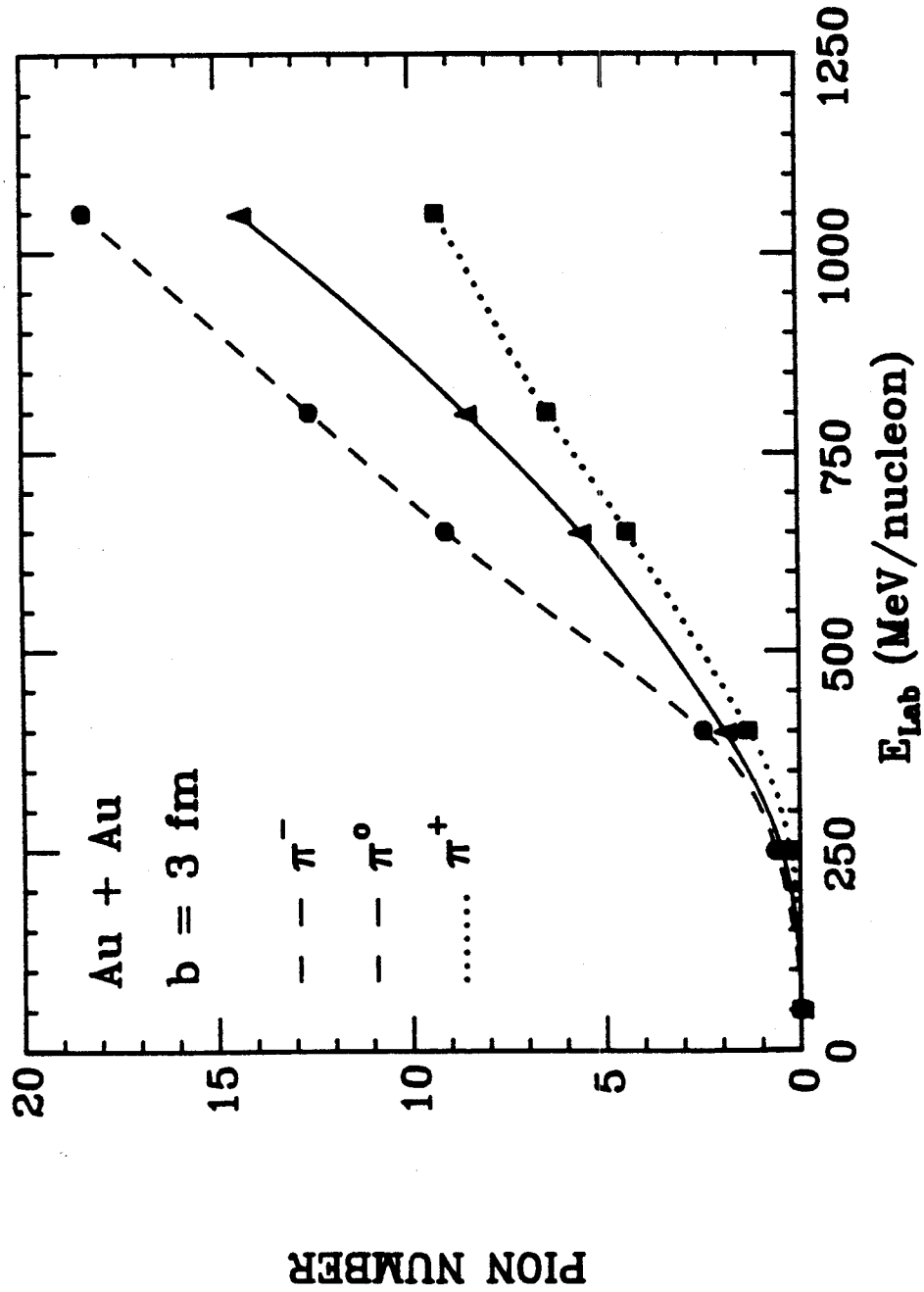

Figure III.29 VUU predictions for pion multiplicities of different isospin versus energy for Au + Au at b = 3 fm.

6. Collective Flow and the Equation of State

Little information about the details of the reaction mechanism can be extracted from comparison of the inclusive data to impact parameter averaged calculations. As has been seen, the pion yields are somewhat sensitive to the EOS. But for example, in spite of it's obvious presence at small impact parameters, no signatures of the collective sidewards flow predicted by the fluid dynamical calculations for central impact parameters seems to be visible in the calculated inclusive cross sections [Ams 75 and 77ab, Buc 83b]: only by triggering for nearly central collisions (high multiplicity selected events) can the sensitivity of the experiments be improved.

First fingerprints for collective flow have been found in early high multiplicity selected particle track detector experiments [Bau 75], which exhibit sidewards maxima in the angular distribution of He nuclei emitted in very asymmetric reactions, e.g. C + Ag. Also the double differential cross sections of light fragments (p,d,t), emitted from high multiplicity selected reactions of Ne + U, exhibits sidewards maxima, in accord with the longstanding predictions of the nuclear fluid dynamical model [Sch 74, Stö 80ab], while the intranuclear cascade model predicts forward peaking [Stö 81c,82b]. Hydrodynamic calculations without thermal breakup yield sidewards peaks which are too narrow [Stö 81c,82b]. The simplified two component and firestreak models give similar results as the three dimensional cascade calculations.

As the bombarding energy is increased, relativistic effects become increasingly important. Already at 400 MeV/nucleon the relativistic

treatment has a substantial influence on the spectra [Stö 80b] of protons, deuterons and tritons emitted from central collisions of Ne + U. The relativistic calculations [Gra 84] give much improved agreement with the data [Stö 80b] compared to the nonrelativistic calculations. The forward emission of particles is still strongly suppressed exhibiting sidewards maxima.

The qualitative features of ϕ-averaged (where ϕ is the azimuthal angle) distributions do not change dramatically with impact parameter, once violent collisions with $b \lesssim 4$ fm are selected. This means, unfortunately, that ϕ-averaged double differential cross sections are of limited value for obtaining information on details of the reaction dynamics and on the nuclear equation of state [Ber 78, Stö 80b].

With the cross sections discussed above the standard observable of nuclear collisions has been discussed. However, this observable describes more or less final state features of the reaction, i.e. the situation after the freeze-out of different clusters. Therefore a lot of different models like the fireball [Wes 76, Gos 78] or the cascade [Yar 79, Cug 80] reproduce at least some (i.e. inclusive) experimental results fairly well. But, the principal difference (e.g. stopping, compression, sidewards emission, bounce-off) between NFD or VUU and other models cannot be seen in the double differential inclusive spectra. Selection of high multiplicity events helps a little, but still more information is needed.

The first step in order to find messengers from the compression phase is to look for the quantitities which are integrated in the equations of motion. Such a quantity is the density, for example. But the density rises and falls off during the reaction. A density

distribution is not observable in experiments. The various momentum components also have very different histories during the collisions. P_z starts with a high value and decreases, whereas p_y and p_x are built up and saturate. On first glance it seems that only the direction of $\vec{p}$ could be interesting. In the experiment there is only a distinction between $p_{||}$ and $p_{\perp}$ possible, reducing the outcome of information. However, in each event there is a distinction between p_x and p_y if the reaction plane is chosen to be the xz-plane; more detailed information can be obtained by an event by event analysis where all the momenta of the fragments from a single nuclear collision are measured.

In an event by event analysis, the individual collisions are analyzed by diagonalizing the kinetic energy flow tensor [Gyu 82]

$$F_{ij} = \sum_{\nu} p_i(\nu)p_j(\nu)/2m(\nu) \tag{9}$$

or the momentum flow tensor:

$$P_{ij}=\sum_{\nu} [p_i(\nu)p_j(\nu)/|p(\nu)|]/\Sigma_{\nu}|p(\nu)| \tag{10}$$

where the sum is over all charged particles in a given event and (i,j) represent the Cartesian components (x,y,z). By diagonalizing this tensor, the flow angle θ_F is obtained for each event.

Let us now turn to the microscopic NFM and VUU theories and compare their event by event predictions to NFD, INC, and experiment. In the Newtonian Force Model [Bod 77, Wil 77, Mol 84a], for Nb (400 MeV/nucleon) + Nb at b = 3 fm, the computations are stopped at t = 30 fm/c, by which the flow results have become constant. The evolution of

a collision at b = 3 fm impact parameter was shown in Figure II.1. The resulting sidewards flow can clearly be seen. The demonstrated strong correlation between configuration space and momentum space can be attributed to the repulsive short range component (see below) of the nucleon-nucleon potential [Mol 84a].

The distribution of flow angles $dN/d\cos\theta_F$ is presented in Figure III.30 for various impact parameter intervals. The qualitative behavior of the flow pattern in the NFM model is as follows: the flow angle θ_F rises smoothly from 0° at large impact parameters to 90° at b=0 fm. Such large changes in the peak flow angle are not seen in models which lack compressional energy like the intranuclear cascade model [Mol 85b]. The contribution of zero impact parameter collisions to the observable cross sections is negligible. Thus a finite range of impact parameters is sampled to compute the distribution of the flow angle, $dN/d\cos\theta_F$, which is to be compared to the experimental data of the GSI/LBL collaboration (Figure III.30).

Figure III.31 shows the experimental data [Gus 84] for the Nb (400 MeV/nucleon) + Nb case discussed above, together with the predictions of the intranuclear cascade and fluid dynamical calculations [Buc 84b]. The data exhibit nonzero average flow angles once high multiplicity, i.e. small impact parameter collisions, are selected. This is in contrast to the intranuclear cascade calculation (using the Yariv Frankel and Cugnon approaches), which yields zero flow angles even at the highest multiplicities (also see Figure III.32 [Mol 85b]). The cascade model only exhibits a spurious flow effect when the nucleons are unbound. The microscopic NFM and macroscopic NFD models, on the other

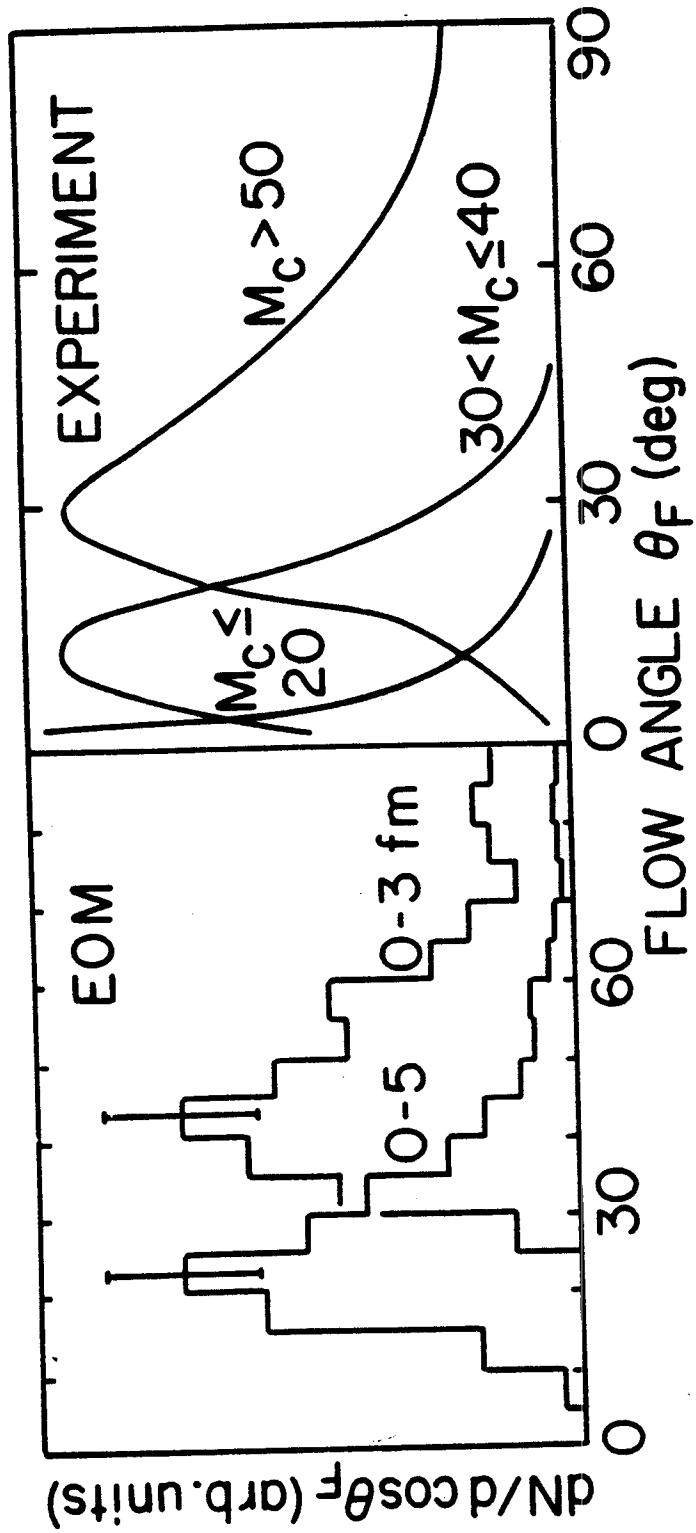

Figure III.30 Kinetic energy flow angle distributions for Nb (400 MeV/nucleon) + Nb in the NFM compared to the experimental data.

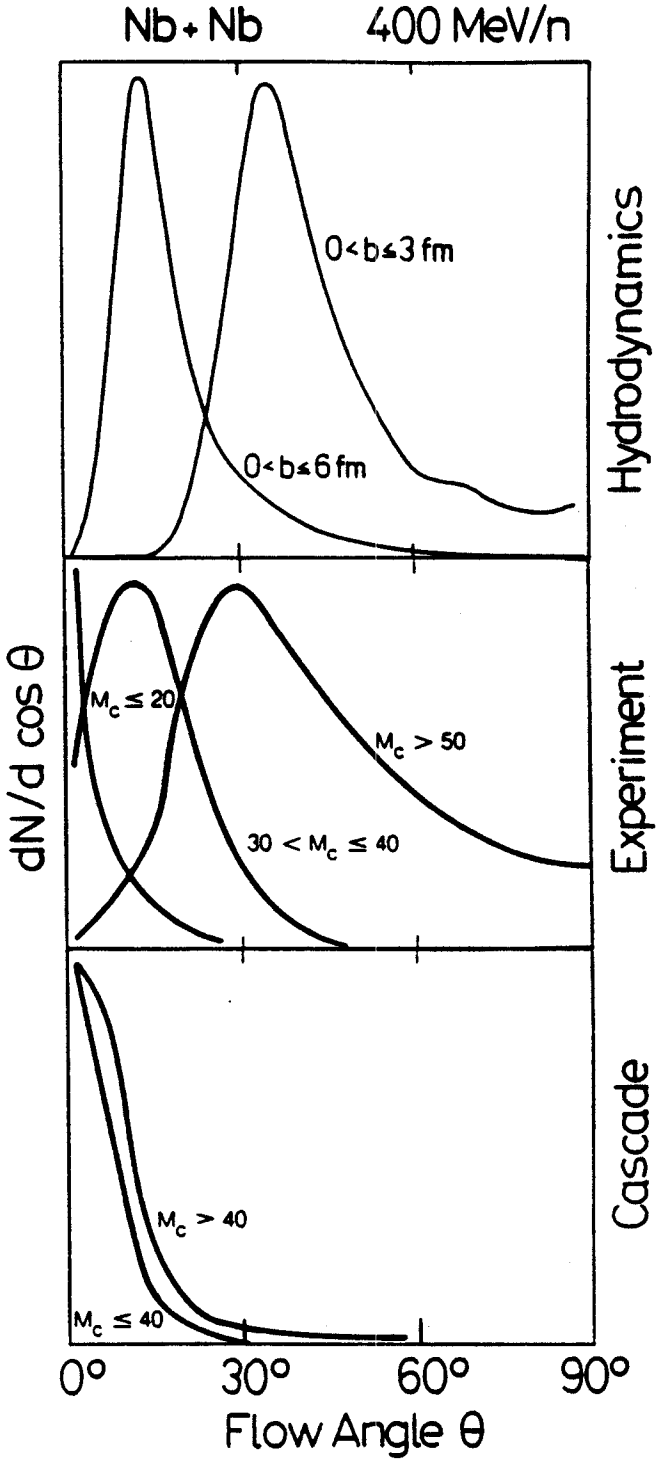

Figure III.31 Kinetic energy flow angle distributions for Nb (400 MeV/nucleon) + Nb from NFD, experiment, and the INC.

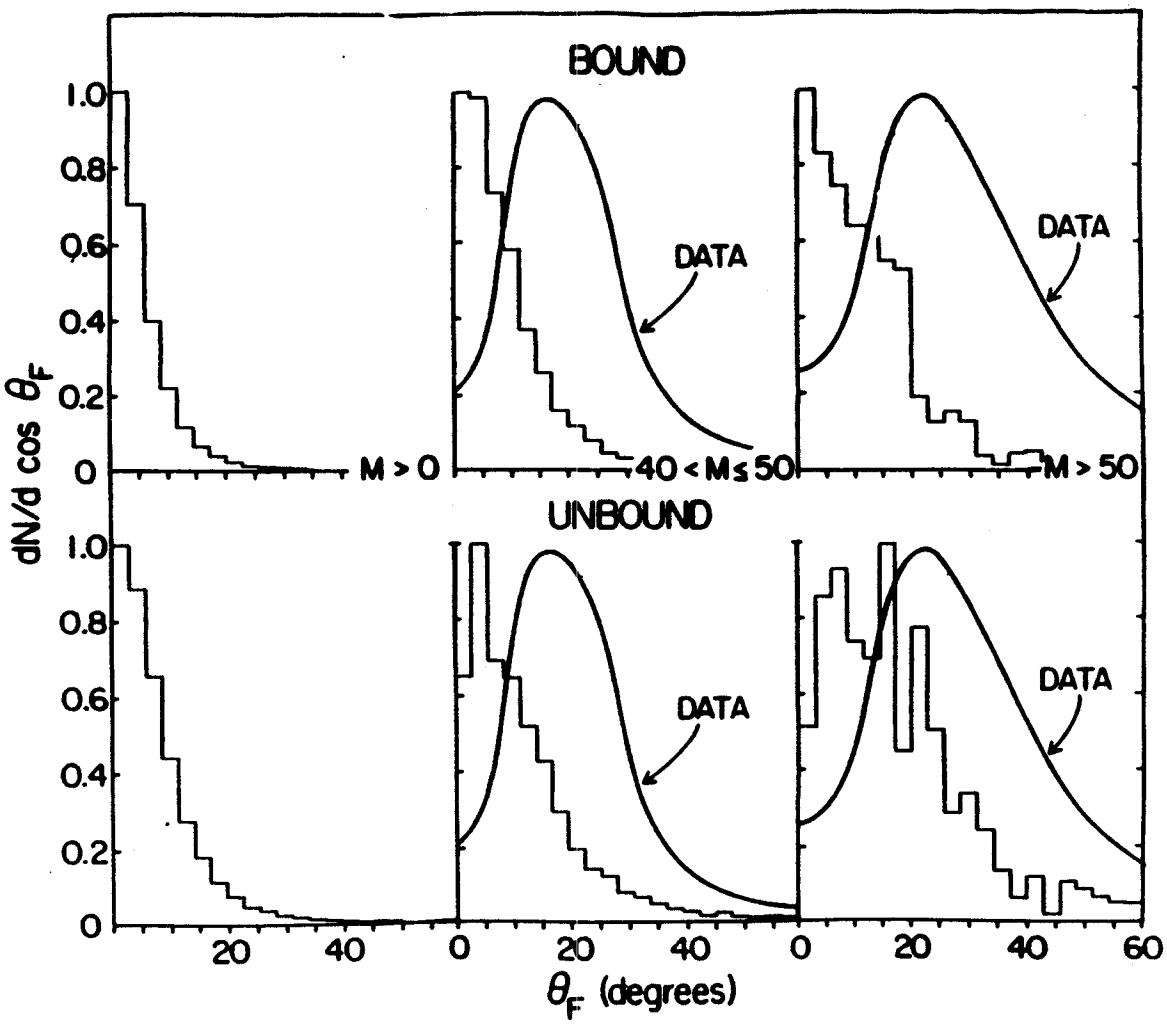

Figure III.32 The bound and unbound Cugnon cascade compared to the experimental data for Nb (400 MeV/nucleon) + Nb in various multiplicity bins.

hand, predicts the observed peaks in the angular distributions of the flow angles, which shift to larger angles with increasing multiplicity.

The physical difference between the INC model and the NFM approach can be traced back to the different treatments of the NN collision process. The INC applies a stochastic 4π scattering at the point of closest approach of straight line trajectories; this allows for substantial transparency. In contrast, the repulsive short range component in the N-N potential used for the NFM approach is a repulsive core and thus effectively results in an excluded volume effect. The nuclei are not as transparent and easily compressible as in the INC. This causes incident nucleons to be deflected away from zones of high density towards sidewards angles.

The soft and hard potentials discussed above in the NFM approach and the medium and stiff EOS in the VUU model have been used to further develop this point. For Nb + Nb at b = 2 fm:

Table III.7

	NFM				VUU			
	hard		soft		stiff		medium	
E	θ_F^{pk}	$\theta_F^{1/4}$	θ_F^{pk}	$\theta_F^{1/4}$	θ_F^{pk}	$\theta_F^{1/4}$	θ_F^{pk}	$\theta_F^{1/4}$
50	-	-	6	18	-	-	-	-
150	23	23	23	18	18	18	0	3
400	23	18	8	8	25	18	18	8
650	17	13	0	3	25	18	18	13
1050	15	13	0	3	23	18	12	8

where 'pk' denotes the peak value and '1/4' denotes the quartile value. Note that there is a clear difference between the hard and the soft potentials or the stiff and medium EOS so that the flow angle provides

information on the short range part of the N-N force. The experimental data may even require a much harder short range force. In fact, if one uses as the force $(\frac{1.2}{r})^5 F_{sof}(r)$ (see equation II.18) in the NFM model, which is much stiffer than the force obtained from the hard potential, one obtains a peak flow angle of 20 degrees and a quartile of 18 degrees at 1050 MeV/nucleon. The flow angles shown previously in Figure III.30 are too high because of the minimization procedure used to prepare the nuclei, which has been abandoned.

The VUU theory also predicts finite flow angles due to the interplay of the collision term and the EOS. Let us study the flow angle as a function of time: in Nb (1050 MeV/nucleon) + Nb, at b = 3 fm, the flow angle reaches a maximum at t = 14 fm/c (see Figure III.33). The compression or density of nuclear matter reaches its maximum value earlier at 5 fm/c (Figure III.5), it takes a finite amount of time for the saturation of the momentum distribution to occur and for the final value of the flow angle to be attained. The density is related to the flow angle for a given system via the EOS: a softer equation of state results in less transverse momentum transfer and therefore lower peak flow angles (Figure III.35).

We have seen for b = 2 fm how the peak flow angle varies as a function of the bombarding energy. At fixed impact parameter (b = 3 fm), the flow angle reaches a maximum value at 400 MeV/nucleon and then does not change further as the collision energy increases (Figure III.36). However, for lower impact parameters, the flow angle actually appears to go down for the highest energies (Figure III.34), as is the case also for the NFM model (Table III.7) and for the experimental data [Rit 85]. There is also a very strong effect due to the atomic number

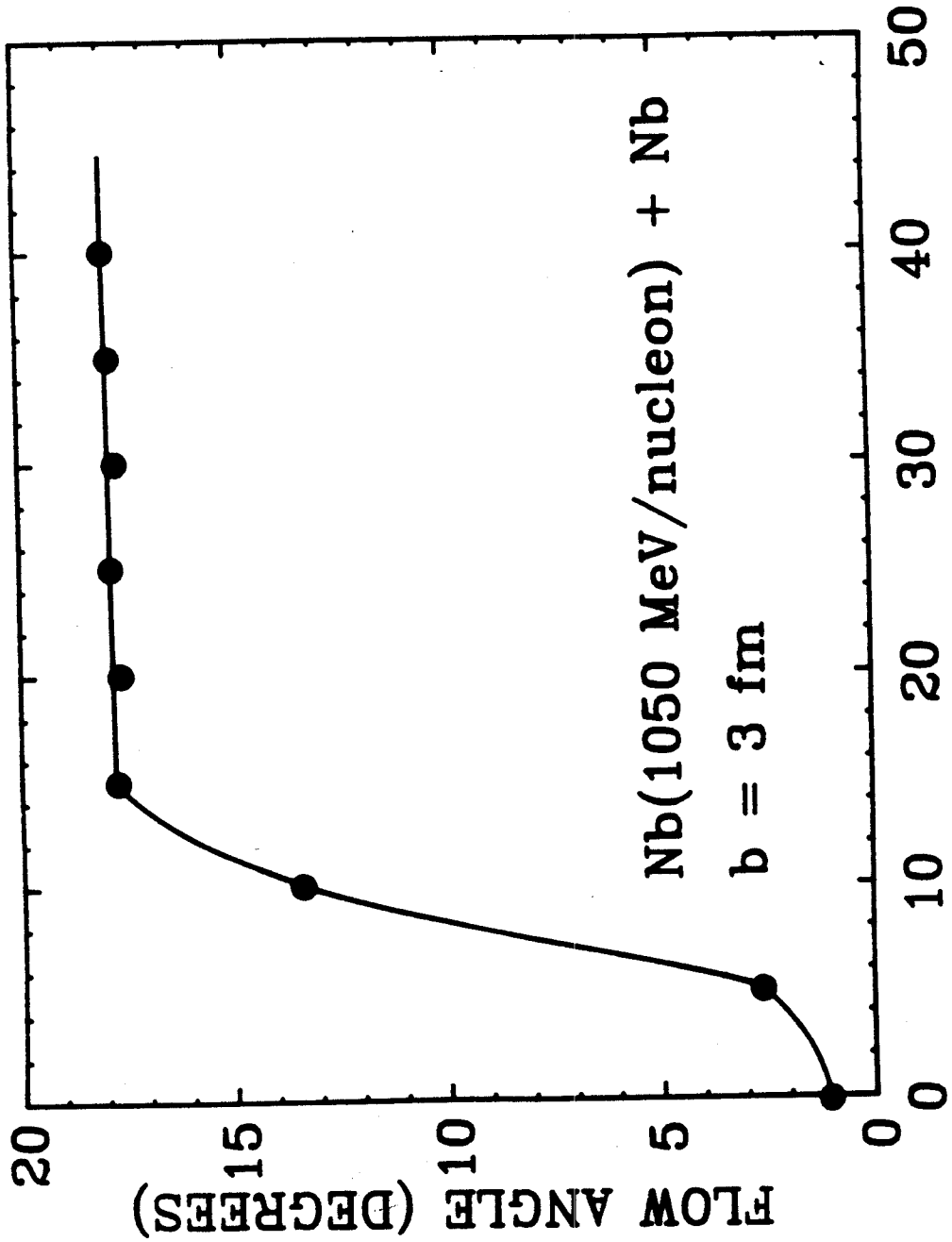

Figure III.33 The average flow angle for Nb (1050 MeV/nucleon) + Nb at b = 3 fm versus time in the VUU approach.

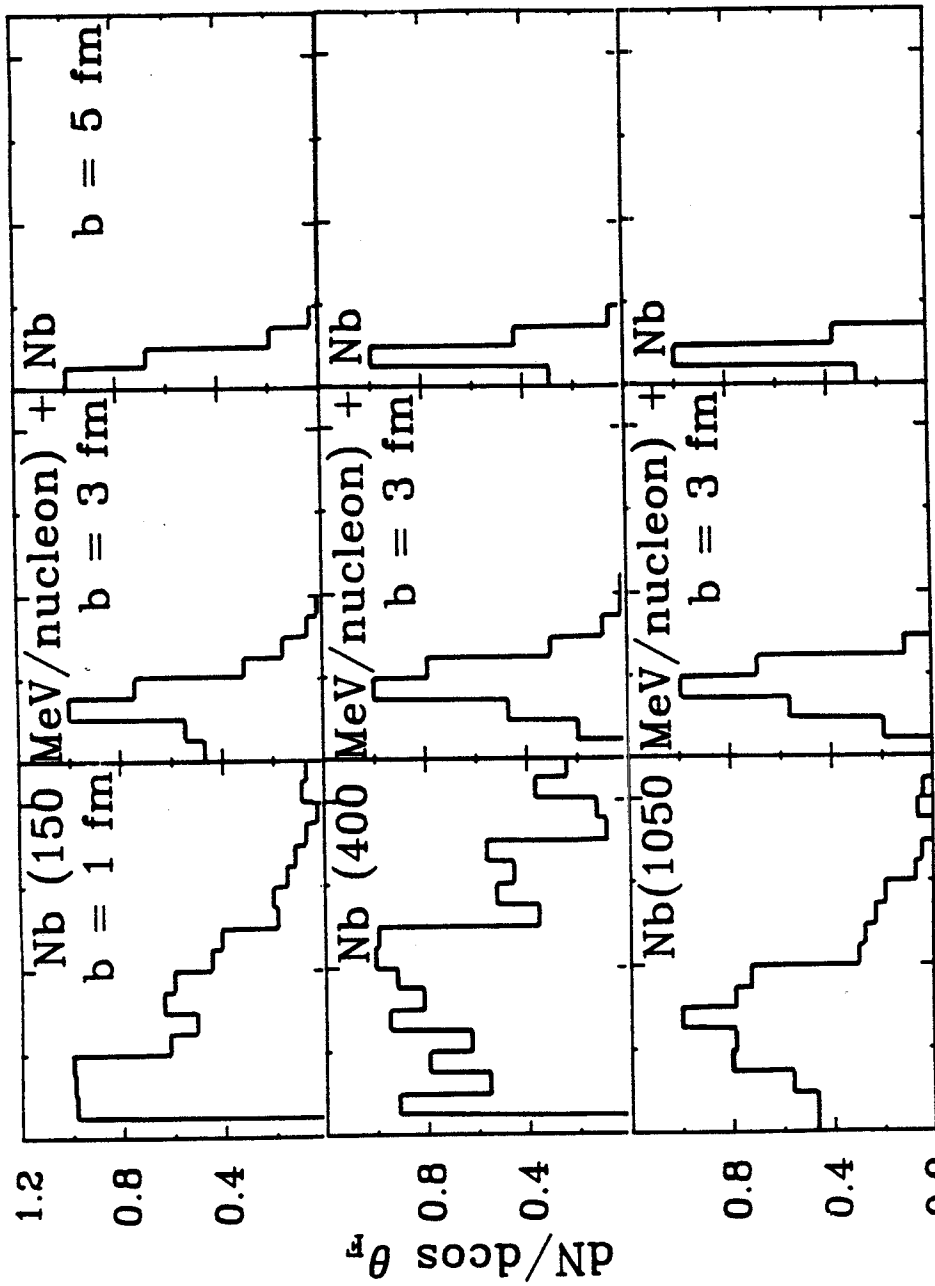

Figure III.34 Kinetic energy flow angular distributions for Nb (150, 400, 1050 MeV/nucleon) + Nb at b = 1, 3, and 5 fm in the VUU approach.

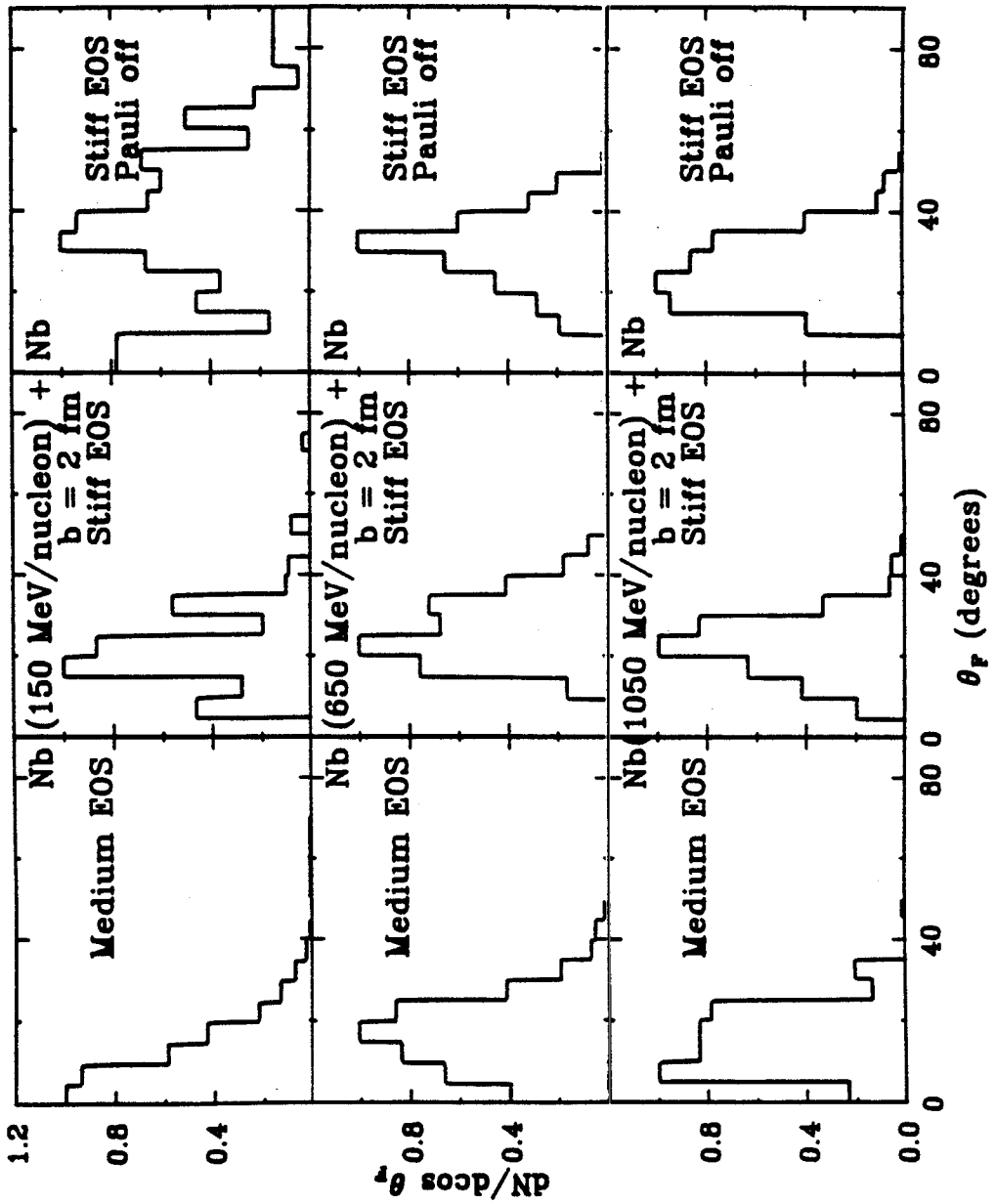

Figure III.35 Kinetic energy flow angular distributions for Nb (150, 650, 1050 MeV/nucleon) + Nb at b = 2 fm with the medium EOS, stiff EOS, and stiff EOS without Pauli blocking cases (VUU).

(Figure III.37) at fixed energy E = 400 MeV/nucleon. This can be understood physically: even though the same densities are reached in these different symmetric systems, there are many more collisions for the higher atomic numbers. The collective flow in the VUU theory thus is determined by an interplay between the collision term and the EOS. We find similar results for the peak flow angle in Au + Au at b = 3 fm as in Nb + Nb except that the maximum flow angle is now twice as large (Figure III.37).

Asymmetric collisions present results somewhat different from the above. Here a new difficulty arises - namely the problem of how to do the flow analysis. E.g. for the Ar (770 MeV/nucleon) + Pb experiment, the data [Ren 84] were interpreted on an event by event basis in a rather complicated way. First, only charged particles were used. Then the center of mass velocity for each event was computed from the momenta of all charged particles with transverse momenta per nucleon greater than the Fermi momentum and, finally, only the forward hemisphere of this participant center of mass frame was considered [Ren 84].

Compare in Figure III.38 these data with the predictions of the Vlasov-Uehling-Uhlenbeck theory with the stiff EOS. Both in theory and experiment a broad bump is observed in the distribution of flow angles for near central collisions, while a rather sharp peak occurs at 15-30 degrees for the medium impact parameters, i.e. intermediate multiplicity events. This contrasts strongly with the results of intranuclear cascade calculations, which exhibit forward peaked angular distributions independent of impact parameter as well for asymmetric as for symmetric collisions.

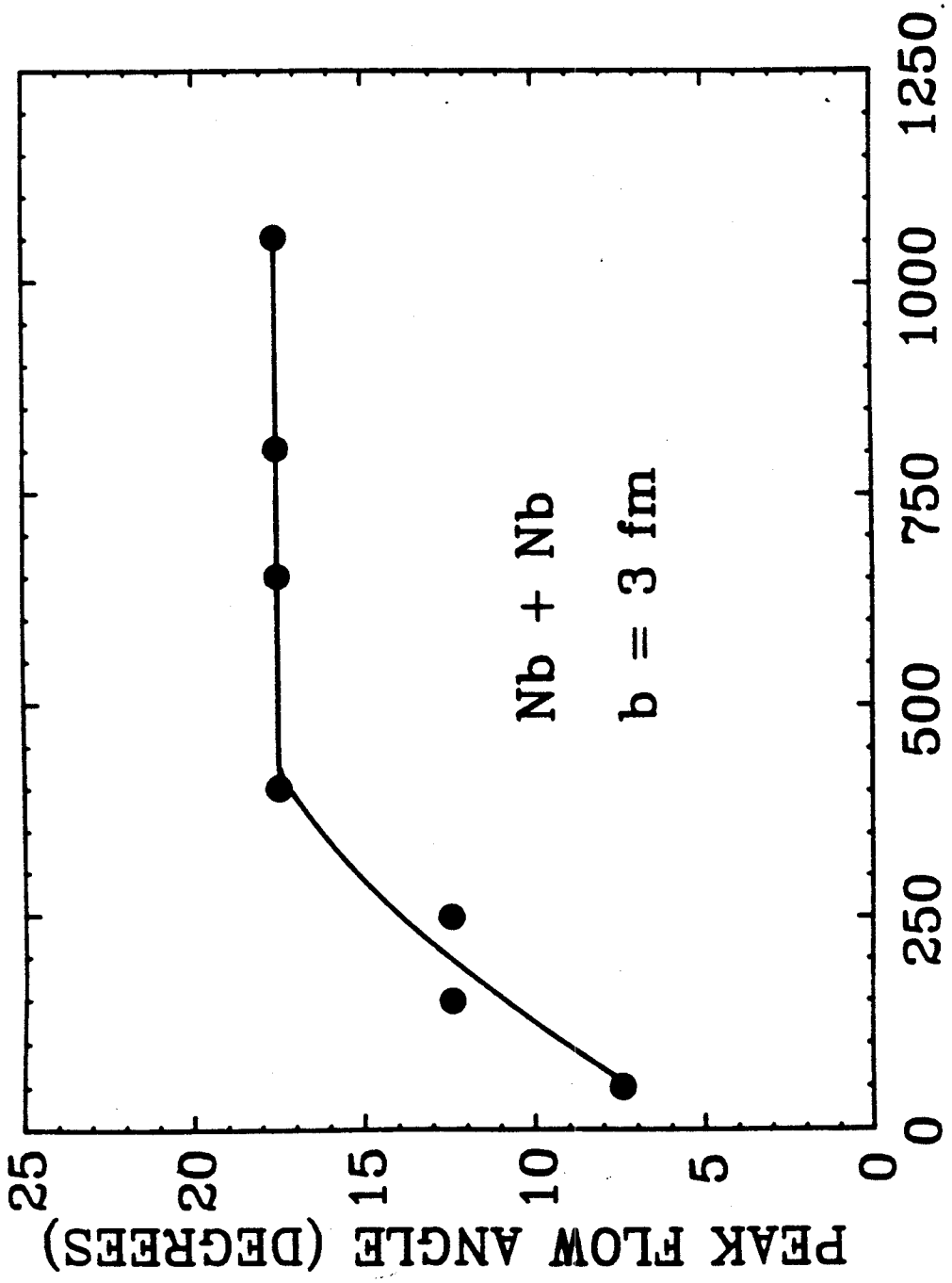

Figure III.36 Peak flow angle versus bombarding energy in the VUU approach for Nb + Nb at b = 3 fm.

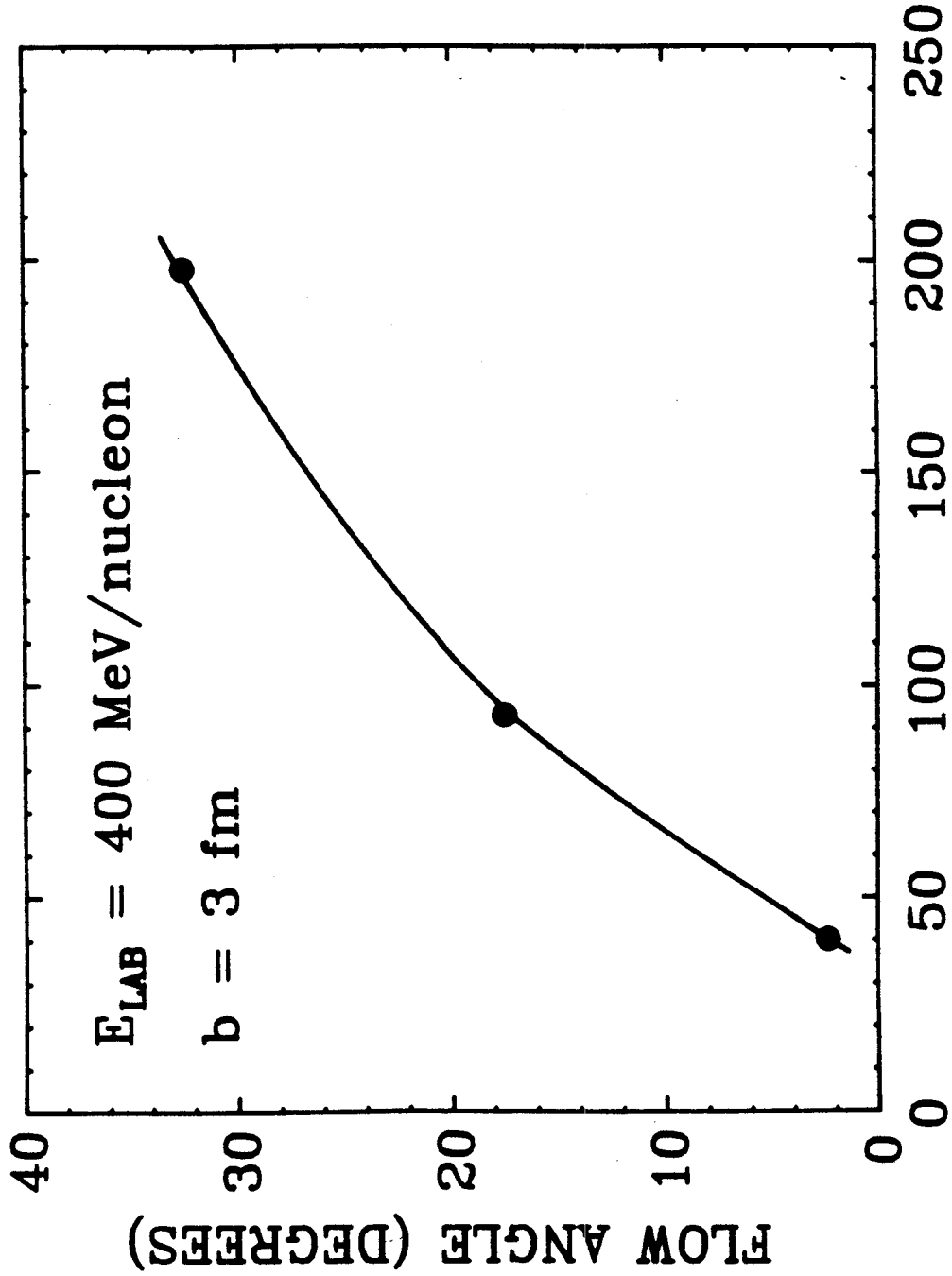

Figure III.37 Peak flow angle in the VUU model for E = 400 MeV/nucleon at b = 3 fm strongly depends on atomic number due to the increased number of collisions.

A different approach is suggested for the data analysis in asymmetric collisions [Mol 84b]. One sees from Figure III.17 that in order to detect the collective sidewards flow of nuclear matter one needs to look at the projectile hemisphere in momentum space for asymmetric systems. An asymmetry here is evidence of collective flow; this is easily recognized at the intermediate impact parameter b = 5 fm in Figure III.17. As in the case for symmetric systems, the flow of nucleons in momentum space is correlated with a flow in configuration space.

Therefore, the flow analysis should be done in the nucleon-nucleon center of momentum system with the usual kinetic energy flow tensor, but restricted to the projectile momentum hemisphere; this will avoid the distortion of the event shape by the large number of target spectators at rather small momenta and thus give the best reflection of the flow of the participant nucleons. We see in Figure III.38 on the bottom that the flow distribution changes it's characteristics in particular for the high multiplicity events. It is skewed towards 90° for the small impact parameters, while the peak remains near 20° degrees for the intermediate impact parameters (also see Figure III.39). This is similar to the results for symmetric systems; the peak of the flow angle distribution decreases with increasing impact parameter. However, the peak flow angle at b = 3 fm appears to be greater than even the one for Au + Au collisions!

In Figure III.39 the standard kinetic energy flow distributions for the system Ar + Pb are compared for individual impact parameters to the new transverse momentum analysis of Danielewicz and Odyniec [Dan 85].

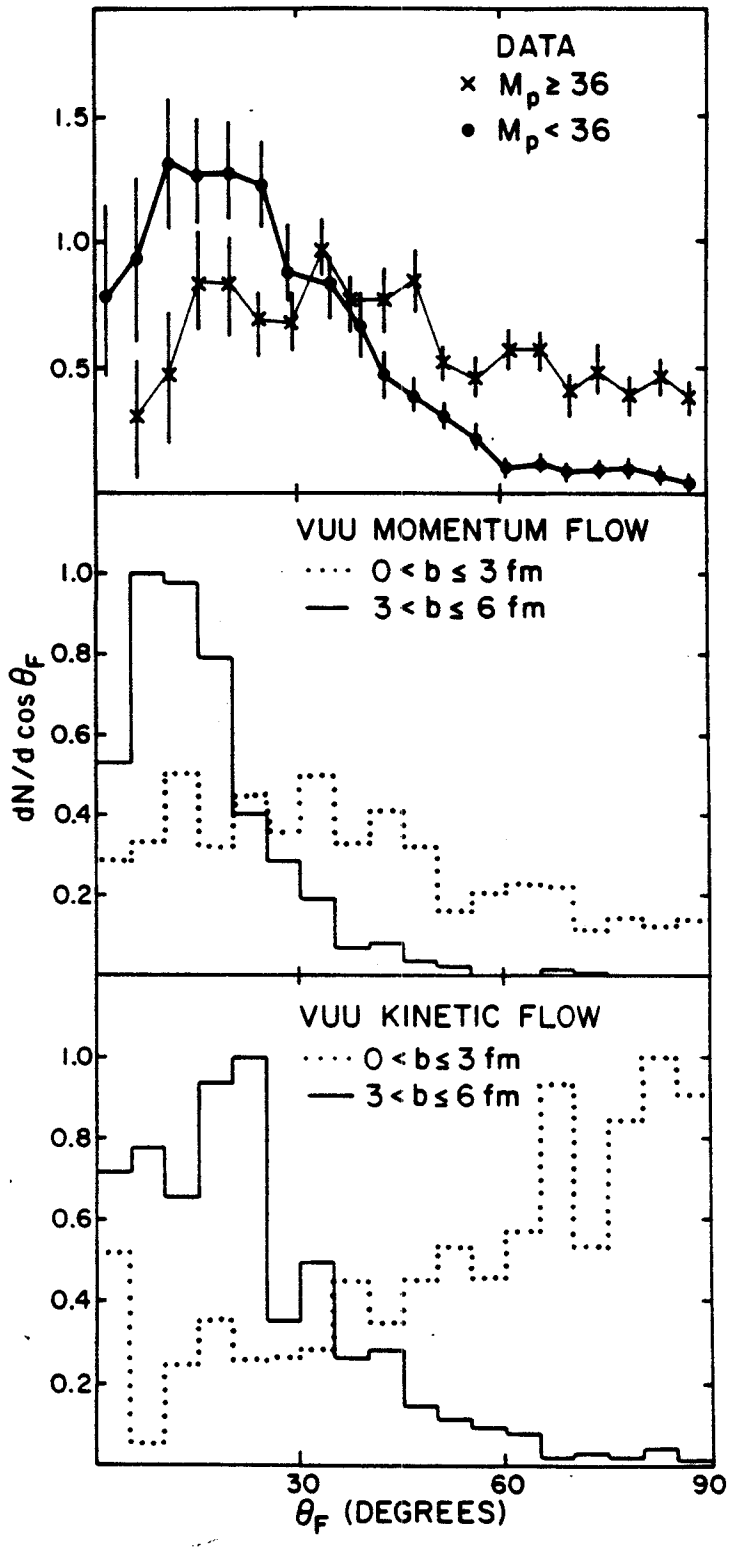

Figure III.38 Flow angle distributions for Ar (770 MeV/nucleon) + Pb for the experimental data (top) with high and low multiplicity cuts using the momentum flow tensor; corresponding predictions of the VUU theory (middle); and a standard kinetic energy flow analysis done in the nucleon-nucleon center of momentum frame using only the projectile momentum hemisphere (bottom).

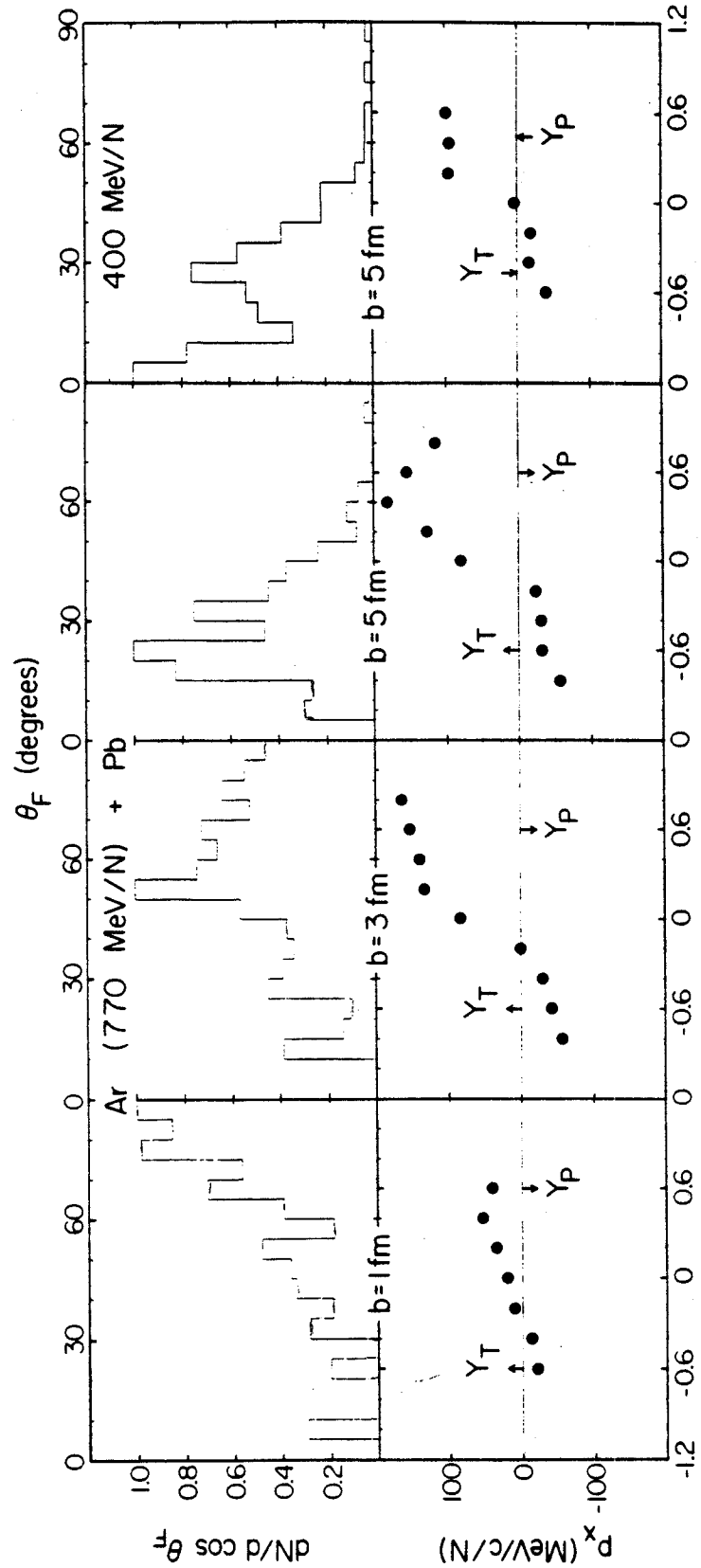

Figure III.39 VUU predictions for two different methods of detecting collective flow are shown for Ar + Pb : the standard kinetic energy flow analysis in the N-N center of momentum frame is done on the forward hemisphere for b = 1, 3, and 5 fm (top) and the transverse momentum analysis is shown at the same impact parameters (bottom).

Here, the transverse momentum spectrum $p_x(y)$ was analyzed, where y is the rapidity

$$y=1/2 \ln (E+p_{||})/(E-p_{||}) \quad (11)$$

E the total energy of the fragment, and $p_{||}$ the momentum in the beam z-direction. Note that in the simulations shown here the projectile has $p_{||} = p_z > 0$. This technique has also been used to predict the presence of collective flow for O (600 MeV/A) + O within a time dependent Dirac equation approach [Cus 85]. One must however be careful in such a continuum theoretical approach to place confidence only in transverse momenta values near the projectile rapidity where there are many particles.

As is evident from Figure III.17, the flow angle approaches it's asymptotic value rather rapidly; indeed at b= 3 fm, the final flow angle distribution is established in less than 20 fm/c. At b = 1 fm, the flow angle distribution is skewed to 90°, i.e., the projectile momentum hemisphere exhibits sidewards peaking (see Figure III.39); a significant number of particles are thrust to the side perpendicular to the beam axis. A broad peak around 55° is observed at b = 3 fm; the flow angle becomes well defined. For b = 5 fm, there is a clear peak at 20-30 degrees. Thus it is only at the intermediate impact parameters where the flow is evident by a sharp peak in such asymmetric systems. Part of the reason why the peak is not so pronounced at lower impact parameters is statistical: the projectile hemisphere contains substantially fewer fragments in the final state in an Ar + Pb collision than in a Nb + Nb collision.

In the transverse momentum plots (Figure III.39), much the same behavior is seen. However, here the analysis is not restricted to the

forward hemisphere in momentum space. Summation over p_x and division by the number of protons in each rapidity bin shows very little flow effects in the target rapidity region, which is dominated by target spectator matter. At b = 1 fm, p_x is about 50 MeV/c/nucleon at the projectile rapidity 0.60, whereas at target rapidity, y_T = -.60, p_x amounts to only 25 MeV/c/nucleon. The flow at b = 3 fm is particularly pronounced in this method of analysis: $p_x(y_P)$ is equal to 150 MeV/c/nucleon whereas $p_x(y_T)$ is only 40 MeV/c/nucleon. At b = 5 fm, we have much the same result as at b = 3 fm. Note that in the massive system studied here the transverse momentum transfer (bounce-off effect) is larger than in lighter systems at higher energies - 100 MeV/c/nucleon have been observed for the system Ar (1.8 GeV/N) + KCl (Figure III.42).

The influence of the nuclear matter equation of state has been studied by varying the EOS from stiff to medium at b = 1, 3 and 5 fm. At the lower impact parameter, the broad distribution prevents any statistically significant difference from being seen in this asymmetric system. At the intermediate impact parameter, one sees a small shifting of the flow angle to the smaller angles as the compressibility decreases, this is consistent with what has been found for symmetric systems (Figure III.35), but less dramatic. Note that one sees a great difference if K = 0 MeV (the cascade model) is used; then the distributions are peaked at zero degrees for all impact parameters. An equation of state with compressional energy seems essential to qualitatively reproduce the data; but asymmetric systems are less sensitive to the details of the equation of state than symmetric ones. Furthermore, one can look for quantum effects by turning off the Pauli principle at b = 3 and 5 fm. No strong effects are seen, which is

somewhat a surprise in view of the strong effect one sees in the symmetric case (Figure III.35) and the fact that about 50% of the collisions are Pauli blocked even at this high energy. However, this may be understood since many of the blocked collisions are between nucleons in the same nucleus, not between nucleons in the compression zone.

Let us consider now the same system Ar + Pb but at a lower energy, 400 MeV/nucleon (see Figure III.39). The kinetic energy flow angular distribution becomes more forward peaked at fixed impact parameter b = 5 fm. The transverse momentum transfer $p_x(y_p)$ decreases to 100 MeV/c/nucleon. Preliminary results from the streamer chamber group indicate an experimental maximum of 76 MeV/c/nucleon [Kea 85]; this is somewhat smaller than our prediction with the stiff EOS. Thus it will be important to relate their experimental multiplicities with finite impact parameters. A similar system, Ar (92 MeV/N) + Au, shows what happens in the VUU model as the energy is decreased further: the flow distributions at b = 2, 3, and 4 fm impact parameter become very broad; the transverse momentum at beam and target rapidities is zero to within 10 MeV/c/nucleon. At still lower energies, the transverse momentum spectra are inverted as the attractive part of the nuclear potential becomes dominant: the bounce-off caused by the short range repulsion at high density is converted into the negative angle deflection known from TDHF calculations in this energy region [Stö 80a and 81b] and from experimental data.

The transverse momentum for the symmetric systems Nb + Nb (Figure III.40) and Au + Au (Figure III.41) is a strong function of energy. At b = 3 fm the transverse momentum $p_x(y_p)$ rises from negative or zero

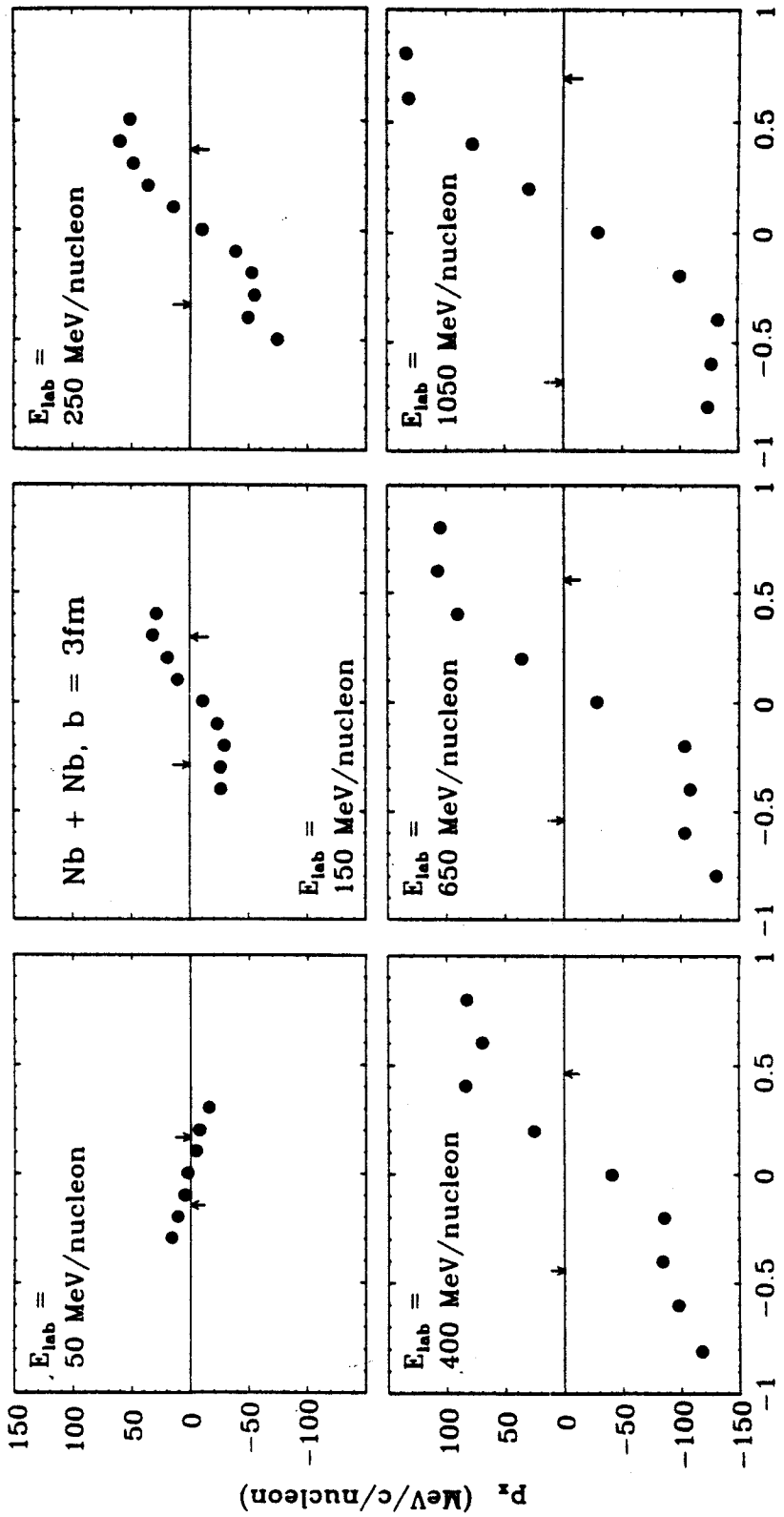

Figure III.40 Transverse momentum distributions for Nb + Nb at b = 3 fm as a function of energy (VUU).

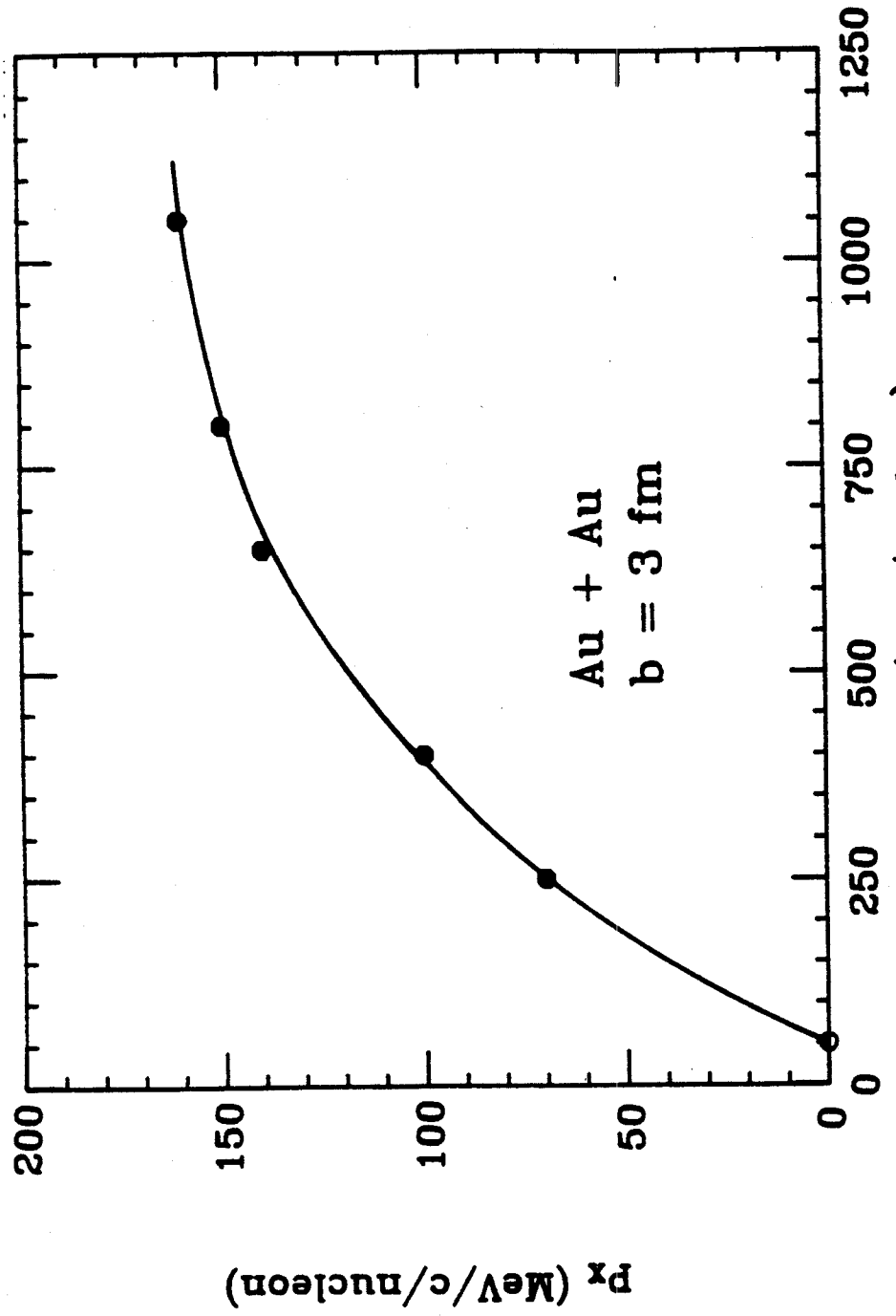

Figure III.41 Transverse momentum at projectile rapidity for Au + Au at b = 3 fm versus energy (VUU).

values for E < 100 MeV/nucleon to 140 to 160 MeV/c/nucleon at 1050 MeV/nucleon for Nb and Au systems, respectively. One probes higher densities at the higher energies so that the bounce-off increases. The bounce-off increases dramatically with energy but only slightly with atomic number. Experimentally, one finds $p_x(y_p)$ = 80 MeV/c/nucleon for 75% multiplicity [Rit 85], which compares rather well with Figure III.40 for the VUU model with the stiff EOS.

A bounce-off effect is thus predicted and may be seen by the variation of $p_x(y_p)$/nucleon with impact parameter (Figure III.2 and 19): from zero at b = 0 (for symmetry reasons) to a maximum at intermediate impact parameters to zero again for the most peripheral interactions. For Au (250 MeV/nucleon) + Au with the stiff EOS, we can emphasize this point

Table III.8

b	$p_x(y_p)$
1	42
3	84
5	70
7	36
9	25

Thus one can in the future compare the maximum transverse momentum obtained versus impact parameter (here at b = 3 fm) to the maximum obtained from multiplicity selection.

For light systems and high energies flow effects are not observed when the standard kinetic energy flow analysis is used [Dan 85, Mol 85a]. In fact, the experimental flow angular distributions for the reaction Ar(1800 MeV/nucleon, b < 2.4 fm) + KCl are peaked at zero

degrees as the cascade model predicts. But also the Vlasov-Uehling-Uhlenbeck approach, which does predict finite flow angles for heavier systems, does not yield any observable sidewards maxima in the flow angle distributions; even less so can a difference between hard and medium equations of state be seen when the standard kinetic energy flow tensor analysis is used. All flow angle distributions are peaked at zero degrees [Mol 85a]. However, one should not hastily conclude that flow effects do not occur for light systems.

Experimentally, one may determine the scattering plane by controlling the finite multiplicity distortions carefully [Dan 85]. Danielewicz and Odyniec detected collective flow effects in the streamer chamber data for Ar (1800 MeV/nucleon) + KCl using this technique (see Figure III.42 top left). There is a transverse momentum accumulation at both the projectile and target rapidities $y = \pm 0.86$ in the center of momentum frame. The collective flow effects are weaker than in the hydrodynamic model, but much stronger than in the cascade (see Figure III.42 bottom left). It is important to point out that the intranuclear cascade model fails to reproduce this data, even though it appeared to be consistent with it when the kinetic energy flow analysis had been applied [Mol 85a].

The transverse momentum analysis technique has been applied to the Vlasov-Uehling-Uhlenbeck results [Mol 85a] for the reaction Ar(1800 MeV/nucleon, $b < 2.4$ fm) + KCl. One finds that the peak in the transverse momentum spectrum $p_x(y)$ depends linearly on the nuclear equation of state: the cascade model predicts $p_x^{max} \approx 25$ MeV/c/nucleon (Figure III.42 bottom left), the medium equation of state in the Vlasov-Uehling-Uhlenbeck approach predicts $p_x^{max} \approx 50$ MeV/c/nucleon (Figure

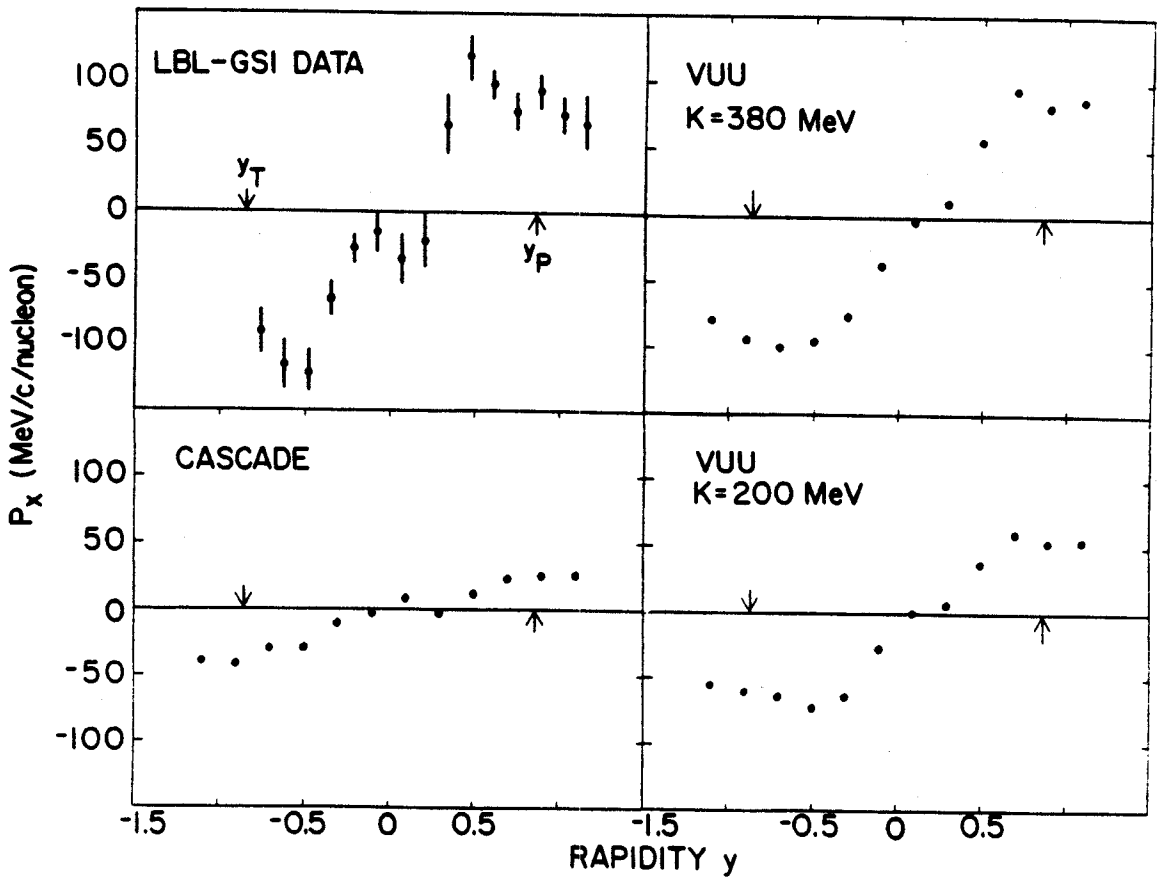

Figure III.42 Transverse momentum spectra for Ar (1800 MeV/nucleon) + KCl for the experimental data (top left), intranuclear cascade (bottom left), and the VUU approach with stiff (top right) and medium (bottom right) equations of state.

III.42 bottom right), and the stiff equation of state yields $p_x^{max} \approx 100$ MeV/c/nucleon (Figure III.42 top right). Only the latter is in agreement with the data. At the lower energy 1.2 GeV/nucleon, one finds experimentally p_x (peak) = 70 MeV/c/nucleon [Kea 85]; the VUU prediction with the stiff EOS is p_x = 80 MeV/c/nucleon. At still lower energies of 770 MeV/nucleon, VUU predicts a value of 70 MeV/c/nucleon. The variation over the energy range 770 - 1800 MeV/nucleon is thus not large. Let us stress that the stiff equation of state reproduces best the pion yields observed in the streamer chamber at this energy (1800 MeV/nucleon) and also at lower energies, down to 360 MeV/nucleon (Figure III.26). This equation of state also agrees well with the one extracted phenomenologically from the pion data.

7) Outlook

In the above, the sensitivity of the nuclear EOS to the pion yields, the transverse momentum transfer, and the flow angle has been demonstrated. Our first glimpse at the nuclear EOS in the Bevalac energy domain seems to reveal surprisingly large energies at densities two to four times the ground state density. At even higher beam energies in the ultra-relativistic realm, the nuclei might be heated strongly enough so that a new state of matter, the quark-gluon plasma, may be created. There the present VUU approach would be inadequate since the parton degrees of freedom are probed.

Partons are quarks, anti-quarks, and gluons. In nuclear physics, they may have significant contributions even in the ground state. In particular, the manner in which the parton degrees of freedom appear in the interaction of nuclei will be important to understand, especially

for nucleus-nucleus collisions at high energies E_{cm} > 20 GeV/nucleon. The high density achieved necessarily implies small distances so that the short range nature of the nuclear force and the internal constituents of the nucleons are probed.

The energy densities attainable in both the central rapidity region (the nucleus-nucleus center of momentum frame) as well as in the fragmentation regions have been estimated to be 1-2 GeV/fm^3. For example, in a quark-gluon cascade code based on QCD applied to ultra-relativistic heavy ion reactions, one finds partial thermalization of quarks and gluons with e ≈ several GeV/fm^3 in the central regions [Boa 85b]. This range of values coincides with the energy densities at which the deconfinement transition is predicted by SU(N) Yang Mills theory (pure gluon matter) on the lattice [Cle 85].

What can be done with the present VUU approach is to extend it to study strangeness production. This is most relevant for the study of very high energy densities at which the quark gluon plasma is expected to be formed. This can be accomplished through the incorporation of the elementary reaction cross sections, as has been done to include pions. The forthcoming heavy ion experiments would thus have a theoretical estimate of the number of strange particles expected just from nucleon-nucleon interactions.

Beyond this estimation of the meson background at higher energies, the difficulty of the many body problem with the parton degrees of freedom will no doubt require the use of phenomenological forces. In view of the success of the microscopic VUU approach, it may be possible to extend some of the ideas and approaches of this thesis to the ultra-relativistic domain. Quark-gluon cascade codes or models based on

relativistic kinetic theory [Hei 83] may be needed to study the transport properties of ultra-relativistic nucleus-nucleus collisions and the quark gluon plasma.

IV Conclusions

The central results of this dissertation were presented in the preceding chapter. They have to do with the application of the recently developed VUU method for modelling relativistic heavy ion collisions. The principal results are essential in interpreting the recent 4π data of the LBL/GSI Plastic Ball group to gain information on the nuclear EOS.

It has been seen that in the Vlasov-Uehling-Uehlenbeck model, for central nucleus-nucleus collisions, rapid equilibration of the participants is predicted within time spans of the order of 10 fm/c. Some stopping or significant degradation of the longitudinal momentum of the projectile occurs at small impact parameters for heavy systems. A sidesplash of nuclear matter is seen due to the interplay of the nuclear compressional energy and the collision term. The intranuclear cascade model lacks this essential compressional energy and so does not give a realistic representation of high energy heavy ion collisions.

Evidence has been presented for a stiff nuclear EOS on three fronts. First, the Ar + KCl pion yields require a stiff EOS in order to best agree with the data; the cascade model, which lacks compressional energy, overestimates these data. Second, the large flow angles observed experimentally for Ar + Pb, Nb + Nb, and Au + Au are better explained with a stiff EOS; the VUU approach with this EOS predicts qualitatively both the energy and the mass dependence of the flow angle distributions. Third, the stiff EOS seems to be necessary to explain the large transverse momentum transfers that have been observed for both Ar + KCl and Nb + Nb.

Much progress has been made both theoretically and experimentally over the past decade in the study of relativistic heavy ion physics. Over the next decade, even more difficult problems must be solved to extend both experimental apparatus and theoretical models to the ultra-relativistic domain. What has been achieved so far is encouraging. Tantalizing insight has been gained into the nuclear equation of state. The sensitivity of physical observables such as pion production, the flow angle, and the transverse momenta to the EOS has been demonstrated above in the context of the microscopic Vlasov-Uehling-Uhlenbeck theoretical model. The precise determination of this equation of state will require much more effort, but it is a prize worth seeking.

LIST OF REFERENCES

LIST OF REFERENCES

Aic 84a J. Aichelin and G. Bertsch, Phys. Lett. 138B, 350, 1984.

Aic 84b J. Aichelin, Phys. Rev. Lett. 52, 2340, 1984.

Aic 84c J. Aichelin and J. Hüfner, Phys. Lett. 136B, 15, 1984.

Aic 84d J. Aichelin, J. Hüfner, R. Ibarra, Phys. Rev. C30, 107, 1984.

Aic 85a J. Aichelin and H. Stöcker, MSUCL-522.

Aic 85b J. Aichelin and G.F. Bertsch, Phys. Rev. C31, 1730, 1985.

Aic 85c J. Aichelin, private communication.

Ald 57 B.J. Alder and T.E. Wainwright, J. Chem. Phys. 27, 1208, 1957.

Ald 59 B.J. Alder and T.E. Wainwright, J. Chem. Phys. 31, 459, 1959.

Ald 72 B.J. Alder and T.E. Wainwright, J. Chem. Phys. 56, 3013, 1972.

Ams 75 A.A. Amsden, G.F. Bertsch, F.H. Harlow, and J.R. Nix, Phys. Rev. Lett. 35, 905, 1975.

Ams 77a A.A. Amsden, F.H. Harlow, and J.R. Nix, Phys. Rev. C15, 2059, 1977.

Ams 77b A.A. Amsden, J.N. Ginocchio, F.H. Harlow, J.R. Nix, M. Danos, E.C. Halbert, and R.K. Smith,Jr., Phys. Rev. Lett. 38, 1055, 1977.

Ana 81 M.R. Anastasio, L.S. Celenza, C.M. Shakin, Phys. Rev. C23, 2258 and 2273, 1981.

Bau 75 H.G. Baumgardt, J.U. Schott, Y. Sakamoto, E. Schopper, H. Stöcker, J. Hofmann, W. Scheid and W. Greiner, Z. Phys. A273, 359, 1975.

Bau 85 W. Bauer, D.R. Dean, U. Mosel, and U. Post, Phys. Lett. 150B, 53, 1985.

Bei 75 M. Beiner, H. Flocard, N.V. Giai, P. Quentin, Nucl. Phys. A238, 29, 1975.

Ber 78 G. Bertsch and A.A. Amsden, Phys. Rev. C18, 1293, 1978.

Ber 81 G. Bertsch and J. Cugnon, Phys. Rev. C24, 2514, 1981.

Ber 83 G. Bertsch and P.J. Siemens, Phys. Lett. 126B, 9, 1983.

Ber 84a G.F. Bertsch, Erice School in Nuclear Physics 1984.

Ber 84b G.F. Bertsch, H. Kruse, and S. das Gupta, Phys. Rev. C29, 673, 1984.

Bet 74 H.A. Bethe and M.B. Johnson, Nucl. Phys. A230, 1, 1974.

Bet 83 H.A. Bethe, G.E. Brown, J. Cooperstein, J.R. Wilson, Nucl. Phys. A403, 625, 1983.

Bla 76 J.P. Blaizot, P. Gogny, B. Grammaticos, Nucl. Phys. A265, 315, 1976.

Blo 58 C. Bloch and C. de Dominicis, Nucl. Phys. 7, 459, 1958.

Boa 85a D.H. Boal and A.L. Goodman, Simon Fraser University preprint, 1985.

Boa 85b D.H. Boal, preprint of RHIC workshop at BNL, 1985.

Bod 71 A.R. Bodmer, Phys. Rev. D4, 1601, 1971.

Bod 76 A.R. Bodmer and C.N. Panos, Proc. of the Symposium on Macroscopic Features of Heavy Ion Collisions, ANL-PHY 76-2.

Bod 77 A.R. Bodmer and C.N. Panos, Phys. Rev. C15, 1342, 1977.

Bod 80 A.R. Bodmer, C.N. Panos, and A.D. MacKellar, Phys. Rev. C22, 1025, 1980.

Bod 81 A.R. Bodmer and C.N. Panos, Nucl. Phys. A356, 517, 1981.

Bog 77 J. Boguta and A.R. Bodmer, Nucl. Phys. A292, 413, 1977.

Bog 82 J. Boguta, Phys. Lett. 109B, 251, 1982.

Bog 83 J. Boguta and H. Stöcker, Phys. Lett. 120B, 289, 1983

Bon 76 P. Bonche, S. Koonin, and J.W. Negele, Phys. Rev. C13, 1226, 1976.

Bow 82 R. Bowers and J.R. Wilson, Astrophys. Jour. 263, 366, 1982.

Boz 85 G. Bozzolo and J.P. Vary, Phys. Rev. C31, 1909, 1985.

Buc 83a G. Buchwald, G. Graebner, J. Theis, J. Maruhn, W. Greiner, H. Stöcker, K. Frankel, and M. Gyulassy, Phys. Rev. C28, 2349, 1983.

Buc 83b G. Buchwald, G. Graebner, J. Theis, J.A. Maruhn, W. Greiner, and H. Stöcker, Phys. Rev. C28, 1119, 1983.

Buc 84a G. Buchwald, Ph.D. thesis, Universität Frankfurt, 1984.

Buc 84b G. Buchwald, G. Gräbner, J. Theis, J. Maruhn, W. Greiner, and H. Stöcker, Phys. Rev. Lett. 52, 1594, 1984.

But 63 S.T. Butler and C.A. Pearson, Phys. Rev. 129, 836, 1963.

Cal 79 D.J.E. Callaway, L. Wilets and Y. Yariv, Nucl. Phys. A327, 250, 1979.

Cam 85 X. Campi and J. Desbois, Proceedings of the 7th High Energy Heavy Ion Study, GSI Darmstadt, October 1984.

Car 85 L. Carlen, H.A. Gustafsson, B. Jakobsen, A. Kristiansson, P. Kristiansson, A. Oskarsson, H. Ryde, M. Westenius, Proc. of Second International Conference on Nucleus-Nucleus Collisions, ed. B. Jakobsen and K. Aleklett, 158, 1985.

Cle 85 J. Cleymans, R.V. Gavai and E. Suhonen, to be published in Phys. Rep.

Cot 73 W.N. Cottingham, M. Lacombe, B. Loiseau, J.M. Richard, R. Vinhmau, Phys. Rev. D8, 800, 1973.

Cse 80a L.P. Csernai, B. Lukacs and J. Zimanyi, Lett. al Nuovo Cimento, 27, 111, 1980.

Cse 80b L.P. Csernai and H.W. Barz, Z. Phys. A296, 173, 1980.

Cse 85 L.P. Csernai and J.I. Kapusta, to be published in Phys.Rep.

Cug 80 J. Cugnon, Phys. Rev. C22, 1885, 1980.

Cug 81 J. Cugnon, T. Mizutani and J. Van der Meulen, Nucl. Phys. A352, 505, 1981.

Cug 82 J. Cugnon, D. Kinet and J. Vandermeulen, Nucl. Phys. A379, 553, 1982

Cug 84a J. Cugnon, D. L'Hote, Phys. Lett. 149B, 35, 1984.

Cug 84b J. Cugnon, Cargese Summer School, 1984.

Cur 65 D.G. Currie, T.F. Jordan, E.C.G. Sudarshan, Rev. Mod. Phys. 35, 350, 1965.

Cus 82 R.Y. Cusson, J.A. Maruhn, H. Stöcker, Nucl. Phys. A385, 76, 1982.

Cus 85 R.Y. Cusson, P.G. Reinhard, H. Stöcker, M.R. Strayer, J.J. Molitoris, and W. Greiner, MSUCL-497, Phys. Rev. Lett., in print.

Dan 79 P. Danielewicz, Nucl. Phys. A314, 465, 1979.

Dan 85 P. Danielewicz and G. Odyniec, Phys. Lett., in print.

Dar 13 C.G. Darwin, Phil. Mag. 25, 201, 1913.

Dos 85 K.G.R. Doss, H.A. Gustafsson, H.H. Gutbrod, B. Kolb, H. Löhner, B. Ludewigt, A.M. Poskanzer, T. Renner, H. Riedesel, H.G. Ritter, A. Warwick, H. Wieman, Phys. Rev. C32, 116, 1985.

Due 56 H.P. Duerr, Phys. Rev. 103, 469, 1956.

Due 58 H.P. Duerr, Phys. Rev. 109, 117 and 1347, 1958.

Eks 65 H. Ekstein, Comm. Math. Phys. 1, 6, 1965.

Eul 37 Euler, Z. Phys., 105, 553, 1937.

Fai 82 G. Fai and J. Randrop, Nucl. Phys. A381, 557, 1982.

Fai 83 G. Fai and J. Randrop, Nucl. Phys. A404, 551, 1983.

Fee 46 E. Feenberg and H. Primakoff, Phys. Rev. 70, 980, 1946.

Fis 67 M.E. Fisher, Phys. 3, 255, 1967.

Fox 85 D. Fox, D.A. Cebra, Z.M. Koenig, J.J. Molitoris, F. Ugorowski, H. Stöcker, G.D. Westfall, MSUCL- , 1985.

Fri 83a W. Friedman and W.G. Lynch, Phys. Rev. C28, 16, 1983.

Fri 83b W. Friedman and W.G. Lynch, Phys. Rev. C28, 950, 1983.

Gal 84 C. Gale and S.D. Gupta, Phys. Rev. C30, 414, 1984.

Gar 79 S.I.A. Garpman, N.K. Glendenning and Y.J. Karant, Nucl. Phys. A322, 382, 1979

Gol 48 M.L. Goldberger, Phys. Rev. 74, 1269, 1948.

Gol 78 A.S. Goldhaber, H.H. Heckman, Ann. Rev. Nucl. Part. Sci. 28, 161, 1978.

Gos 78 J. Gosset, J.I. Kapusta, and G. Westfall, Phys. Rev. C18, 844, 1978.

Gra 84 G. Graebner, Ph.D. Thesis, Universität Frankfurt, 1984, unpublished.

Gus 84 H.A. Gustafsson, H.H. Gutbrod, B. Kolb, H. Löhner, B. Ludewigt, A.M. Poskanzer, T. Renner, H. Riedesel, H.G. Ritter, A. Warwick, F. Weik, and H. Wieman, Phys. Rev. Lett. 52, 1590, 1984.

Gut 85 H.H. Gutbrod, M. Doss, H.A. Gustafsson, B. Kolb, H. Löhner, B. Ludewigt, A.M. Poskanzer, H.G. Ritter, H. Wieman, LBL preprint 1985.

Gyu 77 M. Gyulassy and W. Greiner, Ann. Phys. 109, 485, 1977.

Gyu 82 M. Gyulassy, K.A. Frankel and H. Stöcker, Phys. Lett. 110B, 185, 1982.

Hag 68 R. Hagedorn and J. Ranft, Nuo. Cim. Suppl. 6, 169, 1968.

Hag 71 R. Hagedorn, Academic Training Program Lectures, CERN 1970-71.

Hah 85a D. Hahn and H. Stöcker, MSUCL-505, 1985.

Hah 85b D. Hahn and H. Stöcker, to be published.

Har 85 J.W. Harris, R. Bock, R. Brockman, A. Sandoval, R. Stock, H. Ströbele, G. Odyniec, H.G. Pugh, L.S. Schröder, R.E. Renfordt, D. Schall, D. Bangert, W. Rauch and K.L. Wolf, Phys. Lett. 153B, 377, 1985.

Hei 79 U. Heinz, W. Greiner and W. Scheid, J.Phys. G5, 1383, 1979.

Hei 83 U. Heinz, Phys. Rev. Lett. 51, 351, 1983.

Hir 84 A.S. Hirsch, A. Bujak, J.E. Finn, L.J. Gutay, R.W. Minich, N.T. Porile, R.P. Scharenberg, B.C. Stringfellow, Phys. Rev. C29, 508, 1984.

Hof 76 J. Hofmann, H. Stöcker, U. Heinz, W. Scheid, and W. Greiner, Phys.Rev. Lett. 36, 88, 1976.

Hof 83 J.B. Hoffer, Astro. J. 88, 1420, 1983.

Jac 83 B.V. Jacak, G.D. Westfall, C.K. Gelbke, L.H. Harwood, W.G. Lynch, D.K. Scott, H. Stöcker, M.B. Tsang, and T.J.M.Symons, Phys. Rev. Lett. 51, 1846, 1983.

Jac 84 B.V. Jacak, H. Stöcker, G.D. Westfall, Phys. Rev. C29, 1744, 1984.

Jac 85 B.V. Jacak unpublished.

Jam 81 M. Jaminon, C. Mahaux, P. Rochus, Nucl. Phys. A365, 371, 1981.

Kam 69 N.G. Kampen, Physica 43, 244, 1969.

Kap 84 J.I. Kapusta, Nucl.Phys. A418, 573c, 1984.

Kea 85 D. Keane, UC Riverside, unpublished and private communication.

Kis 84 S.M. Kisalev, Moscow ITEP preprint 123, 1984.

Kit 81 Y. Kitazoe, K. Yamamoto, M. Sano, Lett. Nuo. Cim. 2, 337, 1981.

Kno 84 J. Knoll and B. Strack, Phys. Lett. 149B, 45, 1984.

Köh 80 H.S. Köhler, Nucl. Phys. A343, 315, 1980.

Koo 75 S. Koonin, PhD Thesis, MIT 1975.

Kru 85a H. Kruse, B.V. Jacak, and H. Stöcker, Phys. Rev. Lett. 54, 289 1985.

Kru 85b H. Kruse, B.V. Jacak, J.J. Molitoris, G.D. Westfall, and H. Stöcker, Phys. Rev. C31 1985.

Kun 81 J. Kunz, R. Babinet, L. Wilets and U. Mosel, Nucl. Phys. A367, 459, 1981.

Lan 59 L.D. Landau and E.M. Lifshitz, Fluid Mechanics, Pergamon, NY, 1959.

Lee 74 T.D. Lee and G.C. Wick, Phys. Rev. D9, 2291, 1974

Lem 79 M.C. Lemaire, S. Nagamiya, S. Schnetzer, H. Steiner, I. Tanihata, Phys. Lett. B85, 38, 1979.

Lop 84 J.A. Lopez, P.J. Siemens, Nucl. Phys. A431, 728, 1984.

Lui 85 Y. W. Lui, J.D. Bronson, D.H. Youngblood, Y. Toba, U. Gary, Phys. Rev. C31, 1643, 1985.

Lus 81 L. Lusanna, Nuov. Cim. 65B, 135, 1981.

Mac 85 H. Machner, Phys. Rev. C31, 1271, 1985.

Mad 26 E. Madelung, Z. Phys. 40, 332, 1926.

Mal 81 R. Malfliet, Nucl. Phys. A363, 429, 1981.

Mar 77 J.A. Maruhn, Proc. Topical Conf. on Heavy Ion Collisions, Pikeville, TN 1977 p. 156.

Mar 85 J.A. Maruhn, K.T.R. Davies, M.R. Strayer, Phys. Rev. C31, 1289, 1985.

Mat 65 J.H.E. Mattauch, W. Thiele, A.H. Wapstra, Nucl. Phys. 67, 1, 1965.

Mek 78a A. Mekjian, Phys. Rev. C17, 1051, 1978.

Mek 78b A. Mekjian, Nukl.Phys. A312, 491, 1978.

Met 58 N. Metropolis, R. Bivins, M. Storm, A. Turkevich, J.M. Miller, and G. Friedlander, Phys. Rev. 110, 185, 1958.

Mig 72 A.B. Migdal, JETP 34, 1184

Mil 72 L.D. Miller, A.E.S. Green, Phys. Rev. C5, 241, 1972.

Mol 84a J.J. Molitoris, J.B. Hoffer, H. Kruse, and H. Stöcker, Phys. Rev. Lett. 53, 899, 1984.

Mol 84b J.J. Molitoris and H. Stöcker, MSUCL-514, Phys. Lett. B in print.

Mol 85a J.J. Molitoris and H. Stöcker, Phys. Rev. C32, 346, 1985.

Mol 85b J.J. Molitoris, H. Stöcker, J. Cugnon and D. L'Hote, to be published.

Mon 71 E.J. Moniz, I. Sick, R.R. Whitney, J.R. Ficenec, R.D. Kephart, W.P. Trower, Phys. Rev. Lett. 26, 445, 1971.

Mor 29 P.M. Morse, Phys. Rev. 34, 57, 1929.

Nag 81 S. Nagamiya, M.-C. Lemaire, E. Moeller, S. Schnetzer, G. Shapiro, H. Steiner, and I. Tanihata, Phys. Rev. C24, 971, 1981.

Neg 82 J.W. Negele, Rev. Mod. Phys. 54, 913, 1982.

Nix 69 J.R. Nix, Nucl. Phys. A130, 241, 1969.

Nun 77 L. Nunnely and T.D. Thomas, Nucl. Phys. A301, 119, 1978.

Pan 70 V.R. Pandharipande, Phys. Lett. 31B, 635, 1970.

Pan 84 A.D. Panagioutou, M.W. Curtin, H. Toki, D.K. Scott, P.J. Siemens, Phys. Rev. Lett. 52, 496, 1984.

Pei 79 R. Peierls, Surprises in Theoretical Physics, Princeton, 1979.

Poc 85 J. Pochadzalla, et. al., MSUCL-527, 1985.

Ran 79 J. Randrup, Nucl. Phys. A314, 429, 1979.

Rem 84 B. Remaud, F. Sebille, C. Gregoire and F. Scheuter, Nucl. Phys. A428, 101c, 1984.

Rem 85a E.A. Remler, Phys. Rev. Lett. 54, 989, 1985.

Rem 85b E.A. Remler, April 1985 preprint.

Ren 84 R. E. Renfordt, D. Schall, R. Bock, R. Brockmann, J.W. Harris, A. Sandoval, R. Stock, H. Ströbele, D. Bangert, W. Rauch, G. Odyniec, H.G. Pugh, and L.S. Schroeder, Phys. Rev. Lett. 53, 763, 1984.

Rit 71 A. Rittenberg, A.B. Galtieri, T. Losinski, Rev. Mod. Phys. 43, S1, 1971.

Rit 85 H.G. Ritter, K.G.R. Doss, H.A. Gustafsson, H.H. Gutbrod, K.H. Kampert, B. Kolb, H. Löhner, B. Ludewigt, A.M. Poskanzer, A. Warwick, and H. Wieman, Invited talk at the Second International Conference on Nucleus-Nucleus Collisions at Visby, Sweden, June 1985.

Row 70 D. Rowe, Nuclear Collective Motion, Methuen and Co., London, 1970.

Ruc 76 V. Ruck, M. Gyulassy and W. Greiner, Z. Phys. A277, 391, 1976.

San 80a A. Sandoval, H.H. Gutbrod, W.G. Meyer, R. Stock, C. Lukner, A.M. Poskanzer, J. Gosset, J.C. Jourdain, C.H. King, G. King, N.V. Sen, G.D. Westfall, K.L. Wolf, Phys. Rev. C21, 1321, 1980.

San 80b A. Sandoval, R. Stock, H.E. Stelzer, R.E. Renfordt, J.W. Harris, J.P. Brannigian, J.V. Geaga, L.J. Rosenberg, L.S. Schroeder, and K.L. Wolf, Phys. Rev. Lett. 45, 874, 1980.

Sar 85 S. Sarker and S.K. Chowdhury, Phys. Lett. 153B, 358, 1985.

Sch 68 W. Scheid, R. Ligensa, and W. Greiner, Phys. Rev. Lett. 21, 1479, 1968.

Sch 74 W. Scheid, H. Müller, and W. Greiner, Phys. Rev. Lett. 32, 741, 1974.

Ser 47 R. Serber, Phys. Rev. 72, 1114, 1947.

Ser 85 R.D. Serot and J.D. Walecka in Advances in Nuclear Physics, ed. J.W. Negele and E. Vogt, 1985.

Sie 79 P.J. Siemens and J.I. Kapusta, Phys. Rev. Lett. 43, 1486, 1979.

Sig 85 P.S. Signell, MSU Database and Physik Daten 1981.

Sky 58 T.H.R. Skyrme Proc. R. Soc. London 247 (1958) 260

Sky 59 T.H.R. Skyrme, Nucl. Phys. 9, 615 and 635, 1959.

Sob 75 M.I. Sobel, P.J. Siemens, J.P. Bondorf and H.A. Bethe, Nucl. Phys. A251, 502, 1975.

Sta 79 D. Stauffer, Phys. Rep. 54, 1, 1979.

Sto 80 R. Stock, H.H. Gutbrod, W.G. Meyer, A.M. Poskanzer, A. Sandoval, J. Gosset, C.H. King, G. King, Ch. Lukner, N.V. Sen, G.D. Westfall, and K.L. Wolf, Phys. Rev. Lett. 44, 1243, 1980.

Sto 82 R. Stock, R. Bock, R. Brockman, J.W. Harris, A. Sandoval, H. Stroebele, K.E. Wolf, H.G. Pugh, L.S. Schröder, M. Maier, R.E. Renfordt, A. Dacal, and M.E. Ortiz, Phys. Rev. Lett. 49, 1236, 1982.

Stö 77 H. Stöcker, J. Hofmann, W. Scheid, and W. Greiner, Conf. on Nuclear Collisions, Bled, Yugoslavia, Fizika 9, Supp. 4, 1977a, p. 671.

Stö 78 H. Stöcker, W. Greiner and W. Scheid, Z. Phys. A286, 121, 1978

Stö 79 H. Stöcker, J.A. Maruhn and W. Greiner, Phys. Lett. 81B, 303, 1979.

Stö 80a H. Stöcker, R.Y. Cusson, J.A. Maruhn and W. Greiner, Z. Phys. A294, 125, 1980.

Stö 80b H. Stöcker, J.A. Maruhn, and W. Greiner, Phys. Rev. Lett. 44, 725, 1980.

Stö 81a H. Stöcker, R.Y. Cusson, J.A. Maruhn and W. Greiner, Phys. Lett. 101B, 379 (1981).

Stö 81b H. Stöcker, A.A. Ogloblin and W. Greiner, Z. Phys. A303, 259,1981.

Stö 81c H. Stöcker, C. Riedel, Y. Yariv, L.P. Csernai, G. Buchwald, G. Graebner, J.A. Maruhn, W. Greiner, K. Frankel, M. Guylassy, B. Schürmann, G. Westfall, J.D. Stevenson, J.R. Nix, and D. Strottmann, Phys. Rev. Lett. 47, 1807, 1981.

Stö 82a H. Stöcker, L.P. Csernai, G. Graebner, G. Buchwald, H. Kruse, R.Y. Cusson, J.A. Maruhn, and W. Greiner, Phys. Rev. C25, 1873, 1982.

Stö 82b H. Stöcker, G. Buchwald, L.P. Csernai, G. Graebner, J.A. Maruhn and W. Greiner, Nucl. Phys. A387, 205, 1982.

Stö 82c H. Stöcker, R.Y. Cusson, H.J. Lustig, A. Gobbi, J. Hahn, J.A. Maruhn, W. Greiner, Z. Phys. A306, 235, 1982.

Stö 83 H. Stöcker, G. Buchwald, G. Gräbner, P. Subramanian, J.A. Maruhn, W. Greiner, B.V. Jacak and G.D. Westfall, Nucl.Phys. A400, 63, 1983.

Stö 84 H. Stöcker, J. Phys. Lett 10, 111, 1984.

Stö 85 H. Stöcker and W. Greiner, Phys. Rep. 1985.

Str 83 H. Ströbele, et. al., Phys. Rev. C27, 1349, 1983.

Sub 81 P.R. Subramanian, L.P. Csernai, H. Stöcker, J.A. Maruhn, W. Greiner and H. Kruse, J. Phys. G7, L241, 1981.

Tan 80 I. Tanihata, M.C. Lemaire, S. Nagamiya, S. Schnetzer, Phys. Lett. 97B, 363, 1980.

Ton 83 V.D. Toneev and K.K. Gudima, Nucl. Phys. A400, 173, 1983.

Ueh 33 E.A. Uehling and G.E. Uhlenbeck, Phys. Rev. 43, 552, 1933.

Vas 80a D. Vasak, H. Stöcker, B. Müller and W. Greiner, Phys. Lett. 93B 243, 1980.

Vas 80b D. Vasak, B. Müller and W. Greiner, Physica Scripta 22, 25, 1980.

Vas 84 D. Vasak, W. Greiner, B. Müller, Th. Stahl and M. Uhlig, Nucl.Phys. A428, 291c, 1984.

Vau 72 D. Vautherin and D.M. Brink, Phys. Rev. C5, 626, 1972.

Vic 85 A. Vicentini, G. Jacucci, V.R. Pandharipande, Phys. Rev. C31, 1783, 1985.

Wal 74 J.D. Walecka, Ann. Phys. 83, 491, 1974.

Wes 76 G.D. Westfall, J. Gosset, R.J. Johansen, A.M. Poskanzer, W.G. Meyer, H.H. Gutbrod, A. Sandoval, R. Stock, Phys. Rev. Lett. 37, 1202, 1976.

Wig 32 E. Wigner, Phys. Rev. 40, 749, 1932.

Wil 76 L. Wilets, A.D. Mackellar, G.A. Rinker Jr., Proc. IV Int. Workshop in Gross Properties of Nuclei and Nuclear Excitations, Hirschegg, Austria, 111, 1976.

Wil 77 L. Wilets, E.M. Henley, M. Kraft and A.D. MacKellar, Nucl. Phys. A282, 341, 1977.

Wil 78 L. Wilets, Y. Yariv and R. Chestnut, Nucl. Phys. A301, 359, 1978.

Wil 85 J.R. Wilson, R. Mayle, S.E. Wooseley, T. Weaver, LLNL preprint 1985.

Wit 85 E. Witten, Princeton preprint, 1985.

Sta 79 D. Stauffer, Phys. Rep. 54, 1, 1979.

Sto 80 R. Stock, H.H. Gutbrod, W.G. Meyer, A.M. Poskanzer, A. Sandoval, J. Gosset, C.H. King, G. King, Ch. Lukner, N.V. Sen, G.D. Westfall, and K.L. Wolf, Phys. Rev. Lett. 44, 1243, 1980.

Sto 82 R. Stock, R. Bock, R. Brockman, J.W. Harris, A. Sandoval, H. Stroebele, K.E. Wolf, H.G. Pugh, L.S. Schröder, M. Maier, R.E. Renfordt, A. Dacal, and M.E. Ortiz, Phys. Rev. Lett. 49, 1236, 1982.

Stö 77 H. Stöcker, J. Hofmann, W. Scheid, and W. Greiner, Conf. on Nuclear Collisions, Bled, Yugoslavia, Fizika 9, Supp. 4, 1977a, p. 671.

Stö 78 H. Stöcker, W. Greiner and W. Scheid, Z. Phys. A286, 121, 1978

Stö 79 H. Stöcker, J.A. Maruhn and W. Greiner, Phys. Lett. 81B, 303, 1979.

Stö 80a H. Stöcker, R.Y. Cusson, J.A. Maruhn and W. Greiner, Z. Phys. A294, 125, 1980.

Stö 80b H. Stöcker, J.A. Maruhn, and W. Greiner, Phys. Rev. Lett. 44, 725, 1980.

Stö 81a H. Stöcker, R.Y. Cusson, J.A. Maruhn and W. Greiner, Phys. Lett. 101B, 379 (1981).

Stö 81b H. Stöcker, A.A. Ogloblin and W. Greiner, Z. Phys. A303, 259,1981.

Stö 81c H. Stöcker, C. Riedel, Y. Yariv, L.P. Csernai, G. Buchwald, G. Graebner, J.A. Maruhn, W. Greiner, K. Frankel, M. Guylassy, B. Schürmann, G. Westfall, J.D. Stevenson, J.R. Nix, and D. Strottmann, Phys. Rev. Lett. 47, 1807, 1981.

Stö 82a H. Stöcker, L.P. Csernai, G. Graebner, G. Buchwald, H. Kruse, R.Y. Cusson, J.A. Maruhn, and W. Greiner, Phys. Rev. C25, 1873, 1982.

Stö 82b H. Stöcker, G. Buchwald, L.P. Csernai, G. Graebner, J.A. Maruhn and W. Greiner, Nucl. Phys. A387, 205, 1982.

Stö 82c H. Stöcker, R.Y. Cusson, H.J. Lustig, A. Gobbi, J. Hahn, J.A. Maruhn, W. Greiner, Z. Phys. A306, 235, 1982.

Stö 83 H. Stöcker, G. Buchwald, G. Gräbner, P. Subramanian, J.A. Maruhn, W. Greiner, B.V. Jacak and G.D. Westfall, Nucl.Phys. A400, 63, 1983.

Stö 84 H. Stöcker, J. Phys. Lett 10, 111, 1984.

Stö 85 H. Stöcker and W. Greiner, Phys. Rep. 1985.

Str 83 H. Ströbele, et. al., Phys. Rev. C27, 1349, 1983.

Sub 81 P.R. Subramanian, L.P. Csernai, H. Stöcker, J.A. Maruhn, W. Greiner and H. Kruse, J. Phys. G7, L241, 1981.

Tan 80 I. Tanihata, M.C. Lemaire, S. Nagamiya, S. Schnetzer, Phys. Lett. 97B, 363, 1980.

Ton 83 V.D. Toneev and K.K. Gudima, Nucl. Phys. A400, 173, 1983.

Ueh 33 E.A. Uehling and G.E. Uhlenbeck, Phys. Rev. 43, 552, 1933.

Vas 80a D. Vasak, H. Stöcker, B. Müller and W. Greiner, Phys. Lett. 93B 243, 1980.

Vas 80b D. Vasak, B. Müller and W. Greiner, Physica Scripta 22, 25, 1980.

Vas 84 D. Vasak, W. Greiner, B. Müller, Th. Stahl and M. Uhlig, Nucl.Phys. A428, 291c, 1984.

Vau 72 D. Vautherin and D.M. Brink, Phys. Rev. C5, 626, 1972.

Vic 85 A. Vicentini, G. Jacucci, V.R. Pandharipande, Phys. Rev. C31, 1783, 1985.

Wal 74 J.D. Walecka, Ann. Phys. 83, 491, 1974.

Wes 76 G.D. Westfall, J. Gosset, R.J. Johansen, A.M. Poskanzer, W.G. Meyer, H.H. Gutbrod, A. Sandoval, R. Stock, Phys. Rev. Lett. 37, 1202, 1976.

Wig 32 E. Wigner, Phys. Rev. 40, 749, 1932.

Wil 76 L. Wilets, A.D. Mackellar, G.A. Rinker Jr., Proc. IV Int. Workshop in Gross Properties of Nuclei and Nuclear Excitations, Hirschegg, Austria, 111, 1976.

Wil 77 L. Wilets, E.M. Henley, M. Kraft and A.D. MacKellar, Nucl. Phys. A282, 341, 1977.

Wil 78 L. Wilets, Y. Yariv and R. Chestnut, Nucl. Phys. A301, 359, 1978.

Wil 85 J.R. Wilson, R. Mayle, S.E. Wooseley, T. Weaver, LLNL preprint 1985.

Wit 85 E. Witten, Princeton preprint, 1985.

Won 77 C.Y. Wong, J.A. Maruhn and T.A. Welton, Phys. Lett. 66B, 19, 1977.

Won 82 C.Y. Wong, Phys. Rev. C25, 1460, 1982.

Yar 79 Y. Yariv and Z. Fränkel, Phys. Rev. C20, 2227, 1979.

Yar 81 Y. Yariv and Z. Fränkel, Phys. Rev. C24, 488, 1981.

Zyr 56 P.S. Zyrianov and V.M. Eleonskii, JETP, 620, 1956.